Atom Scattering off Superfluid ^{4}He Clusters and Films

Dissertation

zur Erlangung des akademischen Grades
eines Doktors der technischen Wissenschaften

eingereicht von
DI Robert E. Zillich

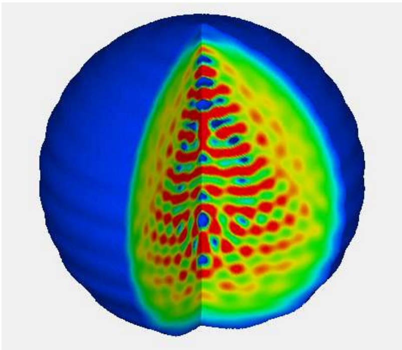

angefertigt am Institut für Theoretische Physik,
Johannes Kepler Universität Linz, Austria

1. Begutachter: o. Univ.-Prof. Dr. Eckhard Krotscheck
2. Begutachter: a. Univ.-Prof. Dr. Dieter Semrad

Linz/Donau, Mai 2001

Teile dieser Arbeit wurden bereits veröffentlicht oder zur Veröffentlichung eingereicht:

1. E. Krotscheck and R. Zillich: "Atom Scattering from Helium Droplets", G. S. Agnastostatos (ed.), 23rd Workshop on Condensed Matter Theories 1999, Nova Science Publishers
2. E. Krotscheck and R. Zillich: "Scattering of ^{3}He and ^{4}He atoms from ^{4}He clusters", J. of Low Temp. Physics **113**, 387 (1998)
3. E. Krotscheck, M. D. Miller, and R. Zillich: "Dynamics of Helium in restricted geometries", Physica B **280**, 59 (2000)
4. R. Zillich and E. Krotscheck: "Elastic and Inelastic Scattering off ^{4}He Droplets", Physica B **284–288**, 154 (2000)
5. R. Zillich and E. Krotscheck: "Atom and Neutron Scattering at ^{4}He Droplets", J. de Physique IV **10**, 173 (2000)
6. E. Krotscheck and R. Zillich: "The Dynamics of ^{4}He Nanodroplets", J. Chem. Phys IV, submitted (2001)
7. R. Zillich: "Hydrogen Scattering at ^{4}He Surfaces: Bound states and sticking probability", J. Low. Temp., submitted (2001)

Ich erkläre eidesstattlich, dass ich die vorliegende Dissertation selbständig verfasst, andere als die angegebenen Quellen und Hilfsmittel nicht benutzt und mich auch sonst keiner unerlaubten Hilfen bedient habe. Diese Arbeit wurde bisher weder im Inland noch im Ausland in irgendeiner Form als Prüfungsarbeit vorgelegt.

Robert E. Zillich

Acknowlegdgements

Most of the work presented in this thesis was carried out at the Institut für Theoretische Physik at the Kepler Universität, Linz, and part of it at the School of Physics and Astronomy, University of Minnesota.

I want to thank my thesis adviser Professor Eckhard Krotscheck for his help and for teaching me many-body physics (how to avoid solving the Schrödinger equation for all 10^{23} particles exactly, for the time being), for providing the means for preparing this thesis, and for his patience with a slower collaborator. He has shown me by example what scientific enthusiasm is.

The pleasant department life is also the merit of my collegues. I am indebted to Jakob and Axel for the professional and non-professional advice, both flavors equally welcome and helpful. I enjoyed the discussions with Norbert, Vesa, and Ferran who enrich(ed) my life with scientific expertise and cartoons. Mentions for their bravery go to my office mates, notably Karl who kept a friendly face although the disorder on my desks was spreading without bounds. For his invitation to the University of Minnesota and for his hospitality I want to thank Professor Charles Campbell.

For their support and for providing a parallel universe beyond doing physics I thank my parents, my brother, cousins and friends, and I hope they understand my preoccupation with physics.

The numerical calculations were largely carried out on an SGI Origin 2000 (and later 3800), the supercomputer of the Kepler University, managed and maintained by the ZID (Zentraler Informatik Dienst). I thank the Origin administrator DI Hans Messner for his cooperativeness and help and apologize for my insatiability for disk space.

ABSTRACT

In this work, the HNC-Euler-Lagrange theory is applied to the many-body scattering problem. We use time-dependent variational correlated wave functions in excitation calculations in order to describe atom scattering off nanoclusters and microscopically thin films of superfluid helium-4. Apart from elastic processes, the level of implementation of the method includes dissipation, *i.e.* processes in which the atom imparts energy to the cluster/film, such as direct inelastic scattering and sticking. From the cross sections/probabilities for elastic and dissipative processes, information about the energetic structure (excitation energies, dispersion relations) of the helium-4 system can be gleaned, and, for scattering off a helium-4 film, about the strength of Van der Waal forces between atom and the substrate, on which the film is adsorbed. For the determination of inelastic scattering cross sections, we develop a method based on the expansion of the expectation value of the probability current to second order in correlation fluctuations which leads to a formulation which allows to identify the decay probability into open scattering channels. Various differential cross sections are calculated such as the probability for energy- and momentum-transfer to the helium cluster which is the analogon to the dynamic structure function measured by inelastic neutron scattering and which allows the determination of the surface wave ("ripplons") dispersion relation. The effect of particle statistics on identical particle scattering is studies by comparing helium-4 scattering to impurity (helium-3) scattering off helium-4 clusters; e.g. we show how the elastic conversion process from helium-4 atom to roton and back can be understood as a resonance phenomenon at the excitation energy of the roton in helium clusters. The connection between resonances in the elastic scattering channel to their counterpart in inelastic channels is highlighted in the example of our results for quantum reflection off films. Furthermore, our theory predicts a long range of interaction between slow atoms and low energy surface waves, which increases the low energy inelastic scattering probability.

Zusammenfassung

In dieser Arbeit wird die HNC-Euler-Lagrange Theorie auf ein Vielteilchenstreuproblem angewandt. We verwenden einen zeitabhängigen Variationsansatz einer korrelierten Wellenfunktion für die Berechnung von angeregten Zuständen zur Beschreibung von Streuprozessen von Atomen an Nanoclustern und mikroskopisch dünnen Filmen von superfluidem Helium-4. Diese Methode berücksichtigt neben elastischen auch dissipative Prozesse, in denen das Atom Energie an den Cluster/Film verliert, wie zum Beispiel direkte inelastische Streuung und Ad- oder Absorption. Die Streuquerschnitte/-wahrscheinlichkeiten für elastische und dissipative Prozesse liefern Informationen über die Energieverhältnisse (Anregungsenergien, Dispersionsrelationen) des Helium-4 Systems, und, im Falle von Streuung an Heliumfilmen, über die Van der Waals-Kräfte zwischen Atom und dem Substrate, auf dem der Film adsorbiert ist. Wir entwickeln eine Method zur Berechnung von inelastischen Streuquerschnitten, in der der Erwartungswert des Wahrscheinlichkeitsstrom bis zweiter Ordung in den Korrelationsfluktuationen entwickelt wird und die Zerfallswahrscheinlichkeit in offene Streukanäle bestimmt wird. Wir berechnen verschiedene differenzielle Streuquerschnitte wie etwa die Wahrscheinlichkeit für Energie- und Impulstransfer an den Heliumcluster, aus der – ähnlich wie aus der durch inelastische Neutronenstreuung bestimmten dynamischen Strukturfunktion – die Dispersionsrelation der Oberflächenwellen ("Ripplonen") folgt. Wir untersuchen den Einfluss der Teilchenstatistik auf Streuung identischer Teilchen durch Vergleich von Helium-4 mit Helium-3 Streuung an Helium-4 Clustern. So stellt sich etwa heraus, dass die elastische Streuung von Helium-4 an der Rotonanregung, bei der das Atom in ein Roton verwandelt wird und wieder zurück, als eine Streuresonanz bei der Anregungsenergie des Rotons zu verstehen ist. Weiters wird der Zusammenhang zwischen Resonanzen im elastischen und in inelastischen Streukanälen am Beispiel der Quantenreflektion am Heliumfilm anhand unserer Ergebnisse besprochen. Ausserdem erhalten wir im Rahmen unserer Theorie eine langreichweitige Wechselwirkung zwischen langsamen Atomen und niederenergetischen Oberflächenwellen, was zu einer erhöhten Wahrscheinlichkeit für inelastische Streuung bei niederen Energien führt.

Contents

List of Figures

CHAPTER 1

Introduction

1. Nature's model system

Helium physics has been the test ground for quantum many body theories for many years. The two isotopes ^{4}He and ^{3}He aggregate to strongly correlated and very "quantum" many-body systems of high density which obey Bose and Fermi statistics, respectively. Helium can be described by the simplest Hamiltonian conceivable for interacting particles[1], yet it is not a model system bearing no relation to real systems, but has been and is studied intensely by experimentalists. Therefore there is a rich set of results that the microscopic theoretical calculations can be compared with: on the one hand, "exact" numerical results are obtained by Diffusion Monte Carlo (DMC) calculations [**Bor98**], the Path Integral Monte Carlo (PIMC) [**Cep95**], Variational Monte Carlo (VMC) [**Gua98**], or the Shadow Wave Function (SWF) method [**Rea97**]. On the other hand, analytic approximation schemes for strongly interacting quantum systems are for example the phenomenological Density Functional Theory (DFT) [**LDPS95**], Coupled Cluster Method (CCM) [**Bis98**], and the HNC-Euler-Lagrange theory which, in different formulations, has been successfully applied to Helium systems such as the homogeneous pure ^{4}He [**CC77**] and ^{3}He–^{4}He mixtures [**KS93b**], inhomogeneous systems [**Kro98a**] (films [**EK88, CFK$^+$94, CKS97**], slabs [**CKS98**], and droplets [**CK95a**]), for both static as well as dynamic properties, and recent efforts to extend the theory to finite temperatures are bearing fruit [**CCKS97**].

While the exactness of the first set of methods is basically a matter of computational effort, if equilibrium properties at $T = 0$ and $T > 0$ (PIMC) are to be determined, the latter set of methods is better suited for the calculation of excitation spectra, damping of excitations, the dynamical structure factor, or the effective mass of impurities in ^{4}He. In this work, the HNC-Euler-Lagrange theory is applied to scattering problems at Helium droplets and films.

2. How many ^{4}He atoms does it take to observe superfluid behaviour?

Droplets of both helium isotopes, pure and mixed, are produced by adiabatic cooling of a beam of helium atoms expanding into a vacuum chamber. The droplets can be doped by sending the cooled beam through pick-up chambers filled with a gas of the dopant atoms/molecules [**Gsp95**].

[1] apart from complications such as three-body forces

A finite size laboratory: Helium droplets offer the possibility to study the continuous transition from a bound few-body system to the bulk limit. The emergence of collective phenomena such as bulk modes (e.g. phonons and rotons in ^{4}He), superfluidity of ^{4}He, or Bose-Einstein condensation are observed without needing to be disentangled from effects stemming from a complicated interaction like those between nucleons or from external influences like the lattice potential acting on the electrons in a solid. Furthermore, closer inspection of the way how properties specific to a finite system evolve with growing size, can shed new light on bulk properties. For example, we will see how the characterisation of the roton as a resonance at wavelengths of the order of the interparticle spacing follows naturally from the examination of scattering solutions of ^{4}He atoms impinging on ^{4}He droplets.

spectroscopy: ^{4}He is not only a very pure matrix for isolating individual molecules; it is cold (typical temperatures of ^{4}He droplets: 0.37K, ^{3}He: 0.15K), but also only weakly perturbing the molecule to be investigated (^{4}He is superfluid at 0.37K), which allows for high resolution molecular spectroscopy [**TVW01**].

Conversely, atoms and molecules with well-known spectra are deployed into helium and onto helium surfaces to probe the properties of helium. Alkali atoms do not dissolve into the bulk of the droplet but instead attach to the surface; electronic excitations hit the helium surface like a hammer, which can be obserbed in femtosecond pump-probe spectroscopy [**SHES95, SMH$^+$99**].

Spectroscopy of molecules with known rotational spectra such SF_6 or OCS has already yielded insight into the phenomenon of superfluidity on a microscopic scale ("nanosuperfluidity") [**KHP$^+$00**], which leads us back to the first aspect of helium droplets used for studying finite size effects: rotationally excited molecules act as a microscopic "stirring straw" inside the ^{4}He droplet. The experimental answer to the question introducing this paragraph is 60 [**GTV98**].

3. The ^{4}He surface

The surface of superfluid ^{4}He is interesting for a variety of experiments, some of them proposed, some carried out. The advantage of ^{4}He over other materials is again its purity, its inertness, and specific for surfaces the fact that it is atomically flat – as any liquid gas interface, but down to zero temperature without freezing –, and it will cover an arbitrarily shaped substrate with a thin film, for example the walls of the experimental cell. Examples where ^{4}He surfaces play a vital role are

- 2-dimensional Fermi systems: electrons floating on Helium films, study of 2D Wigner crystallisation [**KDL00**]; adsorbed ^{3}He [**Hal95, Hal98**]
- recently proposed quantum computing experiment: q-bits are e^- floating on ^{4}He film (large relaxation times!) [**PD99**];
- 2-dimensional Bose gas, quantum degeneracy of a quasicondensate of spin-polarized atomic hydrogen floating on Helium surface, which has been observed [**SVY$^+$98**];

- in the search for Bose condensation of atomic spin-polarized hydrogen the spin-polarized H gas protected by a ^{4}He film from the cell walls in order to prevent degradation by spin-flips at magnetic impurities in the walls;
- surface-state hydrogen maser [**MVSS93**].

Our interest is the interaction of light atoms like atomic H and ^{3}He with ^{4}He surfaces.

4. The goal of this work

In this work, we want to theoretically study the process, which the particles of a gas undergo when they are possibly caught by a ^{4}He droplet and when they hit the helium coated walls of its container — the scattering process. This type of excitation of the many-body system is calculated in the framework of the HNC-Euler-Lagrange theory which has already been applied successfully to excitations in bulk Helium [**AHS99, AS98, Saa86**] and Helium films [**CFK$^+$94, CGK$^+$96**] and elastic scattering, and transmission probabilities have been calculated for ^{4}He slabs [**CKS98**]. The primary information from scattering are cross sections for processes, i.e. the rates for the many possible outcomes when an incoming particle hits the droplet. Apart from absorption cross sections for the probability of being caught, it turns out that inelastic scattering cross sections yield information about the excitation spectrum of the droplet, analogous to inelastic neutron scattering.

Another motivation to study scattering at ^{4}He droplets, is the similarity to nuclear scattering problems [**RR78**]: although Bose statistics, single particle species and the interaction potential are a drastic simplification of a nucleon system, some of the effects that are a consequence of the many body nature could persist in the Helium droplet model. However, we refrain from exploring this possible application, because the method to compute cross section, detailed in section 5, is currently being extended to the Fermi-hypernetted chain formalism (FHNC).

Also, scattering of ^{4}He and ^{3}He atoms at ^{4}He droplets offer the opportunity to observe the effect of statistics on scattering cross sections in an almost perfectly matched pair of experiments: scattering with an identical and with a distinct particle, respectively, both interacting via the same potential and having similar masses.

Finally, there is an interesting proposal to detect the Bose-Einstein condensate (BEC) by transmitting ^{4}He atoms through slabs of ^{4}He. Calculations [**HCGG93, SHC97**] indicate that the inpinging ^{4}He couples to the BEC which could lead to a finite probability of instantaneous emission off the opposite side of the slab.

The text of the first part on ^{4}He droplets is organized as follows: In chapter 2, we give a very concise description of the inhomogeneous version of the HNC-Euler-Lagrange theory, applied to the ground state of the many-boson system that ^{4}He droplets and films constitute, and to the ground state of single impurities in ^{4}He. Also, quantities necessary for the later development are introduced. In chapter 3, we review, in slightly more detail, the extension of the HNC-Euler-Lagrange theory to the calculation of excitations. We choose the linear response approach, but the basic idea of the method was already given by Feynman [**Fey54**].

In this chapter, but more specific for the scattering problem in the following chapter, we also discuss the strengths and limitations of the used methods for excitations. In chapter 4 we furthermore introduce the terms used in the description of scattering, especially the concept of scattering channels. Starting with chapter 5, the main result of this work is presented, the derivation and calculation of currents to *second order* in the correlation fluctuations, which represent the experimentally measureable transport currents in the HNC-Euler-Lagrange theory. These second order currents are applied to the many-body scattering problem in chapter 6 to the calculation of inelastic scattering cross sections. Among other things, the numerical results demonstrate how inelastic scattering of ^{3}He at ^{4}He droplets yields information about the surface excitation spectrum. Furthermore, results for the elastic cross sections are presented and its implications for detecting the roton energy of a ^{4}He droplet are discussed. Finally, chapter 7 deals with inelastic scattering and sticking of atomic hydrogen and of ^{3}He atoms at the surface of adsorbed ^{4}He films. It covers the derivation of the second order impurity currents for the plane surface geometry, which allows the calculation of the total direct inelastic scattering probability and its surprising low energy proportionality, the outgoing flux as it is measured in time-of-flight experiments, the angular distribution of inelastic flux. From unitarity, sticking probabilities are calculated and its sensitivity to the long-ranged Van der Waal potential of the substrate is investigated.

CHAPTER 2

The Basics of HNC-Euler-Lagrange Theory

1. Introduction

The lightest rare gas Helium–4 and Helium–3 liquifies at 4.21 K and 3.19 K, respectively, but both isotopes are too light and its atomic interaction too weakly attracting to freeze at lower temperatures, except at high pressures of 25 atm (^{4}He at $T = 0$) and 34 atm (^{3}He at $T = 0$). Instead, if the temperature is lowered further below the liquefication temperature, the quantum nature of matter manifests itself: the bosonic ^{4}He liquid becomes superfluid at $T_c = 2.17$ K ($p = 0$), and the fermionic ^{3}He, in the millikelvin regime, has even two superfluid phases.

This work is devoted to the study of ^{4}He as a many–body system which ^{4}He droplets of the order of $N = 10^2 - 10^3$ atoms certainly are. $1/N$ is small compared to 1 which allows to apply the HNC-Euler-Lagrange theory, but $N > 3$, *i.e.* semi-analytic methods for the 3-particle problem are not applicable. Yet, N is not large enough to treat the system in the homogeneous bulk limit and to neglect surface effects. Instead the translational symmetry is broken as the atoms condense to a spherical droplet.

If a system of microscopic particles is cooled, and if the Dirac wavelength rises above the mean interparticle spacing d, the system can no longer be described by classical mechanics. In quantum mechanics, the many-body problem can be considered formally solved if all eigenstates of the Hamiltonian H are known, where for N identical particles

$$H = \sum_{i=1}^{N} -\frac{\hbar^2}{2m}\nabla_i^2 + \sum_{i<j} V(|\mathbf{r}_i - \mathbf{r}_j|) + \sum_{i=1}^{N} U(\mathbf{r}_i) \ . \tag{1}$$

H is obtained by decoupling the electronic degrees of freedoms from the motion of the nuclei in the Born-Oppenheimer approximation, yielding an effective interaction potential V between the atoms. For noble gas atoms, V is pairwise additive to a good approximation; it is plotted in Fig. 1. Effects due to three-body terms have been calculated and shown to account for minor corrections [**BC49**]; they are neglected in this work. Furthermore, all inner, electronic excitations can be neglected: for example in bulk ^{4}He at $T = 0$, the mean kinetic energy of the atoms is 17 K and the mean interaction energy is -24 K per particle, which is orders of magnitudes smaller than electronic excitation energies of noble gas atoms.

As the kinetic energy decreases with temperature, the attraction between the particles (the mutual polarization potential) can win over the kinetic energy, and the system undergoes a phase transition to the energetically more favourable solid state. This happens for all

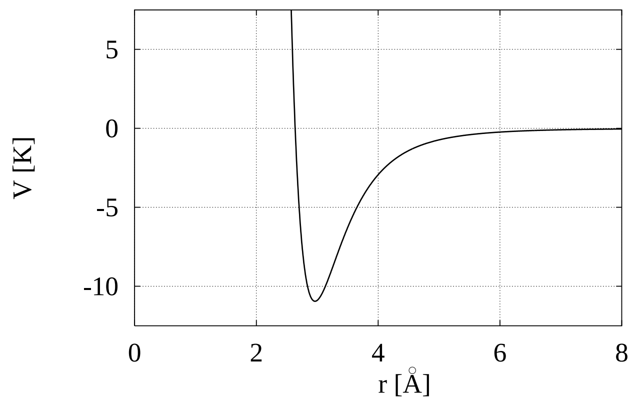

FIGURE 1. The interaction potential used in this work, due to Aziz et. al. [**AMW87**].

atoms and molecules except for ^{4}He and ^{3}He, which remain liquid down to $T = 0$, which is a consequence of their respective low mass of about 4 and 3 atomic mass units and the weak attractive tail of the interaction potential. Brought down to low temperature, where quantum mechanics takes over, *and* still liquid (i.e. the atoms can exchange places with little energetic effort), the Helium isotopes show features which are related to the exchange symmetry. Especially, below 2.17 K a macroscopic fraction of the bosonic ^{4}He "occupies the zero-momentum ground state" (Bose–Einstein Condensation) [**PO56**]. If ^{4}He is cooled down further and thermal excitations (the "normal fraction" in the two fluid model) become negligible, it will be the ground state of the Hamiltonian (1) that carries most information needed to describe the properties of real ^{4}He.

2. Hypernetted chain equations

The microscopic HNC-Euler-Lagrange theory was devised by Feenberg and others [**CF59, Fee69**] to solve the stationary Schrödinger equation

$$H|\Phi\rangle = E|\Phi\rangle \tag{2}$$

for the ground state wave function $|\Phi_0\rangle$ of a dense, strongly correlated quantum many-body system like helium. In order to introduce quantities needed later for excitation calculations, we briefly review the theory for single–component boson systems.

The theory starts with the generalized Jastrow–Feenberg *ansatz* (for our conventions for the notation see Appendix A), which consists of a product of functions

$$\Phi_0(1,\ldots,N) = \prod_i \phi(i) \prod_{i<j} f(i,j)\ldots \;= \exp\frac{1}{2}\Bigg[\sum_{n=1}^{m} \sum_{i_1<\cdots<i_n} u_n(i_1,\ldots,i_n)\Bigg] \tag{3}$$

where u_n, called n–body correlation function, is real and symmetric under exchange of its coordinates. The splitting into functions correlating a different number of particle is made unique be requiring

$$u_n(\mathbf{r}_1,\ldots,\mathbf{r}_n) \to 0 \qquad \text{if } \mathbf{r}_1,\ldots,\mathbf{r}_j \text{ are separated from } \mathbf{r}_{j+1},\ldots,\mathbf{r}_n\,.$$

As long as $m < N$, the exact ground state cannot be cast into this form; however, even for small m ($m = 3$ in our calculations) Φ_0 gives already very accurate results for all important, i.e. few–body quantities: scalar quantities like the ground state energy E_0 and the equation of state for $T = 0$; one–body quantities like density profiles $\rho_1(\mathbf{r})$; two-body quantities like the static structure function $S(k)$.

The expectation value of the Hamiltonian (1) which is to be minimized (see next section) with respect to the Jastrow–Feenberg wave function can be written as a functional of the correlation functions and the particle densities, defined in eq. (242),

$$E[\{u_i,\rho_i\}] = \frac{\langle\Phi_0|H|\Phi_0\rangle}{\langle\Phi_0|\Phi_0\rangle} \equiv \langle T\rangle + \langle V\rangle + \langle U\rangle \tag{5}$$

with

$$\langle T\rangle = -\frac{\hbar^2}{8m}\sum_{n=1}^{m}\frac{1}{n!}\int d1\ldots dn\;\rho(1\ldots n)\sum_{i=1}^{n}\nabla_i^2 u_n(1\ldots n) \tag{6}$$

$$\langle V\rangle = \frac{1}{2}\int d1d2\;\rho(1,2)\,V(1,2) \tag{7}$$

$$\langle U\rangle = \int d1\;\rho(1)\,U(1)\,. \tag{8}$$

However, the densities are functionals of the correlation functions, $\rho_n = \rho_n[\{u_i\}]$ (or vice versa). The functional dependence is the same as between classical densities and potentials $W_n(1\ldots n)$, and the mapping

$$u_n(1\ldots n) \longrightarrow -\frac{1}{k_BT}W_n(1\ldots n) \tag{9}$$

renders the problem of determining ρ_n from u_i, $i = 1,\ldots,m$ a problem of classical statistical mechanics where various approximation schemes are used. These are the equations to related densities and correlation function for $n = 1, 2, 3$ [**LGB59, HM86, MO78, Kro86, Rip79, Puo99, Puo97**]:

One–body correlation: u_1 is expressed in terms of ρ_i, u_2, and u_3 by the Born–Green–Yvon (BGY) equation, obtained by simply applying the gradient operator to the definition of the one–body density

$$\nabla_1 u(1) = \nabla_1 \ln\rho(1) - \int d2\;\frac{\rho(1,2)}{\rho(1)}\nabla_1 u_2(1,2) - \int d23\;\frac{\rho(1,2,3)}{\rho(1)}\nabla_1 u_3(1,2,3) \tag{10}$$

Two–body correlation: Of the numerous approximation schemes for the relation between u_2 and ρ_2 used in statistical mechanics, for our purpose only the *hypernetted chain* (HNC) approximation hierarchy allows for a consistent optimization of the ground state energy expectation value [**Cam78**] (see the appendix for the tilde notation):

$$\begin{aligned} g(1,2) &= e^{u(1,2)+N(1,2)+E(1,2)} && (11)\\ \tilde{N}(1,2) &= [\tilde{h} * \tilde{X}](1,2) \qquad \text{(Ornstein–Zernicke)} && (12)\\ X(1,2) &= h(1,2) - N(1,2) \\ h(1,2) &= g(1,2) - 1 \end{aligned}$$

where g is the *pair distribution*, eq. (248), N is the sum of all so-called *nodal diagrams*, and X is the *direct correlation* function, formally defined as

$$X(1,2) = \frac{\delta^2 C}{\delta\rho(1)\delta\rho(2)}$$

with the transform of the ground state normalization integral $I_{00} = \langle\Phi_0|\Phi_0\rangle$

$$C = \ln I_{00} - \int d1\ \rho(1)\, u(1) - \int d1\ \rho(1)\, [1 - \ln\rho(1)]\,.$$

The HNC equations would be a closed set of equations, if the sum of all *elementary diagrams*, E, were given in analytic form in terms of g or u_2. Unfortulately, E is given only in diagrammatic form. The number of diagrams included in the HNC equations sets the approximation level. Furthermore, for inhomogeneous systems, E is calculated in a local density approximation. It should also be noted, that the validity of the HNC equations relies on the thermodynamic limit, $N \to \infty$, in the same way as the validity of expectation values in the grand canonical ensemble does.

Three–body correlation: For the relations between g_3 and u_3 we need the 3-body direct correlation function (diagrammatically, non-nodal in all three points)

$$X(1,2,3) = \frac{\delta^3 C}{\delta\rho(1)\delta\rho(2)\delta\rho(3)}\,.$$

For the triplet distribution, the exact relation holds

$$\begin{aligned} g(1,2,3) &= h(1,2,3) + h(1,2) + h(1,3) + h(2,3) + 1 && (13)\\ h(1,2,3) &= h(1,2)h(1,3) + h(1,2)h(2,3) + h(1,3)h(2,3) \\ &\quad + \int d4\ \rho(4)\ h(1,4)h(2,4)h(3,4) \\ &\quad + \frac{1}{\sqrt{\rho(1)\rho(2)\rho(3)}} \int d4d5d6\ S(1,4)S(2,5)S(3,6)\tilde{X}(4,5,6) && (14) \end{aligned}$$

where S is defined in (252). The closed set of HNC equations [**Puo97**] would be still to be to computationally demanding, therefore we content ourselves with a less sophisticated approximation such that the sequential property (247) is still fulfilled:

$$X(1,2,3) \approx u(1,2,3)\,.$$

This is the convolution approximation [**Fee69**], including 3–body correlations.

3. Euler-Lagrange equations

Solving the N–body Schrödinger equation for the ground state Φ_0 is equivalent to finding the global minimum of the expectation value of the Hamiltonian with respect to wave functions of the N–body Hilber space. Hence, the variation has to vanish, and the energy has to be minimized by solving the *Euler-Lagrange equation*

$$\delta E = \delta \frac{\langle\Phi|H|\Phi\rangle}{\langle\Phi|\Phi\rangle}\bigg|_{\Phi=\Phi_0} = 0\,, \tag{15}$$

which we now take as the equation to determine Φ_0. Instead of the impossible variation in the full Hilbert space, the variation will be done in the subspace of the Jastrow–Feenberg wave functions.

After we have established the relations between densities and correlations in the previous section, the energy (5) can be expressed in terms of the independent variables ρ_1, g, and u_3 [**Kro98b**]:

$$E[\sqrt{\rho}_1, g, u_3] = E_T + E_U + E_c \tag{16}$$

with

$$\begin{aligned}
E_T &= \int d1\; |\sqrt{\rho(1)}|^2 \\
E_U &= \int d1\; \rho(1)\, U(1) \\
E_c &= E_c^{(2)} + E_c^{(3)} \\
E_c^{(2)} &= \frac{1}{2}\int d1d2\; \rho(1)\rho(2)\left[g(1,2)V(1,2) + \frac{\hbar^2}{2m}|\nabla_1\sqrt{g(1,2)}|^2 + \frac{\hbar^2}{2m}|\nabla_2\sqrt{g(1,2)}|^2\right] \\
&\quad - \frac{1}{4}\int d1d2\; [\tilde{N}(1,2) + \tilde{E}(1,2)]\, H_1(1)\, \tilde{h}(1,2) \\
E_c^{(3)} &= \int d1d2d3\; \tilde{g}(1,2,3)\, [H_1(1) + H_1(2) + H_1(3)]\, \tilde{u}(1,2,3)
\end{aligned} \tag{17}$$

with the one–body operator

$$H_1(1) = -\frac{\hbar^2}{2m}\frac{1}{\sqrt{\rho(1)}}\nabla_1\rho(1)\nabla_1\frac{1}{\sqrt{\rho(1)}} = -\frac{\hbar^2}{2m}\nabla_1^2 + \frac{\hbar^2}{2m}\frac{\nabla_1^2\sqrt{\rho(1)}}{\sqrt{\rho(1)}}\,. \tag{18}$$

The minimization equation (15) for the energy functional (16) are obtained by functional differentiation, leading to Euler-Lagrange (E.L.) equations

$$\frac{1}{2}\frac{\delta(E[\sqrt{\rho}_1, g, u_3] - \mu N)}{\delta\sqrt{\rho(\mathbf{r}_1)}} = 0\,, \qquad \frac{\delta E[\sqrt{\rho}_1, g, u_3]}{\delta g(\mathbf{r}_1, \mathbf{r}_2)} = 0\,, \qquad \frac{\delta E[\sqrt{\rho}_1, g, u_3]}{\delta u(\mathbf{r}_1, \mathbf{r}_2, \mathbf{r}_3)} = 0\,. \tag{19}$$

With the energy functional given, one can derive a set of three coupled equations [**Tym95**]:

One–body E.L.: Variation with respect to the square root of the density, with the constraint of particle conservation, yields a Hartree type of wave equation

$$-\frac{\hbar^2}{2m}\nabla_1^2\sqrt{\rho(1)} + [U(1) + V_H(1)]\sqrt{\rho(1)} = \mu\sqrt{\rho(1)} \tag{20}$$

where μ is the chemical potential. The Hartree potential V_H is

$$\begin{aligned} V_H(1) &= \frac{\delta E_c}{\delta\rho(1)} = \int d2\ \rho(2)\left[V_{\mathrm{p-h}}(1,2) - \frac{1}{2}h(1,2)w_I(1,2)\right] \\ &- \frac{\hbar^2}{16m\rho(1)}\nabla_1\left[\rho(1)\nabla_1\int d2\ \rho(2)h(1,2)N(1,2)\right] \end{aligned} \tag{21}$$

where $V_{\mathrm{p-h}}$ is the *particle-hole interaction*

$$V_{\mathrm{p-h}}(1,2) = \frac{\delta^2 E_c}{\delta\rho(1)\delta\rho(2)} \tag{22}$$

$$\begin{aligned} &= g(1,2)V(1,2) + \left[+\frac{\hbar^2}{2m}|\nabla_1\sqrt{g(1,2)}|^2 + \frac{\hbar^2}{2m}|\nabla_2\sqrt{g(1,2)}|^2\right] \\ &+h(1,2)w_I(1,2) + V_{\mathrm{p-h}}^{(E)}(1,2) + V_{\mathrm{p-h}}^{(T)}(1,2) \end{aligned} \tag{23}$$

$$w_I(1,2) = -\frac{1}{2}\left[[H_1(1)+H_1(2)]\tilde{N}(1,2) + [\tilde{X} * H_1\tilde{X}](1,2)\right]$$

where $V_{\mathrm{p-h}}^{(E)}(1,2)$ and $V_{\mathrm{p-h}}^{(T)}(1,2)$ are terms stemming from the elementary diagrams and the triplet correlations, see [**Tym95**] for their respective definitions. The two above expressions (22) and (23) are equivalent only if *all* elementary diagrams in $V_{\mathrm{p-h}}^{(E)}$ are summed.

Two–body E.L.: The second equation in (19) can be cast into the form

$$[\tilde{X} * H_1\tilde{X}](1,2) - [H_1(1)+H_1(2)]\tilde{X}(1,2) = 2V_{\mathrm{p-h}}(1,2) \tag{24}$$

Three–body E.L.: Using the E.L. equation for g, the third equation in (19) is

$$\begin{aligned} [H_1(1)+H_1(2)+H_1(3)]\tilde{g}(1,2,3) &= \int d4d5\ \frac{\delta u(4,5)}{\delta u(1,2,3)}[H_1(4)+H_1(5)]\tilde{g}(4,5) \\ &+ \int d4d5d6\ \frac{\delta g(4,5,6)}{\delta u(1,2,3)}[H_1(4)+H_1(5)+H_1(6)]\tilde{u}(4,5,6) \end{aligned}$$

The formulation of this equation in a numerically feasable manner in terms of the 3–body nonnodal diagrams $X(1,2,3)$ requires a considerable amount of manipulation. Since we will not explicitly use these 3–body optimization equations nor the definitions therein for the treatment of excitations (which is starting from time-dependent fluctuations of only 1– and 2–body correlations) in the next chapter, we refer to [**Tym95**], where $X(1,2,3)$ is given in eq. (2.76) and (2.80).

Remark 1 For droplets in vacuum, there is no external potential, and the exact ground state has translational invariance which is spontaneously broken only in the limit $N \to \infty$. Nevertheless, the 1–body correlation u_1 is still introduced to break the symmetry for finite N, because a translational invariant ansatz would have to include 4–body correlations to be on the same level of accurracy as the ansatz (3): ρ_1 would be a constant, ρ_2 yields the density profile, etc. Conversely, the ansatz (3) allows the same formalism that has been already used for ^{4}He films.

Remark 2 On a related note, for droplets, the internal energy $E_{\rm int}$ instead of E of eq. (16) is minimized, which is obtained by subtracting the center-of-mass motion, *i.e.* minimizing the expectation value of

$$H_{\rm int} = H + \frac{\hbar^2}{2Nm}\left|\sum_i \nabla_i\right|^2 .$$

Details of this modification can be found in [**CK95a**].

4. Impurity in ^{4}He

In the low concentration limit, impurities in ^{4}He can be treated as single particles interacting with the ^{4}He atoms but not among themselves. Hence, all properties can be derived from the solutions to the Hamiltonian H^I, composed of the Hamiltonian H for the N ^{4}He atoms, as given in eq. (1), the single impurity Hamiltonian, and an interaction part,

$$H^I = H \;-\; \frac{\hbar^2}{2m_I}\nabla_0^2 + U^I(\mathbf{r}_0) \;+\; \sum_{i=1}^{N} V^I(|\mathbf{r}_0 - \mathbf{r}_i|)\,, \tag{25}$$

where m_I is the mass of the impurity with coordinate $\mathbf{r}_0$ and V^I and U^I are the potential between impurity and ^{4}He atom and the external potential, respectively[1]; evidently, for the helium isotope ^{3}He, these potentials are the same as V and U. The Jastrow–Feenberg ansatz for the ground state with an impurity is

$$\Phi_0^{(N+1)}(0,1,\ldots,N) = \exp\frac{1}{2}\left[\sum_{n=1}^{m}\sum_{i_1<\cdots<i_{n-1}} u_n(0,i_1,\ldots,i_{n-1})\right]\Phi_0^{(N)}(1,\ldots,N)\,, \tag{26}$$

where $\Phi_0^{(N)}$ is the ground state (3) of the pure system of N bosons, and, as for the pure system, $m = 3$. The impurity density distributions $\rho_i^I(\mathbf{r}_0,\mathbf{r}_1,\ldots,\mathbf{r}_{i-1}) \equiv \rho(0,1,\ldots,i-1)$ associated with this wave function are defined in appendix A.

The minimization of the energy is described thoroughly in [**Eps92, KSE88, KS93a, CKS97**]. Therefore we will only sketch the idea: the single impurity changes the energy of the system only by an amount of order $\frac{1}{N}$ relative to the pure ground energy E_N, this amount being the chemical potential $\mu_I = E_{N+1}^I - E_N$. It is reasonable — and equivalent, of course — to minimize μ_I instead of E_{N+1}^I. The correlations between impurity and background induces a change in the background quantities ρ_i and u_i of order $\frac{1}{N}$, which may not be neglected in the functional μ_I. Denoting this change by Δ, we find therefore

$$\mu_I = \mu_I^{(0)} - \Delta E_N$$

where E_N is given by eq. (5) and $\mu_I^{(0)}$ is given by the same expression with $\mathbf{r}_1$ being replaced by $\mathbf{r}_0$ and $\frac{1}{m}\nabla_1^2$ by $\frac{1}{m_I}\nabla_0^2$. The optimized correlations and distributions of the pure ground

[1]Following the notational convention summarized in appendix A, we will omit the superscript I, if the function argument(s) are given, thus clarifying whether we are dealing with an impurity or a background function.

state shall be denoted by a superscript p, $u_i^{(p)}$ and $\rho_i^{(p)}$. Then, to first order in $\frac{1}{N}$, the impurity induces a change in the background energy

$$\begin{aligned}\Delta E_N &= E_N[\Delta u_1, \sqrt{\rho}_1^{(p)}, u_2^{(p)}, g^{(p)}, u_3^{(p)}, \rho_3^{(p)}] + E_N[u_1^{(p)}, \sqrt{\rho}_1^{(p)}, \Delta u_2, g^{(p)}, u_3^{(p)}, \rho_3^{(p)}] \\ &\quad + E_N[u_1^{(p)}, \sqrt{\rho}_1^{(p)}, u_2^{(p)}, g^{(p)}, u_3^{(p)}, \Delta\rho_3]\end{aligned}$$

where we used the fact that E_N has already been optimized with respect to $\sqrt{\rho}_1$, g, and u_3, hence the first order variation of E_N vanishes. This not only simplifies the expression for μ_I, but also relieves us of minimizing μ_I with respect to these background quantities. The Euler-Lagrange equations are

$$\frac{1}{2}\frac{\delta\mu_I[\sqrt{\rho_1^I}, g^I, u_3^I]}{\delta\sqrt{\rho_1^I(\mathbf{r}_0)}} = 0\,, \qquad \frac{\delta\mu_I[\sqrt{\rho_1^I}, g^I, u_3^I]}{\delta g^I(\mathbf{r}_0, \mathbf{r}_1)} = 0\,, \qquad \frac{\delta\mu_I[\sqrt{\rho_1^I}, g^I, u_3^I]}{\delta u_3^I(\mathbf{r}_0, \mathbf{r}_1, \mathbf{r}_2)} = 0\,. \tag{27}$$

For expressing u_1^I and u_2^I in terms of ρ_1^I and g^I, we use the impurity versions of the BGY equation and of the HNC equations, respectively, both having exactly the same analytic structure as the pure versions. For the impurity version of (14), we furthermore apply the convolution approximation *without* triplet correlations $X(0,1,2) = 0$.

Lekner approximation The inhomogeneous impurity Euler-Lagrange equations formulated in a numerically tractable manner can by found in the appendix section of [**CKS97**]. They allow for the calculation of ground state properties of light atoms (H, D, ^{3}He, Na) such as chemical potential and the static structure function [**Eps92, KSE88, Kro85a, KS93a, CKS97**]. However, in the case of a ^{3}He impurity, one can take advantage of the similarity of the two isotopes (same interaction potential, similar mass) and employ an approximation due to Lekner [**Lek70**]: instead of determining the 2– and 3–body correlations by solving the 2– and 3–body Euler-Lagrange equations (27), one coordinate in the ground state quantities of $N+1$ ^{4}He atoms is changed to an impurity coordinate, and only the 1–body correlation u_1^B is replaced by u_1^I, and is determined by the 1–body Euler-Lagrange equation. Effectivly, this amounts to settling for the simplified ansatz for the ground state wave function (note the superscripts)

$$\begin{aligned}\Phi_0^{(N+1)}(0,1,\ldots,N) &= \exp\frac{1}{2}\Big[u^I(0) + \sum_i u^B(0,1) + \sum_{i<j} u^B(0,1,2)\Big]\Phi_0^{(N)}(1,\ldots,N) \\ &= e^{\Delta u(0)/2}\bar{\Phi}_0^{(N+1)}(0,1,\ldots,N)\end{aligned} \tag{28}$$

where $\bar{\Phi}_0^{(N+1)}$ denotes the ground state of $N+1$ ^{4}He atoms. $\rho(0)$, and hence $u^I(0)$, is determined by minimizing the energy difference ΔE resulting by replacing the ^{4}He atom at $\mathbf{r}_0$ by the ^{3}He atom. $\sqrt{\rho(0)}$ is the solution of a single-body Schrödinger equation with an effective potential

$$V_H(0) = \frac{\hbar^2}{2m_4}\frac{\nabla^2\sqrt{\rho_B(0)}}{\sqrt{\rho_B(0)}} + (\frac{m_4}{m_3} - 1)\frac{\hbar^2}{8m_4}\int d2\; \rho_B(2)\nabla_1 g(1,2)\cdot\nabla_1 u(1,2) + V_H^T(1)$$

where V_H^T are terms involving triplet correlations.

We have used the Lekner approximation in the droplet calculations, and the full optimization in the film calculations.

5. Discussion of the ground state and results

5.1. Asymptotic behaviour

For the interpretation of the excitation calculation in terms of scattering amplitudes (chapter 4), knowledge of the asymptotic behaviour of the ground state wave function Ψ_0 will turn out helpful. Due to the short-range Van-der-Waal interaction, the Hamiltonians (1) and (25) are separable, if the coordinate of any particle i is separated from all others. Therefore, in this limit, the eigenfunction becomes a (sum of) product(s) of eigenfunctions of the free Hamiltonian for particle i with eigenenergy $\mathcal{E}_1$ and of the Hamiltonian of the remaining particles with eigenenergy $\mathcal{E}_{N-1}$, respectively, where this summation in restricted by requiring $\mathcal{E}_1 + \mathcal{E}_{N-1} = E_N$, with E_N being the ground state energy. We can argue heuristically that, for large N, the N-particle ground state has small overlap with the $(N-1)$-particle states except for the node-less $(N-1)$-particle ground state. Then, only one product is left of the sum and $\mathcal{E}_{N-1} = E_{N-1}$ and therefore $\mathcal{E}_1 = E_N - E_{N-1} = \mu$.

Choosing coordinate $\mathbf{r}_1$ (or $\mathbf{r}_0$ in the impurity case) to tend to infinity while the others are kept near the origin[2], and using the definition of the 1–body density (242) and (243), we find for large N

$$\begin{aligned}\Phi_0^{(N)}(1,\ldots,N) &\overset{r_1\to\infty}{\longrightarrow} \sqrt{\frac{\rho^B(\mathbf{r}_1)}{N}}\Phi_0^{(N-1)}(2,\ldots,N)\\ \Phi_0^{(N+1)}(0,\ldots,N) &\overset{r_0\to\infty}{\longrightarrow} \sqrt{\rho^I(\mathbf{r}_0)}\Phi_0^{(N)}(1,\ldots,N)\end{aligned} \tag{29}$$

and repeating the process for another coordinate

$$\begin{aligned}\Phi_0^{(N)}(1,\ldots,N) &\overset{r_1,r_2\to\infty}{\longrightarrow} \sqrt{\frac{\rho^B(\mathbf{r}_1)\,\rho^B(\mathbf{r}_2)}{N(N-1)}}\Phi_0^{(N-2)}(3,\ldots,N)\\ \Phi_0^{(N+1)}(0,\ldots,N) &\overset{r_0,r_1\to\infty}{\longrightarrow} \sqrt{\frac{\rho^I(\mathbf{r}_0)\,\rho^B(\mathbf{r}_1)}{N}}\Phi_0^{(N-1)}(2,\ldots,N)\end{aligned} \tag{30}$$

where

$$\sqrt{\rho^{(B/I)}(\mathbf{r})} \overset{r\to\infty}{\longrightarrow} \frac{A}{r}\exp\Big[-\sqrt{\frac{2m_{B/I}|\mu_{B/I}|}{\hbar^2}}\,r\Big] \tag{31}$$

and where the double limits $r_i, r_j \to \infty$ have to be carried out independently[3]. Hence, the square root of the one-body density falls off exponentially as if it were the one-body ground state wave function of a particle in a potential, with binding energy $|\mu|$ – which formally it is

[2] In case of helium films, the z–component of coordinate $\mathbf{r}_1$ or $\mathbf{r}_0$ tend to infinity while the others are kept near the holding potential [**Saa71**].

[3] If, in the limit $r_i, r_j \to \infty$, $|\mathbf{r}_i - \mathbf{r}_j|$ is kept finite, $\Phi_0^{(N)}(1,\ldots,N)$ could retain components from the factorization into the $(N-2)$-body ground state and the 2-body ground state φ_B — the ^{4}He dimer, which is known the exist (see text) and has a binding energy $E_B \sim 1.7$mK. For example, for films one finds

$$\Phi_0^{(N)}(1,\ldots,N) \to Ae^{-(\alpha-\lambda)(z_1+z_2)}\varphi_B(|\mathbf{r}_1-\mathbf{r}_2|)\Phi_0^{(N-2)}(3,\ldots,N) \qquad \text{for} \quad z_1, z_2 \to \infty$$

N	μ_4[K]	μ_3[K]
40	-4.04	-2.73
70	-4.49	-2.99
112	-4.84	-3.21
200	-5.17	-3.44
400	-5.48	-3.65
500	-5.56	-3.70
700	-5.66	-3.77
1000	-5.74	-3.83

TABLE 1. The chemical potential μ of ^{4}He droplets and the binding energies of ^{3}He atoms in the Andreev ground state.

in the HNC-Euler-Lagrange theory, since it is determined from eq. (20). The sum of Hartree potential V_H and external potential U is the effective potential which this imaginary particle feels.

5.2. Ground state results

Here we give some results for the ground state energy and density of pure droplets and a ^{3}He impurity in droplets. For ground state results for ^{4}He films see chapter 7.

Ground state energy: Calculations for the ground state energy have appeared in the literature [**CK95a**], the results are in good agreement with DMC calculations. The N-dependence of the ground state energy per particle E_N/N can be fitted by powers of $N^{-1/3}$

$$\frac{E(N)}{N} = -\epsilon_\infty + \left(\frac{36\pi}{\rho_\infty^2}\right)^{1/3} \sigma N^{-1/3} + cN^{-2/3}\ K. \tag{32}$$

where ϵ_∞ is the binding energy of the bulk liquid, ρ_∞ the saturation density, and σ the surface energy. Using the HNC energies for particle numbers $40 \leq N \leq 1000$ leads to the results $\epsilon_\infty = 7.11 \pm 0.03$ and $\sigma = 0.273 \pm 0.006$. The asymptotic limit of $E(N)/N$ is reached only very slowly. The chemical potentials for ^{4}He and ^{3}He are listed in table 1 for several droplet sizes.

Ground state density: The ground state density of N ^{4}He atoms forming a self-bound droplet is of course spherically symmetric, $\rho_1(\mathbf{r}) = \rho_1(r)$. Fig. 2 shows $\rho_1(r)$ for several sizes, $N = 70\ldots1000$, which we used for the scattering calculations. A comparision with density profiles obtained with diffusion Monte Carlo is shown in Fig.3. In HNC-Euler-Lagrange theory, the density–oscillations are weaker than in the DMC calculations; however, these

where

$$\alpha - \lambda = -\sqrt{\frac{2m|\mu|}{\hbar^2}}\left(1 - 2\sqrt{1 - \frac{|E_B|}{2|\mu|}}\right)$$

Note that the exponential decay is slower than that of $\sqrt{\rho(z)} \to e^{-\alpha z}$.

oscillations are very sensitive to the calculational procedure, for example the approximative treatment of the elementary diagrams. Also, there are no directly observable properties connected with these oscillations.

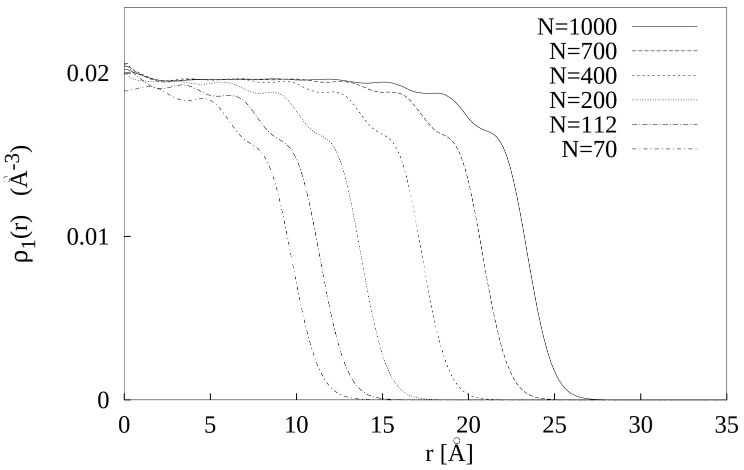

FIGURE 2. The ground state density $\rho_1(r)$ of N ^{4}He atoms forming a spherical droplet, where N ranges from 70 to 1000.

^{3}He chemical potential: The chemical potential, calculated in the above–mentioned Lekner approximation, is reasonably well fitted by the form

$$\mu_3(N) = -4.04 - 0.88N^{-1/3} + 35.93N^{-2/3} - 59.98N^{-1} \text{ K}$$

The asymptotic value of $\mu_3(\infty) = -4.04$ K is less than the -5.1 K found in calculations on adsorbed films [**CKS97**]; we attribute this discrepancy partly to the Lekner–approximation, and partly to the external holding potential of the adsorbed films. Furthermore, the fit is very sensitive on whether the N^{-1} term is included or neglected as in the μ_4-fit. Without it, $\mu_3(\infty) = -4.41$ K, but the fit is much worse.

Andreev state: Like ^{3}He at free ^{4}He surfaces, ^{3}He attached to a ^{4}He droplet has, due to its higher zero-point motion, the lowest energy on the surface (Andreev state [**And66**]). In Fig.4 the ground state density $\rho_1^I(r_0)$ is shown for several droplet sizes, and the binding energies $\mu_3(N)$ of the Andreev state are listed in table 1.

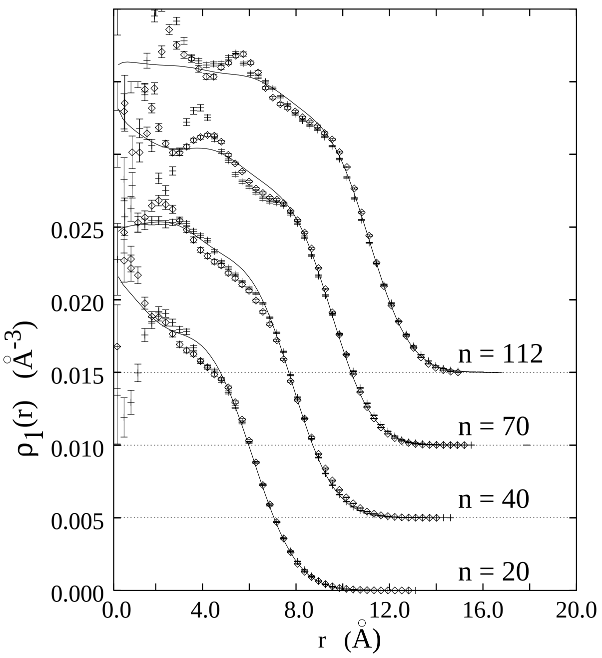

FIGURE 3. The ground state density profiles of ^{4}He droplets from the HNC–EL theory (solid lines) is compared with the DMC results of Ref. [**CK95a**] (asterisks and diamonds with error bars). The curves for higher particles numbers have been shifted upwards by 0.005 each to improve legibility.

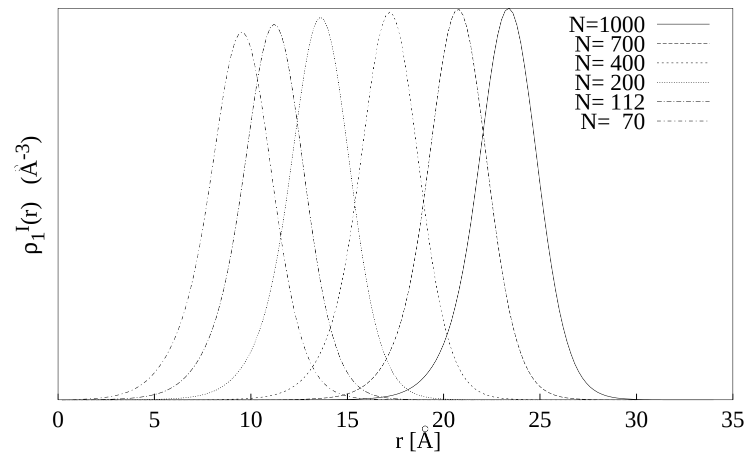

FIGURE 4. The probability distribution $r^2\rho_1^I(r)$ for ^{3}He adsorbed on droplets of N ^{4}He atoms.

CHAPTER 3

Excitations in HNC-Euler-Lagrange Theory

1. Introduction

In the previous chapter, we have reviewed briefly the optimization of the ground state Jastrow-Feenberg wave function Φ_0 up to 3-body correlations $u_n(1,\ldots,n)$. We have also discussed some results of its application to ^{4}He droplets and films. The reliability of the treatment of the many-body problem in the HNC-Euler-Lagrange theory for the ground state gives us confidence that the same method will work fine for calculating excited states. The *nonlinear* problem of fully optimizing $u_n(1,\ldots,n;t)$ is too demanding for excitations in inhomogeneous systems: not only has the whole iterative procedure for solving the HNC/EL equations to be carried out for each excitation independently, but, worse, the high spatial symmetry of the ground state wave function cannot be exploited anymore, which renders the HNC/EL equations intractable[1].

The excitation problem is simplified significantly if the correlations can be split into ground state and excitation contributions, $u_n + \delta u_n$, where the δu_n is assumed to be a *small* time-dependent fluctuation about the ground state correlation u_n:

$$\begin{aligned}\Phi(1,\ldots,N;t) &= \exp\left\{\sum_i [u(i)+\delta u(i;t)] + \sum_{i<j}[u(i,j)+\delta u(i,j;t)] + \ldots\right\} \\ &= \exp\left\{\sum_i \delta u(i;t) + \sum_{i<j}\delta u(i,j;t) + \ldots\right\}\Phi_0(1,\ldots,N) \qquad (33)\end{aligned}$$

If this assumption is valid, the HNC/EL equations can be *linearized* in terms of δu_n. Quantum mechanics in "first quantization" is classical mechanics of fields, i.e. the Schrödinger equation governs the dynamics of the fields $\Re e\ \Phi(t)$ and $\Im m\ \Phi(t)$. In the classical interpretation of $\Phi(t)$, the linearization corresponds to determining the normal modes of the the Hamiltonian around the equilibrium given by Φ_0, with the quantum mechanical eigenenergies given by the normal mode frequencies [**KK76**]. Therefore, linearization does not necessarily fail for high eigenenergies, as it would for classical motion. In fact, linearization works fine for the whole energy range which is of interest for low temperature physics, up to roton and maxon energies and beyond — provided that as little further approximations as possible are

[1]At best, for excitations the optimization with respect to the one-body correlation $u_1(1)$ is feasable, while higher correlations are kept in the ground state — and, of course, only bulk ^{4}He is considered. This could allow, for example, the full optimization treatment of ^{4}He with vortices, of phonon-vortex scattering, and generally of calculations far from equilibrium and involving large amplitude density fluctuations, see appendix C.

applied. Examples for successful application of this scheme include the calculation of the bulk ^{4}He excitation spectrum [**KS93b**], solidification of ^{4}He [**AHS99, Apa00**] and the dynamics of impurities in bulk ^{4}He [**KPM$^+$98**]. Unfortunately, for inhomogeneous systems further approximations are required as will be explained below. However, it should be pointed out that a well-optimized ground state Φ_0 is an essential prerequisite to meaningful solutions of the linearized Euler-Lagrange equations, as it is easily seen by the trivial example of a finite Hilbert space of 2 dimensions with parametrization (a, b) and a trial wave function $\Phi(c)$ of a single parameter c (instead of the Jastrow-Feenberg trial wave *functional* of correlations functions): near the exact ground state, the energy function $E(a, b)$ is a parabola, with the ground state energy $E_0 = E(a_0, b_0)$, see figure 1. $\Phi(c)$ spans a subspace that, in general,

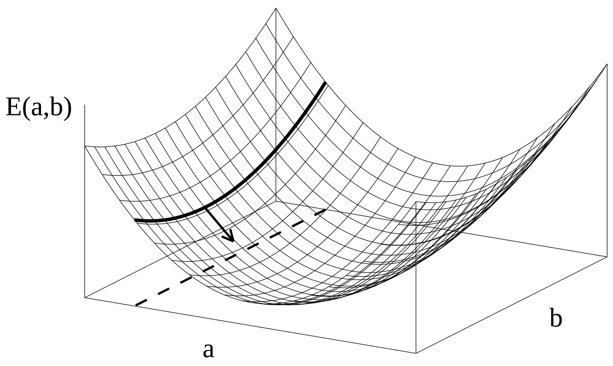

FIGURE 1. Energy of a 2-dimensional Hilbertspace parametrized by (a, b). The dashed line symbolizes a trial wave function subspace and the heavy line the trial wave energy.

will not contain the exact ground state; nevertheless, optimization of $E[\Phi(c)] \equiv E(c)$ results in a close guess for E_0 for the optimal $c = c_0$. Also, the excitation eigenenergies (only one in the example) obtained by normal mode expansion *in the $\Phi(c)$–subspace* are close to superpositions of normal mode energies of the true ground state (*i.e.* the curvature in figure 1). However, if we would try to calculate the normal mode frequency of $\Phi(c_0)$ outside the $\Phi(c)$–subspace, indicated by the arrow, the result would by meaningless, as the energy could be lowered below the approximate ground state energy $E(c_0)$. The same would happen, if c_0 were not the optimal value. In conclusion, two requirements have to be met to assure meaningful excitation obtained by normal mode expansion:

1. The same subspace as for the ground state optimization has to be used, or a subspace of it. In the HNC-Euler-Lagrange theory this is the subspace of Jastrow-Feenberg wave function with up to n–body correlations.
2. The ground state has to be optimized with sufficient accuracy. Apart from the obvious sources of deviations from the solutions of the ground state optimization equations, like discretization, other approximations could in principle hamper proceeding to excitation calculations, e.g. the Lekner approximation, the local density approximation for the

elementary diagrams, or the approximations used for correlations between more than two particles.

Another angle to look at the assumption of small amplitudes is given by Feynman in a well-known paper [**Fey54**] (where the Bijl-Feynman spectrum is derived) and in a successive paper with Cohen [**FC56**]. Both papers provide a useful starting point for literature on excitation calculations in helium, and the study of Feynman's discussion of the features of many-boson ground state and excited wave functions is recommended. Optimizing the energy with respect to (33) and then solving the linearized Euler-Lagrange equations is equivalent to starting out with the ansatz

$$\Phi(1,\ldots,N) \;=\; \left\{ \sum_i \delta u(i) + \sum_{i<j} \delta u(i,j) + \ldots \right\} \Phi_0(1,\ldots,N)$$

which amounts to keeping only the first order term of (33). For the following, the term "Feynman approximation" refers to the original ansatz for Φ, given in [**Fey54**], where only one-body correlations are allowed to fluctuate.

The "small amplitude" excitation resulting from expansion in the δu_i cannot be a vortex solution. This can be easily argued by looking at the one-body correlation: for a vortex line along the z-axis, $u(\mathbf{r})$ must have a contribution $\sim i\varphi$, where φ is the azimutal angle, i.e. far away from the vortex core, the wave function must have the form

$$\Phi(\mathbf{r}_1,\ldots,\mathbf{r}_N) \sim \prod_j e^{i\varphi_j} f(\mathbf{r}_1,\ldots,\mathbf{r}_N)\,. \tag{34}$$

While the rest of the correlations u_n appearing in f might be close enough to the ground state correlations such that the expansion about Φ_0 is justified, the contribution $e^{i\varphi}$, which gives rise to the rotational velocity field around the vortex, cannot be expanded about unity. Nonetheless, efficient vortex calculations can be carried out by using the methods introduced in this chapter and an ansatz similar to (34) by introducing an effective Hamiltonian to account for the kinetic energy of the vortex [**Saa95, SK95**].

One way of implementing the idea of small amplitude excitations is by applying linear response theory, i.e. expanding the wave function in terms of a weakly perturbing one-body potential about the ground state wave function [**Kro85b**]. As a side benefit, the method provides the density response operator $\hat{\chi}(\omega)$, and hence, by means of the fluctutation–dissipation theorem, the dynamic structure operator $\hat{S}(\omega)$. Furthermore, the linear response appoach yields yet another interpretation of the small amplitude approximation, see section 5.

2. Linear Response Theory

Linear response theory is extensively covered in the literature, e.g. in [**For75, NO88**]. Therefore, we restrict ourselves to introduce the quantities we need. We assume that the system of N particles initially is in the ground state Φ_0 of the (time-independent) Hamilitonian

(1). A small time-dependent field coupling to the density operator is added to H

$$
\begin{aligned}
H(\mathbf{r}_1,\ldots\mathbf{r}_N;t) &= H(\mathbf{r}_1,\ldots\mathbf{r}_N) + \sum_{i=1}^{N} U_{\mathrm{pert}}(\mathbf{r}_i;t) \\
&= H(\mathbf{r}_1,\ldots\mathbf{r}_N) + \int d^3r\ U_{\mathrm{pert}}(\mathbf{r};t)\ \hat{\rho}(\mathbf{r})
\end{aligned}
$$

where $\hat{\rho}(\mathbf{r})$ is the coordinate space representation of the density operator

$$
\hat{\rho}(\mathbf{r}) = \sum_{i=1}^{N} \delta(\mathbf{r}_i - \mathbf{r}) .
$$

Due the the time-dependence of the perturbed Hamiltonian and the resulting time-dependence of the perturbed wave function Φ, the Ritz variation principle (15) must be generalized. Solving the time-dependent Schrödinger equation is equivalent to the least action principle

$$
\delta \int_{t_1}^{t_2} dt\ \mathcal{L}(t) = 0 \qquad \text{where} \qquad \begin{aligned} \mathcal{L}(t) = i\hbar\langle\Phi(t)|\dot{\Phi}(t)\rangle - \langle\Phi(t)|H(t)|\Phi(t)\rangle \\ \langle\Phi(t)|\Phi(t)\rangle = 1 \end{aligned} \tag{35}
$$

as can be seen immediately by functional differentiation with respect to Φ^*. Apart from a total time derivative, $\mathcal{L}$ is the classical Lagrange density for the coupled fields $\Re e\,\Phi(t)$ and $\Im m\,\Phi(t)$ [**KK76**].

The perturbing potential induces fluctuations $\delta u_n(1,\ldots,n;t) \in \mathbb{C}$ of the correlations, hence we write the wave function

$$
|\Phi(t)\rangle = e^{-iE_0t/\hbar} \frac{e^{\delta U(t)/2}|\Phi_0\rangle}{\langle\Phi_0|e^{\Re e\ \delta U(t)}|\Phi_0\rangle^{1/2}} \equiv e^{-iE_0t/\hbar}|\Phi_0(t)\rangle \tag{36}
$$

with the fluctuation operator

$$
\delta U(1,\ldots,N;t) = \sum_i \delta u(i;t) + \sum_{i<j} \delta u(i,j;t) + \ldots . \tag{37}
$$

The energy scale is shifted by the kinematic factor $e^{-iE_0t/\hbar}$, which amounts to subtracting the ground state energy E_0. Φ_0 is the real, time-independent ground state, optimized up to n-body correlations. As explained already in the introduction, the fluctuation operator must not contain correlations of higher order than n. In this work, we allow for one- and two-body correlation fluctuations, therefore the requirement is met.

The normalization condition can be included in the Lagrange density. The first term with the time-derivative can be written (apart from the explicit time-derivative of the kinetic factor)

$$
\begin{aligned}
i\hbar \int d1 \dots dN \; & \frac{\Phi_0^*(t)}{\langle \Phi_0(t)|\Phi_0(t)\rangle^{1/2}} \frac{\partial}{\partial t} \frac{\Phi_0(t)}{\langle \Phi_0(t)|\Phi_0(t)\rangle^{1/2}} \\
&= \frac{i\hbar}{2} \int d1 \dots dN \; \frac{\Phi_0^*(t)\dot{\Phi}_0(t) - \dot{\Phi}_0^*(t)\Phi_0(t)}{\langle \Phi_0(t)|\Phi_0(t)\rangle} \\
&= -\hbar \int d1 \dots dN \; |\Phi_0|^2 \; e^{\Re e \; \delta U(t)} \; \Im m \; \delta \dot{U}(t) \\
&= -\frac{\hbar}{2} \int d1 \; \rho(1;t) \; \Im m \; \delta \dot{u}(1;t) - \frac{\hbar}{4} \int d1 d2 \; \rho(1,2;t) \; \Im m \; \delta \dot{u}(1,2;t)
\end{aligned}
$$

where $\rho_1(t)$ and $\rho_2(t)$ are the time-dependent number densities of the excited wave function (36), i.e. functionals of $\Re e \; \delta u_1(t)$ and $\Re e \; \delta u_2(t)$. For the expansion of the Lagrange density to second order in the fluctuations $\delta U(t)$, $\rho_1(t)$ and $\rho_2(t)$ need to be expanded only to first order in $\delta U(t)$.

In the second term, the expectation value of the Hamiltonian, the bare interaction potential can be eliminated by means of the identity for an arbitrary operator F and the (hermitean) Hamiltonian

$$
\langle \Psi | F^+ [H - E_0] F | \Psi \rangle \;=\; \frac{1}{2} \langle \Psi | [F^+, [H, F]] | \Psi \rangle + \langle \Psi | F^+ F [H - E_0] | \Psi \rangle
$$

where for the current purpose $F = e^{\delta U(t)/2}$. The second term on the right hand vanishes exactly only for the nondegenerate ground state, $\Psi = \Phi_0$, i.e. if, in the language of HNC, all correlations up to u_N are optimized. Yet this term is of order $\mathrm{o}(\delta U^{n/2k})$, if δU contains fluctuations of up to δu_k, and the ground state is optimized up to u_n (assuming n to be even). This can be shown by the *dynamical consistency condition* [**Fee69**], which states that optimization of n-body correlations of the ground state is equivalent to the identity

$$
\int d(n+1) \dots dN \; \Phi_0(1 \dots N)[H - E_0]\Phi_0(1 \dots N) = 0 \, .
$$

For the linearized Euler-Lagrange equations, $\mathcal{L}$ has to be expanded to second order – the first order vanishes due to the optimization of the ground state –, which implies, for $k = 2$, that $n = 4$. Unfortunately, it is unfeasable to account for 4-body correlations, and we have to violate requirement 1 stated in the introduction, in order to rid the Euler-Lagrange equations of the bare interaction V.[2] The Hamiltonian term of the Lagrange density (35) becomes

$$
\begin{aligned}
\langle \Phi_0(t) | H - E_0 | \Phi_0(t) \rangle \;&=\; \frac{1}{2} \langle \Phi_0 | [e^{\delta U^*(t)/2}, [H, e^{\delta U(t)/2}]] | \Phi_0 \rangle + \mathrm{O}(\delta U^3) \\
&=\; \frac{1}{8} \langle \Phi_0 | [\delta U^*(t), [\hat{T}, \delta U(t)]] | \Phi_0 \rangle + \mathrm{O}(\delta U^3) \\
&=\; \frac{\hbar^2}{8m} \sum_i \langle \Phi_0 | \; |\nabla_i \delta U(t)|^2 \; | \Phi_0 \rangle + \mathrm{O}(\delta U^3)
\end{aligned}
$$

[2] One should probably not be too concerned about the neglect of 4-body correlations, because already the 3-body correlations cannot be optimized rigorously due to the approximate form of the 3-body number density $\rho_3(1,2,3)$, and hence requirement 2 is not necessarily fullfilled.

where $\delta U(t)$ is given by eq. (37). With the second-order Lagrangian now derived, Euler-Lagrange equations (35) become linear in the fluctuations and henceforth, we call them *equations of motions.* In the following section, we write down and discuss these equations.

3. Equations of motion for pure ^{4}He

The derivation of the equations of motions for the time dependent correlations in inhomogeneous ^{4}He can be found in detail in [**Tym95, CK95a**] and in the appendix of [**CKT96**]. They can be cast into the form of continuity equations:

$$\begin{aligned} \nabla_1 \cdot \mathbf{j}(1;t) + \delta\dot{\rho}(1;t) &= \frac{2}{i\hbar}\sqrt{\rho(1)}[S * \tilde{U}_{\rm pert}](1) && (38)\\ \nabla_1 \cdot \mathbf{j}(1;2;t) + \nabla_2 \cdot \mathbf{j}(2;1;t) + \delta\dot{\rho}(1,2;t) &= \frac{2}{i\hbar}\rho(1,2)[U_{\rm pert}(1) + U_{\rm pert}(2)] && (39)\\ &\quad + \frac{2}{i\hbar}\int d3\ [\rho(1,2,3) - \rho(1,2)\rho(3)]\ U_{\rm pert}(3) \end{aligned}$$

where

$$\begin{aligned} \mathbf{j}(1;t) &= \frac{\hbar}{2m_4 i}\left[\rho(1)\nabla_1\delta u(1;t) + \int d3\ \rho(1,3)\nabla_1\delta u(1,3;t)\right] && (40)\\ \mathbf{j}(1;2;t) &= \frac{\hbar}{2m_4 i}\Big[\rho(1,2)\nabla_1\delta u(1;t) + \rho(1,2)\nabla_1\delta u(1,2;t) && (41)\\ &\quad + \int d3\ \rho(1,2,3)\nabla_1\delta u(1,3;t)\Big]\,. \end{aligned}$$

$\mathbf{j}(1;t)$ and $\mathbf{j}(1,2;t)$ are called transition currents. Their real parts can be obtained by expanding the expectation value of the current operator and the current-density correlation operator to leading, *i.e.* first order in $\delta U(t)$

$$\begin{aligned} \langle\Phi(t)|\hat{\mathbf{j}}(\mathbf{r}_1)|\Phi(t)\rangle &= \Re e\ \mathbf{j}(1;t) + \mathrm{O}(\delta U^2)\\ \langle\Phi(t)|\hat{\mathbf{j}}(\mathbf{r}_1)\hat{\rho}(\mathbf{r}_1)|\Phi(t)\rangle_c &= \Re e\ \mathbf{j}(1;2;t) + \mathrm{O}(\delta U^2) \end{aligned}$$

where the subscript c in $\langle\ldots\rangle_c$ indicates that the auto-correlation term has been substracted.

The density fluctuations $\delta\rho(1;t)$ and $\delta\rho(1,2;t)$ are called transition densities. They are defined as the differences $\delta\rho(1;t) = \bar{\rho}(1;t) - \rho(1)$ and $\delta\rho(1,2;t) = \bar{\rho}(1,2;t) - \rho(1,2)$, where $\bar{\rho}(1;t)$ and $\bar{\rho}(1,2;t)$ are the complex first terms in the respective expansion in the correlation fluctuations, with $\Re e\,\delta u_n$ replaced by δu_n. In other words, the real part of $\delta\rho(1;t)$ and $\delta\rho(1,2;t)$ are the first order terms of the expectation values of the density operator and the static correlation operator

$$\begin{aligned} \langle\Phi(t)|\hat{\rho}(\mathbf{r}_1)|\Phi(t)\rangle &= \Re e\ \delta\rho(1;t) + \mathrm{O}(\delta U^2)\\ \langle\Phi(t)|\hat{\rho}(\mathbf{r}_1)\hat{\rho}(\mathbf{r}_2)|\Phi(t)\rangle_c &= \Re e\ \delta\rho(1,2;t) + \mathrm{O}(\delta U^2)\,. \end{aligned}$$

For $\delta\rho(1;t)$ and $\delta\rho(1,2;t)$ we find

$$\begin{aligned}
\delta\rho(1;t) &= \sqrt{\rho(1)}[S * \delta\tilde{u}(t)](1) + \int d2\ \rho(1,2)\delta u(1,2;t) \\
&\quad + \frac{1}{2}\int d23\ [\rho(1,2,3) - \rho(1)\rho(2,3)]\delta u(2,3;t) \\
\delta\rho(1,2;t) &= [\delta\rho(1;t)\rho(2) + \rho(1)\delta\rho(2;t)]\ g(1,2) + \rho(1)\rho(2)\delta g(1,2;t) \\
\delta g(1,2;t) &= \int d3\ Y(1,2;3)\delta\rho(3;t) + [S * \delta\tilde{X}(t) * S](1,2)
\end{aligned}$$

where Y can be derived from the diagrammatic expansion of $g-1$,

$$\begin{aligned}
\frac{\delta g(1,2)}{\delta\rho(3)} \equiv Y(1,2;3) &= h(1,3)h(2,3) \\
&+ \int d45\ [\delta(1,4) + \rho(4)h(1,4)][\delta(2,5) + \rho(5)h(2,5)]X(3,4,5)
\end{aligned} \tag{42}$$

and $\delta X(1,2;t)$ can be related to $\delta u(1,2;t)$ by linearizing the HNC equations [**Tym95**].

Before we write down an approximate equation for $\delta\rho(1;t)$, obtained by elimination of δu_2 in the pair of equations, we introduce the Feynman approximation mentioned above.

3.1. Feynman approximation

The Feynman ansatz [**Fey54**], generalized to inhomogeneous systems [**CC75**], is recovered by allowing only for one-body fluctuations $\delta u_1(\mathbf{r};t)$. It yields the inhomogeneous version of the Bijl-Feynman excitation spectrum of non-interacting phonons, rotons etc. and, for example, misses the experimental energy gap of the roton in bulk by about a factor of two. At higher momenta, it fails to reproduce qualitativly the features of the dynamic response function, which stem from the coupling between two rotons. Interactions between elementary Feynman modes are mediated by fluctuations in the two-body correlations. Feynman modes provide a useful single-phonon basis for the equations of motion for δu_2.

If U_{pert} is set to zero (see section "Linear response" for more on this), the equation of motion (38) for δu_1 reduces to the generalized eigenvalue equation

$$H_1(1)\delta\tilde{u}(1;t) = i\hbar[S * \delta\dot{\tilde{u}}(t)](1) \qquad \Longrightarrow \qquad H_1(1)\psi_n(1) = \hbar\omega_n[S * \psi_n](1) \tag{43}$$

where we have turned to the stationary equation, with the solution $\delta\tilde{u}(1;t) = \psi_n(1)e^{-i\omega_n t}$. The stationary solutions ψ_n are called Feynman states, each characterized by a triplet of quantum numbers, n. They form a complete basis together with their adjoint states[3]

$$\begin{aligned}
\phi_n(1) := \frac{1}{\hbar\omega_n}H_1(1)\psi_n(1) \quad : \quad & \int d1\ \phi_n^*(1)\psi_m(1) = \delta_{n,m} \\
& \sum_n \phi_n(1)\,\psi_n^*(2) = \sum_n \psi_n(1)\,\phi_n^*(2) = \delta(1,2)
\end{aligned} \tag{44}$$

and the static structure function can be expressed in terms of the Feynman states,

$$S(1,2) = \sum_n \phi_n(1)\,\phi_n^*(2)\,.$$

[3]The ψ_n are not orthogonal, since (43) is not a self-adjoint equation.

In a homogeneous system, eq. (43) can be easily solved in momentum space, because ρ = const and $S(\mathbf{r}_1, \mathbf{r}_2) = S(\mathbf{r}_1 - \mathbf{r}_2)$. Then (43) reduces to the Bijl-Feynman dispersion relation

$$\hbar\omega_F(k) = \frac{\hbar^2 k^2}{2mS(k)}$$

and the Feynman states are simply plane waves. $\hbar\omega_F(k)$ is show in figure 2 for saturation

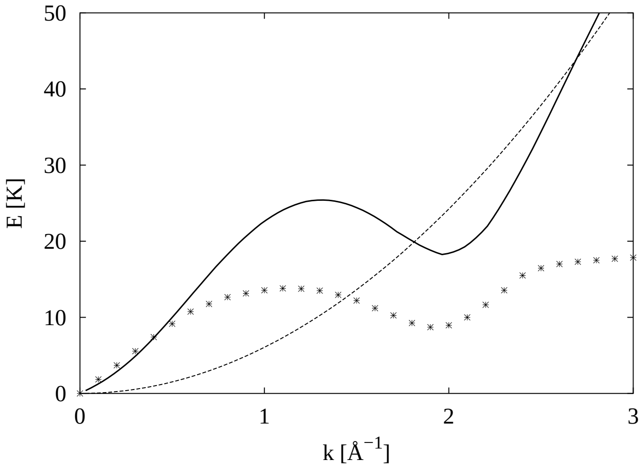

FIGURE 2. Feynman excitation spectrum of bulk ^{4}He at saturation density $\rho = 0.0218\text{Å}^{-3}$ (full line) as well as a fit to the experimentally determined dispersion [**CW71**] and, for comparision, the dispersion of free ^{4}He atoms (dashed line).

density. Except for low momenta (phonons), the excitation energy predicted by Feynman is higher than the dispersion determined by experiment [**DDH81**] by a factor of two in the maxon-roton regime, and fails completely to describe the levelling off at large momenta which is caused by the coupling between two rotons. Instead, since $S(k) \to 1$ for $k \to \infty$, $\hbar\omega_F(k)$ attains the free dispersion.

For films, we assume translational invariance parallel to the film which lies in the xy-plane and which is held by a substrate potential depending only on z. The atomically flat substrate potential is an idealization which cannot account for commensurate structures of the adsorbate at low coverage, but the effect of surface corrugation on the scattering off several layers of adsorbed ^{4}He (such as *Umklapp* processes) can be neglected. Droplets in the ground state exhibit rotational symmetry. For both, films and droplets, the respective symmetry of the density $\rho(\mathbf{r}_1)$ and the static structure operator $S(\mathbf{r}_1, \mathbf{r}_2)$ allow to separate (43) into an easily solvable 1-dimensional integro-differential equation and the operator generating the symmetry group. We summarize for later reference:

Films: have planar symmetry. Feynman states are characterized by the quantum numbers $(n, \mathbf{q})$, where n can be discrete and continuous (bound and scattering states), and

$\mathbf{q} = (q_x, q_y)$ is the momentum parallel to the film.

$$\begin{aligned}
\rho(\mathbf{r}_1) &= \rho(z_1) \\
S(\mathbf{r}_1, \mathbf{r}_2) &= \int \frac{d^2q}{(2\pi)^2}\, e^{-i\mathbf{q}\cdot(\mathbf{r}_1-\mathbf{r}_2)} S_q(z_1, z_2) \\
H_q(z) &= -\frac{\hbar^2}{2m_4}\frac{1}{\sqrt{\rho(z)}}\frac{\partial}{\partial z}\rho(z)\frac{\partial}{\partial z}\frac{1}{\sqrt{\rho(z)}} + \frac{\hbar^2 q^2}{2m_4} \\
\psi_n(\mathbf{r}_1) &= \psi_{n,q}(z_1) e^{i\mathbf{q}\cdot\mathbf{r}}
\end{aligned}$$

Droplets: have spherical symmetry. Feynman states are characterized by the quantum numbers (n, ℓ, m), where n can be discrete and continuous (bound and scattering states), and ℓ and m specify the angular momentum eigenstate.

$$\begin{aligned}
\rho(\mathbf{r}_1) &= \rho(r_1) \qquad (45) \\
S(\mathbf{r}_1, \mathbf{r}_2) &= \sum_{\ell,m} Y^*_{\ell,m}(\Omega_1) Y_{\ell,m}(\Omega_2) S_\ell(r_1, r_2) \\
H_\ell(r) &= -\frac{\hbar^2}{2m_4}\frac{1}{r}\frac{1}{\sqrt{\rho(r)}}\frac{\partial}{\partial r}\rho(r)\frac{\partial}{\partial r}\frac{r}{\sqrt{\rho(r)}} + \frac{\hbar^2}{2m_4}\frac{\ell(\ell+1)}{r^2} \\
\psi_n(\mathbf{r}_1) &= \psi_{n,\ell}(r_1) Y_{\ell,m}(\Omega_1)
\end{aligned}$$

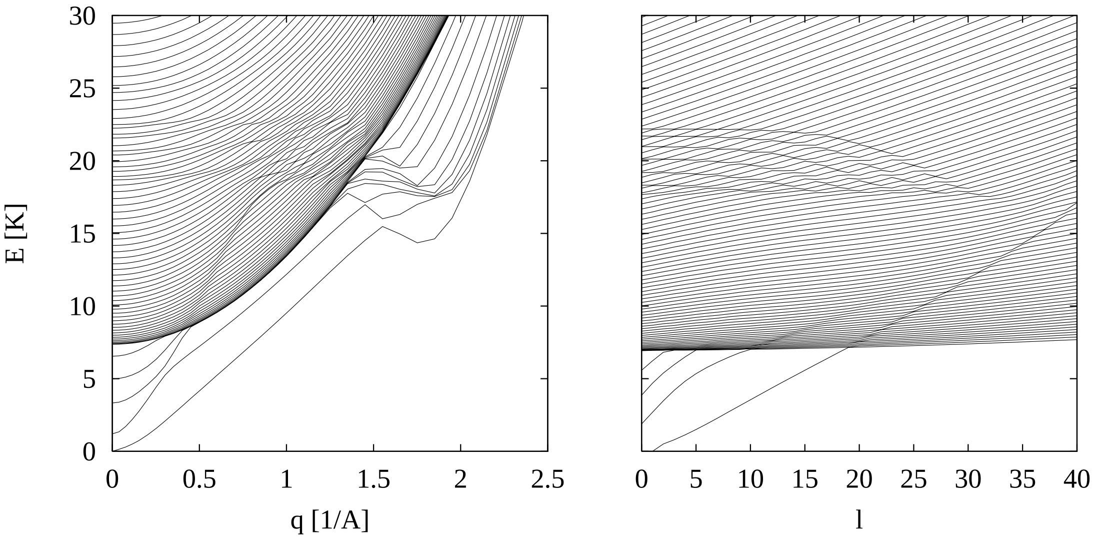

FIGURE 3. Feynman excitation spectrum: (i) $\hbar\omega_n(q)$ as a function of q in graphite-adsorbed film of thickness $n = 0.45\text{Å}^{-2}$ (left); (ii) $\hbar\omega_n(\ell)$ as a function of ℓ in a droplet $^4\text{He}_{1000}$ (right; lines are drawn through the discrete points for better recognition of ripplon and roton).

In figure 3, we show the Feynman dispersion in a ^{4}He film, $\hbar\omega_n(q)$, as a function of q, and in a ^{4}He droplet of 1000 atoms, $\hbar\omega_n(\ell)$, as a function of ℓ. The discreteness of the continuum spectrum, $\hbar\omega_n(q) > |\mu_4| + \frac{\hbar^2 q^2}{2m_4}$ for films, and $\hbar\omega_n(\ell) > |\mu_4|$ for droplets, is a consequence of the finite simulation box size. The inverse of the energy gap between these discretized unbound modes corresponds approximately to the density of states. The lowest excitations of droplets can be identified as free surface ripplons. This is shown in figure 4, where $\omega_{0,\ell}$ is plotted as a function of an effective surface wave number $k = \sqrt{\ell(\ell+1)}/R$ where $R = \sqrt{5/3}r_{\rm rms}$ and $r_{\rm rms}$ is the "root mean square" radius $r_{\rm rms} = \sqrt{\langle r^2 \rangle}$. Obviously, excitation energies of larger droplets lie close to the ripplon dispersion

$$\hbar\omega(k) = \hbar\sqrt{\frac{\sigma}{m\rho_\infty}}k^{3/2}$$

where σ is the surface energy. Going beyond the Feynman approximation (see below) does not alter these surface excitation energies quantitatively.

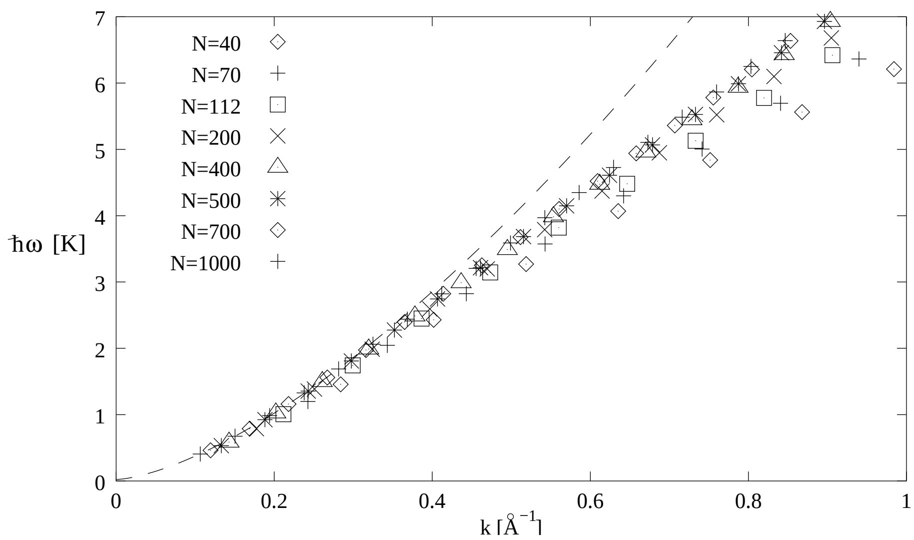

FIGURE 4. Surface Feynman excitation spectrum of droplets $^4\mathrm{He}_N$, $N = 40,\dots,1000$, as a function of the effective surface wave number k, see text. The line is a fit of $a + bk^{3/2}$ to the dispersion of $N = 1000$, for $k < 0.3\text{Å}^{-1}$, yielding a surface energy $\sigma = 0.23$ KÅ^{-2}. This value is still much less than $\sigma(N=\infty)$ extrapolated from the ground state energy dependence on N.

3.2. CBF-BW approximation

In the coupled equations for δu_1 (or $\delta\rho_1$) and δu_2, the latter can be eliminated. The one-body equation can then be brought into a form reminiscent of the second-order Brillouin-Wigner perturbation in terms of Feynman states, i.e. correlated basis function theory (hence the section title, CBF-BW) [**Fee69**].

The pair distribution g is approximated by its uniform limit of a weakly interacting system, as explained in [**Fee69**]. In a nutshell, the *uniform limit approximation* implies the following:

For a weakly interacting system[4] $g(\mathbf{r},\mathbf{r}')$ is close to unity, yet the cluster property (246) has still to be fulfulled, i.e. in words, the correlation hole excludes exactly one particle, $\rho\int d^3r\ [g(r)-1]=-1$. Therefore, while $g(\mathbf{r},\mathbf{r}')-1\approx 0$ in configuration space, g must not be simply set to unity, when it appears in an *integral.* A formal expansion for $g\equiv 1-\alpha G$ can be obtained by the transformation to scaled coordinates $\mathbf{s}=\alpha^{1/3}\mathbf{r}$. The two-body equation of motion is expanded to first order in α.

For the purpose of finding an approximate solution of the equations of motion, the usefulness of the uniform limit approximation lies in its application to a cumulant expansion of ρ_3 in terms of g, as well as in simplifying the HNC equations for $\delta\tilde{X}$ and δu_2. Hence, one finds

$$\begin{aligned} \delta g(1,2;t) &\approx \int d3\ Y(1,2;3)\delta\rho(3;t)+[S*\delta\tilde{u}_2(t)*S](1,2) \\ g(1,2,3)-g(1,2)g(1,3) &\approx g(2,3) \\ \delta\tilde{X}(1,2;t) &= \delta\tilde{u}(1,2;t)\,. \end{aligned} \tag{46}$$

The equations of motion in the uniform limit have a compact form if expanded in the basis of Feynman states:

$$r_n(t) = \int d1\ \psi_n^*(1)\ \frac{\delta\rho(1;t)}{\sqrt{\rho(1)}} \tag{47}$$

$$\delta\tilde{X}_{nm}(t) = \int d1d2\ \phi_n^*(1)\phi_m^*(2)\ \delta\tilde{X}(1,2;t) \tag{48}$$

are the solutions of a 1-body equation and a 2-body equation from which the perturbing 1-body potential can be eliminated (t-dependence omitted from now on for clarity)

$$\begin{aligned} \hbar(\omega_s-i\frac{\partial}{\partial t})r_s\ -\ \frac{1}{2}\sum_{mn}W^s_{mn}\delta\tilde{X}_{nm} &= 2\int d1\ \phi_s^*(1)\ \tilde{U}_{\rm pert}(1) \\ \hbar(\omega_n+\omega_m-i\frac{\partial}{\partial t})\delta\tilde{X}_{nm}\ +\ \sum_{st}T^{mn,st}\delta\tilde{X}_{st}\ -\ \sum_s W^s_{mn}r_s &= 0 \end{aligned} \tag{49}$$

[4]Helium is definitely *not* a weakly interacting system, but remember that the bare interaction has been eliminated from the equations of motion for one- and two-body fluctuations. The assumption of weak interaction between *fluctuations*, not atoms, arguably makes sense for not to high energies. Nonetheless, we agree that g is far from uniform, and only the cross-check with other theories and with experiment can render this approximation valid or obsolete.

where

$$
\begin{aligned}
W^s_{mn} &= \frac{\hbar^2}{2m_4}\int d1\ \frac{\psi_s(1)}{\sqrt{\rho(1)}}\nabla\cdot[\sqrt{\rho(1)}\tilde{\mathbf{W}}^{mn}(1)] \qquad (50)\\
T^{mn,st} &= \frac{\hbar^2}{4m_4}\int d1\ \tilde{\mathbf{W}}^{mn}(1)\cdot\tilde{\mathbf{W}}^{st}(1)\\
\tilde{\mathbf{W}}^{mn}(1) &= {}_a\tilde{\mathbf{W}}^{mn}(1) + {}_b\tilde{\mathbf{W}}^{mn}(1)\\
{}_a\tilde{\mathbf{W}}^{mn}(1) &= \frac{1}{\sqrt{\rho(1)}}\Big[\phi_m(1)\sqrt{\rho(1)}\nabla\frac{1}{\sqrt{\rho(1)}}[\tilde{X}*\phi_n](1)\ +\ (m\leftrightarrow n)\Big]\\
{}_b\tilde{\mathbf{W}}^{mn}(1) &= \sqrt{\rho(1)}\nabla\frac{1}{\sqrt{\rho(1)}}\int d23\ \phi_m(2)\phi_n(3)\ \tilde{X}(1,2,3)\,.
\end{aligned}
$$

In frequency space, $\delta\tilde{X}_{nm}$ can be eliminated by inversion of the operator $\hbar(\omega_n+\omega_m-\omega)\delta_{m,s}\delta_{n,t}+T^{mn,st}$. As this is computationally still unfeasable (remember that m, n, etc. are triplets of quantum numbers), we employ yet another approximation: only the diagonal of $T^{mn,st}$ is kept in the calculations, thus rendering the inversion trivial[5]. For each frequency component of the perturbing potential, $\tilde{U}_{\rm pert}(\omega)$, r_s is obtained from

$$
\hbar(\omega_s-\omega)r_s\ -\ \sum_t\Sigma_{st}(\omega)\ r_t\ =\ 2\int d1\ \phi^*_s(1)\ \tilde{U}_{\rm pert}(1;\omega)\equiv U^s_{\rm pert}(\omega) \qquad (51)
$$

with the *self energy operator*, here in Feynman basis representation,

$$
\Sigma_{st}(\omega)\ =\ \frac{1}{2}\sum_{mn}\frac{W^s_{mn}W^{t*}_{mn}}{\hbar(\omega_m+\omega_n-\omega)} \qquad (52)
$$

Transforming (51) back to configuration space, the equation for $\varphi(1)=[S^{-1}*\frac{\delta\rho}{\sqrt{\rho}}](1)$ reads

$$
H_1(1)\varphi(1)\ -\ \hbar\omega\ [S*\varphi](1)\ -\ [\Sigma(\omega)*\varphi](1)\ =\ 2[S*\tilde{U}_{\rm pert}](1) \qquad (53)
$$

with $\Sigma(1,2;\omega)=\sum_{st}\phi_s(1)\Sigma_{st}(\omega)\phi_t(2)$. Of course, if Σ is set to zero (as well as $U_{\rm pert}$), the Feynman equation (43) is recovered.

The self energy can be expressed in terms of the Green's function G^0 of the Feynman equation

$$
G^0(1,2;\omega)=(H_1(1)-\hbar\omega)^{-1}\ ,\qquad G^0_{st}(\omega)=\int d1d2\ \psi_s(1)G^0(1,2;\omega)\psi_t(2)=\frac{\delta_{st}}{\hbar(\omega-\omega_s)}
$$

The purpose of Green's functions is illuminated in the next section, and single particle Green's functions are discussed in more detail in the appendix B, since we will need them for the calculation of scattering cross sections. Obviously, Σ can be written as

$$
\Sigma_{st}(\omega)\ =\ \frac{1}{2}\sum_{mm'n}W^s_{mn}\,G^0_{mm'}(\omega-\omega_n)\,W^t_{m'n}
$$

The appearence of the Green's function in Feynman approximation or of the Feynman excitation energies in the energy denominator of (52), respectively, means that an excitation of

[5]This is equivalent to employing the Feynman approximation for the one-body current (40) in the two-body equation of motion, after elimination of $\delta\tilde{u}_1$. *I.e.* $\mathbf{j}(1;t)$ is considered only a functional of $\delta\rho(1;t)$, but not of $\delta\tilde{X}(1,2;t)$.

energy $\hbar\omega$ splits into two Feynman modes, whose energy is known to be too high by about a factor of 2. Yet, replacing G^0 by G or the Feynman dispersion by a more realistic disperision would be only a phenomenological treatment, and we refrain from doing this before having gained deeper understanding of the self energy expression obtained in HNC-Euler-Lagrange theory.

4. Density response

Inversion of equation (51) yields the solution to the problem of finding the change of density $\delta\rho(\mathbf{r};t)$ responding to a small perturbing one-body potential $U_{\rm pert}(\mathbf{r};t)$

$$r_s = \sum_t G_{st}(\omega) U^t_{\rm pert}(\omega) \qquad \text{with} \quad G_{st}(\omega) = \left[\hbar(\omega_s - \omega - i\varepsilon)\delta_{s,t} - \Sigma_{st}(\omega)\right]^{-1}.$$

A harmonic time-dependence $U_{\rm pert}(\mathbf{r};t)$,

$$U_{\rm pert}(1;t) = \bar{U}_{\rm pert}(1)\cos(\omega t)\ , \qquad U_{\rm pert}(1;\omega') = \bar{U}_{\rm pert}(1)\ [\delta(\omega'-\omega) + \delta(\omega'+\omega)]$$

defines the dynamic density response operator $\chi(\omega)$ for frequency ω; $\chi(\omega)$ determines $\delta\rho(1;\omega)$ to first order in $\bar{U}_{\rm pert}(1)$,

$$\delta\rho(1;\omega) = [\chi(\omega) * \bar{U}_{\rm pert}](1)$$

and is given by [**CKT96**]

$$\begin{aligned}
\chi_{st}(\omega) &= G_{st}(\omega) + G_{st}(-\omega) \\
\chi(1,2;\omega) &= \sum_{st} \sqrt{\rho(1)}\phi_s(1)\ [G_{st}(\omega) + G_{st}(-\omega)]\ \phi_t(2)\sqrt{\rho(2)}\,.
\end{aligned}$$

The dynamic structure operator $S(1,2;\omega)$ is related to $\chi(1,2;\omega)$ by the fluctuation-dissipation theorem [**PN66a, For75**]

$$S(1,2;\omega) \ = \ -\frac{1}{\pi}\Im m\ \chi(1,2;\omega)$$

$S(\omega)$ serves two purposes:

1. the exact expressions for $S(\omega)$ satisfies sum rules against which approximate expressions can by checked. In fact, the CBF-BW approximation satisfies the ω^0 ane ω^1 sum rules [**CKT96**]

$$\int_0^\infty d\omega\ S(1,2;\omega) \ = \ S(1,2) \qquad \text{and} \qquad \int_0^\infty d\omega\ \omega\ S(1,2;\omega) \ = \ \delta(1,2)H_1(1)$$

2. The projection of $S(1,2;\omega)$ on plane waves is proportional to the inelastic neutron scattering cross section for momentum transfer $\mathbf{k}$ and energy transfer $\hbar\omega$

$$S(\mathbf{k},\omega) \ = \ \sum_f |\langle\Phi_f|\hat{\rho}_\mathbf{k}|\Phi_0\rangle|^2\delta(\omega-\omega_f) \ = \ \int d^3r_1 d^3r_2\ e^{i\mathbf{k}(\mathbf{r}_1-\mathbf{r}_2)}S(\mathbf{r}_1,\mathbf{r}_2;\omega)$$

where $\hat{\rho}_\mathbf{k}$ is the Fourier transform of the density operator and the summation is carried out over all excitations Φ_f of the system. In figure 5, $S(k,\omega)$ of bulk ^{4}H and of a ^{4}He$_{1000}$ droplet are shown as it is obtained in the CBF-BW approximation. In bulk, $S(k,\omega)$ has strength when ω equals an excited energy $\omega(k)$ of the phonon-roton spectrum, which are the plane wave–modes of the system and therefore respond most strongly to a plane wave perturbation induced by a neutron; the next section discusses the connection between linear response and excitations. In droplets, k is no longer a good quantum number, nevertheless $N = 1000$ atoms apparently constitute a large enough droplet to observe phonons and rotons of finite size, yet already of well-defined momentum. Also visible is the dispersion of the surface modes, the "ripplons". Both, the phonon-roton spectrum and the ripplon spectrum are broadened in k-direction due to the finite size of the droplet.

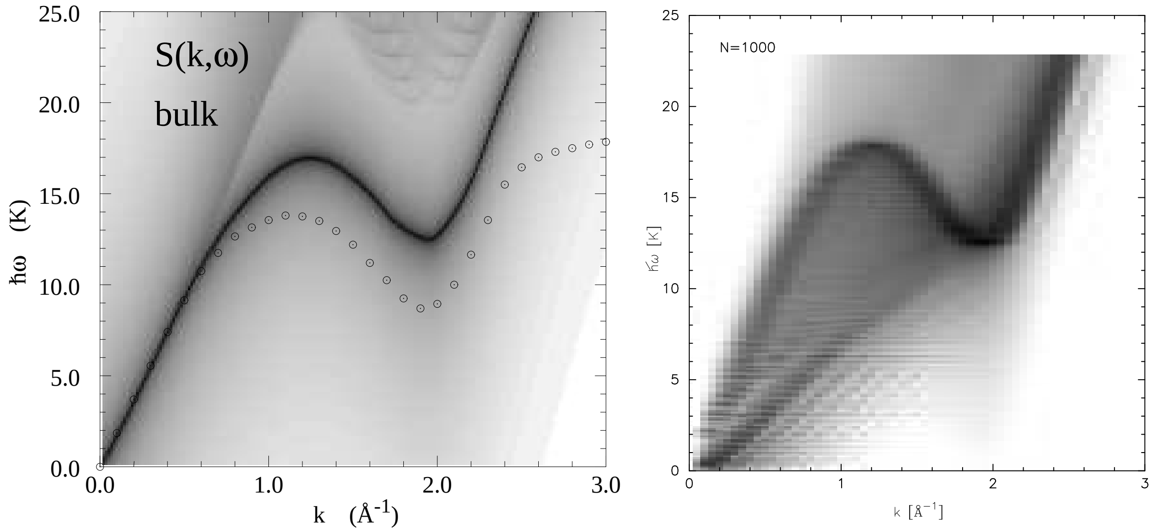

FIGURE 5. The logarithm of the dynamic structure function $S(k, \omega)$ of bulk ^{4}He (left) and of a droplet $^4\mathrm{He}_{1000}$ (right). The circles represent the experimental phonon-roton spectrum in bulk ^{4}He.

5. Discussion of excitations

In this work, the primary application of the equations of motion is not to get the linear response or the dynamic structure function, but the calculation of wave functions of excited states and associated quantities such as scattering cross sections. The purpose of this section is firstly to make plausible that setting $U_{\rm pert} = 0$, equations (38) and (39) describe excited states, and secondly to explain the power and the short-comings of the excitations thus obtained.

The connection between linear response and excitations is quite obvious: the perturbed wave function $\Phi(t)$ can be expanded in the full basis of eigenstates Φ_n

$$\begin{aligned}\Phi(t) &= e^{-iE_0t}e^{\delta U(t)/2}\Phi_0 = e^{-iE_0t}\Phi_0 + \frac{1}{2}e^{-iE_0t}\delta U(t)\Phi_0 + \mathrm{O}(\delta U^2(t)) \\ &= \Phi_0 e^{-iE_0t} + e^{-iE_0t}\sum_{n\neq 0} a_n\Phi_n e^{-i(E_n-E_0)t}\end{aligned}$$

where normalization was disregarded. Hence, we find $\delta U(t)\Phi_0 \propto \sum_n a_n \Phi_n e^{-i(E_n-E_0)t} + \mathrm{O}(\delta U^2(t))$. By setting $U_{\text{pert}} = 0$, the expansion coefficients a_n can be chosen arbitrarily. Specifically for $a_m = \delta_{m,n}$,

$$e^{-i(E_n-E_0)t}|\Phi_n\rangle = \frac{\delta U(t)|\Phi_0\rangle}{\langle\Phi_0|\,|\delta U(t)|^2\,|\Phi_0\rangle^{1/2}} + \mathrm{O}(\delta U^2(t))$$

with a harmonic time-dependence of the correlation fluctuation, $\delta U(t) \equiv e^{-i(E_n-E_0)t}\delta U_n$. Thus all excitations which the perturbation U_{pert} (that is the density operator $\hat\rho(\mathbf{r})$) couples to can be determined, i.e. those excitations Φ_n for which $a_n \neq 0$. In other words, excitations, for which the transition probability $|\langle\Phi_n|\hat\rho(\mathbf{r})|\Phi_0\rangle|^2$ is finite. This can be seen also from the expansion of the density response operator χ in terms of Φ_n [**NO88**]

$$\begin{aligned}
\chi(\mathbf{r}_1,\mathbf{r}_2;\omega) &= \sum_n \left[\frac{\langle\Phi_0|\hat\rho(\mathbf{r}_1)|\Phi_n\rangle\langle\Phi_n|\hat\rho(\mathbf{r}_2)|\Phi_0\rangle}{\hbar\omega-(E_n-E_0)+i\varepsilon} + \frac{\langle\Phi_0|\hat\rho(\mathbf{r}_2)|\Phi_n\rangle\langle\Phi_n|\hat\rho(\mathbf{r}_1)|\Phi_0\rangle}{-\hbar\omega-(E_n-E_0)-i\varepsilon}\right] \\
\chi(\mathbf{q};\omega) &= \sum_n |\langle\Phi_0|\hat\rho_{\mathbf{q}}|\Phi_n\rangle|^2 \frac{2(E_n-E_0)}{(\hbar\omega+i\varepsilon)^2-(E_n-E_0)^2}
\end{aligned}$$

where $\chi(\mathbf{q};\omega)$ is the projection onto $e^{i\mathbf{q}(\mathbf{r}_1-\mathbf{r}_2)}$, needed for the calculation of $S(\mathbf{q},\omega)$. $\chi(\omega)$ has poles at $E_n/\hbar$ which are the exact eigenfrequencies of the system, if χ is the exact density response function.

Exactness is guarateed if δU contains all correlations up to $\delta u_N(1,\ldots,N)$. However, taking into account only 2-body correlation fluctuations means that the excitation described by $\delta U\Phi_0$ are "close" to the ground state in a sense which is explained in the next paragraph. Ruled out are for example: (i) a foreign atom inside ^{4}He is removed in an instant, or excited to a higher electronic state, causing the neighbouring ^{4}He atoms to rearrange [**SMH$^+$99**] — or other processes which involve large changes in the density; (ii) an example where few-body correlation fluctuations fail and which was already mentioned in the introductory section is a vortex for which the simplest ansatz already involves N-body correlations: for a straight vortex along the z-axis, $\delta u_N(1,\ldots,N) = e^{i\varphi_1}\times\cdots\times e^{i\varphi_N}$. Yet the latter example hints the alternative to δu_N: to refrain from linearization of the Euler-Lagrange equations, i.e. to raise the treatment of excitation to the level of the ground state calculation. Then the vortex is well described by mere one-body correlations. More on this can be found in appendix C.

In the probabilistic interpretation of the wave function, the multiplication of factors $f(i,j) = e^{\Re e\,\delta u(i,j)}$ corresponds to an conjunction of probability densities $f(i,j)$, thus effectively correlating all particles $1,\ldots,N$. How are the many-body correlations of collective excitations such as the phonons generated by a *disjunction* (sum) of $f(i,j)$? We repeat the argument given by Feynman [**Fey54**]: the correlations are mediated by the ground state factor of the product $\delta U\Phi_0$. Not only does Φ_0 ensure that the probability of particles overlapping vanishes, but the linearized fluctuation operator δU acts as a projection operator for collective fluctuations contained in the ground state, i.e. zero point collective motion. This is most evident in bulk, where $\sum_i e^{i\mathbf{q}\mathbf{r}_i}\Phi_0$ reproduces the Bijl-Feynman spectrum: the sum over the expontential is merely selecting those configurations of coordinates which fluctuates with wave vector $\mathbf{q}$, but it is Φ_0 which determines the energy and other expectation values.

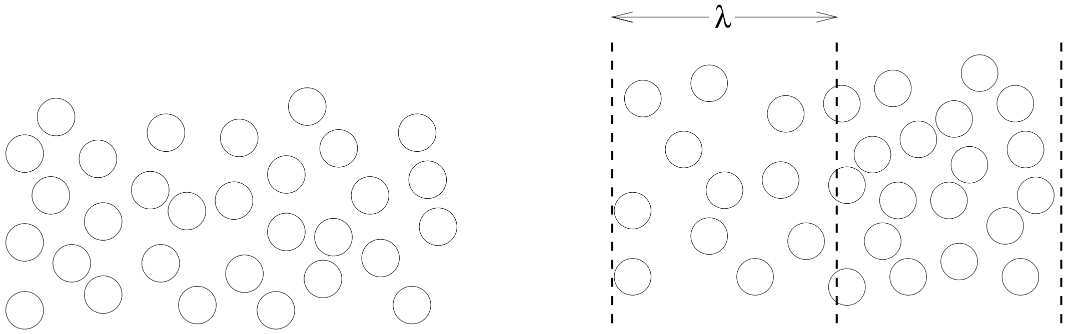

FIGURE 6. Feynman's probabilistic interpretation of the linearized ansatz $\delta U \Phi_0$, with $\delta U = \sum_i e^{i\mathbf{q}\mathbf{r}_i}$. To the left, a typical ground state configuration is shown, which the "projector" δU cancels. One of the few ground state configurations which survives the action of δU is shown to the right, where $\lambda = \frac{2\pi}{q}$.

Remark We want to point out the difference to a more conventional ansatz for scattering at energies below the target fragmentation threshold, which relies on the expansion in eigenstates of the *target* (examples of its application can be found in [**Fes58**] and [**CK92**])

$$\Phi(1, \ldots, N) = \sum_n \phi_n(1) \Psi_n(2, \ldots, N) \tag{54}$$

where $\phi_n(1)$ specifies the various "channels" of the scattering particle 1. The expansion is accurate, if Ψ_n is known accurately and the sum extends over the relevant region in the target Hilbert space. In the case of strongly repulsive interactions, this region has to be large enough to take care of configurations with particle 1 close to or inside the target.[6]

The ansatz (54) leads to an effective one-body equations which is of the same form as (53), i.e. a Schrödinger-like equation with a local potential U and an integral operator Σ, together called *optical potential*; Σ is again of a form similar to the self energy. The difference lies in the calculation of the local potential and of the nominator of Σ, i.e. of the three-phonon matrix elements: in the optical potential methods, these quantities are obtained as expectation values with respect to the states of the target (^{4}He droplet or film), while our matrix elements W^s_{mn} in the denominator of the self energy are calculated using the states of the combined system target+projectile, albeit in an approximate way (Feynman excitations). To allow for hard core interaction potentials, the ansatz (54) can be modified [**Fes58**] by introducing correlation factors similar to the Jastrow-Feenberg ansatz.

[6]Using uncorrelated basis functions as in (54) generally requires huge basis sets, as for example methods based on the LCAO (linear combination of atomic orbitals) in chemistry, or the CIM (configuration interaction method), which lack size-extensivety [**Bis98**].

6. Equations of motion for impurities in ^{4}He

The Lagrange density $\mathcal{L}$ for the dynamics of an impurity at $\mathbf{r}_0$ in inhomogeneous ^{4}He is simpler than for pure ^{4}He, because the correlations are not symmetrized

$$\delta U(0,1,\ldots,N;t) \;=\; \delta u(0;t) + \sum_i \delta u(0,i;t)$$

where we remind of the implicit labelling $\delta u(0;t) = \delta u^I(0;t)$ etc. The steps to expand $\mathcal{L}$ to second order in $\delta U(t)$ are the same as for pure ^{4}He, except that the optimization of the ground state up to 3-body correlations u_3 is sufficient for eliminating the bare interaction *exactly.*

The minimization of $\mathcal{L}$ yields the linearized Euler-Lagrange equations [**CKS97**] (omitting the perturbing potential)

$$\nabla_0 \cdot \mathbf{j}(0;t) + \delta\dot\rho(0;t) \;=\; 0 \tag{55}$$

$$\nabla_0 \cdot \mathbf{j}(0,1;t) + \nabla_1 \cdot \mathbf{J}(0,1;t) + \delta\dot\rho(0,1;t) \;=\; 0 \tag{56}$$

with the transition, i.e. first order currents and current-density correlations

$$\mathbf{j}(0;t) \;=\; \frac{\hbar}{2m_I i}\left[\rho(0)\nabla_0\delta u(0;t) + \int d2\;\rho(0,2)\nabla_0\delta u(0,2;t)\right] \tag{57}$$

$$\mathbf{j}(0;1;t) \;=\; \frac{\hbar}{2m_I i}\left[\rho(0,1)\nabla_0\delta u(0;t) + \rho(0,1)\nabla_0\delta u(0,1;t) + \int d2\;\rho(0,1,2)\nabla_0\delta u(0,2;t)\right]$$

$$\mathbf{J}(0,1;t) \;=\; \frac{\hbar}{2m_4 i}\;\rho(0,1)\nabla_1\delta u(0,1;t)$$

and the transition densities

$$\delta\rho(0;t) \;=\; \delta v(0;t) \;-\; \rho(0)\int d0'\;\delta v(0';t) \tag{58}$$

$$\delta\rho(0,1;t) \;=\; \rho(0,1)\delta u(0;t) \;+\; \rho(0,1)\delta u(0,1;t) \;+\int d2\;\rho(0,1,2)\delta u(0,2;t) \;-\; \rho(0,1)\int d0'\;\delta v(0';t) \tag{59}$$

with

$$\delta v(0;t) \;=\; \rho(0)\delta u(u;t) \;+\int d2\;\rho(0,2)\delta u(0,2;t)\,.$$

Following the same steps as for the CBF-BW approximation in pure ^{4}He, the equations of motion (55) and (56) can be cast into two equations for $\varphi := \frac{\delta\rho}{\sqrt{\rho}}$ (note the difference to φ in pure ^{4}He) and for δu_2. As for pure ^{4}He, they are conveniently expanded in the basis of states obtained by setting $\delta u_2 = 0$. Then the impurity feels only a static, local mean potential and can occupy stationary states $\varphi = \eta_\gamma$ defined by

$$H_1(0)\eta_\gamma(0) \;=\; t_\gamma\eta_\gamma \tag{60}$$

which is simply a single-particle Schrödinger equation for a particle in a potential

$$V_H(0) = \frac{\hbar^2}{2m_I}\frac{\nabla^2\sqrt{\rho(0)}}{\sqrt{\rho(0)}}\;. \tag{61}$$

We will refer to (60) as Hartree equation.

In the uniform limit, the one- and two-body correlations

$$r_\gamma = \int d0\ \eta_\gamma(0)\,\varphi(0) \qquad \delta u_{\gamma n} = \int d0d1\ \eta_\gamma(0)\,\delta\tilde{u}(0,1)\,\phi_n(1)$$

are to be determined from

$$(t_\delta - \hbar\omega)r_\delta = \sum_{\gamma n}(W^\delta_{\gamma n})^*\delta u_{\gamma n} \tag{62}$$

$$(t_\gamma + \hbar\omega_n - \hbar\omega)\,\delta u_{\gamma n} = \sum_\delta W^\delta_{\gamma n} r_\delta \tag{63}$$

where

$$\begin{aligned} W^\delta_{\gamma n} &\equiv \int d0\ \eta_\delta(0)\tilde{W}_{\gamma n}(0) = -\frac{1}{2}\int d0\ \eta_\delta(0)\frac{\eta^*_\gamma(0)}{\sqrt{\rho(0)}}[t_\gamma - t_\delta - H_1(0)]\tilde{X}_n(0) \\ &= \int d0\ \eta_\delta(0)\hat{D}_n(0)\eta_\gamma(0) \end{aligned} \tag{64}$$

$$\tilde{X}_n(0) = \int d1\ \tilde{X}(0,1)\phi_n(1)$$

$$\hat{D}_n(0)f(0) = -\frac{\hbar^2}{2m_I}\frac{1}{\sqrt{\rho(0)}}\nabla f(0)\sqrt{\rho(0)}\nabla\frac{\tilde{X}_n(0)}{\sqrt{\rho(0)}} \tag{65}$$

A further approximation employed in (63) was to discard terms stemming from $X(0,1,2)$, which have been kept in ^{4}He, since they turn out to contribute to scattering cross sections at roton energies. For an impurity in bulk ^{4}He, this and the previous approximations amount to calculating the "unrenormalized" effective mass [**KS93a, Owe81**].

By eliminating $\delta u_{\gamma n}$, the effective single-particle equation for r_γ is analoguous to eq. (51), except for the lack of a static structure operator,

$$(t_\delta - \hbar\omega)r_\delta - \sum_\gamma \Sigma_{\delta\gamma}(\omega)r_\gamma = 0 \tag{66}$$

with the self energy operator in the Hartree basis representation

$$\Sigma_{\delta\gamma}(\omega) = \sum_{\beta n}\frac{W^\delta_{\beta n}(W^\gamma_{\beta n})^*}{\hbar\omega_n + t_\beta - \hbar\omega} \tag{67}$$

Again, with the help of the Green's function of the Hartree equation (60)

$$G^0(0,0';\omega) = (H_1(0) - \hbar\omega)^{-1}\ , \qquad G^0_{\beta\gamma}(\omega) = \int d1d2\ \eta_\beta(0)G^0(0,0';\omega)\eta_\gamma(0') = \frac{\delta_{\beta\gamma}}{\hbar\omega - t_\beta}$$

Σ can be written

$$\Sigma_{\delta\gamma}(\omega) = \sum_{\beta\beta' n} W^\delta_{\beta n}\,G^0_{\beta\beta'}(\omega - \omega_n)\,(W^\gamma_{\beta' n})^*\ . \tag{68}$$

CHAPTER 4

Scattering

1. Scattering Channels

1.1. Definition

Many-body scattering processes are considerably more complicated than potential/two-body scattering. The exact description of many-body scattering implies a large number of coordinates, but also a wealth of qualitatively different processes (grouped into "channels", see below). While the first, kinematic complication is "a nuisance", the second, dynamical one is "subtle and beautiful" [**RS79**]. The description of excitations in the framework of HNC-Euler-Lagrange theory manages to alleviate the burden of dealing with all the N particles potentially participating in the scattering process, yet is subtle enough to retain many important features of many-body scattering. The restrictions of the method are summarized further below.

The outcome of the collision of two structureless particles like ^{4}He atoms is fully characterized by their momenta, i.e. energy and direction of the two particles. This differs from the collision involving three or more particles. Given an initial configuration determined by experimental conditions, the result of the scattering will be a superposition of waves each of which is characterized by the grouping of the particles into fragments, the internal state of the fragments, and the momenta of the fragments. Depending on the author, each grouping or each pair (grouping,internal state) denotes a *scattering channel.* In figure (1), the simplest example of many-body scattering, three-body scattering, is shown schematically.

Describing excited states of an N–body system in terms of channels is especially suited for scattering: channel wave functions help categorizing the scattering solutions of the N–body Hamiltonian into subspaces which have a direct connection to (and in fact define) the experimentally observable scattering cross section; and the mathematical concept of channel Hamiltonians provide not only an exact definition of the channel wave functions, but is the starting point of many approximate treatments of the Schrödinger equation. There is abundant literature on scattering theory, we refer to [**RS79, GW67, Fes62, Fes58, Far75, New66**], especially to the introduction to scattering theory by Taylor [**Tay72**]. The treatment of nuclear scattering by Feshbach [**Fes58**] using multi-channel optical potentials is appropriate complementary material because of some similarities to scattering calculations in the HNC-Euler-Lagrange theory, presented here.

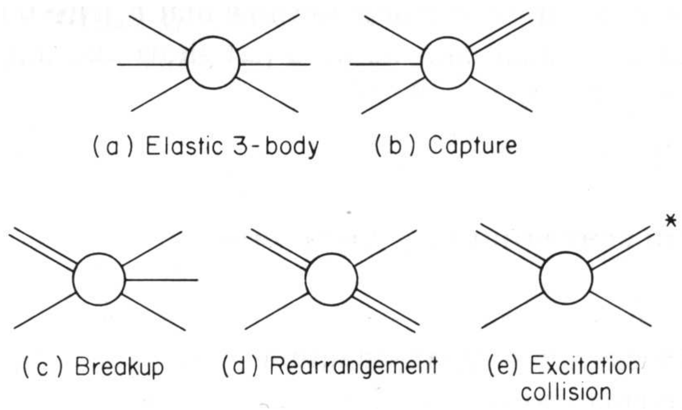

FIGURE 1. Three-body scattering: Time flows in horizontal direction from left to right. Each line corresponds to the path of a particle projected on the drawing plane, i.e. a double line indicates a bound state of two particles. The 5 diagrams represent 5 channels. (From [**RS79**])

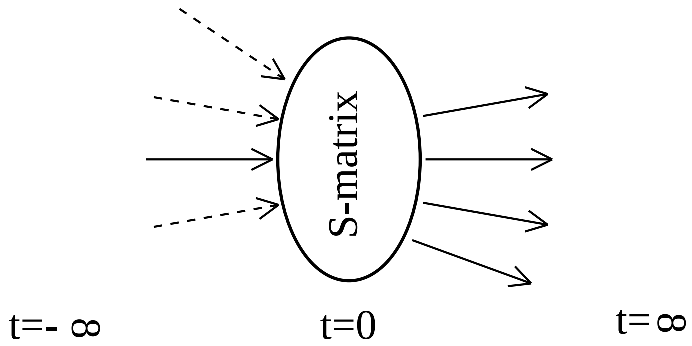

FIGURE 2. Illustration of scattering channels: each line denotes a scattering channel symbolically. In experimental realisations, the asymptotic "in" state lies in a single "in" channel (solid line), and the system evolves into one or a superposition of several "out" channels. The S-matrix transforms from the asymptotic "in" state to the asymptotic "out" state

1.2. Definition

The idea of channel wave functions arises naturally when considering the typical scattering solution: at a time t_- a projectile starts in a state experimentally prepared, evolves until it hits a target at time t_0. The projectile and/or fragments produced during the scattering event are detected at a time t_+. As compared to the time span of projectile and target interacting, the times $t_\pm$ can be considered $\pm\infty$. Only at $t = -\infty / +\infty$, the N–body wave function $\Phi(t)$ is partly known by proper preparation / detection of scattered fragments, hence a description of $\Phi(t)$ in terms of $\Phi(\pm\infty)$ is convenient. For finite interaction potentials, at $t = -\infty / +\infty$ the projectile and target / the scattered fragments move independently and are described by the channel Hamiltonian H_α

$$H_\alpha = h_\alpha^{(1)} + h_\alpha^{(2)} + \dots$$

which is the sum of the Hamiltonians h_i for the particles of the freely moving subsystems (projectile and target / scattered fragments), i.e. the full Hamiltonian devoid of the interaction potential between the subsystems (identity of particles need not be regarded yet, as the wave function can always be (anti-)symmetrized after solving the Schrödinger equation). The subscript α specifies the arrangement of the particles (and possibly other parameters such as internal degrees of freedom): e.g. the arrangement of a projectile and a target (the elastic channel); or the projectile particle bound to the target system and a particle previously bound to the target system freely moving (one of many conceivable inelastic channels).

At $t = \pm\infty$, solutions of H of course factorize into a superposition of products of the wave functions $\Phi_\alpha^{(i)}$ of the subsystems, which are solutions of the respective channel Hamiltonian H_α. This holds for stationary scattering solutions as well, if the condition $t = \pm\infty$ is replaced by the condition that coordinates of particles belonging to different fragments are far apart. $\Phi_\alpha^{(i)}$ are called channel wave functions. For example, for the scattering of a single particle at a bound system of $N-1$ particles in its ground state Φ_0, the incoming and several possible outgoing stationary wave functions are

$$\begin{array}{rcll}
\Phi_{\text{in}}(1,\dots,N) & \to & P\ e^{i\mathbf{k}_{\text{in}}\mathbf{r}_1}\Phi_0(2,\dots,N) & \text{elastic} \\
\Phi_{\text{out}}(1,\dots,N) & \to & P\ e^{i\mathbf{k}_{\text{out}}\mathbf{r}_1}\Phi_0(2,\dots,N) & k_{\text{out}} = k_{\text{in}},\ \text{elastic} \\
 & \to & P\ e^{i\mathbf{k}_1\mathbf{r}_1}\Phi_n(2,\dots,N) & k_1 < k_{\text{in}},\ \text{inelastic} \\
 & \to & P\ e^{i\mathbf{k}_1\mathbf{r}_1}e^{i\mathbf{k}_2\mathbf{r}_2}\Phi_m(3,\dots,N) & \text{inelastic} \\
 & \dots & &
\end{array}$$

where P stands for appropriate symmetrization. Which channels are open (*i.e.* have a real wave vector) depends on the incident energy; the elastic channel is always open. Note that for finite N there is no channel $\Phi_n(1,\dots,N)$: a projectile cannot be scattered into a bound state with the target; the reason is the Orthogonality Theorem [**Tay72**], see section 2.2.

1.3. Channels in HNC-Euler-Lagrange theory

In the previous chapter, we have interpreted the linearization of the Euler-Lagrange equations for the wave function $e^{\delta U/2}\Phi_0$ as an approximative scheme for obtaining excited states of the form $\delta\Phi = \delta U\Phi_0$. With δU including two body correlations (37), we can now identify which channels are supported by the *ansatz* $\delta U\Phi_0$. We will see that the eigenstates of the equation of motion (53) (eq. (66) for impurity scattering) are the elastic channel wave functions, and the eigenstates of the Feynman Hamiltonian and the Hartree Hamiltonian are single particle channels of ^{4}He and ^{3}He, respectively. If P denotes symmetrization with respect to the coordinates $\mathbf{r}_1,\dots,\mathbf{r}_N$, we find for the pure Bose system and for impurity scattering,

$$
\begin{aligned}
&\textbf{pure:}\\
\delta\Phi(1,\ldots,N) &= \delta U(1,\ldots,N)\Phi_0^{(N)}(1,\ldots,N) = [\sum_i \delta u(i) + \sum_{i<j}\delta u(i,j)]\Phi_0^{(N)}(1,\ldots,N)\\
&\rightarrow \frac{1}{\sqrt{N}}P\delta\tilde{u}(1)\Phi_0^{(N-1)}(2,\ldots,N) + \frac{1}{\sqrt{N(N-1)}}P\delta\tilde{u}(1,2)\Phi_0^{(N-2)}(3,\ldots,N)\\
&\rightarrow \frac{1}{\sqrt{N}}P\delta\tilde{u}(1)\Phi_0^{(N-1)}(2,\ldots,N)\\
&\qquad + \frac{1}{\sqrt{N(N-1)}}P\sum_{nm}\delta\tilde{u}^{(B)}_{mn}\Psi_m(1)\Psi_n(2)\Phi_0^{(N-2)}(3,\ldots,N)\\
&\textbf{impurity:}\\
\delta\Phi(0,\ldots,N) &= \delta U(0,\ldots,N)\Phi_0^{(N+1)}(0,\ldots,N) = [\delta u(0) + \sum_i \delta u(0,i)]\Phi_0^{(N+1)}(0,\ldots,N)\\
&\rightarrow \delta\tilde{u}(0)\Phi_0^{(N)}(1,\ldots,N) + \frac{1}{\sqrt{N}}P\delta\tilde{u}(0,1)\Phi_0^{(N-1)}(2,\ldots,N)\\
&\rightarrow \delta\tilde{u}(0)\Phi_0^{(N)}(1,\ldots,N) + \frac{1}{\sqrt{N}}P\sum_{rm}\delta\tilde{u}^{(I)}_{rm}\eta_r(0)\Psi_m(1)\Phi_0^{(N-1)}(2,\ldots,N)
\end{aligned}
$$

For this expansion of $\delta\Phi$ in channel wave functions we have used the asymptotic behaviour of $\delta u^{(X)}$

$$
\begin{aligned}
\delta u^B(1) &\overset{r_1\to\infty}{\longrightarrow} \frac{f_1(\mathbf{r}_1)}{\sqrt{\rho^B(\mathbf{r}_1)}}\\
\delta u^B(1,2) &\overset{r_1,r_2\to\infty}{\longrightarrow} \frac{f_2(\mathbf{r}_1,\mathbf{r}_2)}{\sqrt{\rho^B(\mathbf{r}_1)\rho^((\mathbf{r}_2)}}\\
\delta u^I(0) &\overset{r_0\to\infty}{\longrightarrow} \frac{f_1(\mathbf{r}_0)}{\sqrt{\rho^I(\mathbf{r}_0)}}\\
\delta u^I(0,1) &\overset{r_0,r_1\to\infty}{\longrightarrow} \frac{f_2(\mathbf{r}_0,\mathbf{r}_1)}{\sqrt{\rho^I(\mathbf{r}_0)\rho^B(\mathbf{r}_1)}}\ ,
\end{aligned}
$$

where f_1, f_2 denote non-diverging, but otherwise still arbitrary functions. For the ground states $\Phi_0^{(N)}(1,\ldots,N)$ and $\Phi_0^{(N+1)}(0,\ldots,N)$ we have used the asymptotic behaviour stated in eqns. (29) and (30). The kind of processes that the *ansatz* for $\delta\Phi$ supports are:

1. elastic scattering;
2. inelastic scattering, leaving the target in an excited state;
3. inelastic scattering, and stripping off a target particle in the process
4. sticking, which is accompanied by the emission of a target particle, if $N < \infty$. Therefore, for ^{4}He scattering off finite ^{4}He droplets, *i.e.* identical particle scattering, this process is indistinguishable from 2.

In case of ^{4}He scattering, a further possibility would be the generation of a ^{4}He—dimer: a long-ranged correlation between two ^{4}He atoms excited simultaneously above the chemical potential is necessary to bind them to a dimer of the size of ~ 50Å and binding energy of

~ 1.7mK [**KKZ99**]. There is little hope to numerically resolve effects involving that small energies. On physical grounds we believe the probability for dimer formation is negligible anyway.

Among others, the *ansatz* $\delta U \Phi_0$ excludes the following processes, the cross sections of which vanish only at low energies:

1. Excitation of many target modes: for growing droplet size, the energy spacing between low energy states $^4\mathrm{He}_N$ shrinks, therefore the cross section for excitation of several low energy states might be non-negligible at sub-Kelvin incident energies. For example, the droplet surface waves for large N have an approximate ripplon dispersion [**KZ99, CK95a**]

$$\omega_\ell = \hbar \sqrt{\frac{\sigma}{m\rho_\infty}} k^{3/2} \ , \qquad \text{with} \quad k = \sqrt{\frac{3\ell(\ell+1)}{5\langle r^2 \rangle}} \propto N^{-1} \ .$$

   For scattering off films, multi-excitation process channels are open for arbitrarily small incident energies. For example, the method cannot account for frictionlike slowing-down of the approaching atom by emission of many ripplons [**EP76b, EP76a, SE88**].
2. "Fission" of the target: fitting the droplet ground state energy to the phenomenological law (32), the energy needed to split a large $^4\mathrm{He}_N$ droplet into two equal parts is approximately $4.4 N^{2/3}$ K.
3. Evaporation of many target particles: releasing n ^{4}He atoms from $^4\mathrm{He}_N$, $n \ll N$, after impact of an impurity costs at least $n|\mu_B| - |\mu_I|$, $\mu_B = -7.21$ K, which for all impurities regarded here (^{3}He and H) is positive even for $n = 1$.
4. Scattering of particles off a target which is prepared in an excited state or a superposition of excited states. The only process which can be described by invoking time-reversal symmetry is de-excitation of the target: the scattering particle carries off the excitation energy of the target, leaving the target in the ground state after the event.

In conclusion, we summarize these kinematical considerations: excitations treated in linear response in the HNC-Euler-Lagrange theory can describe the N-body scattering problem exhaustively for low scattering energies, if up to 2-body correlations are allowed to depend on time (corresponding to Feynman's "backflow" [**FC56**]). The precise value of "low energy" is determined by the energy spacing of the low-lying states, i.e. the surface excitations, which is determined by N. By "exhaustive" treatment we mean no channels are missed: because of energy conservation, channels others than the 3-phonon processes are closed at low energies. For higher scattering energies as well as increasing system size $\frac{N}{\rho}$, fluctuating two-body correlations δu_2 in conjunction with linear response accounts for only a subset of all open channels. Unfortunately, lifting both or even one of the restrictions — $\delta u_n = 0$, $n > 2$, and linearization with respect to δU — would lead to currently intractable equations for the inhomogeneous many-body problem.

2. Scattering Cross Sections

After introducing the many-particle scattering problem, and before working out solutions, we need to introduce the quantities of interest: cross sections and — for scattering from surfaces — scattering and sticking probabilities. For the introduction of cross sections, we follow the presentation of [**Tay72**]. The modifications for film scattering are deferred to the next section.

2.1. What can be observed experimentally

Scattering solutions $\Psi(t)$ of a Hamiltonian H are time-dependent wave functions propagating from a given starting state at time $-t_{\text{in}}$ to time t_{out} when they are detected. As we have mentioned already, both t_{in} and t_{out} are large on the scale of the dynamics of the scattering event itself, i.e. large compared to the time span in which the scattering fragments are interacting. Following this premise, many methods of scattering theory are based on the evolution operator $U(t,t') = e^{-iH(t-t')/\hbar}$ and the fact that, for most of the time span $t_{\text{in}} + t_{\text{out}}$, the propagation of (each channel of) $\Psi(t)$ is mediated by the evolution operator(s) of the channel Hamiltonians H_α, $U(t,t') = e^{-iH_\alpha(t-t')/\hbar}$ ("asymptotic condition").

In experiments, the momentum of the incident particle is usually well-defined, and the associated wave packet broad enough to consider stationary solutions of H instead of $\Psi(t)$.[1] The connection between the stationary excited wave function in the HNC-Euler-Lagrange theory as discussed in the previous section and the evolution of a time-dependent scattering solution $\Psi(t)$ is this: the splitting of $\Psi(t)$ into a superposition of a product of non-overlapping wave packets of n_i particles ($\sum n_i = N$) *at large positive and negative times* corresponds to the factorization of the stationary solutions into a superposition of product wave functions *at large separations of the coordinates* of the fragments of channel α. Each of the factors is the wave function of a noninteracting fragment, specified by its center of mass momentum and internal quantum numbers. To sum up the asymptotic behaviour, we have

[1]Nevertheless, there are also methods based on direct application of the evolution operator on wave packets, such as Chebychev expansion of $U(t,t')$ and the split operator method [**Rim00**]

time-dependent

For $t \to -\infty$, the wave function is still in the incoming channel $\alpha_{\rm in}$, for example

$$\Psi(1,\ldots,N;t) \to \Psi_1^{(\alpha_{\rm in})}(1;t)\Psi_2^{(\alpha_{\rm in})}(2,\ldots,N;t)$$

where $\Psi_1^{(\alpha_{\rm in})}$ is the starting wave packet of of the scattering particle 1, and $\Psi_2^{(\alpha_{\rm in})}$ is the state of the target of $N-1$ particles.
For $t \to +\infty$, it has scattered into many channels

$$\Psi(1,\ldots,N;t) \to \sum_\alpha \prod_i \Psi_i^{(\alpha)}(\{j\}_{n_i^{(\alpha)}};t)$$

where the summation is over all open channels.

time-independent

Let the N particles be partitioned into subset $(n_i^{(\alpha_0)})_i$, and each subset be well separated from the others. Then

$$\Psi(1,\ldots,N) \to {\sum_\alpha}' \prod_i \Psi_i^{(\alpha)}(\{j\}_{n_i^{(\alpha)}})$$

where the summation is over all open channels α with fragments partitioned into subsets $(n_i^{(\alpha_0)})_i$. Specifically, the incoming or *elastic* channel $\alpha_{\rm in}$ accounts for elastic scattering, and the corresponding component $\Psi_{\rm el}$ of the wave function is

$$\Psi_{\rm el}(1,\ldots,N) \to \Psi_1^{(\alpha_{\rm in})}(1)\Psi_2^{(\alpha_{\rm in})}(2,\ldots,N)\,.$$

These wave functions have yet to be symmetrized according to the statistics of subsets of identical particles.

Cross sections are defined as the probability that the N-body wave function, which starts from an "in" asymptote in channel $\alpha_{\rm in}$, $\Psi_{\rm in} \equiv \Psi(t=-\infty)$, is found (detected) in the "out" asymptote in channel $\alpha_{\rm out}$, $\Phi_{\rm out}$. Apart from $\alpha_{\rm out}$, $\Phi_{\rm out}$ is characterized by the relative momenta $\bar{p} = (\mathbf{p}_1,\ldots,\mathbf{p}_m)$ of the $m+1$ fragments, produced in the scattering process: $|\Phi_{\rm out}\rangle = |\alpha_{\rm out},\bar{p}\rangle$. Hence, the probability density for the system to end up in state $|\alpha_{\rm out},\bar{p}\rangle$ is

$$\mathcal{W}(\alpha_{\rm in},\alpha_{\rm out},\bar{p}) \;=\; |\langle\alpha_{\rm out},\bar{p}|\Psi(t=+\infty)\rangle|^2 \;=\; |\langle\alpha_{\rm out},\bar{p}|\mathbf{S}|\Psi_{\rm in}\rangle|^2 \tag{69}$$

where we have expressed $\Psi(t=+\infty)$ in terms of the scattering operator $\mathbf{S}$ ("S-matrix"), which transforms from the "in" asymptote to the "out" asymptote[2]. For practical reasons, not all momenta $\bar{p}$ can be determined with a detector, but only, for example, the momentum of the scattering particle, or the recoil of the target etc. This corresponds to integrating (69) over a subspace of the space of m relative momenta

$$\Delta\sigma \;=\; \int_\Delta d^{3m}p\; \mathcal{W}(\alpha_{\rm in},\alpha_{\rm out},\bar{p}) \;=\; \int_\Delta d^{3m}p\; |\langle\alpha_{\rm out},\bar{p}|\mathbf{S}|\Psi_{\rm in}\rangle|^2\,. \tag{70}$$

In order to obtain an observable quantity, $\Delta\sigma$ has yet to be averaged over many wave packets $\Psi_{\rm in}$ according to the experimental preparation. Because $\Psi_{\rm in}$ typically peaks sharply in momentum space at a given incident relative momentum $\mathbf{p}_{\rm in}$, the average has to be taken only over the impact parameter, *i.e.* the deviation from a head-on collision of particle and target. Effectivly, this averaging is equivalent to the calculation of the cross sections from

[2]We will not make explicit use of the scattering operator $\mathbf{S}$ for cross sections calculations. Therefore reference to $\mathbf{S}$ is only symbolical here.

the stationary states[**Tay72**] – which is the final justification to abandon time-dependent solutions for the rest of the paper and henceforth work only with stationary solutions.

Example: $m = 1$

The cross section for scattering into a channel with 2 fragments which have relative momentum in d^3p around $\mathbf{p}$ is

$$d\sigma = \int_{d^3p} d^3p\, \mathcal{W}(\alpha_{\text{in}}, \alpha_{\text{out}}, \mathbf{p})\,, \qquad \frac{d\sigma}{d^3p} = \mathcal{W}(\alpha_{\text{in}}, \alpha_{\text{out}}, \mathbf{p})\,.$$

If only the relative deflection angle is detected, but not the modulus of $\mathbf{p}$, Δ is the solid angle cone $d\Omega$, and the cross section is

$$\frac{d\sigma}{d\Omega} = \int dp\, p^2\, \mathcal{W}(\alpha_{\text{in}}, \alpha_{\text{out}}, \mathbf{p})\,.$$

Conversely, the dependence of the cross section on the energy-transfer E_t from a scattering particle of energy $E_{\text{in}} = \frac{\hbar^2 k_{\text{in}}^2}{2m}$ to a large target is given by

$$\frac{d\sigma}{dE_t} = \int d^3p\, \delta(E_{\text{in}} - \frac{\hbar^2 p^2}{2m} - E_t)\, \mathcal{W}(\alpha_{\text{in}}, \alpha_{\text{out}}, \mathbf{p})$$

The energy transfer dependence is a convenient way to relate measurable scattering probabilities to the internal degrees of freedom of the target, *i.e.* its excitations. For example, in neutron scattering experiments, the scattering probability is measured as a function of E_t and the momentum transfer $\mathbf{q}_t = \mathbf{p}_i - \mathbf{p}_f$

$$\frac{d^2\sigma}{dE_t dq_t} = \frac{p_f}{p_i}\, \frac{d^2\sigma^0}{dE_t dq_t}\, S(\mathbf{q}_t, E_t) \qquad \text{(in Born approximation)}$$

where $\frac{d^2\sigma^0}{dE_t dq_t}$ is the neutron-atom cross section which is a constant in the q_t-range of interest in inelastic neutron scattering measurements of condensed matter. $S(\mathbf{q}_t, E_t)$ is the dynamic structure function from which, by means of the fluctuation-dissipation theorem, the density response function can be obtained if the system is homogeneous [**PN66a**]. But also for ^{3}He–^{4}He$_N$ scattering $\frac{d\sigma}{dE_t dq_t}$ reveals feature of the excitation spectrum of the ^{4}He$_N$ system, as will be shown later.

If Δ is the whole $3m$-dimensional momentum space, $\Delta\sigma$ is called *total* cross section into channel α_{out}, and if furthermore we sum over all open channels except the elastic, $\alpha \neq \alpha_{\text{in}}$, we obtain the total inelastic cross section.

2.2. Orthogonality Theorem

This important theorem states that any state that has evolved from an "in" asymptote in channel α, i.e. a scattering state, is orthogonal to any bound state of *all* particle of the system

$$\left.\begin{array}{ll} \Phi & \text{bound state:} \\ \Psi_\alpha & \text{scattering state:} \end{array}\right\} \qquad \langle \Phi | \Psi_\alpha \rangle = 0\,.$$

In fact, generally states evolving from different "in" asymptotes are orthogonal

$$\langle \Psi_\alpha | \Psi_{\alpha'} \rangle = 0\,.$$

However, scattering states originating in channel α can evolve into a superposition of "out" asympototes of many channels, which is the mathematical way of saying that inelastic scattering can have a finite probability. On the other hand, the overlap of Φ and Ψ_α vanishes for $t \to -\infty$, and therefore for all times. Due to the orthogonality of Φ and Ψ_α, *no bound state of all N particle can result from scattering.* The probability of absorption of the incident particle without emission of a particle of the target is mathematically zero (but it may take long till the particle is emitted, if the target has many degrees of freedom).

3. Scattering from Surfaces

The most important difference between scattering off finite systems like ^{4}He droplets and scattering off surfaces like ^{4}He films is that, for $N \to \infty$, the Orthogonality Theorem is no longer valid, and thus the ab/adsorption or sticking probability s is finite even without emission of a target particle. The physical reason is that, in an infinite system, the energy transferred to the target can by carried off into the system. In classical terms, the Poincaré cycle becomes infinitely long in the thermodynamic limit. Only after taking the limit $N \to \infty$, s is finite; for N large but finite, sharp resonances will be observed, i.e. metastable states of the combined system scattering particle + target system, with a lifetime that increases with N. For a one-dimensional model system, sticking in the thermodynamic limit is discussed very thoroughly in [**CK92**].

Specifically for surface scattering, the target is either bulk matter filling the infinite half space ($z < 0$) with a surface domain near $z = 0$, or a slab of finite thickness [**CKS98**]. In this work, ^{4}He films of several atomic layers are considered which are adsorbed to an inert substrate, which does not respond dynamically. In either case, rather than to speak about cross sections we prefer to stick to the generic terms "scattering probability", "absorption probability", etc. For atom scattering off ^{4}He films, we will calculate the following quantities:

Elastic scattering probability: The elastic scattering probability or reflection probability denotes the probability that the incident particle (coordinate $\mathbf{r}$, momentum $\mathbf{k}_{\rm in} = (k_{x,{\rm in}}, k_{y,{\rm in}}, k_{z,{\rm in}}) = (\mathbf{k}_{\|,{\rm in}}, k_{\perp,{\rm in}})$) is reflected elastically off the surface without losing energy. *I.e.* in a stationary state, the wave function for large z tends to

$$\phi \;\times\; e^{i\mathbf{k}_{\|,{\rm in}}\mathbf{r}} \;\left[e^{-ik_{\perp,{\rm in}}z} + Re^{ik_{\perp,{\rm in}}z}\right]$$

where $\mathbf{k}_{\|,{\rm in}} = \mathbf{k}_{\|,{\rm out}}$ is conserved parallel to the surface, and ϕ is the unperturbed wave function of the target. The reflection is specular just as in potential scattering, but with the difference that the elastic scattering probability $|R|^2 < 1$.

Direct inelastic scattering probability: The inelastic scattering probability r_{inel} denotes the probability that the incident particle is transfering energy (and parallel momentum) to the surface: $k_{\|,\mathrm{out}} < k_{\|,\mathrm{in}}$ and the probability to scatter inelastically into an solid angle Ω_{out} is, other than for elastic scattering, a non-trivial function of Ω_{out}.

Sticking probability: The ad-/absorption probability ("sticking coefficient") s denotes the probability that the incident particle is transfering more energy than its kinetic energy, thus being caught in a state bound to or in the target.

4. Calculation of scattering probabilities

In our work, explicit calculations of cross sections are done via asymptotic probability currents, which is equivalent to using the probability density $\rho = |\Psi|^2$ on the basis of the continuity equation

$$\nabla \cdot \mathbf{j}(1,\ldots,N) + \dot{\rho}(1,\ldots,N) \;=\; 0$$

which asymptotically also holds for each channel α separately by the very definition of channels: asymptotically, the full Hamiltonian H can be replaced by the channel Hamiltonian H_α, therefore for each α–components we find local probability conservation

$$\nabla \cdot \mathbf{j}_\alpha(1,\ldots,n_\alpha) + \dot{\rho}_\alpha(1,\ldots,n_\alpha) \;=\; 0$$

Since the current $\mathbf{j}$ turns out to be easier to be calculated in the HNC-Euler-Lagrange theory, it is the essential quantity in our treatment of scattering properties, and the next chapter is devoted to the calculation of $\mathbf{j}$.

CHAPTER 5

Currents

Probability currents in ^{4}He have been studied in the past with regard to the correlated movement of ^{4}He around each other, particularly the backflow pattern of roton excitations [**FC56, AS98, RG97**]. In the HNC-Euler-Lagrange theory this has been done by expanding the expectation value $\langle \hat{\mathbf{j}}^X \rangle$ of the N-body current operator

$$\hat{\mathbf{j}}^B(\mathbf{r}) = \sum_j \frac{1}{2m^B}(\frac{\hbar}{i}\nabla_j \delta(\mathbf{r}-\mathbf{r}_j) + \delta(\mathbf{r}-\mathbf{r}_j)\frac{\hbar}{i}\nabla_j) \tag{71}$$

to first order in the correlation fluctuations δU (37) and the impurity current operator

$$\hat{\mathbf{j}}^I(\mathbf{r}) = \frac{1}{2m^I}(\frac{\hbar}{i}\nabla_0 \delta(\mathbf{r}-\mathbf{r}_0) + \delta(\mathbf{r}-\mathbf{r}_0)\frac{\hbar}{i}\nabla_0) \tag{72}$$

and by expanding current-density correlations $\langle \hat{\mathbf{j}}^X \hat{\rho}^Y \rangle$.

These first order currents and current-density correlations, called transition currents for reasons that will become clear in the next section, are relatively easy to calculate. The linearized Euler-Lagrange equations (35) $\delta \int dt\, \mathcal{L}(t) = 0$ are formulated as continuity equations for currents and current-density correlations. The first order expectation value of an operator $\mathcal{O}$ provides a picture of how the expectation value due to the excitation is changed with respect to the ground state expectation value (which vanishes in the case of $\mathcal{O} \equiv \hat{j}$). However, it fluctuates with the excitation frequency and therefore vanishes in a measurement, which corresponds to a time integral of the expectation value. Moreover, in case of $\mathcal{O} \equiv \hat{j}$, we will find that the first order current falls off as the square root of the ground state density, and hence does not account for the asymptotic currents necessary for calculating scattering cross sections. It is the second order ^{4}He or impurity current which leads to a mass transport that can be detected in a scattering experiment.

1. Transition Currents and beyond

Assuming, we have solved the Euler-Lagrange equations $\delta \int dt\, \mathcal{L}(t) = 0$ for $\delta U(t)$ and thus obtained the wave function

$$\Phi(1,\ldots,N;t) = e^{-iE_0 t/\hbar} \frac{e^{\delta U(1,\ldots,N;t)/2}\Phi_0(1,\ldots,N)}{\sqrt{\langle \Phi_0 | e^{\Re e\ \delta U(t)} | \Phi_0 \rangle}}$$

as the linear response of the ground state Φ_0, as outlined in chapter 3. Just as the action integral $\mathcal{S}$, the expectation value of an observable $\mathcal{O}$ can be expanded in terms of δU

$$\begin{aligned}\frac{\langle\Phi_0|e^{\delta U^*/2}\mathcal{O}e^{\delta U/2}|\Phi_0\rangle}{\langle\Phi_0|e^{\Re e\ \delta U}|\Phi_0\rangle} &= \frac{\langle\Phi_0|(1+\frac{\delta U^*}{2}+\frac{\delta U^{*2}}{8})\mathcal{O}(1+\frac{\delta U}{2}+\frac{\delta U^2}{8})|\Phi_0\rangle}{\langle\Phi_0|1+\Re e\ \delta U+(\Re e\ \delta U)^2/2|\Phi_0\rangle} \\ &= \langle\hat{\mathcal{O}}\rangle^{(0)}+\langle\hat{\mathcal{O}}\rangle^{(1)}+\langle\hat{\mathcal{O}}\rangle^{(2)}+\ldots\end{aligned}$$

with

$$\begin{aligned}\langle\hat{\mathcal{O}}\rangle^{(0)} &= \frac{\langle\Phi_0|\mathcal{O}|\Phi_0\rangle}{\langle\Phi_0|\Phi_0\rangle} \\ \langle\hat{\mathcal{O}}\rangle^{(1)} &= \frac{\langle\Phi_0|\frac{\delta U^*}{2}\mathcal{O}|\Phi_0\rangle+\langle\Phi_0|\mathcal{O}\frac{\delta U}{2}|\Phi_0\rangle}{\langle\Phi_0|\Phi_0\rangle} \\ \langle\hat{\mathcal{O}}\rangle^{(2)} &= \frac{\langle\Phi_0|\frac{\delta U^{*2}}{8}\mathcal{O}|\Phi_0\rangle+\langle\Phi_0|\frac{\delta U^*}{2}\mathcal{O}\frac{\delta U}{2}|\Phi_0\rangle+\langle\Phi_0|\mathcal{O}\frac{\delta U^2}{8}|\Phi_0\rangle}{\langle\Phi_0|\Phi_0\rangle} \\ &\quad -\frac{1}{2}\frac{\langle\Phi_0|\mathcal{O}|\Phi_0\rangle}{\langle\Phi_0|\Phi_0\rangle}\frac{\langle\Phi_0|(\Re e\ \delta U)^2|\Phi_0\rangle}{\langle\Phi_0|\Phi_0\rangle}\end{aligned}$$

where we have already assumed orthogonalization of the excited state with respect to the ground state, i.e. the overlap of $\Phi(t)$ and Φ_0 vanishes to first order in $\delta U(t)$, $\langle\Phi_0|\delta U(t)|\Phi_0\rangle = 0$. For example, for the impurity current $\mathcal{O}\equiv\mathbf{j}^I$, where $\delta U(1,\ldots,N;t) = \delta u(0;t) + \sum_i \delta u(0,i;t)$

$$\begin{aligned}\langle\hat{\mathbf{j}}^I\rangle^{(0)} &= 0 \qquad (73) \\ \langle\hat{\mathbf{j}}^I\rangle^{(1)} &= \frac{\hbar}{2m^I}\frac{1}{\langle\Phi_0|\Phi_0\rangle}\ \Im m\int d1\ldots dN\ \Phi_0^2\nabla_0\delta U \\ \langle\hat{\mathbf{j}}^I\rangle^{(2)} &= \frac{\hbar}{2m^I i}\frac{1}{\langle\Phi_0|\Phi_0\rangle}\int d1\ldots dN\ \Phi_0^2[-\frac{1}{8}\nabla_0\delta U^{*2}+\frac{1}{4}\delta U^*\nabla_0\delta U \\ &\qquad -\frac{1}{4}\delta U\nabla_0\delta U^*+\frac{1}{8}\nabla_0\delta U^2] \qquad (74) \\ &= \frac{\hbar}{4m^I}\frac{1}{\langle\Phi_0|\Phi_0\rangle}\ \Im m\int d1\ldots dN\ \Phi_0^2[\delta U^*\nabla_0\delta U+\delta U\nabla_0\delta U]\end{aligned}$$

where we have used $\Phi_0\in\mathbb{R}$. In a scattering measurement, a detector, placed far away from the target, measures the time average of the scattered flux caused by the incident wave of well-defined momentum $\mathbf{k}$ (*i.e.* a broad wave packet, sharply peaked in momentum space). From the asymptotic behaviour of the correlation fluctuations $\delta u(0,\ldots,n)\propto\prod_{i=0}^n\rho(i)^{-1/2}$, the first order current $\langle\hat{\mathbf{j}}^I(\mathbf{r}_0)\rangle^{(1)}$ vanishes for $r_0\to\infty$. Even if a detector were placed inside the target system, the time average of $\langle\hat{\mathbf{j}}^I(\mathbf{r}_0)\rangle^{(1)}$ would vanish[1]. From the second order current $\langle\hat{\mathbf{j}}^I\rangle^{(2)}$, only the term containing δU and δU^* contributes to the time average. Therefore we

[1]This time integral has to be performed channel-wise; while this is trivial for the elastic channel $\delta u(0;t)\propto\exp(-i\epsilon t/\hbar)$, $\epsilon=\frac{\hbar^2k^2}{2m^I}$, in case of $\delta u(0,1;t)$ this has to be done seperately for the channels that the detector is able to distinguish.

find for the current describing mass transport

$$\langle \hat{\mathbf{j}}^I \rangle^{\rm trans} = \frac{\hbar}{4m^I} \frac{1}{\langle \Phi_0 | \Phi_0 \rangle} \Im m \int d1 \ldots dN \; |\Phi_0|^2 \delta U^* \nabla_0 \delta U$$

Linearizing the Euler-Lagrange equations amounts to the treatment of the excitations as the linear response of the system out of the ground state $\Phi = \Phi_0 + \delta\Phi$, where $\delta\Phi$ is the (superposition of) excitation(s), as obtained from the linearized Euler-Lagrange equations. For the time average of second order expectation values, the same result[2] as eq. (74) can clearly be obtained by *first* linearizing the yet unnormalized wave function

$$\delta\Phi(1,\ldots,N;t) = e^{-iE_0 t/\hbar} \delta U(1,\ldots,N;t) \Phi_0(1,\ldots,N)$$

and *then* calculating the expectation value

$$\frac{\langle \delta\Phi | \mathcal{O} | \delta\Phi \rangle}{\langle \delta\Phi | \delta\Phi \rangle} = \frac{\langle \Phi_0 | \delta U(t)^* \mathcal{O} \delta U(t) | \Phi_0 \rangle}{\langle \Phi_0 | \delta U(t)^* \delta U(t) | \Phi_0 \rangle} \tag{75}$$

Firstly, this stresses the fact that expanding expection values up to second order is consistent with the expansion of the action integral to second order; secondly, and more important, eq. (75) shows that $\langle \hat{\mathcal{O}} \rangle^{(2)}$, obtained as the exact expectation value with respect to an approximate wave function $\delta\Phi$ rather than as just another term in a Taylor series, is the physically observable quantity. For completness, $\langle \mathcal{O} \rangle^{(1)}$ can also be written in terms of $\delta\Phi$, and it turns out to be (proportional to) $\langle \Phi_0 | \mathcal{O} | \delta\Phi \rangle + c.c.$; formally, it is the real part of the transition matrix element between the ground state and an excited state induced by $\mathcal{O}$ in the role of the perturbation operator; hence the name transition current for $\langle \hat{\mathbf{j}} \rangle^{(1)}$.

2. Currents in Pure Helium

In the case of pure ^{4}He currents, it is more elegant to include terms of the δU-expansion containing the orthogonalization condition $\langle \Phi_0 | \delta U | \Phi_0 \rangle = 0$, which contributes to $\langle \hat{\mathcal{O}} \rangle^{(2)}$,

$$\frac{1}{2} \langle \hat{\mathcal{O}} \rangle^{(1)} \frac{\langle \Phi_0 | \Re e \; \delta U | \Phi_0 \rangle}{\langle \Phi_0 | \Phi_0 \rangle} .$$

Specifically for the current operator $\hat{\mathbf{j}}^B(\mathbf{r})$ as defined in (71), this can be written in terms of the real part of the transition current $\mathbf{j}(\mathbf{r};t)$, eq. (40), appearing in the Euler-Lagrange equation,

$$\mathbf{j}(\mathbf{r};t) = \frac{\hbar}{2mi} \left(\rho(1) \nabla_1 \delta u(1;t) + \int d2 \; \rho(1,2) \nabla_1 \delta u(1,2;t) \right)$$

if we average over time:

$$\begin{aligned} \frac{1}{2} \langle \hat{\mathbf{j}}^B(\mathbf{r}) \rangle^{(1)} \frac{\langle \Phi_0 | \Re e \; \delta U | \Phi_0 \rangle}{\langle \Phi_0 | \Phi_0 \rangle} &\overset{\langle\rangle_T}{=} \frac{1}{2} \frac{\langle \Phi_0 | \Re e \; \delta U^* | \Phi_0 \rangle}{\langle \Phi_0 | \Phi_0 \rangle} \Re e \; \mathbf{j}^B(\mathbf{r}) \\ &= \frac{1}{2} \left[\int d1 \; \rho(1) \delta u^*(1) + \int d1 d2 \; \rho(1,2) \delta u^*(1,2) \right] \Re e \; \mathbf{j}^B(\mathbf{r}) \end{aligned}$$

[2] Except for the normalization constant, which for scattering solutions will be determined by the condition of an unit incident plane wave anyhow.

The full expression for the time average of $\langle\hat{\mathbf{j}}^B(\mathbf{r})\rangle^{(2)}$ is fairly lengthy

$$\langle\hat{\mathbf{j}}^B(1)\rangle^{(2)} \overset{\langle\rangle_T}{\equiv} \frac{\hbar}{4m}\Im m\left[\mathbf{j}_{11}(1)+\mathbf{j}_{12}(1)+\mathbf{j}_{21}(1)+\mathbf{j}_{22}(1)\right]$$

with

$$\begin{aligned}
\mathbf{j}_{11}(1) &= \left[\underline{\rho(1)\delta u^*(1)} + \int d2\ [\rho(1,2)-\rho(1)\rho(2)]\delta u^*(2)\right]\nabla\delta u(1) \\
\mathbf{j}_{12}(1) &= \int d2\ \rho(1,2)[\underline{\delta u^*(1)}+\delta u^*(2)]\nabla\delta u(1,2) \\
&\quad + \int d23\ [\rho(1,2,3)-\rho(1,2)\rho(3)]\delta u^*(3)\nabla\delta u(1,2) \\
\mathbf{j}_{21}(1) &= \int d2\ \underline{\rho(1,2)\delta u^*(1,2)\nabla\delta u(1)} + \frac{1}{2}\int d23\ [\rho(1,2,3)-\rho(1)\rho(2,3)]\delta u^*(2,3)\nabla\delta u(1) \\
\mathbf{j}_{22}(1) &= \int d2\ \underline{\rho(1,2)\delta u^*(1,2)\nabla\delta u(1,2)} + \int d23\ \underline{\rho(1,2,3)\delta u^*(1,3)\nabla\delta u(1,2)} \\
&\quad + \int d23\ \rho(1,2,3)\delta u^*(2,3)\nabla\delta u(1,2) \\
&\quad + \frac{1}{2}\int d234\ [\rho(1,2,3,4)-\rho(1,2)\rho(3,4)]\delta u^*(3,4)\nabla\delta u(1,2)
\end{aligned}$$

where only the the underlined terms contribute in the asymptotic regime $r_1 \to \infty$. Before taking this limit, the above expression for $\langle\hat{\mathbf{j}}^B(1)\rangle^{(2)}$ can be considerably simplified, if the current fluctuations $\delta u^*(1)$, $\delta u^*(1,2)$ are expressed in terms of the density fluctuations $\delta\rho(1)$, $\delta\rho(1,2)$ up to first order

$$\begin{aligned}
\delta\rho(1) &= \int d2\ \frac{\delta\rho(1)}{\delta u(2)}\delta u(2) + \int d23\ \frac{\delta\rho(1)}{\delta u(2,3)}\delta u(2,3) + \mathrm{O}(\delta\mathrm{U}^2) \\
\delta\rho(1,2) &= \int d3\ \frac{\delta\rho(1,2)}{\delta u(3)}\delta u(3) + \int d34\ \frac{\delta\rho(1,2)}{\delta u(3,4)}\delta u(3,4) + \mathrm{O}(\delta\mathrm{U}^2)
\end{aligned}$$

Higher order corrections contribute to $\langle\hat{\mathbf{j}}^B(1)\rangle^{(3)}$ and can therefore be neglected. On the other hand, the functional derivatives can be obtained from the definition of the densities (see appendix A)

$$\frac{\delta\rho(1)}{\delta u(2)} = \rho(1,2)-\rho(1)\rho(2)+\rho(1)\delta(1,2) \tag{76}$$

$$\frac{\delta\rho(1)}{\delta u(2,3)} = \frac{\rho(1,2,3)}{2} - \frac{\rho(1)\rho(2,3)}{2} + \frac{\rho(1,3)}{2}\delta(1,2) + \frac{\rho(1,2)}{2}\delta(1,3) \tag{77}$$

$$\frac{\delta\rho(1,2)}{\delta u(3)} = \rho(1,2,3)-\rho(1,2)\rho(3)+\rho(1,2)[\delta(1,3)+\delta(2,3)] \tag{78}$$

$$\begin{aligned}
\frac{\delta\rho(1,2)}{\delta u(3,4)} &= \frac{\rho(1,2,3,4)}{2} - \frac{\rho(1,2)\rho(3,4)}{2} + \frac{\rho(1,2,4)}{2}[\delta(1,3)+\delta(2,3)] \\
&\quad + \frac{\rho(1,2,3)}{2}[\delta(1,4)+\delta(2,4)] + \frac{\rho(1,2)}{2}[\delta(1,3)\delta(2,4)+\delta(1,4)\delta(2,3)]
\end{aligned} \tag{79}$$

By replacing $\rho(1,2,3,4)$ and $\rho(1,2,3)$ with the help of these equations, $\langle \hat{\mathbf{j}}^B(1)\rangle^{(2)}$ can be expressed as

$$\langle \hat{\mathbf{j}}^B(1)\rangle^{(2)} = \frac{\hbar}{4m}\Im m\left[\ \delta\rho^*(1)\nabla_1\delta u(1) + \int d2\ \delta\rho^*(1,2)\nabla_1\delta u(1,2)\ \right] \equiv \frac{\hbar}{4m}\Im m[\mathbf{j}_a + \mathbf{j}_b] \quad (80)$$

$\delta\rho(1,2)$ and $\delta X(1,2)$ have still to be expressed in terms of the variational variable $\delta\tilde{u}(1,2)$ by variation of the HNC equation (11) and the Ornstein-Zernicke relation (12) [**Tym95, CKT96**]. As for the Euler-Lagrange equations, we use the uniform limit approximation where $\delta g(1,2)$ is given by (46) and $\delta X(1,2) = \delta u(1,2)$.

Putting everything together, yields a still unpleasant expression for $\mathbf{j}_b$, which mixes the elastic component $\delta\rho(1)/\sqrt{\rho(1)}$ with the inelastic ones $\delta\tilde{u}(1,2)$:

$$\begin{aligned}
\mathbf{j}_b \;&=\; \frac{\delta\rho^*(1)}{\sqrt{\rho(1)}}\int d2\ g(1,2)\sqrt{\rho(2)}\ P(1)\ \delta\tilde{u}(1,2) + \sqrt{\rho(1)}\int d2\ \frac{\delta\rho^*(2)}{\sqrt{\rho(2)}}\ g(1,2)\,P(1)\,\delta\tilde{u}(1,2)\\
&\quad + \int d234\ S(1,3)\delta\tilde{u}^*(3,4)S(4,2)\,P(1)\,\delta\tilde{u}(1,2)\\
&\quad + \int d2d3\ \tilde{Y}(1,2;3)\frac{\delta\rho(3)}{\sqrt{\rho(3)}}\,P(1)\,\delta\tilde{u}(1,2)
\end{aligned}$$

where we abbreviated the differential operator

$$P(1) \;\equiv\; \sqrt{\rho(1)}\nabla_1\frac{1}{\sqrt{\rho(1)}}$$

Furthermore, δu_1 in $\mathbf{j}_a$ still has to be eliminated by $\delta\rho_1$ and $\delta\tilde{u}_2$.

The visualization of the mass flow inside the inhomogeneous ^{4}He system is an exciting open problem; however, if we restrict ourselves to determining the scattering cross section (droplets) and reflection and sticking probabilities (films), only the asymptotic current is needed, and terms of $\mathbf{j}_a$ and $\mathbf{j}_b$ proportional to $\sqrt{\rho(1)}$ of $\rho(1)$ may be neglected. In this limit, $\delta u(1)$ may be approximated by $\rho(1)\delta u(1) \to \delta\rho(1) - \int d2\ \rho(1,2)\delta u(1,2)$, and the current is

$$\langle \hat{\mathbf{j}}^B(1)\rangle^{(2)} \overset{r_1\to\infty}{\longrightarrow} \frac{\hbar}{4m}\Im m\left[\ \frac{\delta\rho^*(1)}{\sqrt{\rho(1)}}\ P(1)\ \frac{\delta\rho(1)}{\sqrt{\rho(1)}} + \int d23\ S(3,2)\ \delta\tilde{u}^*(1,3)\,P(1)\,\delta\tilde{u}(1,2)\ \right] \quad (81)$$

where replacing $P(1)$ by ∇_1 would make no difference in this imaginary part. Henceforth, we will abbreviate $\mathbf{j}^{(2)}(1) \equiv \langle \hat{\mathbf{j}}^B(1)\rangle^{(2)}$.

The asymptotic[3] current is clearly constituted of an elastic contribution, which is simply the probability current of the adjoint[4] of the the single-body elastic channel wave function, $\delta\rho(1)/\sqrt{\rho(1)}$, and — less clearly for the moment — of a contribution from inelastically scattered atoms, which is still hidden in the 2-body correlation fluctuations $\delta\tilde{u}_2$.

[3]In the vicinity of the droplet/film, this current still contains interference terms between elastic and inelastic as well as different inelastic channels.

[4]For large r_1, the elastic channel wave function $\varphi(\mathbf{r}_1)$ and the adjoint $\delta\rho(1)/\sqrt{\rho(1)} = [S * \varphi](\mathbf{r}_1)$ coincide.

3. Impurity Currents

The corresponding analysis of the impurity currents is less complicated due to the simpler structure of $\delta U(0,\ldots,N)$. In a similar fashion as above we get two formulations for the second order impurity current

$$\begin{aligned}
\langle \hat{\mathbf{j}}^I(0)\rangle^{(2)} &= \int d1\ldots dN\; |\Phi_0(0,\ldots,N)|^2 \\
&\qquad \times\big[\delta u^*(0)+\sum_i \delta u^*(0,i)\big]\big[\nabla_0\delta u(0)+\sum_i \nabla_0\delta u(0,i)\big] \qquad (82)\\
&= \frac{\hbar}{4m_I}\Im m\Big\{\frac{\delta\rho^*(0)}{\sqrt{\rho(0)}}\;P(0)\;\frac{\delta\rho(0)}{\sqrt{\rho(0)}} - \delta\rho^*(0)\int d1\;\rho(1)\;\delta u(0,1)\nabla_0 g(0,1) \qquad (83)\\
&\quad + \int d12\;A(0,1,2)\;\delta\tilde{u}^*(0,1)\,P(0)\,\delta\tilde{u}(0,2)\Big\}
\end{aligned}$$

with

$$A(0,1,2) \;=\; \delta(1,2)g(0,1)+\sqrt{\rho(1)}[g(0,1,2)-g(0,1)g(0,2)]\sqrt{\rho(2)} \qquad (84)$$

which in the uniform limit approximation simplifies to [**Fee69**]

$$A(0,1,2) \;\approx\; \delta(1,2)+\sqrt{\rho(1)}[g(1,2)-1]\sqrt{\rho(2)}\,.$$

The second formulation is

$$\langle \hat{\mathbf{j}}^I(0)\rangle^{(2)} \;=\; \delta\rho^*(0)\nabla_0\delta u(0)+\int d1\;\delta\rho^*(0,1)\nabla_0\delta u(0,1) \qquad (86)$$

where the complex density fluctuations have been defined in the continuity formulation of the Euler-Lagrange equations (58) and (59).

Similarily to the pure ^{4}He problem, terms proportional to $\sqrt{\rho(0)}$ are negligible in the asymptotic current. In the limit $r_0\to\infty$, we find in the uniform limit approximation

$$\begin{aligned}
\langle \hat{\mathbf{j}}^I(r_0)\rangle^{(2)} \;\stackrel{r_0\to\infty}{\longrightarrow}\; &\tfrac{\hbar}{4m_I}\Im m\Big\{\;\frac{\delta\rho^*(0)}{\sqrt{\rho(0)}}\;P(0)\;\frac{\delta\rho(0)}{\sqrt{\rho(0)}} \qquad (87)\\
&+\int d12\;S(1,2)\;\delta\tilde{u}^*(0,1)\,P(0)\,\delta\tilde{u}(0,2)\;\Big\}\,.
\end{aligned}$$

Henceforth, we will abbreviate $\mathbf{j}^{(2)}(0)\equiv\langle \hat{\mathbf{j}}^I(\mathbf{r}_0)\rangle^{(2)}$.

4. Impurity induced ^{4}He Currents

The momentum transfer $\mathbf{k}_{\rm drop}$ from the impinging atom of momentum $\hbar\mathbf{k}_{\rm in} = \hbar k_{\rm in}\mathbf{e}_z$ to the droplet is given by momentum conservation[5]: vectorial subtraction of the atom's asymtotic scattered momentum from $\mathbf{k}_{\rm in}$ equals the momentum transfered to all ^{4}He atoms, which yet includes both, the momentum of the droplet and possibly evaporated ^{4}He atoms. Hence we need to furthermore subtract the asymptotic ^{4}He current induced by the impurity.

[5] *During* the scattering process the droplet is fixed, therefore the $\ell = 1$-channel is closed

The second order expectation value of $\hat{\mathbf{j}}^B(\mathbf{r}_1)$ with respect to the wave function of excitatition of the impurity $\sim \exp[\delta U(t)/2]\Phi_0$ turns out to be

$$\begin{aligned} \langle \hat{\mathbf{j}}^B(1)\rangle^{(2)} &= \frac{\hbar}{4m_4}\Im m\Big\{ \sqrt{\rho(1)}\int d0\; g(0,1)\; \frac{\delta\rho^*(0)}{\sqrt{\rho(0)}}\,P(1)\,\delta\tilde{u}(0,1) \\ &\quad + \int d02\; A(0,1,2)\;\delta\tilde{u}^*(0,2)\,P(1)\,\delta\tilde{u}(0,1)\Big\}. \end{aligned} \tag{88}$$

In the limit of large r_1, only the first term of A does not fall off as $\sqrt{\rho(\mathbf{r}_1)}$, see eq. (84); and, by the same argument applied to the second order impurity current, the contribution of $g(0,1)-1$ is negligible compared to unity. Hence,

$$\langle \hat{\mathbf{j}}^B(1)\rangle^{(2)} \overset{r_1\to\infty}{\longrightarrow} \frac{\hbar}{4m_4}\Im m\Big\{ \int d0\;\delta\tilde{u}^*(0,1)\,P(1)\,\delta\tilde{u}(0,1)\Big\}. \tag{89}$$

5. Current Conservation

The good news is, the impurity current derived above is conserved, and the bad news is, the ^{4}He current is not [**Fey54**]:

$$(i) \qquad \nabla\cdot\mathbf{j}^{(2)}(0) + \dot{\rho}^{(2)}(0) = 0 \tag{90}$$

$$(ii) \qquad \nabla\cdot\mathbf{j}^{(2)}(1) + \dot{\rho}^{(2)}(1) \neq 0 \tag{91}$$

where $\rho^{(2)}$ is the respective second order inpurity and ^{4}He density expectation value.

ad (i) The current conservation equation to first order, i.e. the equations of motion for $\delta u(0)$ and $\delta u(0,1)$ (55) and (56), guarantee the impurity current conservation to second order. For a proof, we multiply the one–body equation of motion with $\delta u(0)$ and take the real part; we multiply the two–body equation of motion with $\delta u(0,1)$, integrate over the ^{4}He coordinate and take the real part; the sum of the two equations thus obtained is equivalent to (90), which relate the second order current (82) and density

$$\rho^{(2)}(0) = r(0) - \rho(0)\int d0'\; r(0') \tag{92}$$

with

$$r(0) = \int d1\ldots dN\;|\Phi_0(0,\ldots,N)|^2\big[\delta u^*(0) + \sum_i \delta u^*(0,i)\big]\big[\delta u(0) + \sum_i \delta u(0,i)\big]\,.$$

Hence

$$\begin{array}{rlll} & \Re e\Big\{ \quad \delta u^*(0) & \big[\nabla_0\cdot\mathbf{j}^{(1)}(0) + \delta\dot{\rho}^{(1)}(0)\big] \quad \Big\} & = \;0 \\ + & \Re e\Big\{ \int d1\;\delta u^*(0,1) & \big[\nabla_0\cdot\mathbf{j}^{(1)}(0,1) + \nabla_1\cdot\mathbf{J}^{(1)}(0,1) + \delta\dot{\rho}^{(1)}(0,1)\big] \Big\} & = \;0 \\ \hline & & \Longrightarrow \qquad \nabla\cdot\mathbf{j}^{(2)}(0) + \dot{\rho}^{(2)}(0) & = \;0 \end{array}$$

where the (complex) transition current and density fluctuations are defined in (57) and (58). Note that the time derivate of the normalization term in (92) vanishes, as can be seen by integrating over $\mathbf{r}_0$.

The reason for this equivalence is that in (90) as well as in the equations of motions, only probability densities between up to three bodies appear. In contrast, this is no longer true, if the wave function is to be symmetrized with respect to all particle coordinates as we will see now in the case of the pure ^{4}He system.

ad (ii) The non-conservation of the ^{4}He current is readily demonstrated by a counter example: let $\delta u_2 = 0$ (Feynman approximation), *i.e.* $\delta U = \sum_i \delta u(i)$. As a generalisation, δu may also be considered a broad wave packet instead of a stationary Feynman state:

$$\begin{aligned}
\rho^{(2)}(1) &= \frac{\langle\Phi_0|\frac{\delta U^{*2}}{8}\hat\rho(1)|\Phi_0\rangle + \langle\Phi_0|\frac{\delta U^*}{2}\hat\rho(1)\frac{\delta U}{2}|\Phi_0\rangle + \langle\Phi_0|\hat\rho(1)\frac{\delta U^2}{8}|\Phi_0\rangle}{\langle\Phi_0|\Phi_0\rangle} \\
&\quad - \frac{\langle\Phi_0|\hat\rho(1)|\Phi_0\rangle}{\langle\Phi_0|\Phi_0\rangle}\frac{\langle\Phi_0|(\Re e\ \delta U)^2|\Phi_0\rangle}{\langle\Phi_0|\Phi_0\rangle} \\
&\overset{\langle.\rangle_T}{=} \frac{1}{4}\rho(1)\delta u^*(1)\delta u(1) + \frac{1}{4}\int d2\ \rho(1,2)[\delta u^*(1)\delta u(2) + c.c.] \\
&\quad + \frac{1}{4}\int d23\ [\delta(2,3)\rho(1,2) + \rho(1,2,3)]\delta u^*(2)\delta u(3)\,.
\end{aligned}$$

With the help of (78), we can eliminate the 3–body density, if we are consistent with our initial assumption of δU to be small:

$$\begin{aligned}
\rho^{(2)}(1) &= \frac{1}{4}\rho(1)\delta u^*(1)\delta u(1) + \frac{1}{4}\int d2\ \rho(1,2)\delta u^*(1)\delta u(2) + \frac{1}{4}\int d23\ \rho(1,2)\rho(3)\delta u^*(2)\delta u(3) \\
&\quad + \frac{1}{4}\int d2\ \delta u^*(2)\delta\rho(1,2) \\
&= \frac{1}{4}\phi^*(1)\psi(1) + \frac{1}{4}\sqrt{\rho(1)}\int d2\ \psi^*(2)\frac{\delta\rho(1,2)}{\sqrt{\rho(1)\rho(2)}}
\end{aligned}$$

where we used the orthogonality of the Feynman excitation state $\psi \equiv \delta\tilde u_1$ to the ground state density, $\int\sqrt{\rho}\psi = 0$. The current is given by (80) minus the 2–body fluctuation term:

$$\mathbf{j}^{(2)}(0) \overset{\langle.\rangle_T}{=} \frac{\hbar}{4m}\Im m\ \delta\rho^*(1)\nabla\delta u(1) = \frac{\hbar}{4m}\Im m\ \phi^*(1)\sqrt{\rho(1)}\nabla\frac{\psi(1)}{\sqrt{\rho(1)}}\,,$$

i.e. a 2–body term is missing, the current conservation cannot be fulfilled ($\nabla\cdot\mathbf{j}$ only cancels the first term of ρ), because terms involving higher correlations than regarded in equations of motions enter, that could be canceled if higher correlations are allowed to fluctuate in the action principle, and so on ad infinitum. Note, that in the limit that $\mathbf{r}_1$ is far outside the ^{4}He system, this residual term vanishes, and hence there is no net loss or gain of probability density within a surface enclosing the whole system[6],

$$(ii'):\qquad \nabla\cdot\mathbf{j}^{(2)}(1) + \dot\rho^{(2)}(1) = 0 \quad \text{for } |\mathbf{r}_1|\to\infty\,. \tag{93}$$

[6]In case of scattering off film, we assume periodic boundary conditions in the directions parallel to the film.

Therefore, cross sections for ^{4}He scattering calculated from these currents will still yield a unitary S–matrix.

There is an alternative to taking into account all fluctuations up to δu_N (and thus solving the exact Schrödinger equation!) to save current conservation [**Fey54**]: δU is still approximated by $\sum_i \delta u(i)$, but the equation of motion is not linearized. For a more detailed discussion, see appendix C.

6. Impurity Current in Bulk ^{4}He

The simplest example for and the first test of second order currents is excitations in homogeneous ^{4}He. We have shown in the previous section, that the second order impurity current $\mathbf{j}^{(2)}(0)$ is conserved not only asymptotically but also inside the ^{4}He system. Therefore, $\mathbf{j}^{(2)}(0)$ of an impurity moving in bulk ^{4}He is certainly a meaningful quantity. In the following, we briefly derive $\mathbf{j}^{(2)}(0)$ in bulk; for a full discussion of the equations of motion, self energy, and effective mass of an impurity moving in bulk ^{4}He, we refer to Ref. [**KS93a**].

Due to translational symmetry, excitations of impurities in CBF, *i.e.* the solutions $\delta\rho$ of the equation of motion eq. (66), are plane waves, characterized by a wave vector $\mathbf{k}_{\rm in}$, as are the Feynman states ψ_n and Hartree states η_α:

$$
\begin{aligned}
\eta_\alpha(0) &= e^{i\mathbf{p}\mathbf{r}_0} \\
\frac{\delta\rho(0)}{\sqrt{\rho(0)}} &= \frac{1}{2} e^{i\mathbf{k}_{\rm in}\mathbf{r}_0} \\
\psi_n(1) &= \frac{e^{i\mathbf{k}\mathbf{r}_1}}{\sqrt{S(k)}} \\
\tilde{X}_n(0) &= \frac{e^{i\mathbf{k}\mathbf{r}_0}}{\sqrt{S(k)}} S_I(k) \\
\delta\tilde{u}(0,1) &= \sum_n \delta\tilde{u}_n(0)\psi_n(1) \;=\; \sum_k \delta\tilde{u}_{\mathbf{k}}(0)\frac{e^{i\mathbf{k}\mathbf{r}_1}}{\sqrt{S(k)}}
\end{aligned}
$$

where the factor $1/2$ in $\delta\rho(0)/\sqrt{\rho(0)}$ is due to the definition of the correlation operator $\delta U(t)$ generating the excitation wave function $\exp[\delta U(t)/2]\Phi_0$.

In scattering calculations, we will only retain terms in eq. (83) which are finite at large distance from the ^{4}He system. Here we cannot perform this limit. Furthermore, all channels, closed and open, contribute to the current. For $\delta\tilde{u}_{\mathbf{k}}$ we find

$$
\begin{aligned}
\delta\tilde{u}_{\mathbf{k}}(\mathbf{r}_0) &= \frac{1}{2}\sum_\alpha \frac{\eta_\alpha(0)}{\hbar\omega_o + t_\alpha - \hbar\omega^{(I)}} \int d0' \,\frac{\hbar^2}{2m_I}\frac{\delta\rho(0')}{\sqrt{\rho(0')}}\frac{1}{\sqrt{\rho(0')}}\nabla_0' \left[\eta_\alpha^*(0')\sqrt{\rho(0')}\nabla_0' X_o(0')\right] \\
&= \frac{1}{2}\sum_{\mathbf{p}} \frac{e^{i\mathbf{p}\mathbf{r}_0}}{\hbar\omega^{(I)} - \hbar\omega(k) - t(p)} \int d0' \,\frac{\hbar^2}{2m_I} e^{i\mathbf{k}_{\rm in}\mathbf{r}_0'}\nabla' e^{-i\mathbf{p}\mathbf{r}_0'}\nabla' \frac{e^{-i\mathbf{k}\mathbf{r}_0}}{\sqrt{S(k)\rho_I}} S_I(k) \\
&= \frac{1}{2}\frac{S_I(k)}{\sqrt{S(k)\rho_I}}\,\frac{\hbar^2}{2m_I}\mathbf{k}\cdot\mathbf{k}_{\rm in}\; e^{i(\mathbf{k}_{\rm in}-\mathbf{k})\mathbf{r}_0}\,\frac{e^{-i(\omega^{(I)}\pm i\epsilon-\omega(k))t}}{\hbar\omega^{(I)} - \hbar\omega(k) - \frac{\hbar^2}{2m_I}(\mathbf{k}_{\rm in}-\mathbf{k})^2 \pm i\epsilon}
\end{aligned}
$$

where we have retained the time dependence. This yields for the last term, $\mathbf{j}_D^{(2)}(0)$, of eq. (83) in the uniform limit approximation

$$\begin{aligned}
\mathbf{j}_D^{(2)}(0) &= \frac{\hbar}{4m_I}\Im m\sum_{k,k'}\int d12\ S(1,2)\psi^*_{\mathbf{k}}(1)\psi_{\mathbf{k}'}(2)\delta\tilde{u}^*_{\mathbf{k}}(\mathbf{r}_0)\nabla_0\delta\tilde{u}_{\mathbf{k}'}(\mathbf{r}_0)\\
&= \frac{\hbar}{4m_I}\Im m\sum_{k}\delta\tilde{u}^*_{\mathbf{k}}(\mathbf{r}_0)\nabla_0\delta\tilde{u}_{\mathbf{k}}(\mathbf{r}_0)\\
&= \frac{\hbar}{4m_I}\left(\frac{\hbar}{2m_I}\right)^2\int\frac{d^3k}{(2\pi)^3}\frac{S_I^2(k)}{S(k)\rho_I}\frac{(\mathbf{k}\cdot\mathbf{k}_{\rm in})^2(\mathbf{k}_{\rm in}-\mathbf{k})e^{\pm 2\epsilon t}}{(\hbar\omega^{(I)}-\hbar\omega(k)-\frac{\hbar^2}{2m_I}(\mathbf{k}_{\rm in}-\mathbf{k})^2)^2+\epsilon^2}
\end{aligned}$$

The impurity energy dispersion $\hbar\omega^{(I)}(k_{\rm in})$ has to be determined self-consistently by solving the equations of motion $\hbar\omega^{(I)}(k_{\rm in}) = \hbar^2k_{\rm in}^2/2m_I + \Sigma(k_{\rm in},\omega^{(I)})$. If the impurity couples to the phonon-roton excitations, $\omega^{(I)}\in\mathbb{C}$, but as a first approximation, we assume that $\omega^{(I)}$ is real and see if we get a meaningful result for $\mathbf{j}_D^{(2)}(0)$.

If the impurity couples to the background and $\omega^{(I)}\in\mathbb{R}$, $\mathbf{j}_D^{(2)}(0)=\infty$ in the limit $\epsilon\to 0$, because the real $\omega^{(I)}$ corresponds to a steady production of inelastically scattered impurities. Hence we need to calculate the current *rate* $d\mathbf{j}^{(2)}(0)/dt$. Using

$$\frac{d}{dt}\frac{e^{\pm 2\epsilon t}}{(\hbar\omega^{(I)}-\hbar\omega(k)-\frac{\hbar^2}{2m_I}(\mathbf{k}_{\rm in}-\mathbf{k})^2)^2+\epsilon^2}\ \stackrel{\epsilon\to 0}{\longrightarrow}\ \delta\Big(\hbar\omega^{(I)}-\hbar\omega(k)-\frac{\hbar^2}{2m_I}(\mathbf{k}_{\rm in}-\mathbf{k})^2\Big)$$

we find that only $\mathbf{j}_D^{(2)}$ contributes to the second order impurity current rate, which becomes

$$\lim_{\epsilon\to 0}\frac{d}{dt}\mathbf{j}_I^{(2)}(0) = \frac{\hbar}{4m_I}\left(\frac{\hbar}{2m_I}\right)^2\int\frac{d^3k}{(2\pi)^3}\frac{S_I^2(k)}{S(k)\rho_I}(\mathbf{k}\cdot\mathbf{k}_{\rm in})^2(\mathbf{k}_{\rm in}-\mathbf{k})\,\delta\Big(\hbar\omega^{(I)}-\hbar\omega(k)-\frac{\hbar^2}{2m_I}(\mathbf{k}_{\rm in}-\mathbf{k})^2\Big) \tag{94}$$

which has only a component in direction of $\mathbf{k}_{\rm in}$, due to symmetry.

The induced second order background current $\mathbf{j}_B^{(2)}$ is given by eq. (88), of which again only the last term contributes. For $\delta\tilde{u}_{\mathbf{p}}$ the same steps as above are carried out

$$\begin{aligned}
\delta\tilde{u}_{\mathbf{p}}(\mathbf{r}_1) &= \frac{1}{2}\sum_k\frac{\psi_k^*(1)}{\omega_k+t_p-\omega^{(I)}}\int d0'\ \frac{\hbar^2}{2m_I}\frac{\delta\rho(0')}{\sqrt{\rho(0')}}\frac{1}{\sqrt{\rho(0')}}\nabla_0'\left[\eta_p^*(0')\sqrt{\rho(0')}\nabla_0' X_o(0')\right]\\
&= \frac{1}{2}\sum_{\mathbf{k}}\frac{e^{-i\mathbf{k}\mathbf{r}_1}}{\hbar\omega^{(I)}-\hbar\omega(k)-t(p)}\int d0'\ \frac{\hbar^2}{2m_I}e^{i\mathbf{k}_{\rm in}\mathbf{r}_0'}\nabla' e^{-i\mathbf{p}\mathbf{r}_0'}\nabla'\frac{e^{-i\mathbf{k}\mathbf{r}_0}}{\sqrt{S(k)\rho_I}}S_I(k)\\
&= \frac{1}{2}\frac{S_I(|\mathbf{k}_{\rm in}-\mathbf{p}|)}{\sqrt{S(|\mathbf{k}_{\rm in}-\mathbf{p}|)\rho_I}}\ \frac{\hbar^2}{2m_I}(\mathbf{k}_{\rm in}-\mathbf{p})\cdot\mathbf{k}_{\rm in}\ \frac{e^{-i(\mathbf{k}_{\rm in}-\mathbf{p})\mathbf{r}_1}e^{-i(\omega^{(I)}\pm i\epsilon-t(p))t}}{\hbar\omega^{(I)}-\hbar\omega(|\mathbf{k}_{\rm in}-\mathbf{p}|)-\frac{\hbar^2}{2m_I}p^2\pm i\epsilon}
\end{aligned}$$

which yields the rate

$$\lim_{\epsilon\to 0}\frac{d}{dt}\mathbf{j}_B^{(2)}(1) = \frac{\hbar}{4m_B}\left(\frac{\hbar}{2m_I}\right)^2\int\frac{d^3k}{(2\pi)^3}\frac{S_I^2(k)}{S(k)\rho_I}(\mathbf{k}\cdot\mathbf{k}_{\rm in})^2\mathbf{k}\,\delta\Big(\hbar\omega^{(I)}-\hbar\omega(k)-\frac{\hbar^2}{2m_I}(\mathbf{k}_{\rm in}-\mathbf{k})^2\Big) \tag{95}$$

where we have transformed the integration variable $\mathbf{k}_{\rm in}-\mathbf{p}=\mathbf{k}$. Combining (94) and (95) and deviding by the current obtained by setting $\delta u_2\equiv 0$, *i.e.* the free particle current, we find

$$\frac{\dfrac{d}{dt}j_I^{(2)} + \dfrac{m_B}{m_I}\dfrac{d}{dt}j_B^{(2)}}{\dfrac{\hbar k_{\rm in}}{4m_I}} = \Im m\,\Sigma(k_{\rm in},\omega^{(I)})$$

where the analytic form of the self energy $\Sigma(k_{\rm in},\omega^{(I)})$ is derived in Ref. [**KS93a**].

From (94) or (95) we see that the integrand of the imaginary part of the self energy $\Im m\,\Sigma$ can be regarded as the *emission rate* of excitations [**McC95**] or, for that matter, as the *decay rate* of impurities:

$$\dot{p}(\mathbf{k}_{\rm in} \to \mathbf{p};\omega^{(I)}) \;=\; |v(\mathbf{k}_{\rm in} \to \mathbf{p})|^2\;\delta\Big(\,\hbar\omega^{(I)} - \hbar\omega(|\mathbf{k}_{\rm in}-\mathbf{p}|) - \frac{\hbar^2 p^2}{2m_I}\Big)$$

with the matrix element

$$|v(\mathbf{k}_{\rm in} \to \mathbf{p})|^2 \;=\; \left(\frac{\hbar}{2m_I}\right)^2 \frac{S_I^2(k)}{S(k)\rho_I}\,(\mathbf{k}\cdot\mathbf{k}_{\rm in})^2\,, \qquad \mathbf{k} = \mathbf{k}_{\rm in} - \mathbf{p}\,.$$

Hence we have a microscopic approximate expression for the matrix element for the emission rate of excitations generated by dragging an impurity through ^{4}He. Furthermore, the total rate $\dot{P}$ for all process is $\Im m\,\Sigma$ itself:

$$\dot{P}(k_{\rm in},\omega^{(I)}) \;=\; \int\frac{d^3p}{(2\pi)^3}\,\dot{p}(\mathbf{k}_{\rm in} \to \mathbf{p};\omega^{(I)}) \;=\; \Im m\,\Sigma(k_{\rm in},\omega^{(I)})\,,$$

which is an interesting interpretation of the imaginary part of the self energy.

CHAPTER 6

Cross Sections of ^{4}He Droplets

After the stage for scattering calculations has been set in the previous chapters, we are ready to formulate the equations for excitations in ^{4}He and for impurities in ^{4}He for the case of ^{4}He droplets, and to fill the definitions of chapter 4 with substance. After specializing the equations of motion (chapter 3) to the symmetries that prevail in droplets of spherically symmetric ground state, our numerical results for elastic cross sections and, for the purpose of visualisation, the first order density fluctuations (transistion densities) are presented. In section 3, the formulas for inelastic cross sections for identical and distinct particle scattering are derived from the general expressions for inelastic currents obtained in chapter 5. After a discussion of the expressions for the many-body scattering cross sections thus obtained in the framework of HNC-Euler-Lagrange theory, the results of our calculations are presented.

1. Stationary States

In section 2 of chapter 4, it was argued that stationary scattering states are appropriate to derive cross sections for many-body scattering. Hence the first step is to solve the Euler-Lagrange equation — (38) and (39) for pure ^{4}He and (55) and (56) for impurities — for harmonic time-dependence with frequency ω, i.e. for excitations of energy $\hbar\omega$. For scattering, only unbound states need to be considered, where $\hbar\omega$ exceeds the chemical potential $|\mu|$ of the scattering particle in the droplet. Results for bound, low energy modes of ^{4}He droplets can be found in [**CK95a, KZ01**].

1.1. ^{4}He scattering

In the uniform limit approximation of the Euler-Lagrange equations, the single particle equation (53) has to be solved for the elastic channel wave function $\varphi(\mathbf{r})$. Due to the spherical symmetry of the ground state, the integro-differential equation (53) is separable into radial and angular dependence, as we will see below. Therefore, for given energy $E = \hbar\omega + \mu_4 = \frac{\hbar^2 k^2}{2m_4}$, (53) is preferably solved for the partial waves $\varphi(\mathbf{r}) = \varphi_{k,\ell}(r)$, in terms of which a stationary scattering state for an incoming particle of momentum $\mathbf{k}$ can be written [**Sch88**]

$$\varphi_{\mathbf{k}}(\mathbf{r}) = 4\pi \sum_{\ell,m} i^\ell \, Y^*_{\ell,m}(\Omega_k)\, Y_{\ell,m}(\Omega)\ \varphi_{k,\ell}(r) \tag{96}$$

where the asymptotic behaviour $r \to \infty$ of the partial waves and of the stationary scattering state is

$$\varphi_{k,\ell}(r) \;\to\; \frac{1}{2}(h^+_\ell(kr) + S_l(k)h^-_\ell(kr)) \tag{97}$$

$$\varphi_{\mathbf{k}}(\mathbf{r}) \;\to\; e^{i\mathbf{kr}} + f(\theta)\frac{e^{ikr}}{r} \tag{98}$$

with the scattering amplitude $f(\theta)$. The modulus of the amplitude is unity, $|S_l(k)| = 1$, if all inelastic channels are closed, and $|S_l(k)| < 1$ otherwise. The separation of $H(\mathbf{r})$ and $S(\mathbf{r},\mathbf{r}')$ into radial and angular coordinates has already been established in equations (45). What is left is the self energy expanded in spherical harmonics

$$\begin{aligned}\Sigma(\mathbf{r},\mathbf{r}') &= \sum_{\ell_m m_m}\sum_{\ell_n m_n} Y_{\ell_m,m_m}(\Omega)Y_{\ell_n,m_n}(\Omega')^*\Sigma^{\ell_n,m_n}_{\ell_m,m_m}(r,r') \\ &= \sum_{m\ell_m m_m}\sum_{n\ell_n m_n} Y_{\ell_m,m_m}(\Omega)Y_{\ell_n,m_n}(\Omega')^*\phi_{m,\ell_m}(r)\phi_{n,\ell_n}(r)^*\Sigma^{n,\ell_n,m_n}_{m,\ell_m,m_m}\,.\end{aligned}$$

The three-phonon matrix elements W^s_{mn} in the nominator of Σ fulfills selection rules. For ${}_bW^s_{mn}$, eq. (50), they follow immediately from the spherical symmetry of all ground state quantities:

$$\begin{aligned}{}_bW^s_{mn} &= -\int d1d2d3\;\psi_s(1)H(1)\phi_m(2)\phi_n(3)\tilde{X}(1,2,3) \\ &= -\hbar\omega_s\int d1d2d3\;\phi_s(1)\phi_m(2)\phi_n(3)\tilde{X}(1,2,3)\end{aligned} \tag{99}$$

where $\phi_i(1) = \phi_{n_i,\ell_i}(r_1)Y_{\ell_i m_i}(\Omega_1)$ and $\tilde{X}_3$ is rotationally invariant and as such depends only on $|\mathbf{r}_1|$, $|\mathbf{r}_2|$, and $|\mathbf{r}_3|$, and the angles between $\mathbf{r}_i$ and $\mathbf{r}_j$, denoted θ_{12}, θ_{13}, and θ_{23}. Hence $\tilde{X}_3$ can be expanded in Legendre polynomials

$$\tilde{X}(\mathbf{r}_1,\mathbf{r}_2,\mathbf{r}_3) = \sum_{j_1,j_2,j_3=0}^{\infty} P_{j_1}(\theta_{12})P_{j_2}(\theta_{13})P_{j_3}(\theta_{23})X_{j_1,j_2,j_3}(r_1,r_2,r_3)\,.$$

Conversely, $P_j(\theta_{12})$ can be expanded in spherical harmonics,

$$P_j(\theta_{12}) = \frac{4\pi}{2j+1}\sum_{m=-j}^{j} Y_{j,m}(\Omega_1)^*Y_{j,m}(\Omega_2)$$

where θ_{12} denotes the angle between the directions given by Ω_1 and Ω_2. Using equation (254) and (257) the expansion coefficients of $\tilde{X}_3$ in spherical harmonics needed in eq. (99) can be expressed in terms of 3-j and 6-j symbols

$$\begin{aligned}&\int d\Omega_1 d\Omega_2 d\Omega_3\; Y_{l,m}(\Omega_1)Y_{l',m'}(\Omega_2)Y_{l'',m''}(\Omega_3)\;\tilde{X}(\mathbf{r}_1,\mathbf{r}_2,\mathbf{r}_3) = \\ &(4\pi)^{3/2}\sqrt{(2\ell+1)(2\ell'+1)(2\ell''+1)}\begin{pmatrix}\ell & \ell' & \ell''\\ m & m' & m''\end{pmatrix}\times \\ &\sum_{j,j',j''}(-1)^{j+j'+j''}X_{j,j',j''}(r_1,r_2,r_3)\begin{pmatrix}\ell & j & j'\\ 0&0&0\end{pmatrix}\begin{pmatrix}\ell' & j & j''\\ 0&0&0\end{pmatrix}\begin{pmatrix}\ell'' & j' & j''\\ 0&0&0\end{pmatrix}\begin{Bmatrix}\ell & \ell' & \ell''\\ j & j' & j''\end{Bmatrix}\,.\end{aligned} \tag{100}$$

From the properties of the 3-j symbols (see appendix A) which are proportional to the Clebsch-Gordon coefficient, we can infer that (100) vanishes unless

$$m + m' + m'' = 0 \qquad \text{and} \qquad \ell, \ell', \ell'' \text{ satisfy triangular condition } \Delta(\ell, \ell', \ell'')$$

where the triangular condition states that the values of the three ℓ's can be the lengths of the sides of a triangle.

For $\tilde{X}_3$ obtained from the approximative triplet optimization of the ground state wave function, the angular momentum expansion is greatly simplified: according to eq. (2.76) and (2.80) of Ref. [**Tym95**],

$$_bW^s_{mn} = -\frac{\hbar^2}{2m_4}\frac{\omega_s}{\omega_m + \omega_n + \omega_s}\int \left(\phi_m \sqrt{\rho}\, \nabla \frac{\tilde{X}_n}{\sqrt{\rho}} \cdot \nabla \frac{\tilde{X}_s}{\sqrt{\rho}} + \text{cycl.}\right) \tag{101}$$

where

$$\tilde{X}_n(1) \;:=\; [\tilde{X} * \phi_n](1) \tag{102}$$

and where coordinate arguments have been omitted for brevity. Gradients themselves are not rotationally invariant, but their scalar products are, which is seen by expressing it in terms of the rotationally invariant operator $H = -\frac{\hbar^2}{2m_4}\frac{1}{\sqrt{\rho}}\nabla\rho\nabla\frac{1}{\sqrt{\rho}}$

$$\frac{\hbar^2}{2m_4}\sqrt{\rho}\,\nabla\frac{a}{\sqrt{\rho}} \cdot \sqrt{\rho}\,\nabla\frac{b}{\sqrt{\rho}} \;=\; \frac{1}{2}\left(bHa + aHb - H\frac{ab}{\sqrt{\rho}}\right).$$

H commutes with the total angular momentum operator $\hat{L}^2$, and for given ℓ, H_ℓ has already been defined in (45). In $_bW^s_{mn}$, the angular integration can thus be carried out easily, again using (254), to obtain

$$\begin{aligned} {}_bW^{s\ell_s m_s}_{m\ell_m m_m, n\ell_n m_n} &\equiv \begin{bmatrix} \ell_m & \ell_n & \ell_s \\ m_m & m_n & m_s \end{bmatrix} {}_bW^{s\ell_s}_{m\ell_m, n\ell_n} \\ &= \frac{\omega_{s,\ell_s} V_{m\ell_m, n\ell_n, s\ell_s}}{\omega_{m,\ell_m} + \omega_{n,\ell_n} + \omega_{s,\ell_s}} \begin{bmatrix} \ell_m & \ell_n & \ell_s \\ m_m & m_n & m_s \end{bmatrix} \end{aligned} \tag{103}$$

with

$$V_{m\ell_m, n\ell_n, s\ell_s} \;=\; \int dr\; r^2\; \tilde{X}_{s,\ell_s}(r)\; F[\phi_{m,\ell_m}, \phi_{n,\ell_n}](r) \;+\; \text{cycl.}$$

where we defined the functional F of ϕ_{m,ℓ_m} and ϕ_{n,ℓ_n}

$$\begin{aligned} F[\phi_{m,\ell_m}, \phi_{n,\ell_n}](r) \;=\; & \frac{\hbar^2}{2m_4}\frac{1}{\sqrt{\rho(r)}}\frac{\partial}{\partial r}\left[\sqrt{\rho(r)}\,\phi_{m,\ell_m}(r)\,\frac{\partial}{\partial r}\frac{\tilde{X}_{n,\ell_n}(r)}{\sqrt{\rho(r)}}\right] \\ & + \frac{\hbar^2}{2m_4}\frac{1}{2r^2}\Big(\ell_m(\ell_m+1) - \ell_n(\ell_n+1) - \ell_s(\ell_s+1)\Big)\phi_{m,\ell_m}\frac{\tilde{X}_{n,\ell_n}(r)}{\sqrt{\rho(r)}} \end{aligned} \tag{104}$$

and with the abbreviation for the integral over three spherical harmonics

$$\begin{bmatrix} \ell_m & \ell_n & \ell_s \\ m_m & m_n & m_s \end{bmatrix} := \sqrt{\frac{(2\ell_m+1)(2\ell_n+1)(2\ell_s+1)}{4\pi}} \begin{pmatrix} \ell_m & \ell_n & \ell_s \\ 0 & 0 & 0 \end{pmatrix} \begin{pmatrix} \ell_m & \ell_n & \ell_s \\ m_m & m_n & m_s \end{pmatrix}.$$

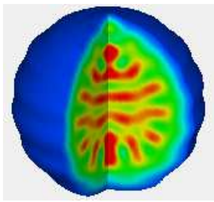

Because the other term ${}_aW^s_{mn}$ of the three-phonon matrix element W^s_{mn} is of the same form as ${}_bW^s_{mn}$ (see eq. (50)), the same steps lead to

$$\begin{aligned} {}_aW^{s\ell_s m_s}_{m\ell_m m_m,n\ell_n m_n} &= \frac{\hbar^2}{2m_4}\int d1\ \frac{\psi_s}{\sqrt{\rho}}\nabla\Big(\sqrt{\rho}\,\phi_m\cdot\nabla\frac{X_n}{\sqrt{\rho}}\ +\ (m\leftrightarrow n)\Big) \\ &= {}_aW^{s\ell_s}_{m\ell_m,n\ell_n}\begin{bmatrix}\ell_m & \ell_n & \ell_s\\ m_m & m_n & m_s\end{bmatrix}\end{aligned}$$

with

$${}_aW^{s\ell_s}_{m\ell_m,n\ell_n} = \int dr\ r^2\ \psi_{s,\ell_s}\big(\ F[\phi_{m,\ell_m},\phi_{n,\ell_n}](r)\ +\ F[\phi_{n,\ell_n},\phi_{m,\ell_m}](r)\ \big)\,.$$

In the expression for the self energy (52), neither the three-phonon vertices depend on the $\hat{J}_z$ quantum numbers m_i, except for the 3-j symbols, nor the energy denominator. This allows to carry out the summation over m_m and m_n using relation (256)

$$\begin{aligned} \Sigma^{t,\ell_t,m_t}_{s,\ell_s,m_s} &= \frac{1}{2}\sum_{mn}\sum_{\ell_m\ell_n}\sum_{m_m m_n}\frac{W^{s\ell_s m_s}_{m\ell_m m_m,n\ell_n m_n}W^{t\ell_t m_t\ *}_{m\ell_m m_m,n\ell_n m_n}}{\hbar(\omega_{m,\ell_m}+\omega_{n,\ell_n}-\omega)} \qquad (105)\\ &= \delta_{\ell_s,\ell_t}\delta_{m_s,m_t}\frac{1}{2}\sum_{mn}\sum_{\ell_m\ell_n}\frac{(2\ell_m+1)(2\ell_n+1)}{4\pi}\begin{pmatrix}\ell_m & \ell_n & \ell_s\\ 0 & 0 & 0\end{pmatrix}^2\frac{W^{s\ell_s}_{m\ell_m,n\ell_n}W^{t\ell_s\ *}_{m\ell_m,n\ell_n}}{\hbar(\omega_{m,\ell_m}+\omega_{n,\ell_n}-\omega)} \\ &= \delta_{\ell_s,\ell_t}\delta_{m_s,m_t}\Sigma^t_{s\ell_s} = \delta_{\ell_s,\ell_t}\delta_{m_s,m_t}\int dr\ r^2\ \psi_{s,\ell_s}(r)\,\Sigma_{\ell_s}(r,r')\,\psi_{t,\ell_t}(r')\,.\end{aligned}$$

The Kronecker δ's show that, indeed, in the equation of motion for the elastic channel (53) the radial and the angular dependence separate; thus the equation for the partial wave $\varphi_{\omega,\ell}$ is

$$H_\ell(r)\,\varphi_{\omega,\ell}(r) - \int dr'\,r'^2\ \Sigma_\ell(r,r')\,\varphi_{\omega,\ell}(r')\ =\ \hbar\omega\int dr'\,r'^2\ S_\ell(r,r')\,\varphi_{\omega,\ell}(r') \qquad (106)$$

which is not simply a generalized eigenvalue problem as Σ_ℓ depends on ω. This equation can be solved for $\hbar\omega < |\mu_4|$ and $> |\mu_4|$. In the first case, only a discrete set of solutions $\hbar\omega = E_i$ exists, and the iterative scheme to find E_i and $\varphi_{i,\ell}$ is given in detail in the appendix of [**CFK+94**]. The second case, which yields the scattering solutions we are interested in, is easier to deal with, because the equation can be solved for any given ω in a single step.

1.2. Impurity scattering

For excitations of an impurity, a further approximation is to discard terms involving $\tilde{X}(0,1,2)$. For the impurity calculations in droplets, ground state multi-particle quantities have been calculated in the Lekner approximation [**Lek70**], and before including more terms in the three-phonon matrix element, these quantities (such as $\tilde{X}(0,1,2)$) would have to be improved by a full optimization of the impurity wave function.

The three-phonon matrix element of the impurity self energy is basically ${}_aW^s_{mn}$ without symmetrization. Hence the self energy

$$\Sigma^\delta_{\gamma\ell_\gamma} = \sum_{\beta n}\sum_{\ell_\beta\ell_n}\frac{(2\ell_\beta+1)(2\ell_n+1)}{4\pi}\begin{pmatrix}\ell_\beta & \ell_n & \ell_\gamma\\ 0 & 0 & 0\end{pmatrix}^2\frac{W^{\gamma\ell_\gamma}_{\beta\ell_\beta,n\ell_n}W^{\delta\ell_\gamma\ *}_{\beta\ell_\beta,n\ell_n}}{t_{\beta,\ell_\beta}+\hbar\omega_{n,\ell_n}-\hbar\omega} \qquad (107)$$

with

$$
\begin{aligned}
W^{\gamma\ell_\gamma}_{\beta\ell_\beta,n\ell_n} &= \int dr\, r^2\, \eta_{\gamma\ell_\gamma}(r) \hat{D}^{\ell_\gamma}_{\ell_\beta,n\ell_n} \eta_{\beta\ell_\beta}(r) && (108)\\
\hat{D}^{\ell_\gamma}_{\ell_\beta,n\ell_n} &= \frac{\hbar^2}{2m_I}\Bigg\{ \frac{1}{2r^2}\Big(\ell_\beta(\ell_\beta+1) - \ell_n(\ell_n+1) - \ell_\gamma(\ell_\gamma+1)\Big) \frac{\tilde{X}_{n,\ell_n}(r)}{\sqrt{\rho(r)}} && (109)\\
&\quad - \frac{H(r)\tilde{X}_{n,\ell_n}(r)}{\sqrt{\rho(r)}} + \frac{\partial}{\partial r}\frac{\tilde{X}_{n,\ell_n}(r)}{\sqrt{\rho(r)}} \sqrt{\rho(r)}\frac{\partial}{\partial r}\frac{1}{\sqrt{\rho(r)}} \Bigg\}\\
H(r) &= -\frac{\hbar^2}{2m_I}\frac{1}{\sqrt{\rho(r)}}\frac{\partial}{\partial r}\rho(r)\frac{\partial}{\partial r}\frac{1}{\sqrt{\rho(r)}}
\end{aligned}
$$

and the equation to be solved for each partial wave is of the same form as (106) except for S

$$
H_\ell(r)\,\varphi_{\omega,\ell}(r) - \int dr'\, r'^2\, \Sigma_\ell(r,r')\,\varphi_{\omega,\ell}(r') = \hbar\omega\,\varphi_{\omega,\ell}(r)\,. \tag{110}
$$

2. Elastic Cross Section

The cross section $\frac{d\sigma_{\rm el}(k)}{d\Omega}$ of an incoming particle of momentum $\mathbf{k}$ for elastic scattering into a solid angle Ω can be immediately deduced from the asymptotic behaviour of the elastic channel wave function, eq. (98), and the well-known result is $\frac{d\sigma_{\rm el}(k)}{d\Omega} = |f(\theta)|^2$. This follows also from the first term of (81) and of (87), respectively: the elastic channel wave function φ is related to the linearized density fluctuation by $\frac{\delta\rho(\mathbf{r})}{\sqrt{\rho(\mathbf{r})}} = [S*\varphi](\mathbf{r})$. But for $r\to\infty$, the nonlocal part of $S(\mathbf{r},\mathbf{r}')$, $\sqrt{\rho(\mathbf{r})}[g(\mathbf{r},\mathbf{r}')-1]\sqrt{\rho(\mathbf{r}')}$, vanishes, hence

$$
\frac{\delta\rho(\mathbf{r})}{\sqrt{\rho(\mathbf{r})}} \stackrel{r\to\infty}{\longrightarrow} \varphi(\mathbf{r})
$$

and substituting (98) for $\frac{\delta\rho}{\sqrt{\rho}}$ in (81) and (87) yields the stated result for the scattered flux. From eqns. (96) – (98), we find the common expressions for the elastic scattering amplitude and the angle-integrated elastic cross section $\sigma_{\rm el}$

$$
\begin{aligned}
f(\theta) &= \frac{1}{2ik}\sum_{\ell=0}^{\infty}(2\ell+1)(S_\ell(k)-1)P_\ell(\cos\theta)\\
\frac{d\sigma_{\rm el}(k)}{d\Omega} &= |f(\theta)|^2\\
\sigma_{\rm el}(k) &= \int d\Omega\,\frac{d\sigma_{\rm el}(k)}{d\Omega} = \frac{\pi}{k^2}\sum_{\ell=0}^{\infty}(2\ell+1)|S_\ell(k)-1|^2
\end{aligned}
$$

and from calculating, by integrating over Ω, the flux lost in the elastic channel [**Sch88**], we obtain $\sigma_{\rm inel}(k)$, the cross section of all inelastic processes, and the total cross section $\sigma_{\rm tot}(k)$

$$
\begin{aligned}
\sigma_{\rm inel}(k) &= \frac{\pi}{k^2}\sum_{\ell=0}^{\infty}(2\ell+1)(1-|S_\ell(k)|^2) && (111)\\
\sigma_{\rm tot}(k) &= \sigma_{\rm el}(k)+\sigma_{\rm inel}(k) = \frac{2\pi}{k^2}\sum_{\ell=0}^{\infty}(2\ell+1)(1-\Re e\, S_\ell(k))\,.
\end{aligned}
$$

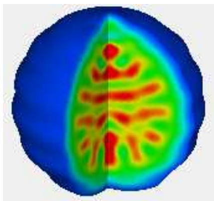

For impurity scattering, $\sigma_{\rm inel}$ is the sum of the absorption cross section and the inelastic scattering cross section

$$\text{for impurity:} \quad \sigma_{\rm inel}(k) = \sigma_{\rm insc}(k) + \sigma_{\rm ab}(k) \tag{112}$$

while the absorption cross section for ^{4}He vanishes, according to the orthogonality theorem, see section 2.2 of chapter 4. The theorem states that the scattering states are mutually orthogonal to the bound states of the N-body system. Hence, a particle (e.g. the incident impurity) cannot be absorbed without another particle (e.g. an ^{4}He atom) being ejected. In case of identical particle scattering, this process is of course indistinguishable from inelastic scattering of the incident particle. In order to seperate to two contributions to $\sigma_{\rm inel}$ for impurity scattering, the inelastic scattering cross section $\sigma_{\rm insc}$ will have to be calculated, from which $\sigma_{\rm ab}$ can finally be obtained using equation (112). This will be done in section 3.1.

2.1. Results for $\sigma_{\rm el}$ and $\sigma_{\rm inel}$

We have performed calculations of the scattering states of ^{4}He and ^{3}He scattered off droplets of $N = 70 \ldots 1000$ ^{4}He atoms. Here we report on the results for $\sigma_{\rm el}^{(X)}$ and $\sigma_{\rm inel}^{(X)}$, where the superscript $X = 4, 3$ discriminate between ^{4}He and ^{3}He.

The $\sigma_{\rm el}^{(X)}$ and $\sigma_{\rm inel}^{(X)}$ for ^{4}He and ^{3}He scattering are shown in Fig. 1 and 2. The energetically lowest droplet excitation is the quadrupole mode, below its energy $\sigma_{\rm inel}^{(X)} = 0$. The features of $\sigma_{\rm el}^{(X)}$ are discussed in the next two sections.

Table 1 lists the total cross sections $\sigma_{\rm tot} = \sigma_{\rm el} + \sigma_{\rm inel}$ for ^{4}He and ^{3}He with an impact energy of $E = 10\,$K and $E = 15\,$K, divided by a "classical" cross section $\sigma_{\rm class} = \pi R^2(N)$. The effective radius $R(N)$ is the sum of the radius of an equivalent droplet of density ρ_∞ *plus* the hard core radius of the interaction potential, $R(N) = r_0 + (3N/\rho_\infty 4\pi)^{1/3}$, $r_0 = 2.56\,$Å. The N-dependence of $\sigma_{\rm tot}$ can be fitted by the functional form $a_1\pi(R(N)+a_2)^2$ which yields, for 10K and 15K, $a_1 = 1.93; 1.84$ and $a_2 = 4.97; 6.17\,$Å for ^{4}He and $a_1 = 1.98; 2.21$ and $a_2 = 5.10; 4.25\,$Å for ^{3}He. Evidently, the scattering particle "sees" a target whose radius is larger than the equivalent hard sphere radius by the order of $a_2 \approx 5\,$Å. Furthermore, $\sigma_{\rm tot}$ is roughly twice as large as the classical cross section. This fits the picture that atoms scatter almost completely inelastically off large droplets, which would lead to $\sigma_{\rm tot} = 2\sigma_{\rm class}$ because of the forward diffraction contribution ("shadow scattering") [**Sch88**]. From the fit, we obtain $\sigma_{\rm tot} \to 29.9; 28.5\,N^{1/3}\,$Å^2 and $30.7; 34.2\,N^{1/3}\,$Å^2 for ^{4}He and ^{3}He, respectively, for $E = 10; 15$K and $N \to \infty$. But even the largest droplet ^{4}He$_{1000}$ is still far from the limiting behavior.

2.2. Coupling between bound states: Feshbach resonances

For incident energies $E < |\mu_4|$, where μ_4 is the chemical potential of ^{4}He, the equation $\hbar\omega - \hbar\omega_i - \hbar\omega_j = 0$ (^{4}He scattering), or $\hbar\omega - \hbar\omega_i - t_j = 0$ (^{3}He scattering) has solutions such that both, i and j label discrete, bound states. At such energies E, the real part of Σ diverges as $(\hbar\omega - \hbar\omega_i - \hbar\omega_j)^{-1}$, causing a peak in the elastic cross section. Fig.3 shows the elastic scattering cross section $\sigma_{\rm el}(E)$ of ^{4}He and ^{3}He scattered at one of the smaller

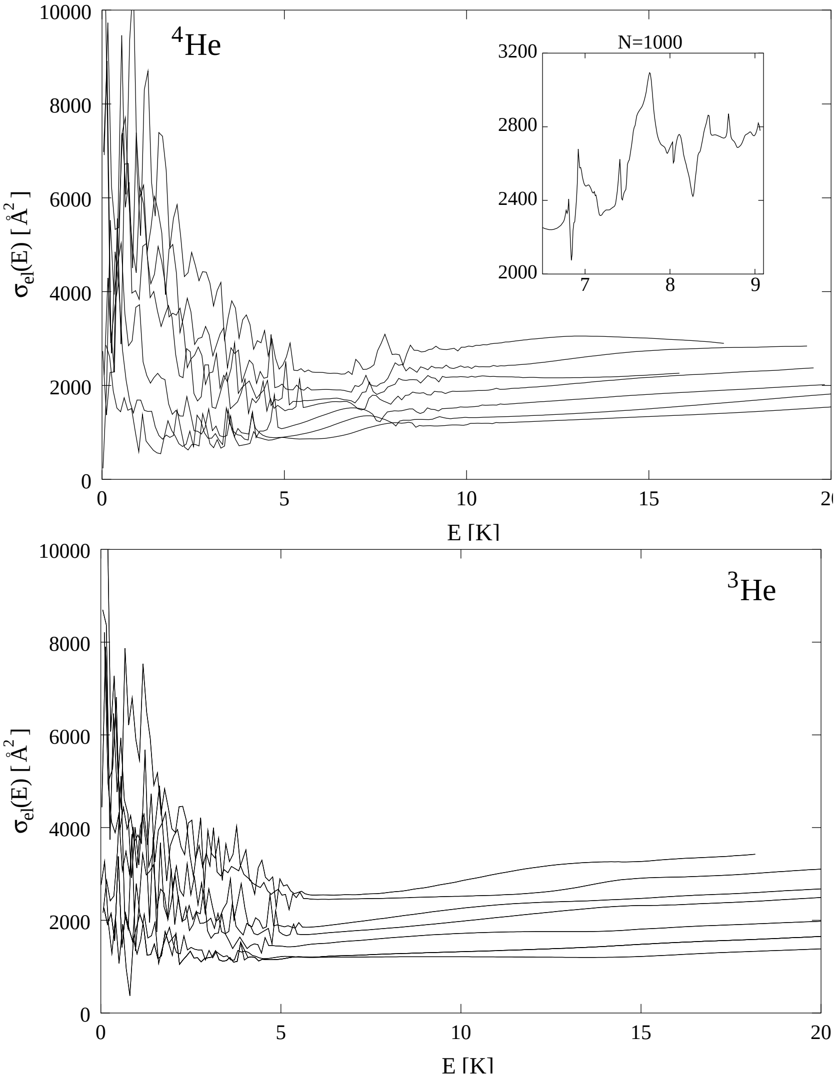

FIGURE 1. The elastic cross section $\sigma_{\mathrm{el}}^{(X)}$ is plotted as a function of the incoming energy for scattering of ^{4}He (top) and ^{3}He (bottom) off $^4\mathrm{He}_N$, $N = 70; 112; 200; 400; 500; 700; 1000$; larger values for $\sigma_{\mathrm{el}}^{(X)}$ correspond to larger N. The insert shows $\sigma_{\mathrm{el}}^{(4)}$ for $N = 1000$ at roton energies and above.

droplets ($N = 112$), where the resonance peaks can still be distinguished from each other. For large droplets, the number of bound droplet excitations n_B and of bound impurity states n_b^I increases, causing an according increase in the number of peaks n_σ in $\sigma_{\mathrm{el}}(E)$, given simply be all distinct combinations: $n_\sigma = n_B(n_B + 1)/2$ for ^{4}He scattering and $n_\sigma = n_B^I n_B$.

The peaks correspond to resonances, i.e. metastable states of the incident particle in the droplet. The mathematical background of these resonances has been already discussed in chapter 4. In the thermodynamic limit $N \to \infty$, the peaks become infinitely sharp and dense, and the life-time τ of the metastable states diverges. Only when N is large enough

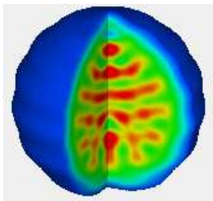

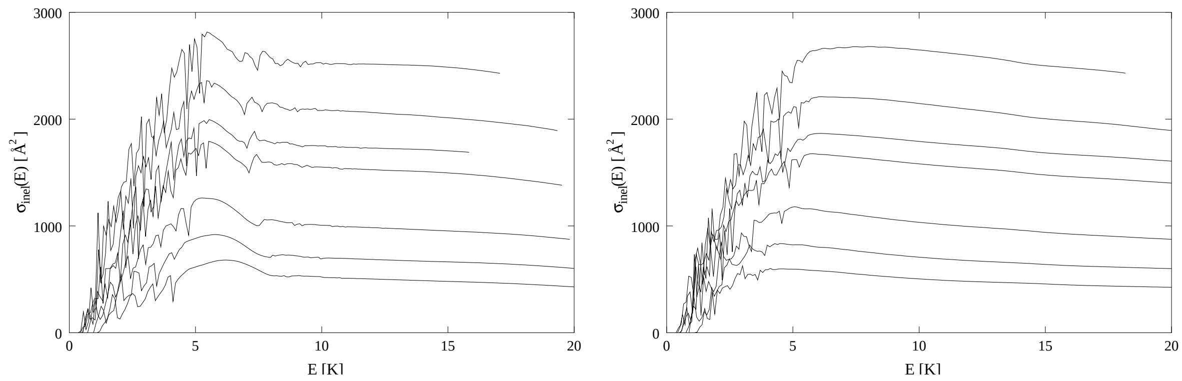

FIGURE 2. The inelastic cross section σ_{inel} is plotted as a function of the incoming energy for scattering of ^{4}He (left) and ^{3}He (right) off $^4\text{He}_N$, $N = 70; 112; 200; 400; 500; 700; 1000$.

N	$\sigma^{(4)}_{\text{tot}}/\sigma_{\text{class}}$	$\sigma^{(3)}_{\text{tot}}/\sigma_{\text{class}}$	$\sigma^{(4)}_{\text{tot}}/\sigma_{\text{class}}$	$\sigma^{(3)}_{\text{tot}}/\sigma_{\text{class}}$
70	3.91	3.99	4.22	3.89
112	3.64	3.67	3.93	3.84
200	3.35	3.62	3.64	3.62
400	3.05	3.17	3.26	3.37
500	3.07	3.17	3.07	3.25
700	2.87	2.99	3.05	3.15
1000	2.78	2.86	2.85	2.99
∞	1.93	1.98	1.84	2.21

TABLE 1. The total cross section $\sigma_{\text{tot}} = \sigma_{\text{el}} + \sigma_{\text{inel}}$ for ^{4}He and ^{3}He scattering off $^4\text{He}_N$, in units of the classical cross section σ_{class}. Incident energy is 10K (left) and 15K (right). The last line is an extrapolation obtained from a fit, see text.

that τ is longer than the duration of a scattering experiment, sticking of the droplet and the atom is observed.

The relations between the energy of two bound states, the according 3-phonon matrix element in Σ, and the features of the peaks in σ_{el} can be found in Feshbach's discussion of derivation of the optical potential from a coupled Hamiltonian [**Fes58**]. Large parts of his discussion can be applied to the elastic channel in our formulation of the N-body scattering problem, as the optical potential is of similar form as our self energy. To sum up the results of [**Fes58**]: the divergence in $\Sigma(E/\hbar)$ at an energy $E_{ij} = \hbar(\omega_i + \omega_j)$ leads to a Lorentzian shaped resonance peak in σ_{el}; the peak width and its energy shift relative to E_{ij} can be calculated in a straightforward manner by splitting Σ into the term responsible for the divergence of Σ

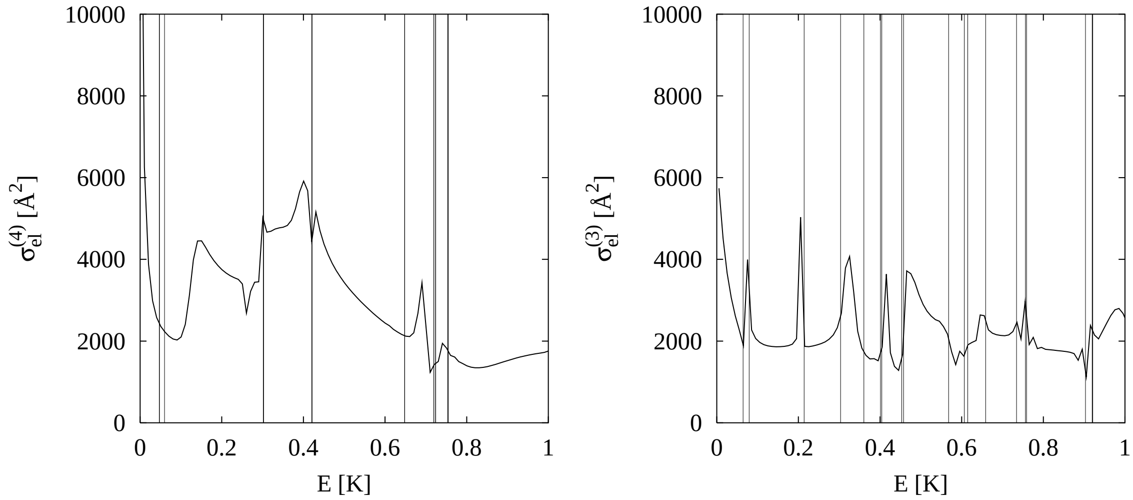

FIGURE 3. Elastic scattering cross section $\sigma_{\mathrm{el}}^{(X)}(E)$ of ^{4}He (left) and ^{3}He (right) scattering at $^4\mathrm{He}_{112}$, $E = 0 \ldots 1\mathrm{K}$. As reference, vertical lines are drawn at energies E, where the incident particle couples to two bound states, $E = \hbar\omega_n + \hbar\omega_m - |\mu|$ (left) and $E = \hbar\omega_n + t_m - |\mu_I|$ (right).

and the rest $\Sigma^{(ij)}$. For example for ^{4}He scattering, for the partial wave $\varphi_{\omega,\ell}$

$$[(H_\ell - \Sigma_\ell^{(ij)}(\omega) - \hbar\omega S_\ell) * \varphi_{\omega,\ell}](r) \;=\; \Lambda^{(ij)}\, W_\ell^{(ij)}(r) \tag{113}$$

and

$$\Lambda^{(ij)} \;=\; \frac{1}{\hbar}\,\frac{[W_\ell^{(ij)^*} * \varphi_{\omega,\ell}]}{\omega_i + \omega_j \;-\; \omega} \tag{114}$$

where $W_\ell^{(ij)}$ denotes the 3-phonon matrix element (times the square root of the prefactors according to eq. (105)) for the two discrete states i and j, *i.e.* the pole strength. Eqns (113) and (114) can be solved for $\varphi_{\omega,\ell}$ and $\Lambda^{(ij)}$:

$$\varphi_{\omega,\ell}(r) \;=\; \varphi_{\omega,\ell}^{(ij)}(r) \;+\; \Lambda^{(ij)}\,[G_\ell^{(ij)}(\omega) * W_\ell^{(ij)}](r) \tag{115}$$

which is inserted in eq. (114) and solved for $\Lambda^{(ij)}$,

$$\Lambda^{(ij)} \;=\; \frac{[W_\ell^{(ij)^*} * \varphi_{\omega,\ell}^{(ij)}]}{\hbar\omega_i + \hbar\omega_j \;-\; \hbar\omega \;-\; [W_\ell^{(ij)^*} * G_\ell^{(ij)}(\omega) * W_\ell^{(ij)}]} \tag{116}$$

$G_\ell^{(ij)}(\omega)$ is the Green's operator, $G_\ell^{(ij)}(\omega) = (H_\ell - \Sigma_\ell^{(ij)}(\omega) - \hbar\omega S_\ell)^{-1}$ and $\varphi_{\omega,\ell}^{(ij)}$ is the homogeneous solution of eq. (113). It is clear from eq. (115) that $\Lambda^{(ij)}$ is responsible for the resonance, and that the real and imaginary part of the convolution product in the denominator yield the energy shift and the width of the resonance, the first being determined by solving

$$\hbar\omega \;=\; \hbar\omega_i + \hbar\omega_j \;-\; \Re e[W_\ell^{(ij)^*} * G_\ell^{(ij)}(\omega) * W_\ell^{(ij)}]$$

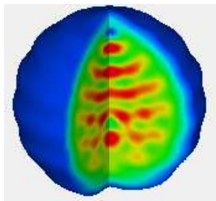

If two or more poles are close to each other on the ω-axis, the corresponding contributions are subracted from Σ.

In the case of helium scattering, however, the experimental energy resolution of the incoming beam is of the order of the incoming energy itself, hence there is no chance of resolving peaks in $\sigma_{\rm el}$. Even if a low-energy beam of helium of precise energy could be produced, one would still have to address the problem of producing ^{4}He droplets of a single size N. Therefore we have refrained from a detailed analysis of the peaks. In future work, it may be worthwile to analyse the density and life times of resonances with regard to the thermodynamic limit.

2.3. Quantum scattering: the ^{4}He$\longrightarrow$roton$\longrightarrow$^{4}He process

For the free ^{4}He surface, the observation of quantum emission and the associated possibility of measuring the presumed enhancement of the bose condensed fraction at the surface, has recently drawn some attention [**Wya98**]. Quantum emission is caused by the elastic scattering of an elementary excitation with an energy above the chemical potential at the free surface, where it transfers its energy and parallel momentum to an atom which is ejected. In the case of finite pure ^{4}He droplets, excited states of energy $E > |\mu_4|$ are by definition scattering states, hence quantum emission cannot be observed in a straightforward manner[1]. Nevertheless, the elastic scattering of ^{4}He at ^{4}He droplets bears some similarity, which tempts us to call it "quantum scattering": the incoming ^{4}He atoms is quantum absorbed and subsequently quantum emitted; in between it propagates as a phonon or roton, as we shall see now.

For $\hbar\omega > -\mu_4 - \mu_X$, $\sigma_{\rm el}^{(3)}$ is smooth, whereas $\sigma_{\rm el}^{(4)}$ has as series of peaks around $E = 8$K, the insert in Fig. 1 shows a zoom into this energy region. These peaks come from the coupling to the roton excitations of the droplet. Note that the roton excitation energy Δ lies above the chemical potential, hence rotons are scattering states. Therefore, for droplet sizes where $\Delta > -2\mu_4$, rotons constitute a second set of resonances, set apart from the Feshbach resonances, while for larger droplets, these two sets of resonances merge. But for small droplets, ^{4}He scattering is in theory a probe for detecting rotons: the ^{4}He atom enters the droplet, where it is converted to a roton, which travels through the droplet to be converted back to an atom, which is ejected and leaves the droplets in its ground state.

The transition density $\delta\rho(\mathbf{r};t)$ for a stationary scattering state of energy E also pictures the quantum scattering at elementary excitations, and especially the change from phonon-like to roton-like propagation, once $\hbar\omega$ reaches the roton energy. Fig.4 shows the transition densities of phonon and roton, for a large droplet of 1000 atoms, where the characteristics of phonons and rotons are seen best; for the $S(k,\omega)$ map of ^{4}He$_{1000}$ see figure 5 of chapter 3. For an incident energy below the roton energy, the elastically scattered ^{4}He atom propagates as a phonon, with a well-defined wave vector inside the droplet. A ^{4}He atom of roton energy

[1] Superposition of scattering states to a small wave packet which fits into the droplet and propagates towards the droplet surface might be similar to the experimental situation where a heater generates a statistical distribution of excitations.

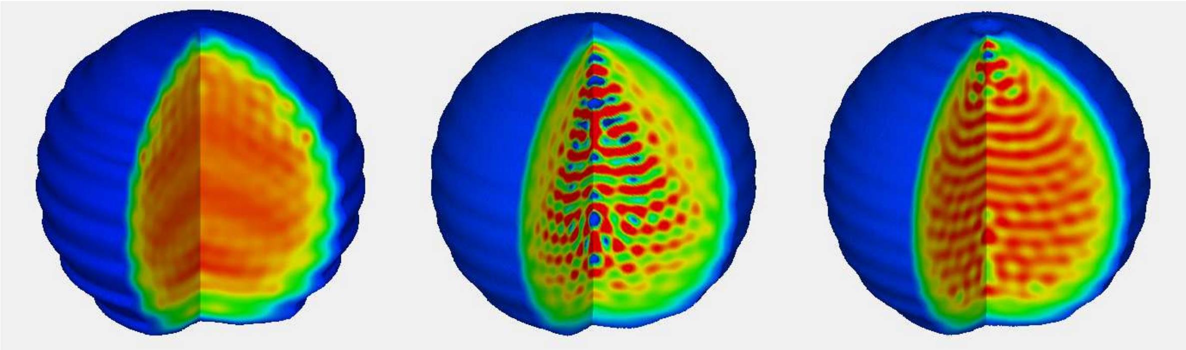

FIGURE 4. The transition density $\delta\rho(\mathbf{r};t)$ of a ${}^4\mathrm{He}_{1000}$ droplet, when an ^{4}He atom impinges from below with energy, from left to right, 5.3, 6.8 and 9.0 K.

not only leads to a much stronger density response (which illuminates the nature of the roton as a *resonance* much better than looking at roton in bulk ^{4}He), but the wave number inside the droplet rises rapidly to about 1.9Å^{-1}. Unlike the phonon scattering state, the roton scattering state has not yet reached the bulk form of a plane wave, but instead is still inhomogeneous.

In the right bottom corner, a short flip book animation shows $\delta\rho(\mathbf{r};t)$ at the roton resonance of a smaller droplet ($N = 112$).

2.3.1. Importance of the self energy. As the calculation of the self energy Σ is the numerically most demanding part of the cross section calculation, it is worth checking whether the influence of Σ is important, if only $\sigma_{\rm el}$ is sought (obviously, Σ is important for the calculation of $\sigma_{\rm inel}$ which would vanish without it). In Fig.5 $\sigma_{\rm el}$ and $\sigma_{\rm tot}$ is compared to $\sigma_{\rm el}$ calculated by omitting Σ in (53) — i.e., in Feynman approximation —, for scattering of ^{4}He at ${}^4\mathrm{He}_{150}$. The feature in $\sigma_{\rm el}(E)$ at about E=12K can be attributed to the roton which shows the familiar excess of the roton energy gap in Feynman approximation.

3. Inelastic Cross Sections

The remainder of the chapter is devoted to the derivation of inelastic cross sections from the second order currents which have been introduced in chapter 5, and to the results for ^{4}He and ^{3}He scattered off ^{4}He droplets. Specializing these currents for spherical geometry produces lengthy equations, even for the asymptotic current needed for the cross sections. Therefore, unlike in the previous sections, we begin with the simpler case of impurity scattering.

3.1. Impurity scattering

The inelastically scattered impurity atoms produce, at large distance from the droplet, the current given by the third term of (87),

$$\mathbf{j}^{(2)}_{\rm inel}(\mathbf{r}_0) \;=\; \frac{\hbar}{4m^I}\Im m \int d12\; S(1,2)\;\delta\tilde{u}^*(0,1)\,P(0)\,\delta\tilde{u}(0,2) \tag{117}$$

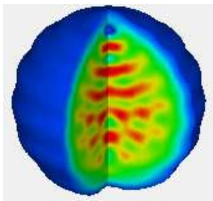

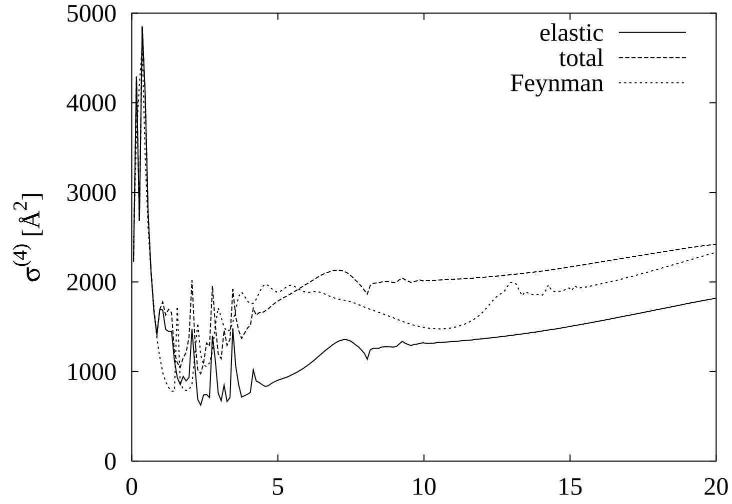

FIGURE 5. For ^{4}He (left) and ^{3}He (right) scattering at ^{4}He$_{150}$, the elastic cross section $\sigma_{\rm el}$ obtained in Feynman approximation (full line) is compared to $\sigma_{\rm el}$ (dashed) and $\sigma_{\rm tot}$ (dotted) in the full CBF calculation.

The fluctuating 2-body correlations are determined in the Euler-Lagrange equations derived in chapter 3. Writing equation (63) in coordinate space yields

$$\delta\tilde{u}(0,1) \equiv \sum_n \psi_n(1)\delta\tilde{u}^{(n)}(0) \tag{118}$$

with the "expansion coefficient"

$$\begin{aligned}
\delta\tilde{u}^{(n)}(0) &= \sum_\gamma \eta_\gamma(0)\frac{\sum_\delta W^\delta_{\gamma n} r_\delta}{t_\gamma + \hbar\omega_n - \hbar\omega} = \int d0'\ \varphi(0')\sum_\gamma \frac{\eta_\gamma(0)\hat{D}_n(0')\eta^*_\gamma(0')}{t_\gamma + \hbar\omega_n - \hbar\omega} \\
&= \frac{\hbar^2}{2m_I}\int d0' \left[\frac{1}{\sqrt{\rho(0')}}\nabla'_0 G^0(0,0';E-\hbar\omega_n)\sqrt{\rho(0')}\nabla'_0 X_n(0')\right]\varphi(0')
\end{aligned}$$

where G^0 is the single-particle Green's function of the Hartree equation (60). A more general formulation is obtained by tranforming the 3-phonon matrix elements to a channel operator acting in coordinate space,

$$W_n(0'',0') \equiv \frac{2m_I}{\hbar^2}\sum_{\gamma,\delta} W^\delta_{\gamma n}\eta_\gamma(0'')\eta^*_\delta(0') \tag{119}$$

which in the impurity case is actually the diagonal differential operator $\hat{D}_n(0')$. $\delta\tilde{u}^{(n)}$ becomes

$$\delta\tilde{u}^{(n)}(0) = \frac{\hbar^2}{2m_I}\int d0''d0'\ G^0(0,0';E-\hbar\omega_n)W_n(0'',0')\varphi(0')\,. \tag{120}$$

Inserting the expansion (118) in (117) and using the orthonormalization condition (44) of the Feynman states, $\int d12\ \psi_n(1)S(1,2)\psi_m(2) = \delta_{nm}$, we find for the asymptotic current

$$\begin{aligned}\mathbf{j}^{(2)}(\mathbf{r}_0) &= \mathbf{j}^{(2)}_{\rm el}(\mathbf{r}_0) + \mathbf{j}^{(2)}_{\rm inel}(\mathbf{r}_0) \;=\; \mathbf{j}^{(2)}_{\rm el}(\mathbf{r}_0) + \sum_n \mathbf{j}^{(2)}_n(\mathbf{r}_0) \\ &= \frac{\hbar}{4m^I}\Im m\Big\{\varphi^*(0)\,P(0)\,\varphi(0) \;+\; \sum_n \delta\tilde{u}^{(n)}(0)^*\,P(0)\,\delta\tilde{u}^{(n)}(0)\Big\} \qquad (121)\end{aligned}$$

The solution φ of the Schrödinger-like equation of motion (110) was called elastic channel wave function; accordingly, $\delta\tilde{u}^{(n)}$ will be called n–channel wave function or generally inelastic channel wave function.

Actually, one could have guessed the result (121) right from the start: from the discussion of scattering in the HNC-Euler-Lagrange theory, we know that, in the limit $r_0 \to \infty$ and otherwise arbitrary ^{4}He coordinates, the asymptotic excited many-body wave function is (remember $\delta\tilde{u}(0) \to \varphi(0)$ for $r_0 \to \infty$)

$$\begin{aligned}\delta\Phi(0,1,\ldots,N;t) &\stackrel{r_0\to\infty}{\longrightarrow} \varphi(0)\Phi_0^{(N)}(1,\ldots,N) + \sum_i \delta\tilde{u}(0,i)\Phi_0^{(N)}(1,\ldots,N) \\ &= \varphi(0)\Phi_0^{(N)}(1,\ldots,N) + \sum_n \delta\tilde{u}^{(n)}(0)\sum_i \psi_n(i)\Phi_0^{(N)}(1,\ldots,N)\end{aligned}$$

where $\psi_n(1,\ldots,N) := \sum_i \psi_n(i)\Phi_0^{(N)}(1,\ldots,N)$ is the excited many-body wave function in Feynman approximation[2]. It means that, for $r_0 \to \infty$, $\delta\Phi(t)$ factorizes into a product of N-body Feynman states $\psi_n(1,\ldots,N)$ for the background and single-body wave functions for the impurity, which are the channel wave functions:

$$\delta\Phi(0,1,\ldots,N) \;=\; \sum_{\rm open}\{\text{channel wave function}\}(\mathbf{r}_0)\;\times\;\{\text{Feynman state}\}(\mathbf{r}_1,\ldots,\mathbf{r}_N)$$

is the asymptotic limit of the $(N+1)$-body scattering wave in the HNC-Euler-Lagrange theory. The symbolic sum over open channels will be substantiated below.

Expressing $\delta\tilde{u}^{(n)}$ in terms of the Hartree Green's function turns out to be convenient if only the limit $r_0 \to \infty$ is of interest: for spherical symmetry, G^0 can be expanded in spherical harmonics,

$$G^0(\mathbf{r}_0,\mathbf{r}_0';\epsilon) \;=\; \sum_{\ell,m} Y_{\ell,m}(\Omega_0)\,G^0_\ell(r_0,r_0';\omega)\,Y^*_{\ell,m}(\Omega_0')$$

where the effectively *one-dimensional* G^0_ℓ has a simple analytic expression for positive energy ϵ

$$G^0_\ell(r_0,r_0';\epsilon) = -\frac{2m_I}{\hbar^2}\frac{1}{k}\eta_{k,\ell}(r_<)\chi^+_{k,\ell}(r_>)e^{i\delta_\ell(k)}$$

where $k = \sqrt{2m_I\epsilon/\hbar}$, $\delta_\ell(k)$ is the phase shift of the Hartree state $\eta_{k,\ell}$, and $\chi^+_{k,\ell}$ is the outgoing *irregular* solution of the Hartree equation; $r_< = \min(r_0,r_0')$ and $r_> = \max(r_0,r_0')$. For negative ϵ, G^0_ℓ decays exponentially, implying a closed channel. All definitions and properties of the single-particle Green's functions of the Hartree and Feynman equation are summarized in appendix B. With (109) and choosing for φ a stationary scattering state (96) — multiplied

[2] In fact, it is precicely the ansatz used by Feynman [**Fey54**].

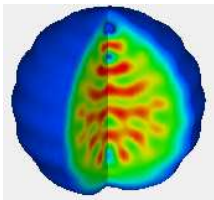

by 2 to account for the factor $\frac{1}{2}$ in the definition of the correlation operator, $\frac{1}{2}\delta U(t)$ —, the wave function of the *open* channel (n, ℓ_n, m_n), i.e. where $E > \hbar\omega_{n,\ell_n}$, is

$$\begin{aligned}
\delta\tilde{u}^{n,\ell_n,m_n}(\mathbf{r}_0) &= 8\pi \sum_{\ell,m}\sum_{\ell',m'} Y_{\ell',m'}(\Omega_0)\, Y^*_{\ell,m}(\Omega_{\mathbf{k}_\mathrm{in}})\, i^\ell \begin{bmatrix} \ell' & \ell_n & \ell \\ m' & m_n & m \end{bmatrix} \\
&\quad \times \int dr_0'\, {r_0'}^2\; \varphi_{k_\mathrm{in},\ell}(r')\, \hat{D}^\ell_{\ell',n\ell_n}(r_0')\, G^0_{\ell'}(r_0, r_0'; E - \hbar\omega_{n,\ell_n}) \\
&\stackrel{r_0\to\infty}{\longrightarrow} -8\pi \sum_{\ell,m}\sum_{\ell',m'} Y_{\ell',m'}(\Omega_0)\, Y^*_{\ell,m}(\Omega_{\mathbf{k}_\mathrm{in}})\, i^\ell \begin{bmatrix} \ell' & \ell_n & \ell \\ m' & m_n & m \end{bmatrix} \\
&\quad \times \chi^+_{k_\mathrm{out},\ell'}(r_0)\, e^{i\delta_{\ell'}(k_\mathrm{out})} \mathcal{W}^{k_\mathrm{in},\ell}_{k_\mathrm{out},\ell';n,\ell_n}
\end{aligned}$$

with the incident and the outgoing wave vectors

$$k_\mathrm{in} = \sqrt{2m_I E/\hbar^2} \tag{122}$$

$$k_\mathrm{out} = \sqrt{2m_I(E - \hbar\omega_{n,\ell_n})/\hbar^2} \tag{123}$$

the latter depending on the channel quantum numbers n and ℓ_n. $\mathcal{W}^{k_\mathrm{in},\ell}_{k_\mathrm{out},\ell';n,\ell_n}$ is the "renormalized" three-phonon matrix element

$$\mathcal{W}^{k_\mathrm{in},\ell}_{k_\mathrm{out},\ell';n,\ell_n} = \frac{2m_I}{\hbar^2}\int dr_0'\, {r_0'}^2\; \varphi_{k_\mathrm{in},\ell}(r_0')\, \hat{D}^\ell_{\ell',n\ell_n}(r_0')\, \frac{\eta_{k_\mathrm{out},\ell'}(r_0')}{k_\mathrm{out}} =: \frac{\mathcal{K}^{k_\mathrm{in},\ell}_{k_\mathrm{out},\ell';n,\ell_n}}{k_\mathrm{out}} \tag{124}$$

In the Distorted Wave Born approximation (DWBA)[3], $\varphi_{k_\mathrm{in},\ell}(r_0')$ is to be replaced by $\eta_{k_\mathrm{in},\ell}(r_0')$, and thus the above expression is approximated by the three-phonon matrix element (108)

$$\text{DWBA:} \qquad \mathcal{W}^{k_\mathrm{in},\ell}_{k_\mathrm{out},\ell';n,\ell_n} \longrightarrow \frac{2m_I}{\hbar^2}\frac{1}{k_\mathrm{in}k_\mathrm{out}} W^{k_\mathrm{in},\ell}_{k_\mathrm{out},\ell';n,\ell_n}\,.$$

As the calculation of $\varphi_{k_\mathrm{in},\ell}$ is numerically straigthforward once the self energy is calculated, there is, in this work, no reason for the application of the DWBA. The DWBA has been used in the calculation of the sticking coefficient for surface scattering and its validity has been discussed in [**CK92, CC92, CC98**].

From the asymptotic behaviour $\frac{1}{k}\chi^+_{k,\ell}(r) \to h^+_\ell(kr)$ (see appendix B), we see that $\delta\tilde{u}^{n,\ell_n,m_n}$ is a superposition of expanding spherical waves. Hence, only the radial component $\mathbf{e}_r\sqrt{\rho}\frac{\partial}{\partial r}\frac{1}{\sqrt{\rho}}$ of the vector operator $P(0)$ needs to be considered for large r_0, giving rise to a radially outflowing current — as it should be for scattering. Without loss of generality $\mathbf{k}_\mathrm{in}$ may be aligned with the z-axis. Then $Y^*_{\ell,m}(\Omega_{\mathbf{k}_\mathrm{in}}) = \delta_{m,0}\sqrt{(2\ell+1)/4\pi}$, which removes not only the sum over m, but also, thanks to the properties of the 3-j symbols, the sum over m'.

[3]In the DWBA, the interaction potential is split into two, $V = V_1 + V_2$, where the scattering solutions for $H = T + V_1$ are assumed to be known, and the effect of V_2 is treated in a Born series [**Tay72**]. For the elastic channel equation (110), DWBA means Born approximation with the Hartree solutions as the unperturbed states, i.e. $V_1 = V_H$, eq. (61) and $V_2 = \Sigma(\omega)$.

Inserting the asymptotic inelastic channel wave functions thus obtained into (121), and using $\chi^+_{k,\ell}(r) \to e^{i(kr-\ell\pi/2)}/r$ gives the inelastic asymptotic current

$$\mathbf{j}^{(2)}_{\mathrm{inel}}(\mathbf{r}_0) \;\to\; \frac{1}{r_0^2} \sum_{n,\ell_n,m_n}{}' \frac{\hbar k_{\mathrm{out}}}{m_I}\, |f_{n,\ell_n,m_n}(k_{\mathrm{in}},\Omega_0)|^2$$

with the inelastic scattering amplitude

$$f_{n,\ell_n,m_n}(k_{\mathrm{in}},\Omega_0) \;=\; 4\pi \sum_{\ell,\ell'} Y_{\ell',m_n}(\Omega_0)\, e^{i\delta_{\ell'}(k_{\mathrm{out}})}\, i^{\ell-\ell'} \sqrt{\frac{2\ell+1}{4\pi}} \begin{bmatrix} \ell' & \ell_n & \ell \\ -m_n & m_n & 0 \end{bmatrix} \mathcal{W}^{k_{\mathrm{in}},\ell}_{k_{\mathrm{out}},\ell';n,\ell_n} \tag{125}$$

where the primed sum denotes summation over all open channels, $E > \hbar\omega_{n,\ell_n}$).

The *differential inelastic cross section* is defined as the ratio between the current flowing throught an area element $r_0^2 d\Omega_0$ and the incident flux $\frac{\hbar k_{\mathrm{in}}}{m_I}$,

$$\frac{d\sigma_{\mathrm{insc}}(k_{\mathrm{in}})}{d\Omega_0} \;=\; \sum_{n,\ell_n,m_n}{}' \frac{k_{\mathrm{out}}}{k_{\mathrm{in}}} |f_{n,\ell_n,m_n}(k_{\mathrm{in}},\Omega_0)|^2 \tag{126}$$

The angle-integrated *inelastic scattering cross section*

$$\sigma_{\mathrm{insc}}(k_{\mathrm{in}}) \;=\; \int d\Omega_0\, \frac{d\sigma_{\mathrm{insc}}(k_{\mathrm{in}})}{d\Omega_0}$$

is calculated by making use of the orthonormalization of the spherical harmonics which appear in $f_{n,\ell_n,m_n}(k_{\mathrm{in}},\Omega_0)$ and of the relation (256). This removes all remaining interference terms in $|f_{n,\ell_n,m_n}(k_{\mathrm{in}},\Omega_0)|^2$, and the calculation of the total inelastic cross section simplifies to evaluating

$$\sigma_{\mathrm{insc}}(k_{\mathrm{in}}) \;=\; 4\pi \sum_{n,\ell_n}{}' \frac{k_{\mathrm{out}}}{k_{\mathrm{in}}} \sum_{\ell,\ell'} L(\ell_n,\ell,\ell')\, |\mathcal{W}^{k_{\mathrm{in}},\ell}_{k_{\mathrm{out}},\ell';n,\ell_n}|^2 \tag{128}$$

with

$$L(\ell_n,\ell,\ell') \;=\; \frac{(2\ell_n+1)(2\ell+1)(2\ell'+1)}{4\pi} \begin{pmatrix} \ell_n & \ell & \ell' \\ 0 & 0 & 0 \end{pmatrix}^2 .$$

Finally, the form of (126) suggests to define a channel-wise differential cross section

$$\frac{d\sigma_{n,\ell_n,m_n}(k_{\mathrm{in}})}{d\Omega_0} \;=\; \frac{k_{\mathrm{out}}}{k_{\mathrm{in}}} |f_{n,\ell_n,m_n}(k_{\mathrm{in}},\Omega_0)|^2 \tag{129}$$

for all open channels (n,ℓ_n,m_n). Although (129) is only an abbreviation at the moment, it is plausible that, for discrete, *i.e.* bound droplet states (n,ℓ_n,m_n), $\frac{d\sigma_{n,\ell_n,m_n}}{d\Omega_0}$ can be discerned from each other by measuring the outgoing momentum $\hbar k_{\mathrm{out}}$ of the inelastically scattered impurity, as will be seen in the results for ^{3}He scattering. Subtraction of the differential cross sections of channels corresponding to bound droplet states from (129) yields the impurity cross section for processes where both, the impurity atom and a ^{4}He atom leave the droplet.

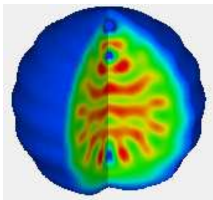

Writing $\sum_n = \int dn = \int \frac{dk_n}{\pi}$,

$$\frac{d\sigma_{\rm cont}(k_{\rm in})}{d\Omega_0} = \sum_{\ell_n, m_n} \int_0^{k_{\rm max}} \frac{dk_n}{\pi} \frac{k_{\rm out}}{k_{\rm in}} |f_{n,\ell_n,m_n}(k_{\rm in}, \Omega_0)|^2 \tag{130}$$

$$\sigma_{\rm cont}(k_{\rm in}) = 4\pi \sum_{\ell_n,\ell,\ell'} L(\ell_n, \ell, \ell') \int_0^{k_{\rm max}} \frac{dk_n}{\pi} \frac{k_{\rm out}}{k_{\rm in}} |\mathcal{W}^{k_{\rm in},\ell}_{k_{\rm out},\ell';n,\ell_n}|^2 \tag{131}$$

where $k_{\rm out}$ is given by (123) with $\hbar\omega_{n,\ell_n} = |\mu_4| + \frac{\hbar^2 k_n^2}{2m_4}$, and hence $k_{\rm max} = \sqrt{2m_4(E - |\mu_4|)/\hbar^2}$.

Unitarity The N-body Hamiltonian is of course hermitean, which implies the unitarity of the S-matrix [**Tay72**]. This means that the incoming flux of particles is divided into open channels, with weights determined by the dynamics, and no flux is lost. Although the N-body excitation wave functions in the HNC-Euler-Lagrange theory are only approximations, we have shown in section 5 of chapter 5 that the second order currents fulfill current conservation: impurity currents everywhere; ^{4}He currents only in the asymptotic regime, which is all we need for scattering cross sections. As mentioned in chapter 5, other channels which might be open at a given incident energy and through which flux would be lost, are simply not contained in the ansatz for the excited wave function $e^{\delta U(t)/2}\Phi_0$.

Therefore, calculation of $\sigma_{\rm insc}$, and of the inelastic cross section $\sigma_{\rm inel}$, eq. (111), allows to determine the *ab-/adsorption cross section*

$$\sigma_{\rm ab}(k_{\rm in}) = \sigma_{\rm inel}(k_{\rm in}) - \sigma_{\rm insc}(k_{\rm in}) \tag{132}$$

which is the difference between the number of *all* particles losing energy (removed from the elastic channel) and of those retaining enough energy to leave the droplet, divided by the areal density of incoming particles. In fig. 6, the definitions of the various cross sections are illustrated.

It is instructive to return to the effective Schrödinger equation for the elastic channel wave function (110) which serves to provide an alternative to the determination of the inelastic cross section from (111). It is convenient, though not necessary, for the following to express the self energy (107) in terms of the Hartree Green's function, as done in eq. (68) generically. For droplets the impurity self energy becomes, in r-space,

$$\Sigma(\mathbf{r}_0, \mathbf{r}_0') = \sum_{\ell,m} Y_{\ell,m}(\Omega_0)\, \Sigma_\ell(r_0, r_0')\, Y^*_{\ell,m}(\Omega_0') \tag{133}$$

with the partial components

$$\Sigma_\ell(r_0, r_0') = \sum_{n,\ell_n} \sum_{\ell'} \frac{L(\ell_\beta, \ell_n, \ell)}{2\ell+1} \hat{D}^\ell_{\ell',n\ell_n}(r_0)\, G^0_{\ell'}(r_0, r_0'; E - \hbar\omega_{n,\ell_n}) \left[\hat{D}^\ell_{\ell',n\ell_n}(r_0')\right]^+ \tag{134}$$

If the stationary scattering solution $\varphi_{\mathbf{k}_{\rm in}}$ to (110) is multiplied with (110) itself and integrated over a large sphere of radius R enclosing the droplet, the imaginary part of the resulting

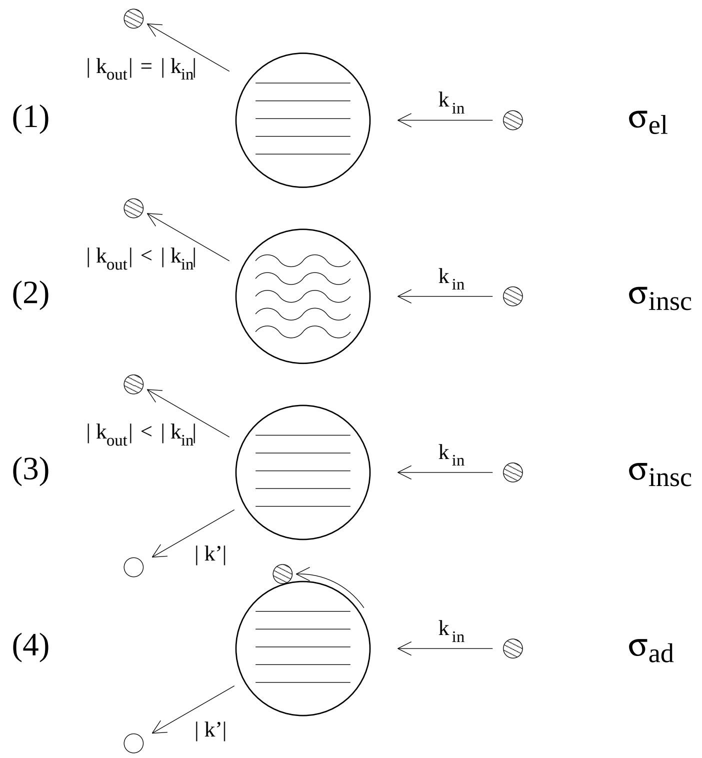

FIGURE 6. For impurity scattering, four types of processes contribute to σ_{el}, σ_{insc}, and σ_{ad}; see also section 1.3 of chapter 4.

equation is

$$-\frac{\hbar^2}{2m_3}\Im m \int_R d^3r_0\ \varphi^*_{\mathbf{k}_{\mathrm{in}}}(\mathbf{r}_0)\nabla^2\varphi_{\mathbf{k}_{\mathrm{in}}}(\mathbf{r}_0) \;=\; \Im m \int_R d^3r_0 \int_\infty d^3r'_0\ \varphi^*_{\mathbf{k}_{\mathrm{in}}}(\mathbf{r}_0)\Sigma(\mathbf{r}_0,\mathbf{r}'_0)\varphi_{\mathbf{k}_{\mathrm{in}}}(\mathbf{r}'_0)$$

The *lhs* can be partially integrated and is proportional to the surface integral over the combined incoming and outgoing elastic current, i.e. the loss rate of particles in the elastic channel, which is of course the negative of the inelastic cross section. For the rhs, $\varphi_{\mathbf{k}_{\mathrm{in}}}$ and Σ are expanded, see (96) and (133). This yields

$$\sigma_{\mathrm{inel}}(k_{\mathrm{in}}) \;=\; 4\pi\left(\frac{\hbar^2 k_{\mathrm{in}}}{2m_I}\right)^{-1}\sum_\ell \int dr_0^3 \int dr_0'^{\,3}\ (2\ell+1)\,\varphi^*_{\omega,\ell}(r_0)\,\Im m\ \Sigma_\ell(r_0,r'_0)\,\varphi_{\omega,\ell}(r'_0)$$

The imaginary part of Σ stems from (*i*) the imaginary part of the Green's function G^0_ℓ for positive energy argument; (*ii*) the integration of the continuous Feynman basis $\sum_n$ over the poles of $G^0_\ell(\omega)$ at the bound state energies t_i of the impurity in the droplet in Hartree approximation (60). The latter contribution to dissipation (as seen from the elastic channel) accounts for the absorption channels generating σ_{ab}, while the first one describes inelastic scattering, producing σ_{insc}. Accordingly we define $\Im m\,\Sigma^{\mathrm{insc}}$ and $\Im m\,\Sigma^{\mathrm{ab}}$ as those two contributions to $\Im m\,\Sigma$

$$\Im m\,\Sigma \;=\; \Im m\,\Sigma^{\mathrm{insc}} + \Im m\,\Sigma^{\mathrm{ab}}$$

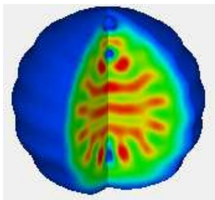

If we use (134) and that, for positive energy argument $\epsilon = \frac{\hbar^2 k^2}{2m_I}$, the imaginary part of G^0 is

$$\Im m\ G^0_\ell(r_0, r_0'; \omega) = -\left(\frac{\hbar^2 k}{2m_I}\right)^{-1} \eta_{k,\ell}(r_0)\, \eta_{k,\ell}(r_0')$$

then comparison with (128) shows that the absorption and inelastic scattering cross section can indeed be calculated separately (and thus providing an alternative to calculating $\sigma_{\rm insc}$ according to eq. (128) which will be used for checking the numerical accuracy)

$$\begin{aligned} \sigma_{\rm insc}(k_{\rm in}) &= 4\pi \left(\frac{\hbar^2 k_{\rm in}}{2m_I}\right)^{-1} (2\ell+1) \\ &\times \sum_\ell \int\!\!\int dr_0^3 dr_0'^{\,3}\ \varphi^*_{\omega,\ell}(r_0)\, \Im m\, \Sigma^{\rm insc}_\ell(r_0, r_0')\, \varphi_{\omega,\ell}(r_0') \qquad (135) \\ \sigma_{\rm ab}(k_{\rm in}) &= 4\pi \left(\frac{\hbar^2 k_{\rm in}}{2m_I}\right)^{-1} (2\ell+1) \\ &\times \sum_\ell \int\!\!\int dr_0^3 dr_0'^{\,3}\ \varphi^*_{\omega,\ell}(r_0)\, \Im m\, \Sigma^{\rm ab}_\ell(r_0, r_0')\, \varphi_{\omega,\ell}(r_0') \qquad (136) \end{aligned}$$

We will see in the next section, about ^{4}He scattering, how this result is modified for identical particle scattering.

***T*-matrix formulation** The inelastic scattering amplitude (125) can be cast into a form reminiscent of expressions involving the T-matrix which are found in the literature [**Mes85, Tay72, GW67**]. Instead of the full expansion in spherical harmonic in (125), only the Green's function G^0 is expanded in eq. (120), which is necessary for writing G^0 as a product of the regular and the irregular solution. Then the inelastic channel wave function asymptotically becomes

$$\delta\tilde{u}^{(n)}(0) \to f_n(k_{\rm in}, \theta_0) \frac{e^{ik_{\rm out} r_0}}{r_0}$$

where the amplitude for scattering from $\mathbf{k}_{\rm in}$ to $\mathbf{k}_{\rm out}$, both spanning an angle θ_0, can be written without referring to the specific set of chosen quantum numbers (although is was necessary as an intermediary step)

$$f_n(k_{\rm in}, \theta_0) = (\eta^-_{\mathbf{k}_{\rm out}} | W_n | \varphi_{\mathbf{k}_{\rm in}}) = (\eta^-_{\mathbf{k}_{\rm out}} | \hat{D}_n^+ | \varphi_{\mathbf{k}_{\rm in}})$$

where $k_{\rm out}$ is determined by energy conservation, W_n is defined by (119), and $\hat{D}^+_n$ is the adjoint of $\hat{D}_n$, eq. (65),

$$\hat{D}^+_n = \frac{\hbar^2}{2m_I} \sqrt{\rho(0)}\, \nabla \frac{\tilde{X}_n(0)}{\sqrt{\rho(0)}}\, \nabla \frac{1}{\sqrt{\rho(0)}}$$

$\eta^-_{\mathbf{k}_{\rm out}}$ is a stationary scattering state solution of the Hartree equation, normalized similarily to $\varphi_{\mathbf{k}}$, except that asymptotically $\eta^-_{\mathbf{k}_{\rm out}}$ is the sum of a plane wave and a *converging* spherical wave:

$$\eta^\pm_{\mathbf{k}}(\mathbf{r}_0) = \sum_{\ell,m} i^\ell Y^*_{\ell,m}(\Omega_{\mathbf{k}}) Y_{\ell,m}(\Omega) e^{\pm i\delta_\ell(k)} \frac{\eta_{\ell,k}(r)}{k} \to e^{i\mathbf{k}\mathbf{r}_0} + f^\pm(\theta) \frac{e^{\pm ikr_0}}{r_0}$$

The T-matrix is the transition operator defined such that its matrix elements with respect to two reference states (the Hartree solutions in our case) are the transition amplitudes between the two reference states. To obtain the inelastic contributions to the T-matrix, we simply need to formally express $\varphi_{\mathbf{k}}$ in terms of which $\eta^{+}_{\mathbf{k}}$, using the Green's function G of the *full* equation of motion of the elastic channel (110)

$$\varphi_{\mathbf{k}} \;=\; \eta^{+}_{\mathbf{k}} \;+\; G(\omega)\,\Sigma(\omega)\,\eta^{+}_{\mathbf{k}}$$

yielding for the inelastic scattering amplitude for channel n

$$f_n(k_{\rm in},\theta) \;=\; (\eta^{-}_{\mathbf{k}_{\rm out}}\,|\,W_n\,(1+G(\omega)\,\Sigma(\omega))\,|\,\eta^{+}_{\mathbf{k}_{\rm in}}) \tag{137}$$

which is the "on-shell" matrix element[4] of the transition operator of channel n defined as

$$T_n \;=\; W_n\,(1+G(\omega)\,\Sigma(\omega))$$

where T_n is an operator acting in the single-particle space of the elastic channel. The inelastic scattering cross section in terms of T is given by eq. (126)

$$\frac{d\sigma_{\rm insc}(k_{\rm in})}{d\Omega_0} \;=\sum_n{}' \frac{k_{\rm out}}{k_{\rm in}}\left|(\eta^{-}_{\mathbf{k}_{\rm out}}\,|\,W_n|\,\varphi_{\mathbf{k}_{\rm in}})\right|^2 \;=\sum_n{}' \frac{k_{\rm out}}{k_{\rm in}}\left|(\eta^{-}_{\mathbf{k}_{\rm out}}\,|\,T_n|\,\eta^{+}_{\mathbf{k}_{\rm in}})\right|^2 \tag{138}$$

3.2. Rearrangement collisions: ejection of ^{4}He

For incident energies larger than $E = |\mu_4| - |\mu_I|$ (which is positive for ^{3}He scattering), an ^{4}He atom can be ejected from the droplet, giving rise to a current whose general expression was given in (89). The ^{4}He current per incoming impurity current defines a cross section.

The derivation is very similar to the one of the ^{3}He scattering cross section, and we only point out the differences: instead of (118), the fluctuations of the 2-body correlations is expanded with respect to the impurity coordinate in the Hartree basis, in terms of which the asymptotic ^{4}He current (89) is expressed as a sum of all "channels", which now are labelled by the Hartree quantum numbers,

$$\begin{aligned}
\delta\tilde{u}(0,1) &= \sum_\alpha \eta_\alpha(0)\,\delta\tilde{u}_\alpha(1)\\
\mathbf{J}^{(2)}(\mathbf{r}_1) &= \frac{\hbar}{4m_4}\Im m\Big\{\sum_\alpha \delta\tilde{u}^*_\alpha(1)\,P(1)\,\delta\tilde{u}_\alpha(1)\Big\}
\end{aligned}$$

In the expression for $\delta\tilde{u}_\alpha(1)$, summation over the Feynman states yields the single-body Green's function of the Feynman equation. Due to the non-locality of the Feynman equation, the partial Green's functions $G^0_\ell(r_1,r_1';\omega)$ do not separate into a product of two appropriate solutions to eigenvalue $\hbar\omega$ for arbitrary r_1, r_1', but they do for $r_1\to\infty$ or $r_1'\to\infty$; see appendix B for details. The cross section for ejecting ^{4}He after impact of an impurity is given

[4] "On-shell" means on the shell of energy $\hbar\omega$, i.e. refers to the fact that the outgoing wave vector is chosen to fulfill energy conservation.

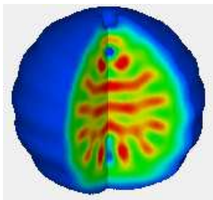

by the outgoing ^{4}He current divided by the incoming impurity current per area. Following the same steps as for the derivation of $\sigma_{\rm insc}$, we find

$$\sigma^{(4)}_{\rm insc}(k_{\rm in}) \;=\; \frac{m_4}{m_I}\,4\pi \sum_{\alpha,\ell'}{}' \frac{k_{\rm out}}{k_{\rm in}} \sum_{\ell,\ell_n} L(\ell_n,\ell,\ell') \left| \frac{\mathcal{K}^{k_{\rm in},\ell}_{\alpha,\ell';k_{\rm out},\ell_n}}{k_{\rm out}} \right|^2 \tag{139}$$

where now the outgoing wave vector is given by $\sqrt{2m_4(\hbar\omega - |\mu_4| - t_{\alpha,\ell'})/\hbar^2}$. Comparison of the inelastic ^{3}He and ^{4}He scattering cross sections of the respective *continous* channels, defined in (131), reveals a simple relation between them (but not between the respective differential cross sections). The transformation $k' = \sqrt{2m_I(\hbar\omega - |\mu_I| - |\mu_4| - \hbar^2 k_n^2/2m_4)/\hbar^2}$ in the k_n-integral of (131) shows that

$$\sigma_{\rm cont}(k_{\rm in}) \;=\; \sigma^{(4)}_{\rm cont}(k_{\rm in})$$

which is, in fact, the trivial statement that the probability of (i) the ^{3}He atom being inelastically scattered and ejecting a ^{4}He atom equals the probability of (ii) the ejection of a ^{4}He atom but leaving enough energy for the ^{3}He atom for not being trapped in the droplet; hence the difference between $\sigma_{\rm cont}$ or $\sigma^{(4)}_{\rm cont}$ is just the perspective.

3.3. Identical particle scattering

In analogy to impurity scattering, we apply the results for the second order currents to the calculation of inelastic cross sections, which are contained in the second term of (81),

$$\mathbf{j}^{(2)}_{\rm inel}(1) \;=\; \frac{\hbar}{4m_4}\Im m \int d23\; S(2,3)\;\delta\tilde u^*(1,2)\,P(1)\,\delta\tilde u(1,3)\,. \tag{140}$$

The 2-body correlation fluctuation $\delta\tilde u_2$, which is equated to the fluctuation of the direct correlation $\delta\tilde X$ in the uniform limit, is expanded in the Feynman states, see (48)

$$\delta\tilde u(1,2) \;=\; \sum_{mn} \psi_m(1)\psi_n(2)\delta\tilde X_{mn} \;=:\; \sum_m \delta\tilde X_m(1)\psi_m(2)$$

where $\delta\tilde X_m$ are now the inelastic channel wave functions. We find for (140)

$$\mathbf{j}^{(2)}_{\rm inel}(1) \;=\; \frac{\hbar}{4m_4}\Im m \sum_m \delta\tilde X^*_m(1)\,P(1)\,\delta\tilde X_m(1)\,.$$

$\delta\tilde X_{mn}$ is obtained from the 2-body Euler-Lagrange equation (48), with r_s calculated from (106). In order to solve (48) for $\delta\tilde X_{mn}$, the same approximation, namely neglecting the operator $T^{mn,st}$, is applied. Hence, upon insertion of the orthonormalization relation of the Feynman states, the wave function of channel m becomes

$$\delta\tilde X_m(1) \;=\; \int d1'\;\delta\tilde X_m(1,1')\,\varphi(1') \;=\; \int d1'\;\sum_n \frac{\psi_n(1)W_{mn}(1')}{\hbar(\omega_m+\omega_n-\omega)}\,\varphi(1')\,. \tag{141}$$

As for impurity scattering, $\delta\tilde X_m$ can be expressed in terms of a single-particle Green's function. Before deriving the working formulas, we define the three-phonon matrix operator in coordinate space

$$W_m(1'',1') \equiv \frac{2m_4}{\hbar^2}\sum_n \psi_n(1'')W_{mn}(1') = \frac{2m_4}{\hbar^2}\sum_{ns}\psi_n(1'')W^s_{mn}\phi^*_s(1')$$

which is non-diagonal, unlike the corresponding impurity operator. The sum over n in (141) yields the Green's function of the Feynman equation,

$$\delta\tilde{X}_m(1) \;=\; \int d1'd1''\;{}_{\psi\phi}G^0(1,1'';E-\hbar\omega_m)W_m(1'',1')\varphi(1') \tag{142}$$

where the "dressed" Green's function ${}_{\psi\phi}G^0$ is defined in (268) in the appendix B.

Now, the 3-phonon matrix element is

$$\begin{aligned} W_{mn}(1) \;&=\; \frac{\hbar^2}{2m_4}\frac{1}{\sqrt{\rho(1)}}\nabla\cdot\Big[\phi_m(1)\sqrt{\rho(1)}\nabla\frac{\tilde{X}_n(1)}{\sqrt{\rho(1)}} + \;(m\leftrightarrow n)\Big] \\ &\quad - H(1)\int d23\;\phi_m(2)\phi_n(3)\,\tilde{X}(1,2,3) \end{aligned}$$

which yields for $\delta\tilde{X}_m(1,1')$, which is implicitly defined in eq. (141),

$$\delta\tilde{X}_m(1,1') \;=\; \delta_a\tilde{X}_m(1,1') \;+\; \delta_b\tilde{X}_m(1,1')$$

with

$$\begin{aligned} \delta_a\tilde{X}_m(1,1') \;&=\; \frac{\hbar^2}{2m_4}\frac{1}{\sqrt{\rho}}\nabla'\sqrt{\rho}\Big[{}_{\psi\phi}G^0(1,1';E-\hbar\omega_m)\nabla'\frac{[\tilde{X}*\phi_m](1')}{\sqrt{\rho}} \\ &\qquad\qquad +\phi_m(1')\nabla'\frac{[{}_{\psi\phi}G^0(E-\hbar\omega_m)*\tilde{X}](1,1')}{\sqrt{\rho}}\Big] \\ \delta_b\tilde{X}_m(1,1') \;&=\; -H(1')\int d23\;{}_{\psi\phi}G^0(1,2;E-\hbar\omega_m)\phi_m(3)\tilde{X}(1',2,3) \\ &=\; \sum_{sn}\phi_s(1')\int d2\;{}_{\psi\phi}G^0(1,2;E-\hbar\omega_m)\psi_n(2)\,{}_bW^s_{mn} \end{aligned}$$

where ${}_bW^s_{mp}$ is given by (101). Without assigning a real physical meaning to the two terms, we note that $\delta_a\tilde{X}_m$ describes the coupling to mode m via the 2–body direct correlation $X(1,2)$, and $\delta_b\tilde{X}_m$ describes coupling via the 3–body generalisation of $X(1,2)$, $X(1,2,3)$, both of which are determined in the ground state calculation. We remember that $\delta_b\tilde{X}_m$ is neglected in inelastic ^{3}He scattering and rearrangement collisions, derived in the two previous sections.

Specifically for the droplet geometry, we use the expansion in spherical harmonics obtained in section 1.1. As noted in the previous section, the expansion coefficients of ${}_{\phi\psi}G^0(1',1)$, ${}_{\phi\psi}G^0_\ell(r'_1,r_1)$, factorize into a product of two solutions of the Feynman equation, if at least one of the arguments, r_1 or r'_1, go to infinity. Then ${}_{\phi\psi}G^0_\ell(r'_1,r_1)$ is given by (267), *i.e.*

$$\begin{aligned} {}_{\phi\psi}G^0(2,1;\epsilon) \quad&=\quad \sum_{\ell',m'} Y_{\ell',m'}(\Omega_2)\,{}_{\phi\psi}G^0_{\ell'}(r_2,r_1)\,Y^*_{\ell',m'}(\Omega_1) \\ {}_{\phi\psi}G^0_{\ell'}(r_2,r_1) \quad&\overset{r_1\to\infty}{\longrightarrow}\quad -\frac{2m}{\hbar^2 k_\epsilon}\,\phi_{\epsilon,\ell'}(r_2)\,\psi^+_{\epsilon,\ell'}(r_1)\,e^{i\delta_{\ell'}(k_\epsilon)}\,. \end{aligned} \tag{143}$$

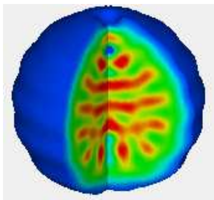

We find for $\delta_a\tilde{X}_m(\mathbf{r}_1) \equiv \delta_a\tilde{X}_{m,\ell_m,m_m}(\mathbf{r}_1)$, in the limit $r_1 \to \infty$,

$$\delta_a\tilde{X}_{m,\ell_m,m_m}(\mathbf{r}_1) \;=\; 8\pi \sum_{\ell,m} i^\ell Y^*_{\ell,m}(\Omega_{\mathbf{k}_{\rm in}}) \int dr'_1 {r'_1}^2\; \delta_a\tilde{X}^{\ell,m}_{m,\ell_m,m_m}(r_1,r'_1,\Omega)\,\varphi_{k_{\rm in},\ell}(r'_1)$$

with

$$\delta_a\tilde{X}^{\ell,m}_{m,\ell_m,m_m}(r_1,r'_1,\Omega) \;\stackrel{r_1\to\infty}{\longrightarrow}\; \sum_{\ell_n,m_n} \frac{2m_4}{\hbar^2 k_{\rm out}}\, Y_{\ell_n,m_n}(\Omega) \begin{bmatrix} \ell & \ell_n & \ell_m \\ -m & m_n & m_m \end{bmatrix} \times$$
$$e^{i\delta_{\ell_n}(k_{\rm out})}\; \psi^+_{k_{\rm out},\ell_n}(r_1)\, \Big(\; F[\phi_{k_{\rm out},\ell_n},\phi_{m,\ell_m}](r'_1) + F[\phi_{m,\ell_m},\phi_{k_{\rm out},\ell_n}](r'_1)\;\Big)$$

where the functional F is defined in eq. (104) and the incident and outgoing wave vectors are

$$k_{\rm in} \;=\; \sqrt{\frac{2m_4 E}{\hbar^2}} \tag{144}$$

$$k_{\rm out} \;=\; \sqrt{\frac{2m_4(E-\hbar\omega_{m,\ell_m})}{\hbar^2}}\,. \tag{145}$$

As for impurity scattering, $\varphi(\mathbf{r})$ has been assumed to be a stationary scattering state, i.e. of the form (96), and ψ^+ is the asymptotically outgoing irregular solution of the Feynman equation.

For $\delta_b\tilde{X}_m(1)$

$$\sum_{sn} \phi_s\; {}_bW^s_{mn} \int d2\;\, {}_{\phi\psi}G^0(2,1;\omega-\omega_m)\psi_n(2)$$

the stationary scattering state is expanded in the Feynman basis

$$\int d1\;\varphi_{\mathbf{k}_{\rm in}}(1)\,\varphi_s(1) \equiv \phi_s\;, \qquad \varphi_{\mathbf{k}_{\rm in}}(1) = \sum_s \varphi_s\psi_s(1)\;;$$

in spherical symmetry,

$$\int d1\;\varphi_{\mathbf{k}_{\rm in}}(1)\,\phi_s(1) = 4\pi i^{\ell_s} Y^*_{\ell_s,m_s}(\Omega_{\mathbf{k}_{\rm in}}) \int dr\;\varphi_{k_{\rm in},\ell_s}(r)\phi_{s,\ell_s} \equiv 4\pi i^{\ell_s} Y^*_{\ell_s,m_s}(\Omega_{\mathbf{k}_{\rm in}})\varphi^{k_{\rm in}}_{s,\ell_s}$$

and for large r_1, the Green's function acting on ψ_n can be simplified using (143). Orthogonality of $\phi_{\epsilon,\ell'=,\ell_n}$ and ψ_{n,ℓ_n} in the ℓ_n–subspace can be used:

$$\int d2\;\, {}_{\phi\psi}G^0(2,1;E-\hbar\omega_m)\psi_n(2) \;\stackrel{r_1\to\infty}{\longrightarrow}\; -\delta(k_{\rm out}-k_n)\,\frac{2m_4}{\hbar^2 k_{\rm out}}\,\psi^+_{k_{\rm out},\ell_n}(r_1)\; e^{i\delta_{\ell_n}(k_{\rm out})}$$

and $\delta_b\tilde{X}_m(1)$ becomes

$$\delta_b\tilde{X}_{m,\ell_m,m_m}(\mathbf{r}_1) \;=\; \sum_{s,\ell_s,m_s}\sum_{\ell_n,m_n} 4\pi i^{\ell_s}\, Y^*_{\ell_s,m_s}(\Omega_{\mathbf{k}_{\rm in}})\,\varphi^{k_{\rm in}}_{s,\ell_s}\,\frac{2m_4}{\hbar^2 k_{\rm out}}\, e^{i\delta_{\ell_n}(k_{\rm out})}\,\psi^+_{k_{\rm out},\ell_n}(r_1)$$
$$\times\; Y_{\ell_n,m_n}(\Omega_1)\;{}_bW^{s\ell_s}_{m\ell_m;k_{\rm out}\ell_n} \begin{bmatrix} \ell_m & \ell_n & \ell_s \\ m_m & m_n & m_s \end{bmatrix}\,.$$

For ${}_bW^{s\ell}_{m\ell_m;k_{\rm out}\ell_n}$, we insert $k_{\rm out}$ (145) in equation (103) to obtain

$${}_bW^{s\ell}_{m\ell_m;k_{\rm out}\ell_n} = \frac{\omega_{s,\ell_s}}{\omega+\omega_{s,\ell_s}}\; V_{m\ell_m,k_{\rm out}\ell_n,s\ell}\,.$$

Evidently, for large incident energy, the triplet contribution to the inelastic scattering cross section vanishes as $\frac{1}{\omega}$. See Fig.7 for a comparison of the elastic and inelastic ^{4}He cross sections, including and omitting triplet correlations, respectively.

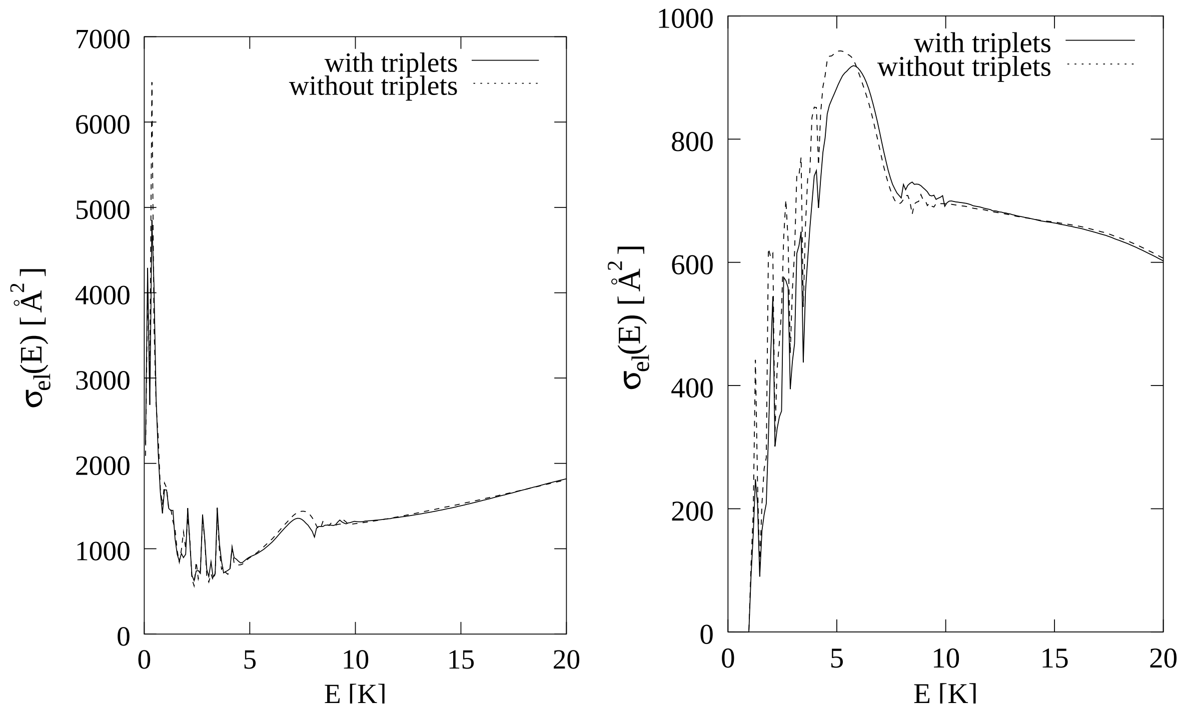

FIGURE 7. $\sigma_{\rm el}(E)$ and $\sigma_{\rm insc}(E)$ for ^{4}He scattering at $^4{\rm He}_{112}$, calculated with (full) and without (dashed) triplet correlations in eq. (147).

The calculation of the ^{4}He cross section proceeds in the same way as for ^{3}He scattering: $\Omega_{\mathbf{k}_{\rm in}}$ points into the z-direction, and the outgoing Feynman wave function assumes its asymptotic plane wave form, $\psi^+_{k_{\rm out},\ell_n}(r) \to \frac{1}{r} e^{ik_{\rm out}r - i\ell_n\pi/2}$. The asymptotic inelastic current is again split into kinetic part and probability part

$$\begin{aligned}
\mathbf{j}^{(2)}_{\rm inel}(r_1,\Omega_1) &= \frac{\hbar}{4m_4}\Im m \sideset{}{'}\sum_{m,\ell_m,m_m} \delta\tilde{X}^*_{m,\ell_m,m_m}(r_1,\Omega_1)\nabla_1\delta\tilde{X}_{m,\ell_m,m_m}(r_1,\Omega_1) \\
&\to \frac{\mathbf{e}_{r_1}}{r_1^2} \sideset{}{'}\sum_{m,\ell_m,m_m} \frac{\hbar k_{\rm out}}{m_4}\,|f_{m,\ell_m,m_m}(k_{\rm in},\Omega_1)|^2
\end{aligned}$$

with the amplitude

$$\begin{aligned}
f_{m,\ell_m,m_m}(k_{\rm in},\Omega) &= 4\pi\sum_{\ell,\ell_n} i^{\ell-\ell_n} e^{i\delta_{\ell_n}(k_{\rm out})}\sqrt{\frac{2\ell+1}{4\pi}}\,Y_{\ell_n,m_m}(\Omega)\begin{bmatrix}\ell & \ell_n & \ell_m \\ 0 & -m_m & m_m\end{bmatrix} \\
&\qquad\times\left[{}_a\mathcal{W}^{k_{\rm in},\ell}_{k_{\rm out},\ell_n;m,\ell_m} + {}_b\mathcal{W}^{k_{\rm in},\ell}_{k_{\rm out},\ell_n;m,\ell_m}\right]
\end{aligned}$$

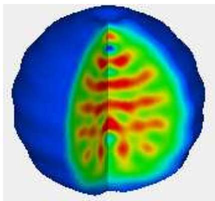

and the three-phonon matrix elements

$$
\begin{aligned}
{}_a\mathcal{W}^{k_{\rm in},\ell}_{k_{\rm out},\ell_n;m,\ell_m} &= \frac{2m_4}{\hbar^2}\int drr^2\ \varphi_{k_{\rm in},\ell}(r)\Big(\ F[\frac{\phi_{k_{\rm out},\ell_n}}{k_{\rm out}},\phi_{m,\ell_m}](r)+F[\phi_{m,\ell_m},\frac{\phi_{k_{\rm out},\ell_n}}{k_{\rm out}}](r)\ \Big)\\
{}_b\mathcal{W}^{k_{\rm in},\ell_s}_{k_{\rm out},\ell_n;m,\ell_m} &= \frac{2m_4}{\hbar^2 k_{\rm out}}\sum_s \varphi^{k_{\rm in}}_{s,\ell_s}\ {}_bW^{s\ell_s}_{m\ell_m;k_{\rm out}\ell_n}\,.
\end{aligned}
$$

In terms of the above quantities, the differential inelastic cross section for ^{4}He is of the same form as for ^{3}He scattering

$$
\frac{d\sigma_{\rm insc}(k_{\rm in})}{d\Omega_1} = \sum_{m,\ell_m,m_m}{}' \frac{k_{\rm out}}{k_{\rm in}}\,|f_{m,\ell_m,m_m}(k_{\rm in},\Omega_1)|^2 \tag{146}
$$

and the inelastic cross section irregardless of scattering angle is

$$
\sigma_{\rm insc}(k_{\rm in}) = 4\pi\sum_{m,\ell_m}{}'\frac{k_{\rm out}}{k_{\rm in}}\sum_{\ell_s,\ell_n}L(\ell_m,\ell_s,\ell_n)\,|\mathcal{W}^{k_{\rm in},\ell_s}_{k_{\rm out},\ell_n;m,\ell_m}|^2\,. \tag{147}
$$

Unitarity From the equation of motion (106), we can calculate the flux of particles missing in the elastic channel, just as we did for impurity scattering: mulitplication with $\varphi_{k_{\rm in},\ell}$ and integration yields for the imaginary part

$$
\begin{aligned}
\sigma_{\rm inel}(k_{\rm in}) &= 4\pi\left(\frac{\hbar^2 k_{\rm in}}{2m_4}\right)^{-1}\Im m\sum_\ell\int dr^3\int dr'^3\ (2\ell+1)\,\varphi^*_{\omega,\ell}(r)\,\Sigma_\ell(r,r')\,\varphi_{\omega,\ell}(r')\\
&= 4\pi\left(\frac{\hbar^2 k_{\rm in}}{2m_4}\right)^{-1}\frac{1}{2}\Im m\sum_{\ell_m,\ell_n,\ell}\sum_{m,n}L(\ell,\ell_m,\ell_n)\,\frac{|\frac{\hbar^2 k_n}{2m}\,\mathcal{W}^{k_{\rm in},\ell_s}_{n,\ell_n;m,\ell_m}|^2}{\hbar(\omega_{m,\ell_m}+\omega_{m,\ell_m}-\omega)}
\end{aligned}
$$

where eq. (105) was used. The connection to (147) is made by splitting the sum over the radial quantum number m and n into discrete and continuous spectrum, respectively,

$$
\begin{aligned}
\sum_{m,n} &= \sum_{i_m,i_n} + \sum_{i_m}\int\frac{dk_n}{\pi} + \int\frac{dk_m}{\pi}\sum_{i_n} + \int\frac{dk_m}{\pi}\int\frac{dk_n}{\pi}\\
&= \sum_{i_m,i_n} + 2\sum_{i_m}\int\frac{dk_n}{\pi} + \int\frac{dk_m}{\pi}\int\frac{dk_n}{\pi}\,.
\end{aligned}
$$

The purely discrete sums do not contribute to $\sigma_{\rm inel}$, and the integrals are to be regarded as

$$
\frac{1}{f(k)} = P\frac{1}{f(k)} + i\frac{\pi}{|f'(k_0)|}\delta(k-k_0)
$$

Thus we obtain

$$
\begin{aligned}
\sigma_{\rm inel}(k_{\rm in}) = 4\pi\sum_{\ell_m,\ell_n,\ell}{}' L(\ell,\ell_m,\ell_n)\,\Big[\ &\sum_{i_m}\frac{k_{\rm out}}{k_{\rm in}}|\mathcal{W}^{k_{\rm in},\ell_s}_{k_{\rm out},\ell_n;i_m,\ell_m}|^2\\
&+\frac{1}{2}\int\frac{dk_m}{\pi}\,\frac{k_{\rm out}}{k_{\rm in}}\,|\mathcal{W}^{k_{\rm in},\ell_s}_{k_{\rm out},\ell_n;k_m,\ell_m}|^2\ \Big]
\end{aligned} \tag{148}
$$

where $k_{\rm out}$ is the root of the energy denominator of the self energy, i.e. is given by energy conservation eq. (145). Recalling impurity scattering, $\sigma_{\rm inel}$ obtained in the same way turned out to be the sum of both, scattering, $\sigma_{\rm insc}$, and absorption, $\sigma_{\rm ab}$. For identical particle scattering, $\sigma_{\rm ab}$ of course vanishes due to the orthogonality theorem, see section 2.2, which requires that if the incident particle is absorbed, another particle must be ejected; since they are all identical, this process contributes to $\sigma_{\rm insc}$, and therefore by definition $\sigma_{\rm ab} = 0$.

However, despite $\sigma_{\rm ab} = 0$, $\sigma_{\rm inel}$ does not equal $\sigma_{\rm insc}$, but the contributions of continuum–continuum channels, *i.e.* where both, the scattered particle and the droplet excitation have energy $> |\mu_4|$, differ by a factor 1/2. Again, this difference is a trivial consequence of the identity of scattering and droplet particles:

Eq. (147) : sums the flux of all scattering products coming from the droplet, because this is how (147) was calculated: as the expectation value of the particle current operator. This flux contains contributions from bound–continuum channels (one particle escapes), as well as from continuum–continuum channels (two particle escape and *both contributing to the flux equally*). This is what a spherical detector surrounding the target would measure.

Eq. (148) : is the flux missing from the elastic channel. Therefore, in continuum–continuum channels, only one of the particles (or due to symmetry, both of them with a weight 1/2) are counted as detection event, detection meaning here that it was lost from the incoming beam of particles.

Eq. (148) is the common definition of the inelastic cross section, therefore we apply the factor $\frac{1}{2}$ to the continuum–continuum channels for the inelastic ^{4}He scattering cross section. Fig.8 shows the difference between $\sigma_{\rm inel}$ and $\sigma_{\rm insc}$ for a range of incident energies E: for energies below the chemical potential, $E < |\mu_4|$, those channels are closed, and $\sigma_{\rm inel}$ and $\sigma_{\rm insc}$ are equal.

T-matrix formulation As for impurity scattering, we close the section with giving a formal expression for the inelastic scattering cross section, *i.e transition* probabilities for inelastic processes, im terms of a T-matrix. The steps leading to the T-matrix are exactly the same as in section 3.1, resulting in

$$\frac{d\sigma_{\rm insc}(k_{\rm in})}{d\Omega_1} = \sum_n{}' \frac{k_{\rm out}}{k_{\rm in}} \left|(\phi^-_{\mathbf{k}_{\rm out}}\,|\,W_n|\,\varphi_{\mathbf{k}_{\rm in}})\right|^2 = \sum_n{}' \frac{k_{\rm out}}{k_{\rm in}} \left|(\phi^-_{\mathbf{k}_{\rm out}}\,|\,T_n|\,\psi^+_{\mathbf{k}_{\rm in}})\right|^2 \tag{149}$$

where $\phi^\pm_{\mathbf{k}_{\rm out}}$ and $\psi^\pm_{\mathbf{k}_{\rm out}}$ are the analog to $\eta^\pm_{\mathbf{k}_{\rm out}}$ for the Feynman equation, and where we formally solved the elastic channel equation

$$\varphi_{\mathbf{k}} = \psi^+_{\mathbf{k}} + G(\omega)\,\Sigma(\omega)\,\psi^+_{\mathbf{k}}$$

with $G(\omega) = [H - \Sigma - \hbar\omega S]^{-1}$. Hence, the T-matrix for channel n has the same form as for impurity scattering,

$$T_n = W_n\,(1 + G(\omega)\,\Sigma(\omega))\,.$$

3.4. Representation of inelastic cross sections

Before we report on the results, we introduce convenient representations of the inelastic differential cross section $\frac{d\sigma_{\rm insc}(k_{\rm in})}{d\Omega}$ for ^{4}He and ^{3}He scattering.

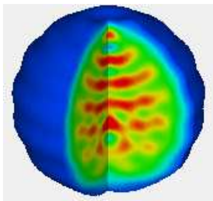

3.4.1. Spatio-kinetic distribution function. The doubly differential inelastic cross section bins the outgoing particles not only with respect to their direction, but also to their momentum,

$$\frac{d^2\sigma_{\rm insc}(k_{\rm in})}{dkd\Omega} = \sum_{n,\ell_n,m_n}{}' \delta(k-k_{\rm out})\frac{k_{\rm out}}{k_{\rm in}}|f_{n,\ell_n,m_n}(k_{\rm in},\Omega)|^2 \tag{150}$$

The spatio-kinetic distribution function $dp/d\mathbf{k}$ is obtained by omitting the quotient of the outgoing and incoming wave numbers in eq. (150), *i.e.* it is the probability for the incoming particle of energy $E_{\rm in}$ to be scattered into a momentum $\mathbf{k}=(k,\Omega)$.

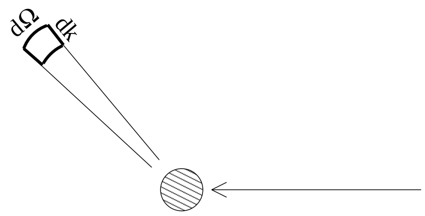

Evidently, $\frac{d^2\sigma_{\rm insc}(k_{\rm in})}{dkd\Omega}$ or $dp/d\mathbf{k}$ are more suitable quantities than the merely spacial distribution $\frac{d\sigma_{\rm insc}(k_{\rm in})}{d\Omega}$ if one is interested in the excitation energies E_i of the target: by energy conservation, they are given by the energy lost by the particle, $E_i=\hbar^2k_{\rm in}^2/2m-\hbar^2k^2/2m$.

Note that $dp/d\mathbf{k}$ directly corresponds to a spatial representation of the scattered flux because $\mathbf{r}=\hbar\mathbf{k}t/m$ is the location of the scattered particles a time t after the event (disregarding very long-lived metastable states which would shift t by the life-time of the state).

$dp/d\mathbf{k}$ can be defined channelwise, e.g. $dp_{\rm ripplon}/d\mathbf{k}$, which is helpful in analyzing the numerical data, although of course in experiment the detector signal cannot be assigned to separate channels.

3.4.2. Energy and momentum transfer. A simple transformation of $dp(\omega)/d\mathbf{k}$ yields the probability for a particle of incident energy $E_{\rm in}$ to transfer energy E_t and momentum

$$k_t=|\mathbf{k}_{\rm in}-\mathbf{k}_{\rm out}|=\sqrt{k_{\rm in}^2+k_{\rm out}^2-2k_{\rm in}k_{\rm out}\cos\theta} \tag{151}$$

to the droplet: similarly to the dynamic structure function $S(k,E)$, which is — apart from kinematic factors — the inelastic neutron scattering cross section, we define an atom cross section $\sigma(k_t,E_t)$ in the same fashion and have good reason to expect to gain similar information about the excitations of the target as from $S(k,E)$.

$$\sigma(k_t,E_t) = 2\pi\sum_{m,\ell_m,m_m}{}'\int d(\cos\theta)\ \delta(k_t-|\mathbf{k}_{\rm in}-\mathbf{k}_{\rm out}|)\ \delta(E_t-(E_{\rm in}-E_{\rm out})) \tag{152}$$

$$\times\ \frac{k_{\rm out}}{k_{\rm in}}\ |f_{m,\ell_m,m_m}(k_{\rm in},\Omega)|^2$$

$$= 2\pi\frac{k_t}{k_{\rm in}^2}\sum_{m,\ell_m}{}'\delta(E_t-(E_{\rm in}-E_{\rm out}))\sum_{m_m}|f_{m,\ell_m,m_m}(k_{\rm in},\Omega)|^2 \tag{153}$$

where in numerical calculations $\sigma(k,E)$ is obtained by binning with respect to the E-dependence, or weighted with a function $w(E-E')$, $\int dE'\,w(E-E')\,\sigma(k,E')$, see below.

In contrast to $S(k,E)$, $\sigma(k_t,E_t)$ cannot be expected to be independent of incident energy. For slow thermal neutrons, the energy $E_{\rm in}$ is too low to resolve the bare interaction potential between neutron and the atoms of the target, but is still high enough to excite the target. This is not the case for ^{3}He scattering at ^{4}He droplets.

The cross section for energy transfer, irregardless of momentum transfer, is

$$\sigma(E_t) \equiv \int dk_t \sigma(E_t, k_t)\,.$$

4. Results for inelastic scattering

4.1. Inelastic scattering cross section $\sigma_{\rm insc}$

The inelastic scattering cross section of $^4{\rm He}_N$ for ^{4}He and ^{3}He is calculated according to eq. (148) and (128), respectively. As the absorption cross section for ^{4}He vanishes, $\sigma_{\rm insc}$ as obtained from unitarity (eq. (148)) reproduces the inelastic cross section (111), which is defined as the number of inelastically scattered particles *lost* from the beam of incoming particles. If, however, $\sigma_{\rm insc}$ is simply calculated from the inelastic current (147), it differs for energies higher than the chemical potential, $E > |\mu_4|$. Both cross sections are compared in Fig. 8 for $^4{\rm He}_{112}$; it depends on the type of experiment which one is measured.

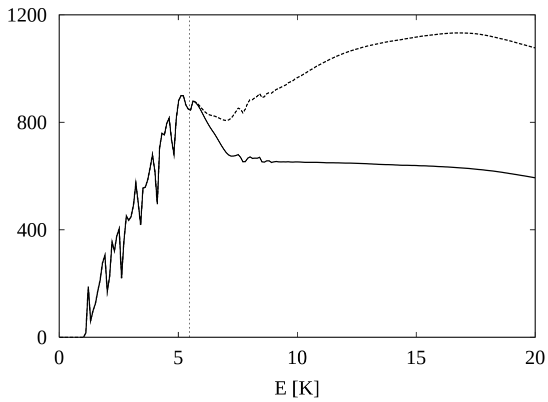

FIGURE 8. $\sigma_{\rm insc}(E)$ for ^{4}He scattering at $^4{\rm He}_{112}$, determined from unitarity (full) and from the whole inelastic current (dashed). The vertical line separates $E < |\mu_4|$ from $E > |\mu_4|$.

For ^{3}He scattering, Fig. 9 shows the inelastic scattering cross section $\sigma_{\rm insc}(E)$ and the adsorption cross section $\sigma_{\rm ad}(E)$ of $^4{\rm He}_N$. In that figure, eq. (135) and (136) are used to calculate the two cross sections, the sum of which reproduces $\sigma_{\rm inel}(E)$ by definition. Unitarity can achieve this level of consistency of the respective calculation of the inelastic cross section and of the self energy only for full cross sections, but not for differential cross sections, discussed below. Therefore, we take the opportunity to compare $\sigma_{\rm insc}(E)$ as obtained by eq. (135) with $\sigma_{\rm insc}(E)$ as obtained by eq. (128). This is done in Fig. 10 for ^{4}He scattered at $^4{\rm He}_{112}$, where $\sigma_{\rm insc}(E) = \sigma_{\rm inel}(E)$. The result of this test is not very satisfactory. The reason for the discrepancy is that the matrix elements in eq. (128) contain Feynman states

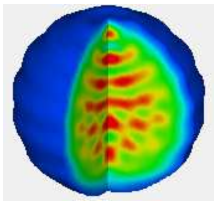

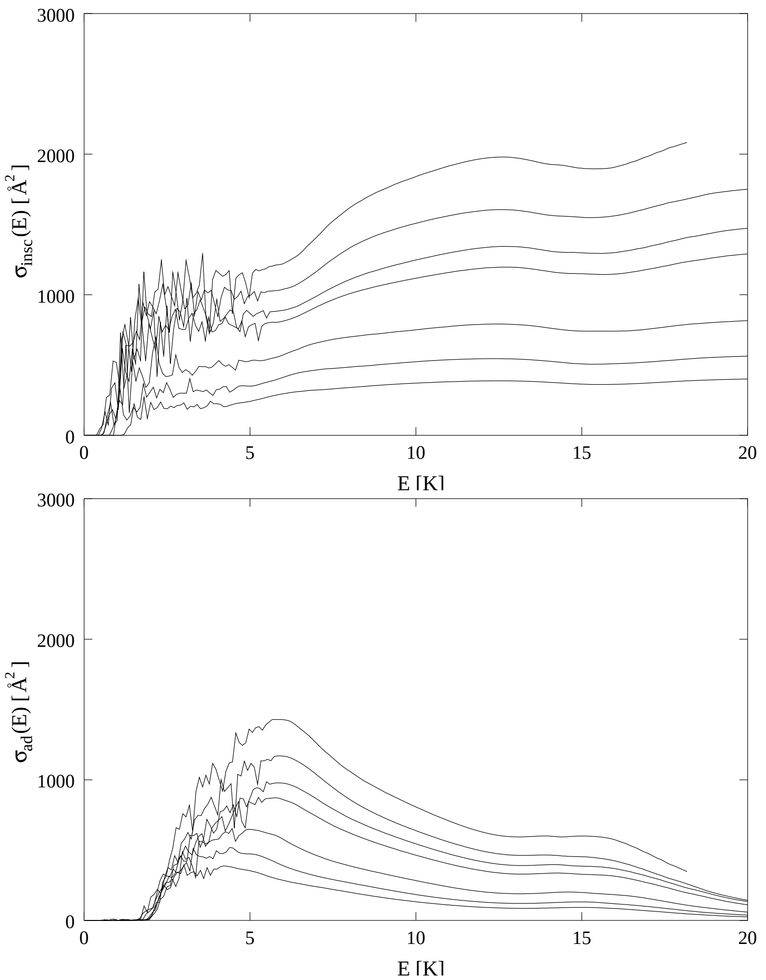

FIGURE 9. The inelastic *scattering* cross section $\sigma_{\rm insc}(E)$ and the adsorption cross section $\sigma_{\rm ad}(E)$ for ^{3}He scattering off $^4{\rm He}_N$, as a function of incident energy E; $N = 70; 112; 200; 400; 500; 700; 1000$. The threshold energy for the opening of inelastic scattering channels is the excitation energy of the quadrupole mode, and the chemical potential difference $|\mu_4| - |\mu_3|$ for the adsorption channels.

(for ^{4}He scattering) / impurity Hartree states (^{4}He scattering) of energy $\frac{\hbar^2 k_{\rm out}^2}{2m}$, given by energy conservation; in contrast, the self energy $\Im m\,\Sigma$ is calculated using a complete basis of Feynman/Hartree solutions in a large box (approx. 5 times droplet radius). The spikes for lower energies are caused by shape resonances of the Hartree potential, which shift to higher energies for increasing angular momentum ℓ; in general, these resonances are less pronounced for the solutions confined to the box. For higher scattering energies, the results of the two formlulas converge, because coupling to low-energy virtual scattering states becomes negligible; resonances at high energies, $E > 10$K, are not sharp anymore, and the explained numerical effect is less severe.

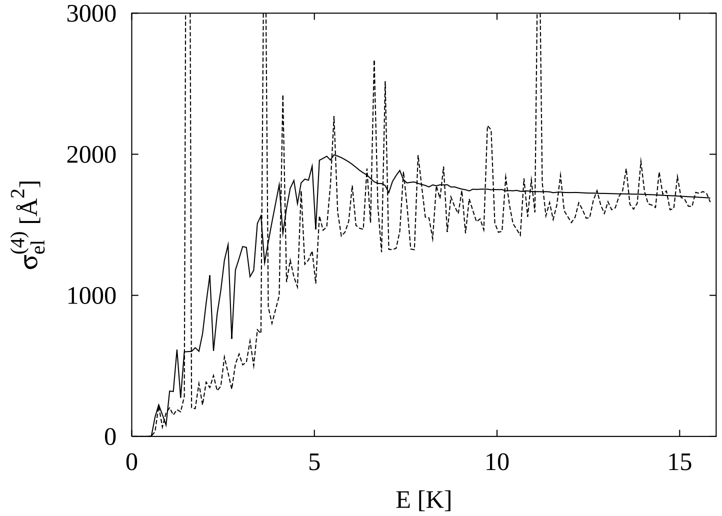

FIGURE 10. $\sigma_{\rm insc}$ for ^{3}He scattering at ^{4}He$_{112}$, as a function of incident energy E, using eq. (135) (full) and (128) (dashed).

The poor numerical consistency of our current results at lower energies has certainly to be improved. In the next two sections, we discuss differential cross sections mostly at high incident energies.

4.2. Spatio-kinetic distribution function

$dp_n/d\mathbf{k}$ of the ripplon channel, $n = 0$, and for the next two channels $n = 2, 3$, is shown in Fig. 11 for ^{3}He scattering with incident energy $\hbar\omega = 26$K at ^{4}He$_{1000}$. We distinguish between contributions from bound droplet excitations, $\hbar\omega_n < -\mu_4$, (red lines) and those from the continuum, $\hbar\omega_n > -\mu_4$ (green mesh).

The spatio-kinetic distribution provides a qualitative understanding of the inelastical scattering process, if we associate the particle location after time t, $\mathbf{r} = \hbar\mathbf{k}t/m$, with the wave number $\mathbf{k}$: not surprisingly, ^{3}He atoms which are only slightly deflected loose little energy, hence excite long wave-length modes, preferably on the surface; higher modes $n \leq 2$ contribute less to the cross section at the incident energies regarded here. Also short wave-length surface excitation, which would deflect the ^{3}He atom stronger, are less likely to be excited. The strongest coupling is to the lowest energy excitation, the quadrupole mode. Its angular dependence deviates from those of the other contributions, in that it has a second maximum at a larger scattering angle than its main peak. However, this feature was sensitive to the way the elementary diagrams were treated in the ground state calculations, and it may be an artifact.

4.3. Energy and momentum transfer

The cross section $\sigma(k_t, E_t)$ of ^{4}He$_N$ for energy E_t and momentum transfer $\hbar k_t$, eq. (153), is shown in Fig. 12 for ^{3}He scattering, where N ranges from 70 to 1000. $\sigma(k_t, E_t)$ has been

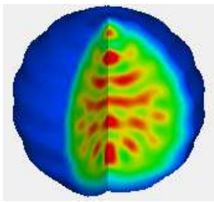

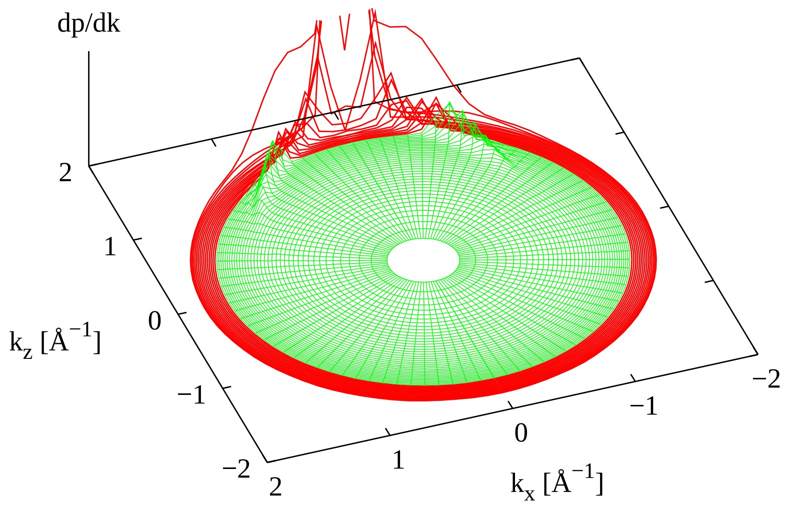

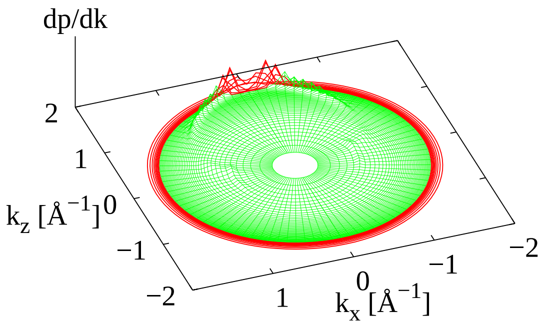

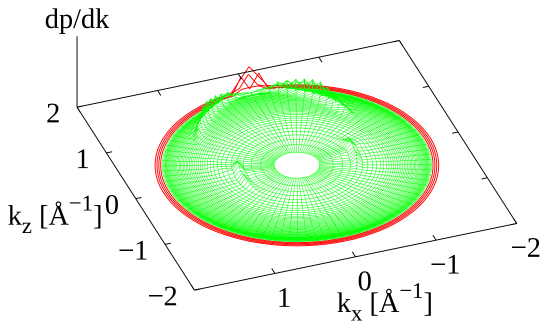

FIGURE 11. Spatio-kinetic distribution function for ^{3}He scattering at $^4\mathrm{He}_{1000}$, separated into contributions of the ripplon channel and the next two higher energy channels, $dp_n/d\mathbf{k}$ with $n = 1, 2, 3$; see text for explanation. Incident energy $E_{\text{in}} = 26$K, the scale is arbitrary, but equal for all three plots.

broadened with a Lorentzian $(E_t^2 + \Delta_E^2)^{-1}$ in E_t-direction. The parabola where $\sigma(k_t, E_t) \neq 0$ is kinematically allowed is determined by eq. (151). The energies $\hbar\omega_{n=0,\ell}$ of the lowest modes, the ripplons, are drawn with squares (bound ripplon) and lines (ripplon-like scattering states). The dispersion relation $\hbar\omega_{n=0,\ell} = \hbar\omega_0(k)$ of these surface excitations follows closely the free surface ripplon dispersion $\propto k^{3/2}$, already for small droplets [**CK95b**], although the wave number k is not a good quantum number yet; here k is determined from ℓ by

$$k = \sqrt{\frac{3\ell(\ell+1)}{5r_{\text{rms}}^2}} \qquad \text{with } r_{\text{rms}}^2 = \frac{1}{N}\int d^3r\ \rho(r)\, r^2$$

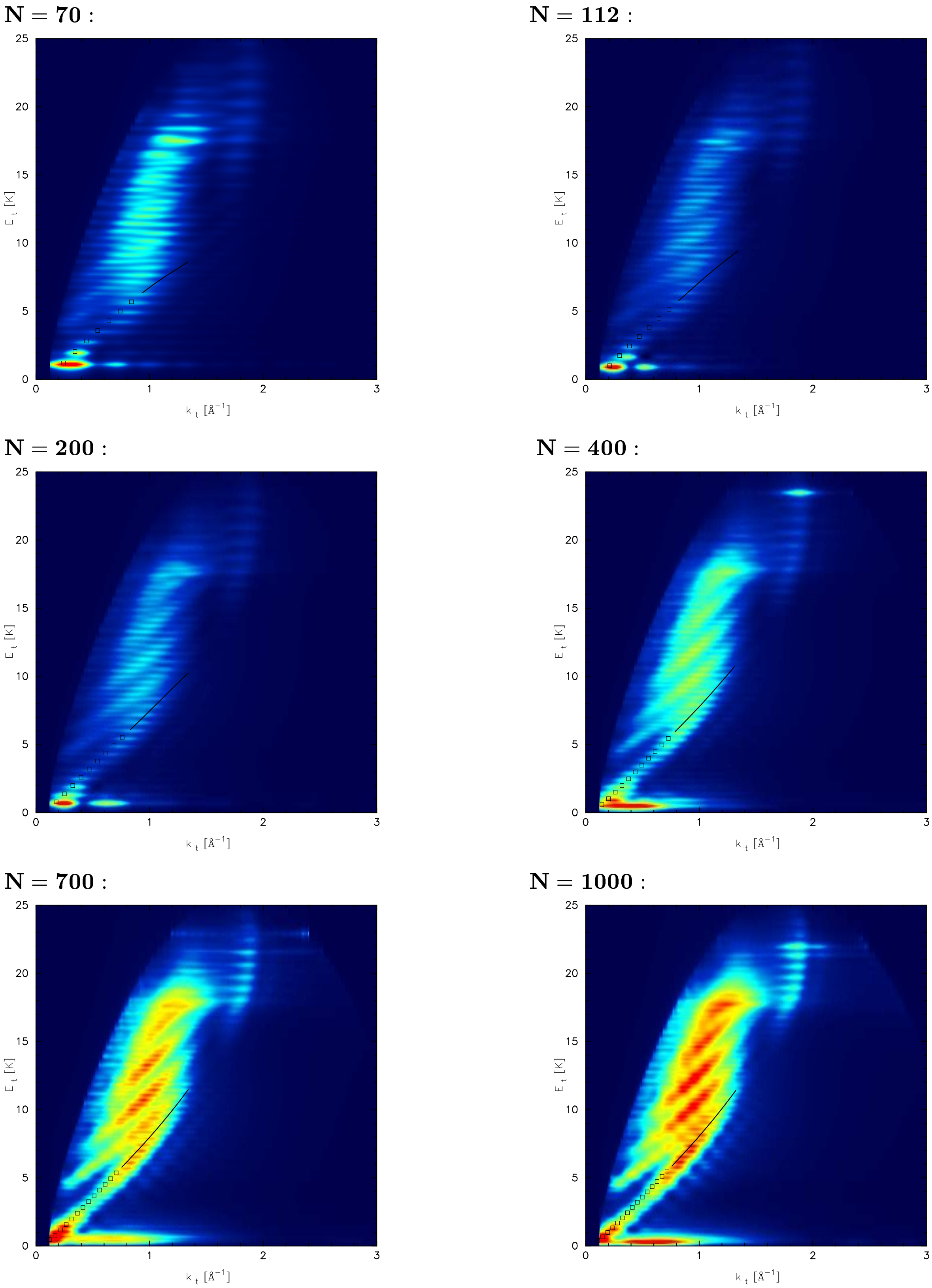

FIGURE 12. $\sigma(k_t, E_t)$ of ^{3}He scattering at $^4\text{He}_N$, $E_{\text{in}} = 26\text{K}$, $\Delta_E = 0.2\text{K}$.

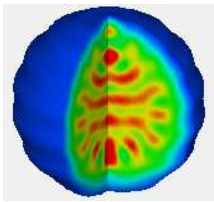

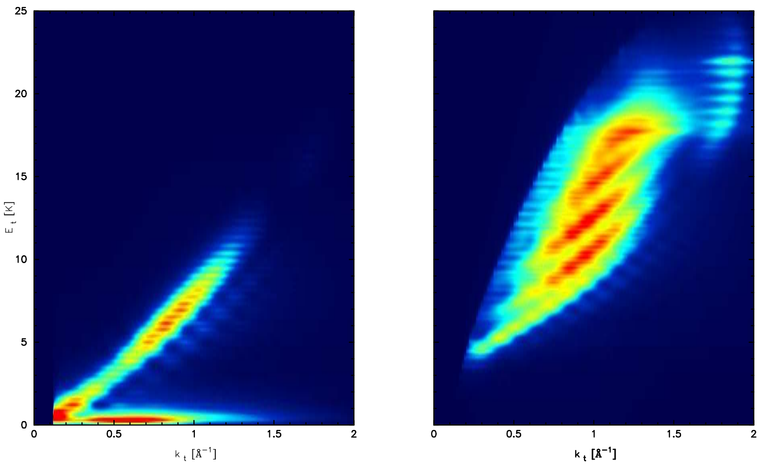

FIGURE 13. $\sigma(k_t, E_t)$ of ^{3}He scattering at ^{4}He$_{1000}$, separated into ripplon (left) and the other contributions.

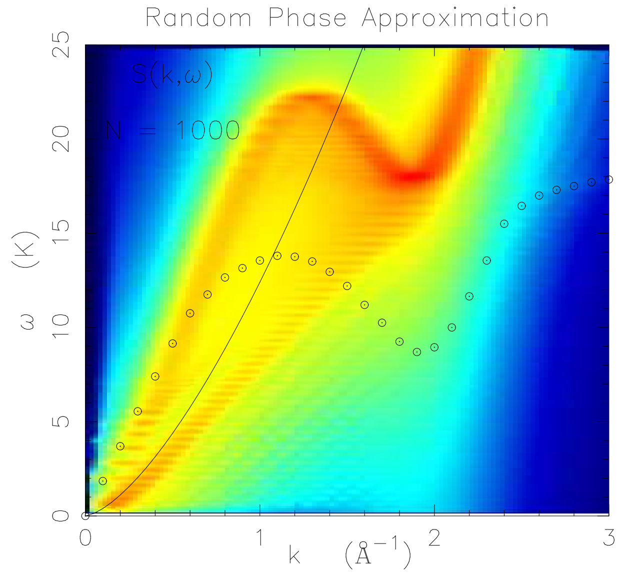

FIGURE 14. Logarithm of the dynamic structure funtion $S(k, E)$ of ^{4}He$_N$, in Feynman approximation.

In analogy of the mapping of excitation energies by inelastic neutron scattering providing the dynamic structure function $S(k, E)$, $\sigma(k_t, E_t)$ for ^{3}He scattering clearly yields the ripplon dispersion of the droplet. $\sigma(k_t, E_t)$ is particularly sensitive to ripplon excitation — in Fig. 13 we separate the ripplon modes contributing to $\sigma(k_t, E_t)$ from all other contributions —, while $S(k, E)$, shown for comparision in Fig. 14 in Feynman approximation, is suitable for probing the maxon–roton region. Both, $\sigma(k_t, E_t)$ and $S(k, E)$, show still an expected finite size broadening for $N = 1000$. Note, that the "stripes" above the ripplon in $\sigma(k, E)$, which stem from other channels, persist for all droplet sizes, instead of developing into a single signature for the phonon.

The coupling of ^{3}He to the "favourite" response of ^{4}He, the roton, is considerably weaker (see further below) than for neutron scattering. The most likely inelastic process seems to be scattering of ^{3}He off surface excitations, before the ^{3}He atom enters the interior of the droplet where it could interact with the roton. We remember that at the current level of the theory, where excitations include time-dependent one- and two-body correlations, *multiple* inelastic scattering processes are excluded; hence, an atom cannot excite more than two modes (e.g. no roton after a ripplon). The situation differs fundamentally from ^{3}He in bulk, where dissipation is only via roton creation.

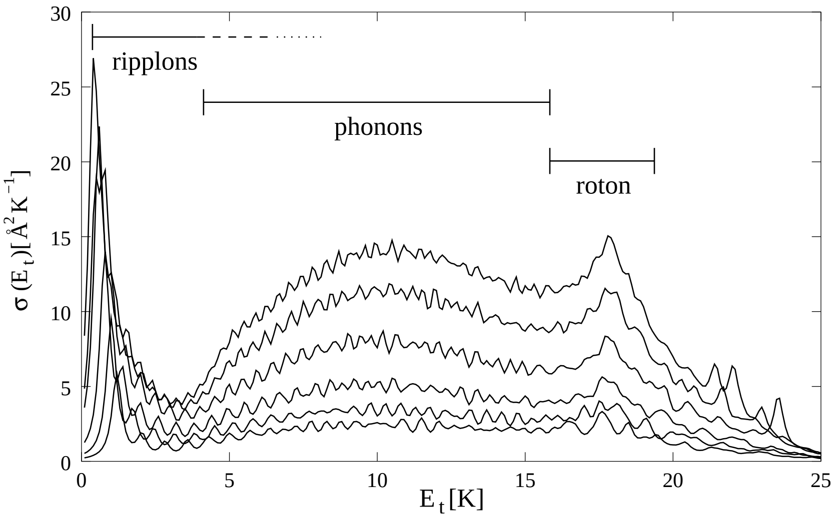

FIGURE 15. The cross section for energy transfer $\sigma(E_t)$ for ^{3}He scattering at ^{4}He$_N$, for incident energy $E = 26K$, $N = 70; 112; 200; 400; 700; 1000$.

While $\sigma(E_t, k_t)$ did not reveal any signs of increase scattering probability at roton momenta, we find in the cross section for energy transfer $\sigma(E_t)$ an increased probability at the roton energy. In Fig.15, this is seen as a peak at about 18K, which is exactly the roton energy in Feynman approximation: it is evident from the self energy (67), from the matrix elements (124), and from the energy conservation (123) that the elastic channel is coupled to excitations in Feynman approximation, the energy of which can considerably deviate from the CBF energy. The difference between Feynman excitation energies and CBF corrected energies is minor in the case of surface excitations [**KZ99**]. However, the roton peak in $\sigma(E_t)$ would have to go to smaller energies in an improved theory.

The most noticable feature in Fig.15 is not the roton peak, but again the small energy transfer to ripplon. Between ripplon- and roton contributions to $\sigma(E_t)$, there is a broad range of phonon excitations.

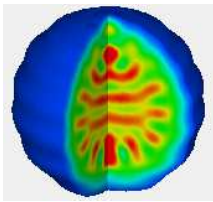

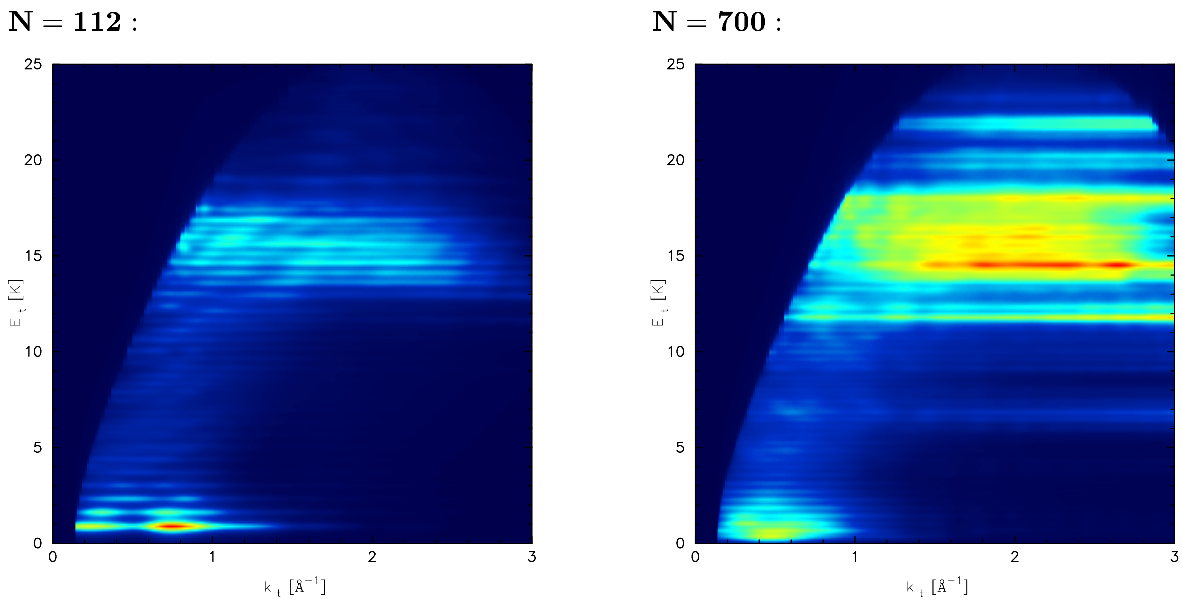

FIGURE 16. $\sigma(E_t, k_t)$ for ^{4}He scattering off ^{4}He$_N$, $\Delta_E = 0.2$K. Incident energy $E_{\text{in}} = 26$K.

The picture is very different for identical particle scattering: Fig. 16 shows $\sigma^{(4)}(k_t, E_t)$ of ^{4}He$_{112}$ and ^{4}He$_{700}$ for ^{4}He atoms of incident energy $E_{\text{in}} = 26$K.[5] $\sigma^{(4)}(k_t, E_t)$ does not have features in its k_t-dependence that can be related to a dispersion relation. Furthermore, $\sigma^{(4)}(k_t, E_t)$ for large N depends much more on E_{in} than $\sigma^{(3)}(k_t, E_t)$; the stripes at several energies E_t are probably spurious resonances similarly to those described above, see also Fig.10. The only systematic feature is a broad maximum energy transfer probability centered around $E_t = \hbar\omega/2$, *i.e.* when the impinging ^{4}He decays into two excitations of similar energy: In Fig. 17 we compare the dependence of $\sigma(E_t)$ on E_{in} for ^{4}He and ^{3}He scattering off ^{4}He$_{112}$. We remember that $\sigma(E_t)$ as well as $\sigma(E_t, k_t)$ are fundamentally different quantities for ^{4}He scattering and for ^{3}He scattering, because for the latter, energy/momentum transfer due to adsorption is not regarded, while due to the identity of ^{4}He atoms, all inelastic processes are indistinguishably contained in $\sigma^{(4)}(E_t, k_t)$.

Our preliminary conclusion for inelastic ^{4}He scattering is that $\sigma^{(4)}(E_t, k_t)$ does not reveal information about droplet excitations, of course except for the values of the discrete energies below $-\mu_4$.

4.4. Experimental considerations

Scattering of a ^{3}He atom at a single droplet of (a) well-defined size N which is (b) in its ground state, is an idealization and currently cannot be realized in experiment. The latter condition (b) — scattering at excited droplets, *i.e.* droplets having a temperature — is an

[5]For the calculation of $\sigma^{(4)}(k_t, E_t)$, we have not applied a weight $\frac{1}{2}$ to the continuum channels, as we have done for $\sigma^{(4)}_{\text{inel}}$.

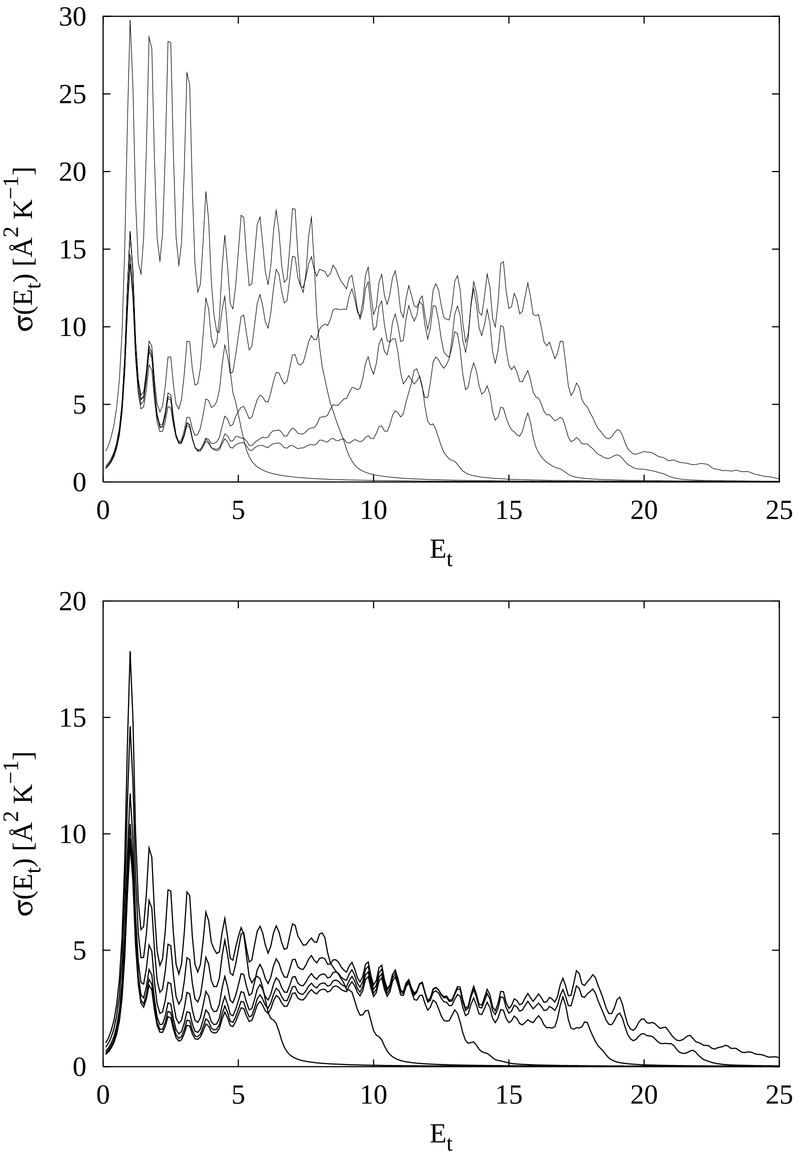

FIGURE 17. The cross section for energy transfer $\sigma(E_t)$ for ^{4}He (top) and ^{3}He (bottom) scattering at $^4\mathrm{He}_{112}$, for incident energy $E = \hbar\omega + \mu_X$, $\hbar\omega = 10; 14; 18; 22; 26; 30$K.

open question and cannot be answered here; see the subsection 1.3 for a list of processes which elude the level of treatment of excitations in the HNC-Euler-Lagrange theory, that is feasable for inhomogeneous systems.

The technique of ^{4}He droplet experiments was developed by the group of P. Toennies [**EST88, TV98**] and the setup for measuring inelastic ^{3}He scattering is sketched in Fig. 18. In the beam of ^{4}He atoms expanding from vacuum, droplets of various sizes are formed, following approximately a log-normal distribution $P(N) = \exp[-(\ln N - \mu)^2/2\sigma^2]/\sqrt{2\pi}N\sigma$

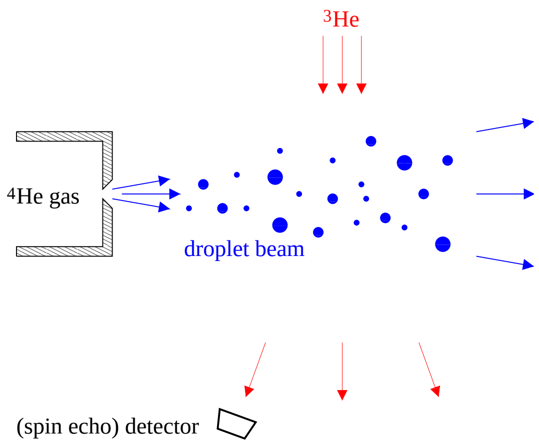

FIGURE 18. Measuring the inelastic cross section of ^{3}He scattering at a beam of ^{4}He droplets.

[**LST93**]. To answer the question whether discrete excitation energies can still be measured by scattering at a distribution of droplets, we simply have to generate the statistical superposition of the cross sections $\sigma(N)$,

$$\sigma = \int dN \; P(N)\,\sigma(N)$$

where $\sigma(N)$ is one of the $^4\mathrm{He}_N$ cross section introduced above.

In Fig.19, the small angle current of the ripplon channel is shown for N =70,112,200,400,700, and 1000, each weighted with a broad distribution $P(N)$ of droplet sizes ($\mu = 6.1$, $\sigma = 0.4$, see inset); the incident energy is 25.0K.

It may be concluded that, given the high precision of the spin-echo measurement of the transferred energy, the energy of the first three ripplon modes $\hbar\omega_{\ell,\mathrm{ripplon}}$ of small ^{4}He droplets, N <1000, can by measured. Although we cannot calculate cross sections of droplets of sizes of the order of $N = \mathrm{O}(10^4)$ or larger, the convergence of the strong, increasingly sharp ripplon feature in $\sigma(k, E)$ is obvious from the series in Fig. 12. Hence, for large droplets, the measurement of the energy *and* momentum transfer (by varying the measured scattering angle) of ^{3}He atoms to a distribution of ^{4}He droplets yields the free ripplon disperion relation.

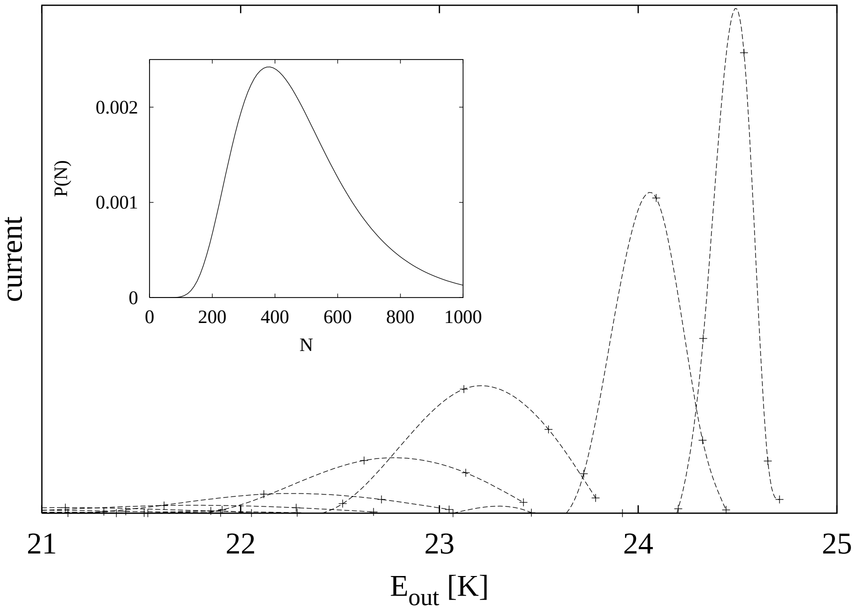

FIGURE 19. The ripplon contribution to the inelastic cross section of ^{3}He of incoming energy 25.0K scattered at a log-normal distribution (see inset), for scattering angles 7.8°. Contribution of other droplet excitations are negligible in the shown range of outgoing energies.

CHAPTER 7

Impurity scattering off ^{4}He films

1. Introduction

In the previous chapter, we have applied the HNC-Euler-Lagrange theory to the calculation of asymptotic second order currents, *i.e.* cross sections, for scattering of ^{4}He and ^{3}He off ^{4}He droplets. In this chapter, we apply it to impurity scattering off ^{4}He films. The ground state of ^{4}He on various substrates has been studied extensively in Refs. [**Kro85a, EK88, CEKS93**]; Refs. [**KT92, CGK$^+$96, CKT96**] extend these calculations to time-dependent correlations to describe excitations of pure ^{4}He films, and Refs. [**KSE88, CKS97**] extend them to impurity motion in the films. In Ref. [**Zil97, KZ98**], we have calculated elastic reflection probabilities $|R|^2$ of ^{3}He, which are less than unity due to time-dependent two-body correlations. Here we continue this work and investigate the residual probability $1 - |R|^2$, which is the sum of the sticking probability and the inelastic reflection probablity, defined in section 3 of chapter 4:

$$1 = |R|^2 + s + r_{\mathrm{inel}}\,. \tag{154}$$

For this purpose, the asymptotic second order currents are calculated in the plane surface geometry of ^{4}He adsorbed on a translationally invariant graphite substrate. The steps involved are essentially the same as for droplet scattering.

When an atom approaches a ^{4}He film, adsorbed on a substrate, from a large distance, it first feels the Van der Waals attraction of the substrate. We assume that the substrate is inert and fills the half space $z < 0$. Closer to the film, the atom-^{4}He interaction leads to a coupling of the motion of H and the ^{4}He atoms of the film, and hence potentially to dissipation. For low energies, the most important process is the emission of surface waves (ripplons in the case of the free surface of an infinitely thick film, or third sound on the surface of thin films). Therefore, most theoretical methods applied to this surface scattering problem reduce the number of freedoms to those of an atom scattering at a mean potential, and coupling to elementary excitations of the N-body target. To simplify matters, many calculations adjust an effective potential such that the experimental binding energy of H on the film is reproduced, and use a continuum model to describe the surface waves of the film. Conversely, our microscopic calculation takes as only input the many-body Hamiltonian and *yields* the mean potentials as well as the "optical potential" (self energy) describing the coupling between atom and elementary excitations. We give a comprehensive study of scattering off the superfluid ^{4}He surface, and supplement previous theoretical work [**Goo71,**

BBS82, Gol86, EF78, HWS92, CC92, CC98, BL95, CK92, BGG94] by a many-body calculation.

Unlike classical particles, which stick with unit probability to a dissipative surface in the limit of zero incident energy E, quantum particles like hydrogen and ^{3}He atoms are scattered elastically with the elastic reflection probability $|R|^2$ approaching unity. This well–known phenomenon, called "universal quantum reflection", is due to the mismatch of the wave function at the potential well [**LJSD36a, LJSD36b**]. Quantum reflection occurs also for long-ranged Van der Waals potentials [**BBS82**] which fall off with the inverse third power of the distance from the surface, $-C_3/z^3$. However, the strength C_3 crucially determines below which energies the asymptotic behavior $1-|R|^2 \propto \sqrt{E}$ starts: universal quantum reflection may be suppressed by low energy resonances as well as weakly bound states, as we shall see.

The solvation energy of H atoms in bulk liquid ^{4}He is rather high (theoretical prediction [**KS93a**] is 31.6 K), hence low energy H atoms will not penetrate the helium film. H scattering is therefore by surface dynamics, especially by creating surface waves which have a typical wave number $k \approx 0.13\text{Å}^{-1}$ due to energy conservation. These surface properties are not affected beyond a few atomic layers of ^{4}He. However, the film acts as a buffer between H and the substrate which interacts much stronger with H than ^{4}He. That way, the effect of the substrate potential can be tuned by changing the film thickness.

By evaporation–cooling trapped atomic hydrogen [**YDSea93**], Yu *et. al.* have measured the dependence of s on the energy and the film thickness for the sticking of H atoms on ^{4}He films adsorbed on sintered silver. For films consisting of more than two liquid layers, substrate corrugation is negligible, we can therefore assume a plane–surface geometry. We choose as background the ^{4}He film calculations on graphite substrates from Ref.[**CEKS93**] because the detailed nature of the substrate is irrelevant: The most important quantities for the low energy sticking coefficient are C_3, the coefficient of the atom–substrate potential, and the coupling between the atom and ^{4}He surface modes.

2. Plane surface geometry

We assume from now on translational invariance in the $x-y$–plane. Then the ^{4}He density is only a function of the coordinate perpendicular to the film, the z–coordinate, $\rho_1(\mathbf{r}) = \rho_1(z)$, and the areal density of the film is given by $n = \int dz\, \rho_1(z)$. All states are characterized by two quantum numbers, α and $\mathbf{k}_\alpha$, associated with the motion perpendicular (α) and parallel to the symmetry plane ($\mathbf{k}_\alpha$). We shall use bold labels (*e.g.* $\boldsymbol{\alpha}$, $\boldsymbol{\beta}$, … for impurity states and $\boldsymbol{m}$, $\boldsymbol{n}$, … for film states) to collectively represent both quantum numbers, *i.e.* $\boldsymbol{\alpha} \equiv \{\alpha, \mathbf{k}_\alpha\}$ and $\boldsymbol{m} \equiv \{m, \mathbf{k}_m\}$.

The phonon states $\phi^{(\boldsymbol{m})}(\mathbf{r})$ and the $X_{\boldsymbol{m}}(\mathbf{r}_0)$ are of the form

$$\phi^{(\boldsymbol{m})}(\mathbf{r}) = \frac{1}{L}\, \phi^{(m)}(z, \mathbf{k}_m) e^{i\mathbf{k}_m \cdot \mathbf{r}_\parallel}\,, \qquad X_{\boldsymbol{m}}(\mathbf{r}_0) = \frac{1}{L}\, e^{i\mathbf{k}_m \cdot \mathbf{r}_\parallel} X_m(z, \mathbf{k}_m)\,, \tag{155}$$

where

$$X_{\boldsymbol{m}}(\mathbf{r}_0) \equiv \int d^3 r_1 X^I(\mathbf{r}_0, \mathbf{r}_1) \sqrt{\rho_1(\mathbf{r}_1)}\, \phi^{(\boldsymbol{m})}(\mathbf{r}_1)\,. \tag{156}$$

and where L^2 is the size of the normalization area parallel to the surface.

The impurity states $\eta^{(\boldsymbol{\alpha})}(\mathbf{r}_0)$ depend only trivially on the parallel coordinate,

$$\eta^{(\boldsymbol{\alpha})}(\mathbf{r}_0) = \frac{1}{L}\eta^{(\alpha)}(z_0)e^{i\mathbf{k}_\alpha\cdot\mathbf{r}_\parallel} . \tag{157}$$

The corresponding energies are

$$\varepsilon_{\boldsymbol{\alpha}} = \epsilon_\alpha + \frac{\hbar^2 k_\alpha^2}{2m_I} , \tag{158}$$

where ϵ_α are the eigenvalues of Eq. (60) for $k_\alpha = 0$. In particular,

$$\eta^{(0)}(\mathbf{r}_0) = \sqrt{\rho_1^I(z)}e^{i\mathbf{k_0}\cdot\mathbf{r}_\parallel} \tag{159}$$

and $\varepsilon_0 = \hbar^2 k_0^2/2m_I$.

The coupling matrix elements (64) depend on the parallel momentum $\mathbf{k}_\alpha$ only through momentum conservation; they have the form

$$W_{\boldsymbol{\gamma m}}^{(\boldsymbol{\alpha})} = \frac{1}{L}\delta_{\mathbf{k}_m+\mathbf{k}_\gamma,\mathbf{k}_\alpha} W_{\gamma m}^{(\alpha)}(\mathbf{k}_m,\mathbf{k}_\gamma) \equiv \frac{1}{L}\delta_{\mathbf{k}_m+\mathbf{k}_\gamma,\mathbf{k}_\alpha}\int dz\ \eta^{(\alpha)}(z)W_{\gamma m}(z,\mathbf{k}_m,\mathbf{k}_\gamma) \tag{160}$$

In coordinate space, and in the adopted plane–surface geometry, Eq. (66) reads

$$\left[H_1^I(z) + \frac{\hbar^2 k_\parallel^2}{2m_I}\right]\varphi_\omega(z) - \int dz'\,\Sigma(z,z',\mathbf{k}_\parallel;\omega)\varphi_\omega(z') = \hbar\omega\varphi_\omega(z) , \tag{161}$$

where

$$H_1^I(z) = -\frac{\hbar^2}{2m_I}\frac{1}{\sqrt{\rho_1^I(z)}}\frac{d}{dz}\rho_1^I(z)\frac{d}{dz}\frac{1}{\sqrt{\rho_1^I(z)}} \tag{162}$$

$$\Sigma(z,z',\mathbf{k}_\parallel;\omega) = \frac{1}{L^2}\sum_{m,\mathbf{k}_m}\sum_\gamma \frac{W_{\gamma m}(z,\mathbf{k}_m,\mathbf{k}_\parallel-\mathbf{k}_m)\ W_{\gamma m}^*(z',\mathbf{k}_m,\mathbf{k}_\parallel-\mathbf{k}_m)}{\hbar\omega_m(k_m)+\epsilon_\gamma+\frac{\hbar^2(\mathbf{k}_m-\mathbf{k}_\parallel)^2}{2m_I}-\hbar\omega} \tag{163}$$

Equations (66) and (67) or, alternatively, Eq. (161) determine the energetics of bound states, the impurity motion parallel to the surface, and the dynamics of atom scattering. The solutions have, in configuration space, the form

$$\varphi_\omega(\mathbf{r}) = \varphi_\omega(z)e^{i\mathbf{k}_\parallel\cdot\mathbf{r}_\parallel} . \tag{164}$$

Depending on the energy $\hbar\omega$, the solutions describe the motion of physisorbed adatoms or scattering states. In the latter case, $\hbar\omega = E - \mu_I = \hbar^2(k_\perp^2 + k_\parallel^2)/2m_I - \mu_I$, where $k_\perp$ is the perpendicular component of the wave number.

2.1. Elastic scattering and unitarity

The continuum solutions of the effective Schrödinger equation (161) describe scattering processes. The equation is solved subject to the boundary conditions

$$\psi_\omega(\mathbf{r}) = \psi_\omega(z)e^{i\mathbf{k}_\parallel\cdot\mathbf{r}_\parallel} \stackrel{z\to\infty}{\longrightarrow} e^{i\mathbf{k}_\parallel\cdot\mathbf{r}}\left[e^{-ik_\perp z} + R(k_\perp,\mathbf{k}_\parallel)e^{ik_\perp z}\right] . \tag{165}$$

Superficially, we appear to be describing a quantum mechanical single–particle scattering problem. In fact, a number of notions such as that of a reflection coefficient can be carried over from single particle models, and simple phenomenological descriptions can be constructed at the level of a one–body theory. But the physical situation is far richer: Since the scattering film is composed of helium atoms, this is a generically *non-local* problem when viewed at the one-body level. Moreover, the film is *dynamic:* the incoming particle may produce excited states of the background. This may result in the capture of the particle and/or the emission of particles in states other than the elastic channel.

One of the key quantities of interest is the elastic reflection coefficient $R(k_\perp, \mathbf{k}_\|)$. This quantity is directly determined by the coupling of the motion of the impinging particle to the excitations of the quantum liquid. The absolute value of the reflection coefficient can differ from unity only if the self–energy $\Sigma(\mathbf{r}, \mathbf{r}', \omega)$ is non-hermitian. This happens when the energy denominator in the self–energy (67) has zeroes; note that the quantum numbers $\boldsymbol{m}$ and $\boldsymbol{\gamma}$ include both the motion of the particles parallel to the surface as well as the discrete or continuous degrees of freedom in the z-direction. A detailed discussion of the elastic reflection coefficient $R(k_\perp, \mathbf{k}_\|)$ and its relation to properties of the film as well as results for ^{3}He scattering can be found in Ref. [**KZ98**].

Unitarity of the *many–body* scattering matrix implies that the sum of all probabilities $p_{\boldsymbol{m}}$ to scatter into channel $\boldsymbol{m}$ is unity. We utilize this property to obtain the sticking probability s from the asymptotic elastic and inelastic currents,

$$\mathbf{j}_{\rm el} = -(1 - |R|^2)\frac{\hbar k_\perp}{m_I}\mathbf{e}_z + \frac{\hbar}{m_I}\mathbf{k}_\| \tag{166}$$

and $\mathbf{j}_{\rm inel}$ which will be calculated in the next section. Surface integration of the total current $\mathbf{j} = \mathbf{j}_{\rm el} + \mathbf{j}_{\rm inel}$ over a plane parallel to and at large distance from the film yields the flux of particles lost due to sticking; the sticking probability is therefore

$$s \equiv 1 - |R|^2 - r_{\rm inel}\,, \tag{167}$$

where $r_{\rm inel}$ is the probability for inelastic scattering, also termed *direct* inelastic scattering as opposed to the combination of sticking and subsequent desorption at finite film temperatures [**BW93**]. $|R|^2$ is easily obtained from the equation of motion either by appropriately scaling and fitting the asymptotic form of the solution of Eq. (161) to the form (165), or by integrating Eq. (161) with $\psi^*_\omega(\mathbf{r})$ and subtracting its complex conjugate:

$$1 - |R|^2 = \frac{2m_I}{\hbar^2 k_\perp}\int dz dz'\ \psi^*_\omega(z)\Im m\,\Sigma(z, z', \mathbf{k}_\|; \omega)\psi_\omega(z')\,, \tag{168}$$

where we have used again the asymptotic form (165).

We will show in section 2.5 that, for low incident energies $E = \frac{\hbar^2 k^2}{2m_I}$, $r_{\rm inel}$ falls off as $r_{\rm inel} \propto E^2$. Inelastic reflection can therefore be neglected compared to $1 - |R|^2$ and s for low energies, and we can obtain the sticking coefficient from $s = 1 - |R|^2$, which turns out to be proportional to $\sqrt{E}$. This is no longer valid for energies of the order of 1K or higher, where all three probabilities $|R|^2$, $r_{\rm inel}$, and s are of comparable magnitude.

2.2. Inelastic scattering

Elastic and inelastic scattering processes are described by their respective asymptotic second order current (87), where, for the rest of the paper, the superscript (2) denoting second order is omitted. As for droplets, we simplify Eq. (87) by using the uniform limit approximation to obtain

$$\mathbf{j}_{\text{inel}}(\mathbf{r}_0) = \Im m\ \frac{\hbar}{4m_I} \sum_{\boldsymbol{m}} \delta\tilde{u}^*_{\boldsymbol{m}}(\mathbf{r}_0) \nabla \delta\tilde{u}_{\boldsymbol{m}}(\mathbf{r}_0)\,, \tag{169}$$

where

$$\delta\tilde{u}_{\boldsymbol{m}}(\mathbf{r}_0) = \sum_{\boldsymbol{\alpha}} \eta^{(\boldsymbol{\alpha})}(\mathbf{r}_0)\delta\tilde{u}_{\boldsymbol{\alpha m}} = \int d^3r\,\delta\tilde{u}_2(\mathbf{r}_0,\mathbf{r})\phi^{(\boldsymbol{m})}(\mathbf{r}) \tag{170}$$

are the inelastic scattering channel wave functions, and the matrix–elements $\delta\tilde{u}_{\boldsymbol{\alpha m}} \equiv (\eta^{(\boldsymbol{\alpha})} \mid \delta\tilde{u}_2 \mid \phi^{(\boldsymbol{m})})$ of the time–dependent correlations are given by eq. (63). Hence we can write the currents as

$$\mathbf{j}(z\to\infty) \;=\; \mathbf{j}_{\text{el}} + \mathbf{j}_{\text{inel}} \;=\; \mathbf{j}_{\text{el}} + {\sum_{\boldsymbol{m}}}' \mathbf{j}^{(\boldsymbol{m})}_{\text{inel}}\,, \tag{171}$$

where the first term is the elastic current which takes the asymptotic form (166) with wave number $k = (2m_I E)^{1/2}/\hbar$. The prime denotes summation over all open inelastic scattering channels, *i.e.* those where $\delta\tilde{u}_{\boldsymbol{m}}(\mathbf{r}_0)$ is characterized by an outgoing wave vector $\mathbf{k}_{\text{out}} \in \mathbf{R}^3$.

Having specified the geometry, we will now further evaluate the $\delta\tilde{u}_m(\mathbf{r}_0)$. The first–order current is characterized by the energy $\hbar\omega$ and a parallel momentum $\mathbf{k}_{\|}$, *i.e.* it has the form

$$\mathbf{j}^{(1)}(\mathbf{r}_0) = \mathbf{j}^{(1)}(z_0,\mathbf{k}_{\|})e^{i\mathbf{k}_{\|}\cdot\mathbf{r}_{\|}}\,. \tag{172}$$

We adopt the Feynman–approximation for the incoming current $\mathbf{j}^{(1)}(\mathbf{r}_0)$,

$$\mathbf{j}^{(1)}(\mathbf{r}_0) \;\approx\; \frac{\hbar}{2m_I i}\rho^I_1(\mathbf{r}_0)\nabla_0\frac{\delta\rho^I_1(\mathbf{r}_0)}{\rho^I_1(\mathbf{r}_0)} \;=\; \frac{\hbar}{2m_I i}\rho^I_1(\mathbf{r}_0)\nabla_0\frac{\varphi_\omega(\mathbf{r}_0)}{\sqrt{\rho^I_1(\mathbf{r}_0)}}\,. \tag{173}$$

With the definition

$$\frac{1}{L}e^{i(\mathbf{k}_m+\mathbf{k}_{\|})\cdot\mathbf{r}_{\|}}F_m(z,\mathbf{k}_m,\mathbf{k}_{\|}) \equiv \frac{1}{\sqrt{\rho^I_1(\mathbf{r}_0)}}\mathbf{j}(\mathbf{r}_0)\cdot\nabla_0 X_{\boldsymbol{m}}(\mathbf{r}_0)\,, \tag{174}$$

the matrix elements (63) of the fluctuating pair distribution function are, in this geometry,

$$(\varepsilon_{\boldsymbol{\alpha}} + \hbar\omega_{\boldsymbol{m}} - \hbar\omega)\delta\tilde{u}_{\boldsymbol{\alpha m}} = i\hbar\delta_{\mathbf{k}_m+\mathbf{k}_{\|},\mathbf{k}_\alpha}\int dz\,\eta^{(\alpha)}(z)F_m(z,\mathbf{k}_m,\mathbf{k}_{\|})\,. \tag{175}$$

We are now ready to calculate

$$\begin{aligned}\delta\tilde{u}_{\boldsymbol{m}}(\mathbf{r}_0) &= \frac{i\hbar}{L}e^{i(\mathbf{k}_m+\mathbf{k}_{\|})\cdot\mathbf{r}_{\|}}\int dz'\left[\sum_\alpha \frac{\eta^{(\alpha)}(z)\eta^{*(\alpha)}(z')}{\epsilon_\alpha + \frac{\hbar^2}{2m_I}(\mathbf{k}_m+\mathbf{k}_{\|})^2 + \hbar\omega_m - \hbar\omega}\right]F_m(z',\mathbf{k}_m,\mathbf{k}_{\|})\\ &= \frac{i\hbar}{L}e^{i(\mathbf{k}_m+\mathbf{k}_{\|})\cdot\mathbf{r}_{\|}}\int dz' G(z,z';\epsilon_\lambda+\mu_I)F_m(z',\mathbf{k}_m,\mathbf{k}_{\|})\,,\end{aligned} \tag{176}$$

where $G(z,z';\epsilon_\lambda+\mu_I)$ is the Green's function of the Hartree–equation (60) with energy

$$\epsilon_\lambda = \hbar\omega - \frac{\hbar^2}{2m_I}(\mathbf{k}_m+\mathbf{k}_{\|})^2 - \hbar\omega_m\,. \tag{177}$$

The Green's function may also be written as, see appendix B,

$$G(z,z';\epsilon_\lambda+\mu_I) = -\frac{2m_I}{\hbar^2 k_{\perp,\text{out}}}\chi^{+(\lambda)}(z_>)\eta^{(\lambda)}(z_<)\,. \tag{178}$$

We are interested in scattering states, *i.e.* the energy ϵ_λ associated with the state (λ) must be above the evaporation threshold $-\mu_I$ and can, hence, be written as

$$\epsilon_\lambda = -\mu_I + \frac{\hbar^2 k_{\perp,\text{out}}^2}{2m_I} . \tag{179}$$

The wave function $\eta^{(\lambda)}(z)$ is regular as $z \to 0$ whereas the irregular solution $\chi^{+(\lambda)}(z)$ has the form of an outgoing plane wave: for $z \to \infty$,

$$\chi^{+(\lambda)}(z) \to e^{ik_{\perp,\text{out}}z + i\delta_\lambda} , \qquad \eta^{(\lambda)}(z) \to \sin(k_{\perp,\text{out}}z + \delta_\lambda) . \tag{180}$$

We can now go back to Eqs. (176) and (174) and write, for large z,

$$\begin{aligned} \delta\tilde{u}_{\boldsymbol{m}}(\mathbf{r}_0) &= -\frac{2m_I}{\hbar^2 k_{\perp,\text{out}}}\frac{1}{L} e^{i((\mathbf{k}_m+\mathbf{k}_{\|})\cdot\mathbf{r}_{\|}+k_{\perp,\text{out}}z+i\delta_\lambda)} i\hbar \int dz'\, \eta^{(\lambda)}(z') F_m(z',\mathbf{k}_m,\mathbf{k}_{\|}) \\ &\equiv \frac{2}{L} e^{i((\mathbf{k}_m+\mathbf{k}_{\|})\cdot\mathbf{r}_{\|}+k_{\perp,\text{out}}z+i\delta_\lambda)} M_m(\mathbf{k}_m,\mathbf{k}_{\|}) . \end{aligned} \tag{181}$$

with

$$M_m(\mathbf{k}_m,\mathbf{k}_{\|}) = \frac{2m_I}{\hbar^2 k_{\perp,\text{out}}} \int dz\, W_{\lambda\, m}(z,\mathbf{k}_m,\mathbf{k}_{\|})\, \varphi_\omega(z) . \tag{182}$$

With this we can now write Eq. (169) as

$$\mathbf{j}_{\text{inel}} = \sum_{m,\mathbf{k}_m}{}' \mathbf{j}_{\text{inel}}^{(m,\mathbf{k}_m)} \tag{183}$$

with

$$\mathbf{j}_{\text{inel}}^{(m,\mathbf{k}_m)} = \frac{\hbar}{m_I L^2}\left(\mathbf{k}_m + \mathbf{k}_{\|} + k_{\perp,\text{out}}\mathbf{e}_z\right)|M_m(\mathbf{k}_m,\mathbf{k}_{\|})|^2 = \frac{\hbar}{m_I L^2}\mathbf{k}_{\text{out}}|M_m(\mathbf{k}_m,\mathbf{k}_{\|})|^2 . \tag{184}$$

The wave number of the inelastically scattered impurity is

$$\mathbf{k}_{\text{out}} \equiv \mathbf{k}_m + \mathbf{k}_{\|} + k_{\perp,\text{out}}\mathbf{e}_z , \qquad k_{\perp,\text{out}}^2 = \frac{2m_I}{\hbar^2}(E - \hbar\omega_m(k_m)) - |\mathbf{k}_{\|,\text{out}}|^2 ; \tag{185}$$

it is a function of the energy and parallel wave number of the incoming current as well as of the energy and wave number of the film mode which is excited: the parallel component $\mathbf{k}_{\|,\text{out}}$ is determined by momentum conservation in the direction parallel to the film whereas the perpendicular component $k_{\perp,\text{out}}$ by energy conservation, Eq. (177). Similarly to Eq. (182), the prime on the sum in eq. (183) denotes summation over open channels, where the impurity states are unbound, $\varepsilon_\lambda > |\mu_I|$, *i.e.* $k_{\perp,\text{out}} \in \mathbf{R}$.

From $\mathbf{j}_{\text{inel}}$ we can finally determine r_{inel} as the ratio of the inelastically scattered current perpendicular to the film and the incoming current $\mathbf{j}_{\text{in}} = \hbar\mathbf{k}/m_I$,

$$r_{\text{inel}} = \left|\frac{j_{\perp,\text{inel}}}{j_{\perp,\text{in}}}\right| = \frac{2m_I}{\hbar^2 k_\perp}\frac{1}{L^2}\sum_{m,\mathbf{k}_m}{}' \frac{2m_I}{\hbar^2 k_{\perp,\text{out}}}\left|\int dz\, W_{\lambda\, m}(z,\mathbf{k}_m,\mathbf{k}_{\|})\, \varphi_\omega(z)\right|^2 . \tag{186}$$

More detailed information than merely the total probability r_{inel} for any kind of inelastic scattering, can be obtained by "binning" into the various decay channels, which amounts to weighing the current operator $\hat{\mathbf{j}}(\mathbf{r})$ with appropriate functions of finite support. For example, the expectation value of the operator $\hat{\mathbf{j}}(\mathbf{r})\delta(\Omega - \Omega_{\hat{\mathbf{j}}})$ gives the flux into the solid angle element $d\Omega$ pointing into the direction $\hat{\mathbf{e}}_\Omega$, where $\Omega_{\hat{\mathbf{j}}}$ is the solid angle in the direction of $\hat{\mathbf{j}}$. This gives

$$\mathbf{j}_{\text{inel}}(\Omega) = \sum_{\boldsymbol{m}}{}' \delta(\Omega - \Omega_{\text{out}}^{(\boldsymbol{m})})\ \mathbf{j}_{\text{inel}}^{(\boldsymbol{m})} = \hat{\mathbf{e}}_\Omega \sum_{\boldsymbol{m}}{}' \delta(\Omega - \Omega_{\text{out}}^{(\boldsymbol{m})})\ j_{\text{inel}}^{(\boldsymbol{m})} \tag{187}$$

where $\Omega_{\text{out}}^{(\boldsymbol{m})}$ is the solid angle in the direction of $\mathbf{j}_{\text{inel}}^{(\boldsymbol{m})}$, *i.e.* of $\mathbf{k}_{\text{out}}$. For the plane surface geometry, where $\boldsymbol{m} = \left\{m, \mathbf{k}_{\|}^{(m)}\right\}$, the differential current can be calculated in the limit $L \to \infty$

$$j_{\text{inel}}(\Omega) = \sum_m{}' \int \frac{d^2k_m}{(2\pi)^2}\ \delta(\Omega - \Omega_{\text{out}}^{(m,\mathbf{k}_m)})\ j_{\text{inel}}^{(m,\mathbf{k}_m)} \tag{188}$$

$$= \frac{1}{(2\pi)^2} \sum_m{}' \sum_i \left[\frac{d\Omega_{\text{out}}^{(m,\mathbf{k}_m)}}{d\mathbf{k}_m}\right]_{\mathbf{k}_m^{(i)}}^{-1} j_{\text{inel}}^{(m,\mathbf{k}_m^{(i)})} \tag{189}$$

where $\mathbf{k}_m^{(i)}$ are the roots of $\Omega - \Omega_{\text{out}}^{(m,\mathbf{k}_m)} = 0$ and the functional determinant is

$$\left[\frac{d\Omega_{\text{out}}^{(m,\mathbf{k}_m)}}{d\mathbf{k}_m}\right] = \frac{1}{\cos\theta\ k_{\text{out}}^2} \left|1 + \hbar\omega_m'(k_m)\ \frac{\mathbf{k}_m \cdot \mathbf{k}_{\|,\text{out}}}{k_{\text{out}}^2}\right| \tag{190}$$

where $\omega_m'(k_m)$ denotes the derivative of the dispersion relation $\omega_m(k_m)$ with respect to $\frac{\hbar^2 k_m{}^2}{2m_I}$. We can then define the inelastic differential scattering probability per particle as the ratio between outgoing inelastic current $j_{\text{inel}}(\Omega)$ and incoming current $\frac{\hbar k}{m_I}$

$$\frac{d\sigma_{\text{inel}}(\Omega)}{d\Omega} = \frac{1}{(2\pi)^2} \sum_m{}' \sum_i \left[\frac{d\Omega_{\text{out}}^{(m,\mathbf{k}_m)}}{d\mathbf{k}_m}\right]_{\mathbf{k}_m^{(i)}}^{-1} \frac{k_{\text{out}}}{k}\ |M_m(\mathbf{k}_m^{(i)}, \mathbf{k}_{\|})|^2\,, \tag{191}$$

where the definition of $j_{\text{inel}}^{(m,\mathbf{k}_m^{(i)})}$, eq. (184), was used.

Other differential scattering probabilities can be defined in similar fashion as the ratio between the inelastic current of outgoing energy E_{out} or perpendicular momentum $k_{\perp,\text{out}}$, and the incoming current,

$$\frac{d\boldsymbol{\sigma}_{\text{inel}}(E_{\text{out}})}{dE_{\text{out}}} = \sum_m{}' \int \frac{d^2k_m}{(2\pi)^2}\ \delta\left(E_{\text{out}} - \frac{\hbar^2 k_{\text{out}}^2}{2m_I}\right)\ \frac{\mathbf{k}_{\text{out}}}{k}\ |M_m(\mathbf{k}_m, \mathbf{k}_{\|})|^2 \tag{192}$$

$$\frac{d\boldsymbol{\sigma}_{\text{inel}}(\bar{k}_{\perp,\text{out}})}{d\bar{k}_{\perp,\text{out}}} = \sum_m{}' \int \frac{d^2k_m}{(2\pi)^2}\ \delta\left(\bar{k}_{\perp,\text{out}} - k_{\perp,\text{out}}\right)\ \frac{\mathbf{k}_{\text{out}}}{k}\ |M_m(\mathbf{k}_m, \mathbf{k}_{\|})|^2\,. \tag{193}$$

The latter would be measured in a time-of-flight experiment, while the first corresponds to measuring the outgoing energy or the energy lost to the film $E - E_{\text{out}}$. Finally, the spatio-kinetic distribution function contains all information about the film one can obtain from scattering data

$$p_{\text{inel}}(\bar{\mathbf{k}}_{\text{out}}) = \sum_m{}' \int \frac{d^2k_{\|}^{(m)}}{(2\pi)^2}\ \delta(\bar{\mathbf{k}}_{\text{out}} - \mathbf{k}_{\text{out}})\ |M^{(m,\mathbf{k}_{\|}^{(m)})}|^2 \tag{194}$$

It combines the cross sections defined by (193) and (191) and specifies the probability to find an inelastically scattered particle with wave vector $\bar{\mathbf{k}}_{\text{out}}$.

2.3. Relation between s, r_{inel}, and $\Im m\,\Sigma$ and

We can now close the circle and relate the result for r_{inel}, Eq. (186), to the expression of the elastic reflection probability $|R|^2$, in terms of the imaginary part of the self energy, eq. (168).

The summation over the Hartree states λ in the expression (163) for the self energy consists of a sum over the bound states, $\sum_{\lambda_i}$ plus an integral, $\int \frac{dk_{\perp,\lambda}}{\pi/2}$, over all scattering states of wave number $k_{\perp,\lambda}$ and energy $\epsilon_\lambda = \frac{\hbar^2 k_{\perp,\lambda}^2}{2m_I} - \mu_I$.

$$\Sigma_{\gtrless}(z,z',\mathbf{k}_{||};\omega) = -\frac{1}{L^2}\sum_{m,\mathbf{k}_m}\sum_{\lambda}^{\gtrless} \frac{W^*_{\lambda m}(z,\mathbf{k}_m,\mathbf{k}_{||}-\mathbf{k}_m)\; W_{\lambda m}(z',\mathbf{k}_m,\mathbf{k}_{||}-\mathbf{k}_m)}{\hbar\omega_m(k_m)+\epsilon_\lambda+\frac{\hbar^2(\mathbf{k}_m-\mathbf{k}_{||})^2}{2m_I}-\hbar\omega}\,, \tag{195}$$

where the superscripts $>$ and $<$ stand for $\epsilon_\lambda + \mu_i > 0$ and < 0, respectively.

For the imaginary part of the latter contribution we find

$$\Im m\,\Sigma_{>}(z,z',\mathbf{k}_{||};\omega) = -\frac{1}{L^2}\sum_{m,\mathbf{k}_m}{}' \frac{W_{\lambda m}(z,\mathbf{k}_m,\mathbf{k}_{||}-\mathbf{k}_m)\; W^*_{\gamma m}(z',\mathbf{k}_m,\mathbf{k}_{||}-\mathbf{k}_m)}{\hbar^2 k_{\perp,\text{out}}/m_I} \tag{196}$$

where λ is determined just as for the inelastic current, Eq. (177), and the prime on the sum denotes again summation over open channels, *i.e.* such that Eq. (177) yields $\epsilon_\lambda + \mu_I > 0$. We conclude that, by comparison with Eq. (186),

$$r_{\text{inel}} = \frac{2m_I}{\hbar^2 k_\perp}\int dzdz'\;\varphi^*_\omega(z)\,\Im m\,\Sigma_{>}(z,z',\mathbf{k}_{||};\omega)\,\varphi_\omega(z')\,, \tag{197}$$

By unitarity, the remainder of $1-|R|^2-r_{\text{inel}}$ must be s and comparison with (168) finally yields

$$s = \frac{2m_I}{\hbar^2 k_\perp}\int dzdz'\;\varphi^*_\omega(z)\,\Im m\,\Sigma_{<}(z,z',\mathbf{k}_{||};\omega)\,\varphi_\omega(z')\,, \tag{198}$$

Thus we conclude that the probability s for the incoming atom to be scattered into any of the sticking channels (only one for H) is given by $2m_I/\hbar^2 k_\perp$ times the expectation value of $\Im m\,\Sigma_<$ with respect to the elastic channels wave function φ_ω, where $\Im m\,\Sigma_<$ is the contribution of the *bound* Hartree states (i.e. the sticking channels) to $\Im m\,\Sigma$. And conversely, the probability r_{inel} that the atom is scattered back inelastically is determined by the expectation value of $\Im m\,\Sigma_>$, the part of $\Im m\,\Sigma$ contributed by the *scattering* states of the Hartree equation. One should, of course, expect such a result from an exact calculation, but the fact that our approximate treatment leads to the same conclusion documents the validity of our treatment especially because r_{inel} and $1-|R|^2$ were obtained by entirely different calculations.

2.4. Low energy limit of s

A number of exact statements can be made in the low–energy limit; for simplicity we restrict ourselves to scattering perpendicular to the surface, *i.e.* the parallel momentum $\mathbf{k}_{||}$ of the incoming current is zero. For the sticking coefficient $s(\mathbf{k})$ discussed in the following, this poses no restiction, because, in the low–energy limit, s depends only on the perpendicular component of the wave number $k_\perp$, $s = s(k_\perp)$.

To study the low–energy features of the solutions of either the Hartree–equation (60) or the full equation of motion (161), we divide the z-axis into three regions. The interaction region (I) is the one that coincides with the actual position of the film and its surface *i.e.* where the film density $\rho_1(z_1)$ is finite; the self–energy may be complex there. The intermediate region (II) is where both the substrate potential and a possible static potential due to the ^{4}He particles are larger or comparable to the energy of the incoming particle. Finally, the interaction is negligible in the far region (III). We give a brief summary of the properties of the solutions of the equation of motion (161) (and of the Hartree equation (60) for that matter):

(I): Close to and within the ^{4}He film, only fully solving Eq. (161) can yield φ_ω. Since E is assumed much smaller than the interaction energy between the scattered atom and the film, we are allowed to set $E = 0$, *i.e.* $\hbar\omega = |\mu_I|$, in Eq. (161). Provided that there is no resonance at $E = 0$, the correctly normalized solution can depend, to leading order, only through a scaling factor on the energy, which is determined by the *asymptotic* behavior of the solution.

(II): In the region II, we have to distinguish between Van der Waals fields that have a potential $U(z) \to -C_3 z^{-3}$, and shorter–ranged substrate potentials. The Van der Waals potential has been studied in detail in Ref. [**BBS82**]. Eq. (161) for $E = 0$ has the solution

$$\bar{\varphi}(z) = a\sqrt{z}J_1\Big(\sqrt{\frac{D}{z}}\Big) + b\sqrt{z}Y_1\Big(\sqrt{\frac{D}{z}}\Big)\,, \quad \text{with} \quad D = \frac{8m_I C_3}{\hbar^2} \tag{199}$$

where a and b are integration constants In the limit $C_3 = 0$ the solution is

$$\bar{\varphi}(z) \sim a_0 + b_0 z\,. \tag{200}$$

(III): The solution in region III is a free wave given, for Eq. (161), by (165)

$$\varphi_\omega(z) = 2i\sin[k_\perp(z + \frac{\delta_{k_\perp}}{k_\perp})] \tag{201}$$

The three expressions for the wave functions in region (I) — (III) have to be matched at their respective boundaries. In region (I), we can write the wave function of the incoming particle as

$$\varphi_\omega(z) \equiv k_\perp\bar{\varphi}(z) \tag{202}$$

where $\bar{\varphi}(z)$ is the zero–energy solution of Eq. (161), normalized such that $b = i\pi\sqrt{D}$ or $b_0 = 2i$, respectively, implying the leading behavior $\bar{\varphi}(z) \sim iz$ in region (III). The factorization (202) of the elastic channel wave function φ_ω in the limit $k_\perp \to 0$ leads for the elastic reflection probability (168) to

$$|R(k_\perp)|^2 \to 1 - s_1 k_\perp \tag{203}$$

where the proportionality constant s_1 is determined by the expectation value of $\Im m\Sigma$ with respect to $\bar\varphi(z)$, and is calculated below. The limiting behavior $|R(k_\perp)|^2 \to 1$ is the well-known effect of universal quantum reflection [**LJSD36a, LJSD36b**].

Our analysis of inelastic scattering, in particular the splitting of $\Im m\Sigma$ into contributions from bound and unbound Hartree states, allows us to determine the individual contributions to $1-|R|^2$ from sticking and from inelastic scattering, and to calculate s and $r_{\rm inel}$ from Eq. (198) and (197) independently. The calculation of *low–energy* scattering becomes particularly simple if the impurity has only one bound state attached to the ^{4}He surface. Atomic hydrogen is such a case; the following analysis does not apply to ^{3}He which not only has two Andreév states [**Hal95**], but also can penetrate into the bulk.

For low scattering energy, the impinging H atom can only couple to ripplons for scattering at a free ^{4}He surface or to third sound modes for scattering at thin ^{4}He films (*i.e.* the modes of perpendicular quantum number $m=0$, henceforth denoted by a subscript r), we therefore only need to retain the coupling matrix element of the incoming atom to the ripplon and the bound state

$$W_{\gamma,m}(z,\mathbf{k}_m,-\mathbf{k}_m) \equiv W_{r0}(z,k_m) = -\frac{\hbar^2}{2m_I}H_1^I(z)\tilde X_{rk_r}(z) \tag{204}$$

which yields for (198), in the limit of small E and $L\to\infty$

$$\begin{aligned} s \;&\to\; -\frac{8m_I}{\hbar^2 k_\perp}\int dz dz'\; k_\perp\bar\varphi^*(z)\;\Im m\int\frac{d^2k_r}{(2\pi)^2}\frac{W^*_{r0}(z,k_m)\,W_{r0}(z',k_m)}{\hbar\omega_m(k_m)+\frac{\hbar^2k_m^2}{2m_I}-|\mu_I|}\;k_\perp\bar\varphi(z') \\ &\to\; k_\perp\,\frac{4m_Ik_0}{\hbar^2}\,\frac{|\left(\bar\varphi\mid H_1^I(z)\mid \tilde X_{r,k_0}\right)|^2}{\hbar\omega_r'(k_0)+\frac{\hbar^2k_0}{m_I}}\end{aligned}$$

where k_0 is the solution of $\hbar\omega_r(k)+\frac{\hbar^2k^2}{2m_I}-|\mu_I|=0$.

In the Distorted Wave Born Approximation (DWBA), $\bar\varphi(z)$ in the expression for s is replaced by the analogously normalized Hartree eigenstate $\bar\eta(z)$, with $\hbar^2k_\perp^2/2m_I=E$. We can use the two-body Euler equation [**CKS97**]

$$(\eta^{(\boldsymbol\alpha)}|\tilde X^I|\phi^{(\boldsymbol m)}) = -2\frac{(\eta^{(\boldsymbol\alpha)}|\tilde V^I_{\rm p-h}|\phi^{(\boldsymbol m)})}{\varepsilon_{\boldsymbol\alpha}+\hbar\omega_{\boldsymbol m}} \tag{205}$$

to write s as

$$\begin{aligned} s \;&\to\; k_\perp\,\frac{16m_Ik_0}{\hbar^2}\left(\frac{|\mu_I|+E}{|\mu_I|+\omega_r(k_0)+\frac{\hbar^2k_0^2}{2m_I}}\right)^2\frac{\left|\left(\bar\eta\mid\tilde V_{r,k_0}\right)\right|^2}{\hbar\omega_r'(k_0)+\frac{\hbar^2k_0}{m_I}} \\ &\to\; k_\perp\,\frac{4m_Ik_0}{\hbar^2}\,\frac{\left|\left(\bar\eta\mid\tilde V_{r,k_0}\right)\right|^2}{\hbar\omega_r'(k_0)+\frac{\hbar^2k_0}{m_I}}\qquad\text{for } E\to 0\,, \end{aligned}\tag{206}$$

where $V_{m,k_m}(z)$ is defined analogously to $X_{m,k_m}(z)$, eq. (156). This is the result that would be obtained from a conventional Green's function theory.

The situation is more complicated for scattering of atoms which are bound more strongly to the film, like for example ^{3}He: firstly, falling into a lower chemical potential μ_I releases more energy, and film modes other than the ripplon mode can be excited; secondly, the atom can be trapped into states other than the Hartree ground state, located on the surface (*i.e.* the Andreev state [**And66**]). Both of these effects are essential; we will discuss these questions together with the results for s in section 3.

2.5. Low energy limit of r_{inel}

The next task is to derive the low energy limit of r_{inel}. For simplicitly, we restrict ourselves again to perpendicular incidence, $\mathbf{k}_{\|} = 0$. From the previous section, we know the total inelastic current (183). Hence, in the limit $L \to \infty$,

$$r_{\text{inel}} = \frac{1}{2\pi} \sum_m{}' \int dk_m k_m \; \frac{k_{\perp,\text{out}}}{k_\perp} \left| M_m(\mathbf{k}_m, 0) \right|^2 \,. \tag{207}$$

For low incident energies $E = \hbar^2 k^2/2m_I$, only third sound modes can be excited by processes where the incident particle is inelastically scattered with a lower energy $E_{\text{out}} = \hbar^2 k_{\text{out}}^2/2m_I < E$. All energetically higher modes $m > 0$ can again be neglected since, for films (as opposed to a free surface) they are seperated by an energy gap from the third sound modes. As above, the subscript r denotes this lowest (ripplon or third sound) mode.

If $\varepsilon_{\boldsymbol{\delta}} \eta^{(\boldsymbol{\delta})}$ in (64) is replaced by $H_1^I(\mathbf{r}_0)\eta^{(\boldsymbol{\delta})}$, we find for (182), for perpendicular incidence,

$$M_r(\mathbf{k}_r, 0) = \frac{2m_I}{\hbar^2 k_{\perp,\text{out}}} \frac{1}{2} \int dz \; \frac{\eta^{(\lambda)}(z)}{\sqrt{\rho_1^I(z)}} \left[\epsilon_\lambda \varphi_\omega(z) - (H_1^I(z)\varphi_\omega(z)) - \varphi_\omega(z) H_1^I(z) \right] \tilde{X}_{r,k_r}(z) \tag{208}$$

where $\epsilon_\lambda = |\mu_I| + E_{\text{out}}$. $H_1^I(z)\varphi_\omega(z)$ can be expressed by ω and the self energy using the equation of motion (161). Furthermore, from Eq. (205) in plane surface geometry $H_1^I(z)\tilde{X}_{r,k_r}(z)$ can be expressed by

$$H_1^I(z)\tilde{X}_{r,k_r}(z) \;\; = \;\; -(\hbar\omega_r(k_r) + \frac{\hbar^2 k_r^2}{2m_I})\tilde{X}_{r,k_r}(z) - 2\tilde{V}_{r,k_r}(z) \tag{209}$$

Using energy conservation, Eq. (177),

$$\begin{aligned} M_r(\mathbf{k}_r, 0) \;\; = \;\; \frac{2m_I}{\hbar^2 k_{\perp,\text{out}}} \;\; & \Bigg(\int dz \; \eta^{(\lambda)}(z)\, V_{r,k_r}(z) \varphi_\omega(z) \\ & + \frac{1}{2} \int dz dz' \; \eta^{(\lambda)}(z)\, X_{r,k_r}(z)\, \Sigma(z, z', 0; \omega)\, \varphi_\omega(z') \Bigg) \end{aligned} \tag{210}$$

According to eq. (207), the matrix element $M_r(\mathbf{k}_r, 0)$ is the probability amplitude for transitions from the elastic channel (φ_ω) to an exit channel ($\eta^{(\lambda)}$). We have brought $M_r(\mathbf{k}_r, 0)$ now into a form where the integrands vanish for large z irregardless of k_r, which is convenient for taking the low energy limit of r_{inel}. The operator for the "interaction" between in ($\mathbf{r}_0$) and out ($\mathbf{r}_0'$) channels, mediated by excitation of a film mode ($\mathbf{r}_1$), can be defined therefore

$$\hat{M}(\mathbf{r}_0, \mathbf{r}_0', \mathbf{r}_1) = \delta(\mathbf{r}_0 - \mathbf{r}_0') V_{p-h}(\mathbf{r}_0, \mathbf{r}_1) + \frac{1}{2} [X * \Sigma(\omega)](\mathbf{r}_0, \mathbf{r}_0', \mathbf{r}_1)$$

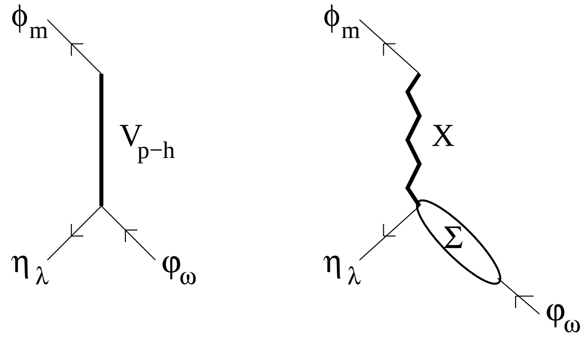

FIGURE 1. Diagrammatic representation of the two terms contributing to the operator $\hat{M}$ coupling elastic and inelastic scattering channels.

from which $M_r(\mathbf{k}_r, 0)$ is obtained by calculating the on-shell matrix element and summing over all unbound impurity states, *i.e.* over the exit channels,

$$M_m(\mathbf{k}_m, 0) = \sum_{\varepsilon_{\boldsymbol{\lambda}} > -\mu_I} \delta(\hbar\omega - \hbar\omega_{\boldsymbol{m}} - \varepsilon_{\boldsymbol{\lambda}}) \int d^3r_0 d^3r_0' d^3r_1 \; \varphi_\omega(\mathbf{r}_0)\eta^{(\boldsymbol{\lambda})}(\mathbf{r}_0')\phi_{\boldsymbol{m}}(\mathbf{r}_1) \; \hat{M}(\mathbf{r}_0, \mathbf{r}_0', \mathbf{r}_1)$$

In Fig.1, the two terms are represented as diagrams. The first term V_{p-h} of $\hat{M}$ is the particle-hole potential operator. For the free surface and for small k_r, V_{r,k_r} can be shown to be proportional to the z-derivative of the static Hartree potential V_H seen by the atom; the free surface limit is discussed in the next section. The second term $X * \Sigma(\omega)$, which has a longer range than the first, has no simple interpretation. In the following, we will see that, for low energy scattering, the second term of M_r dominates, while the first term can be neglected.

We have argued in section 2.4 that for low energies the wave functions $\varphi_\omega(z)$ and $\eta^{(\lambda)}(z)$, of energies E and $E_{\rm out}$, are proportional to $\sqrt{E}$ and $\sqrt{E_{\rm out}}$, respectively, within the interaction region *cf.* Eq. (202). We can therefore use that

$$\varphi_\omega(z) = k_\perp \bar{\varphi}(z) \ , \quad \eta^{(\lambda)}(z) = k_{\perp,{\rm out}} \bar{\eta}(z) \ , \tag{211}$$

where $k_{\perp,{\rm out}} = \sqrt{2m_I(E - \hbar\omega_r(k_r))/\hbar^2} = \sqrt{k_\perp^2 - 2m_I\omega_r(k_r)/\hbar}$; $\bar{\eta}$ is defined such that $\bar{\eta}(z) \to z$ for $z \to \infty$.

We finally must utilize the long–wavelength behavior of the third–sound wave function $\phi_r(z, k_r)$. In Ref. [**CKS94**] it was shown that, for $k_r \to 0$, the third sound wave function factorizes as

$$\phi_{r,k_r}(z_1) \;=\; \sqrt{\frac{\hbar k_r^2}{2m_B n \omega_r(k_r)}} \; \Phi_R(z_1) \tag{212}$$

which vanishes as $\sqrt{k_r}$ for $k_r \to 0$. $\Phi_R(z_1)$ is the shape of the long–wavelength density fluctuation, it is normalized to the areal density, $\int dz_1 \, \Phi_R(z_1)\sqrt{\rho(z_1)} = n$. Furthermore, we need the low-momentum behavior of $\tilde{X}_{r,k_r}(z_0)$ which is gained by solving Eq. (209) via expansion in Hartree states η_α,

$$\begin{aligned}\tilde{X}_{r,k_r}(z_0) &= -2\frac{\sqrt{\rho_1(z_0)}}{\hbar\omega_r(k_r)+\frac{\hbar^2k_r^2}{2m_I}}\int dz_0'\ \sqrt{\rho_1(z_0')}\tilde{V}_{r,k_r}(z_0') \\ &\quad -2\sum_{\alpha>0}\frac{\eta_\alpha(z_0)}{\epsilon_\alpha+\hbar\omega_r(k_r)+\frac{\hbar^2k_r^2}{2m_I}}\int dz_0'\ \eta_\alpha(z_0')\tilde{V}_{r,k_r}(z_0')\end{aligned}$$

In the limit of small k_r, only the term involving the overlap with the Andreev state needs to be taken into account

$$\tilde{X}_{r,k_r}(z_0)\to -\frac{2}{\hbar c_3 k_r}\sqrt{\frac{\hbar k_r}{2m_B n c_3}}V_r^{(0)}\sqrt{\rho_1(z_0)} \tag{213}$$

where

$$V_r^{(0)}=\int dz_0 dz_1\ \rho_1(z_0)V_{p-h}^I(z_0,z_1,0)\sqrt{\rho_1(z_1)}\Phi_R(z_1) \tag{214}$$

In the same limit, the channel amplitude $M_r(\mathbf{k}_r,0)$ is dominated by the second term of Eq. (210)

$$M_r(\mathbf{k}_r,0)=\sqrt{\frac{\hbar k_r^2}{2m_B n\omega_r(k_r)}}\frac{2m_I k_\perp}{\hbar^2}\frac{1}{\hbar\omega_r(k_r)}V_r^{(0)}M_r^{(0)} \tag{215}$$

where

$$M_r^{(0)} = \int dz_0 dz_0'\ \bar{\eta}(z_0)\,\Sigma(z_0,z_0';0,0)\,\bar{\varphi}(z_0') \tag{216}$$

The upper bound Q of the momentum–integration in Eq. (207) is determined by energy conservation: Q is the root of $E-\hbar\omega_r(k_r)-\hbar^2k_r^2/2m_I$, which, for low E and a third sound dispersion relation $\omega_r(k_r)=c_3k_r$ can be approximated by $Q\sim E/\hbar c_3$. Finally, we find for the inelastic scattering probability of slow particles hitting the ^{4}He film perpendicularly

$$\begin{aligned}r_{\rm inel} &\to k|M_r^{(0)}|^2|V_r^{(0)}|^2\left(\frac{2m_I}{\hbar^2}\right)^2\int_0^{E/\hbar c}\frac{dk_r}{2\pi}k_r\frac{\hbar^2k_r^2}{2m_B n\hbar c k_r}\frac{1}{(\hbar c k_r)^2}\sqrt{\frac{2m_I(E-\hbar c_3 k_r)}{\hbar^2}} \\ &= k^4\ \frac{2}{3}\frac{1}{2\pi n}\frac{m_I}{m_B}\frac{|M_r^{(0)}|^2|V_r^{(0)}|^2}{(\hbar c_3)^4}\end{aligned} \tag{217}$$

This result would not be expected in superficial inspection of (207): a matrix element which is localizied at the surface would lead to a proportionality $r_{\rm inel}\propto E^4$. It is the divergence of the third sound contribution to the direct correlation $X_{r,k}(z)$ with vanishing parallel wave number k_r which leads to $r_{\rm inel}\propto E^2$.

This divergence for k_r is linked to its exponentially slow decay with z, $X_{r,k}(z)\propto e^{-ak_rz}$ for large z and small k_r, and $a=\sqrt{m_I/2|\mu_I|}c_3k_r$, which follows from the differential equation (209) for $\tilde{X}_{r,k}(z)$ with given inhomogeneity $\tilde{V}_{r,k}(z)$. Hence, in the formulation (208) of the matrix element $M_r(\mathbf{k}_r,0)$, the interaction between incoming state φ_ω and outgoing state $\eta^{(\lambda)}$ is not limited to the surface region for small k_r: the incoming low-energy atom scatters well above the surface at a third sound mode; it need not travel all the way to the film surface, which is inhibited by quantum reflection, in order to create a surface wave and be deflected inelastically.

In DWBA, the second term of $M_m(\mathbf{k}_m, 0)$ as given by Eq. (210) is neglected altogether, because φ_ω is replaced by $2\eta^{(\omega)}$ (the factor is due to the different normalization). According to Eq. (207), $r_{\rm inel}$ in the DWBA is proportional to E^4 instead of E^2. Unlike the DWBA of the sticking coefficient s, which yields the same proportionality, albeit a different proportionality factor, the DWBA of $r_{\rm inel}$ leads to an altogether different proportionality. Further investigation is necessary to gain full confidence that the $r_{\rm inel} \propto E^2$ behavior is not an artifact caused by an approximation applied in the derivation of the equations of motion and of the second order impurity current, for example the uniform limit approximation.

We want to stress that, in our implementation of the HNC-Euler-Lagrange theory for excitations, only the elastic channel wave function φ_ω is improved over the Hartree states, but not the decay channels. This not only provides expressions for the Hartree potential and the self energy from a microscopic theory, but also fulfilles unitarity, $s + r_{\rm inel} + |R|^2 = 1$. In an exact theory, however, one could expect that the equation of motion, Eq. (161), has to be solved for the elastic channel wave function φ_ω self-consistently, *i.e.* the self-energy contains φ_{ω_γ} and ω_γ itself instead of the Hartree wave function $\eta^{(\gamma)}$ and ε_γ. The same holds for the currents, which will be matrix elements of the form $(\varphi_\omega|W|\varphi_{\omega_{\rm out}})$, and not of the mixed form $(\varphi_\omega|W|\eta_{k_{\rm out}})$, as it is the case here. Assuming that introducing the solutions of eq. (161) self-consistently back into the matrix elements is a step towards the exact solution of the N-body scattering problem, we could, in an ad hoc fashion, replace in Eq. (208) $\eta^{(\lambda)}$ by φ_λ. Eq. (210) would have to be replaced by

$$\begin{aligned} M_m(\mathbf{k}_m, 0) &= \frac{2m_I}{\hbar^2 k_{\perp,\rm out}} \Bigg(\int dz\ \varphi_\lambda^*(z)\, V_{r,k_r}(z) \varphi_\omega(z) \\ &+ \frac{1}{2} \int dz dz'\ X_{r,k_r}(z)\, [\varphi_\omega(z')\Sigma(z,z',0;\omega)\varphi_\lambda^*(z) - \varphi_\omega(z)\Sigma^*(z,z',0;\epsilon_\lambda)\varphi_\lambda^*(z')] \Bigg) \end{aligned} \tag{218}$$

which can be shown to yield $r_{\rm inel} \propto E^4$, because $\Im m\Sigma$ vanishes in the limit $E \to 0$. But we stress that to our knowledge there is no mathematical reason to believe that (218) is an improvment over (210).

A final word about the energy regime where Eq. (217) is valid:

1. In the derivation of the low energy properties we assumed to be in the quantum reflection regime, *i.e.* the long wavelength factorization (211) is fulfilled. As it is well known, long-ranged substrate potentials can reduce this regime to energies below 1 mK, and hence (217) fails for higher energies.
2. The estimate for the effect of the film thickness d is straightforward: typically, the linear third sound dispersion holds if the parallel wave number is less than the inverse film thickness, $k_r \ll \frac{1}{d}$. The same is true for the low k_r behavior of the other ingredients V_{r,k_r} and X_{r,k_r}. Hence, with increasing E (but still small enough for condition (211) to be fulfilled) or with increasing film thickness, there will be a crossover to a free surface behavior of $r_{\rm inel}$, which is discussed in the following section.

2.6. Low energy inelastic reflection at a free surface

For completeness, we also derive the case of a free liquid surface. Some important identities follow from the fact that all impurity states shift with a rigid displacement of the profile of the background density. In the absence of a substrate, the Hartree–potential is a functional of the background density alone, hence we can write

$$V_H^I[\rho_1(z+\xi)](z_0) = V_H^I[\rho_1(z)](z_0+\xi) \tag{219}$$

Expanding the Hartree–equation (60) to first order in the displacement ξ and noting that $V_{\rm p-h}^I(\mathbf{r}_0,\mathbf{r}) = \delta V_H^I(\mathbf{r}_0)/\delta\rho_1(\mathbf{r})$ we obtain the identity

$$H_1^I(z_0)\frac{d\eta^{(\alpha)}(z_0)}{dz_0} + \eta^{(\alpha)}(z_0)\int dz V_{\rm p-h}(z_0,z,0+)\frac{d\rho_1(z)}{dz} = \epsilon_\alpha \frac{d\eta^{(\alpha)}(z_0)}{dz_0}\,. \tag{220}$$

A special consequence is

$$\frac{dV_H(z_0)}{dz_0}\sqrt{\rho_1^I(z_0)} = -H_1^I(z_0)\frac{d\sqrt{\rho_1^I(z_0)}}{dz_0} = \sqrt{\rho_1^I(z_0)}\int dz V_{\rm p-h}(z_0,z,0+)\frac{d\rho_1(z)}{dz} \tag{221}$$

because $H_1^I(z_0)\sqrt{\rho_1^I(z_0)} = 0$.

The ripplon wave function in an infinite half space is [**KSE88, CKS94**]

$$\phi_r(z) = \left(\frac{2\hbar k_r}{m_B\rho_\infty\omega_r(k_r)}\right)^{1/2}\frac{d\sqrt{\rho_1(z)}}{dz} \tag{222}$$

where $\omega_r^2(k_r) = \sigma k_r^3/(m_B\rho_\infty)$ is the ripplon disperion, ρ_∞ is the bulk density, and σ is the surface energy. Therefore, we have

$$V_{r,k_r}(z_0) = \left(\frac{2\hbar k_r}{m_B\rho_\infty\omega_r(k_r)}\right)^{1/2}\frac{dV_H(z_0)}{dz_0} \tag{223}$$

Secondly, we need $X_{r,k_r}(z_0)$ for small k_r, to be determined from (209): expansion in the Hartree states η_α yields

$$\tilde{X}_{r,k_r}(z) \to -2\sum_{\alpha\neq 0}\eta_\alpha(z)\frac{1}{\epsilon_\alpha}\int dz'\ \eta_\alpha(z')\tilde{V}_{r,k_r}(z') \tag{224}$$

where we have used, that, due to Eq. (221), η_0 and $\tilde{V}_{r,0}(z_0)$ do not overlap. Inserting Eq. (223) and the Hartree equation $H_1^I(z)\eta_\alpha(z) = \epsilon_\alpha\eta_\alpha(z)$ and parital integration leads to

$$\tilde{X}_{r,k_r}(z) = 2\sqrt{\frac{2\hbar k_r}{m\rho_\infty\omega(k_r)}}\ \frac{d\sqrt{\rho_1^I(z)}}{dz} \tag{225}$$

With these expressions for the long wave length limits of $V_{r,k_r}(z)$ and $X_{r,k_r}(z)$ the channel amplitude can be determined according to Eq. (210), of which now both terms contribute to the low-energy limit of $r_{\rm inel}(E)$:

$$M_r(\mathbf{k}_r,0) = \frac{2m_I k_\perp}{\hbar^2}\left(\frac{2\hbar k_r}{m_B\rho_\infty\omega_r(k_r)}\right)^{1/2} M_r^{(0)} \tag{226}$$

with

$$M_r^{(0)} = \int dz\ \bar{\eta}(z)\ \frac{dV_H(z)}{dz}\ \bar{\varphi}(z) + \int dzdz'\ \bar{\eta}(z)\ \frac{\eta_0'(z)}{\eta_0(z)}\ \Sigma(z,z',0;0)\ \bar{\varphi}(z') \tag{227}$$

where $\eta_0 = \sqrt{\rho_1^I}$. This yields for $r_{\rm inel}$ the low energy limit

$$\begin{aligned} r_{\rm inel} &= \frac{k_\perp}{2\pi} \int dk_r k_r\ k_{\perp,{\rm out}} \frac{2\hbar k_r}{m_B \rho_\infty \omega_r(k_r)} \left(\frac{2m_I}{\hbar^2}\right)^2 \left|M_r^{(0)}\right|^2 \\ &= \frac{4}{9\pi} \left(\frac{2m_I}{\hbar^2}\right)^3 \left|M_r^{(0)}\right|^2 \left(\frac{E}{\sqrt{\sigma}}\right)^2 \end{aligned} \tag{228}$$

In DWBA, where $\bar{\varphi}$ is replaced by $2\bar{\eta}$, we are left with only the first term of $M_r^{(0)}$, see the previous section. Partial integration and using the equations (60) and (211) yields for $M_r^{(0)}$

$$\begin{aligned} M_r^{(0)} &= 2\int dz\, \frac{dV_H(z)}{dz}\, [\bar{\eta}(z_0)]^2 = -\frac{\hbar^2}{m_I} 2 \int dz\, \frac{d^2\bar{\eta}(z_0)}{dz^2} \frac{d\bar{\eta}(z_0)}{dz} \\ &= -\frac{\hbar^2}{m_I} \left[\frac{d\bar{\eta}(z_0)}{dz}\right]^2_{z_0\to\infty} = -\frac{\hbar^2}{m_I} \end{aligned}$$

where we used the asymptotic behaviour $\bar{\eta}(z) \to z$. *I.e.* the matrix element, and thus the inelastic reflection probability, for low energy is independent of the structure of the surface, except for the surface energy,

$$r_{\rm inel} = \frac{16}{9\pi} \frac{2m_I}{\hbar^2} \left(\frac{E}{\sqrt{\sigma}}\right)^2 \tag{229}$$

to first order DWBA. A similar result has been shown for the small angle inelastic scattering for penpendicular incidence on finite temperature films [**HS89, TSV90**], see also the next section.

The effect of higher orders of the full Born series (228), *i.e.* the full solution of the equation of motion (161), is to introduce a dependence of $r_{\rm inel}(E \to 0)$ on the dynamical quantities of the scattering process: the scattering wave function $\bar{\varphi}$ and the self energy $\Sigma(z,z',0;0)$.

2.7. Small angle inelastic scattering

The discussion of inelastic small angle deflection (*quasi-elastic* scattering) is similar to the above discussion about inelastic scattering at low energies, in that only long wave-length surface modes are excited. Again we restrict ourselves to perpendicular incidence for simplicity, but the qualitative features of the conclusions are the same for any angle of incidence.

The probability for inelastic scattering into an angle θ is given by Eq. (191). The contribution from third sound to inelastic small angle scattering, $\theta \to 0$, is obtained by expanding (191) for small $k_m \equiv k_r$

$$\lim_{\theta\to 0} \frac{d\sigma(\theta)}{d\Omega} = \frac{k^2_{\perp,{\rm out}}}{4\pi^2} \left|M_r(\mathbf{k}_r, 0)\right|^2 \tag{230}$$

with $k_r \to k_\perp \sin\theta$ and $\epsilon_\lambda = \frac{\hbar^2 k^2_{\perp,{\rm out}}}{2m_I} - \mu_I$, and we can use that, for $\theta \to 0$, $k_{\perp,{\rm out}} \to k_\perp$. For thin films, at incident energies lower than $\hbar\omega_m(0)$, $m > 0$, generation of third sound is the only open channel for inelastic scattering. We have already worked out the low momentum matrix element for the third sound channel in section 2.5. $\frac{d\sigma}{d\theta} = 2\pi \sin\theta \frac{d\sigma}{d\Omega}$ becomes for almost specular reflection

$$\lim_{\theta\to 0} \frac{d\sigma(\theta)}{d\theta} = \frac{1}{2\pi n} \frac{m_I}{m_B} \frac{2m_I}{\hbar^2 k_\perp} \frac{|V_r^{(0)}|^2}{(\hbar c_3)^3} \left| \int dz_0 dz_0' \, \eta_{k_{\rm out}}(z_0)\, \Sigma(z_0, z_0', 0; \omega)\, \varphi_\omega(z_0') \right|^2 \tag{231}$$

As for the low energy limit of $r_{\rm inel}$, the DWBA would lead to a qualitatively different result: $\frac{d\sigma}{d\Omega}$ would vanish linearly in θ; *i.e.* $\frac{d\sigma}{d\Omega}$ would have a hole in the specular direction. Instead we find that the inelastic reflection of an impurity at a ^{4}He film in specular direction has finite probability, and accordingly $\frac{d\sigma}{d\Omega}$ diverges as $1/\theta$.

For low energy scattering, Eq. (215) can be inserted

$$\lim_{k_\perp\to 0} \lim_{\theta\to 0} \frac{d\sigma(\theta)}{d\theta} = \frac{k_\perp^3}{2\pi n} \frac{m_I}{m_B} \frac{2m_I}{\hbar^2} \frac{|V_r^{(0)}\, M_r^{(0)}|^2}{(\hbar c_3)^3} \tag{232}$$

Comparison of this result with the low-energy limit scattering probability $r_{\rm inel}$ (217) shows that the latter vanishes fast with $k_\perp$:

$$\frac{d\sigma(\theta=0)}{d\theta} \propto k_\perp^3 \qquad \text{and} \qquad r_{\rm inel} \propto k_\perp^4\, . \tag{233}$$

According to the definitions (186) and (187), both quantities are related via

$$r_{\rm inel} = \int d\theta \, \cos\theta \, \frac{d\sigma(\theta)}{d\theta}\, , \tag{234}$$

therefore the width of the angular distribution $\frac{d\sigma(\theta)}{d\theta}$ must be of order $k_\perp$: the inelastic scattering probabilite distribution of low-energy impurities at ^{4}He films is sharply peaked in the specular direction.

3. Results

We consider liquid ^{4}He adsorbed to a plane attractive substrate which is translationally invariant in the $x-y$ plane, *i.e.* $U_{\rm sub}(\mathbf{r}) = U_{\rm sub}(z)$. The systems under consideration are characterized by a Van der Waals substrate potential whose long range $U_{\rm sub}(z) \to -C_3/z^3$ is crucial for low energy scattering properties, as we shall see; and by the surface coverage

$$n = \int_0^\infty dz \rho_1(z)\ , \tag{235}$$

where $\rho_1(\mathbf{r}) = \rho_1(z)$ is the density profile of the ^{4}He host system. This density profile is, along with the energetics, structure functions, and excitations of the film, obtained through the optimization of the ground-state as outlined above, and in much more detail in our previous work [**CEKS93**]. However, unlike in earlier work, where the dependence of the features of the films on the substrate potential has been studied explicitly, we choose here a graphite substrate for all calculations.

The H-He potential has been the subject of several *ab initio* calculations. Jochemsen *et al.* [**JBH84**] have discussed the available potentials, measured the diffusion of H in He gas at low temperature and proposed a potential (R2) which has become the *de facto* standard

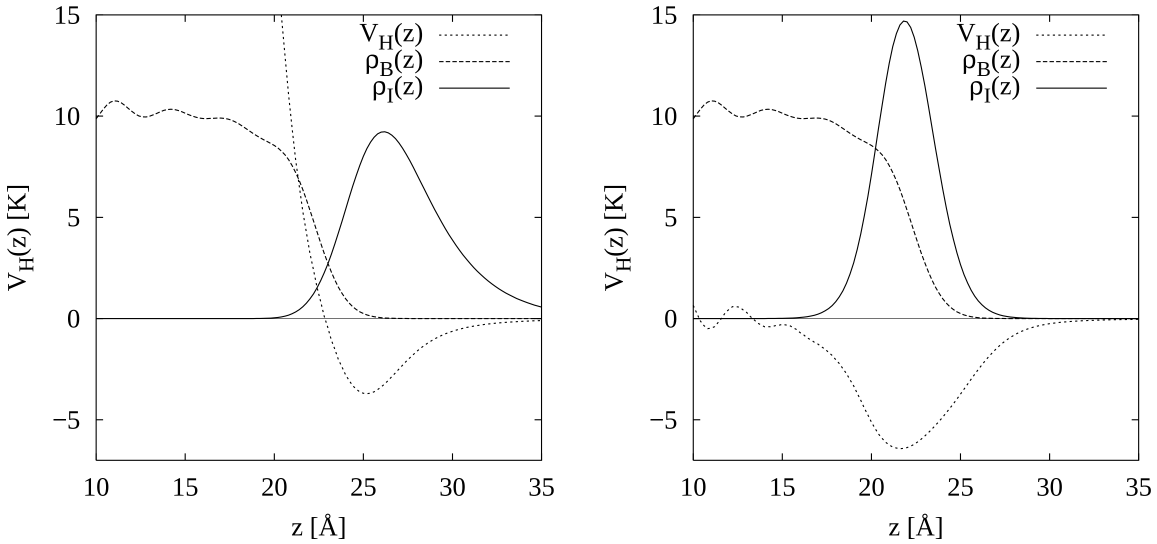

FIGURE 2. The figure shows the profile of the ^{4}He background, the ground state density $\rho_I(z)$ of hydrogen (left) and ^{3}He (right) and the respective one–body Hartree potential V_H seen by the impurity. The underlying model is always a ^{4}He films with areal density $n = 0.45\,\text{Å}^{-2}$.

for atomic hydrogen researchers. However, Jochemsen *et al.* themselves preferred to use the older potential of Das *et al.* [**DWW78**], which is essentially the same as R2. For the sake of simplicity, we have, however, used the Lennard-Jones 6-12 potential by Toennies *et al.*[**TWW76**]; we have compared the results, in the bulk liquid, with those obtained from the potential of Ref. [**DWW78**] and found that the binding energies differ by less than five percent.

3.1. Static structure

We have carried out a sequence of ground state calculations for our model of a helium film adsorbed to a graphite substrate [**CEKS93**], with a coverage up to $n = 0.45$ Å^{-2}, corresponding to about seven liquid layers or to a thickness of $d = 22.3$Å, where d is defined as the first minimum of $\frac{d\rho_1(z)}{dz}$ coming from the vacuum side. d is only meaningful for films where the surface profile has attained its asymptotic form, while for graphite-adsorbed films of 3 or less atomic layers d and n are not proportional. Starting at a coverage of $n = 0.20$ Å^{-2}, the energy of the ground state of the hydrogen impurity is fairly independent of the coverage.

The impurity ground states are shown, for a hydrogen and a ^{3}He atom, in Fig.2. The figure also shows the background as a reference, and the effective potential $V_H^I(z)$. More than the binding energy or the shape of the ground state, the effective potential $V_H^I(z)$ highlights the difference between the helium and the hydrogen impurities: While the hydrogen impurities have to overcome a rather steep potential well to intrude into the film, such a potential well is – as it is well known – absent in the case of helium. Our results for the Andreev ground state energy μ_I of H and ^{3}He are -1.1K and -4.8K, respectively, for $n = 0.45$ Å^{-2}. Fig.3

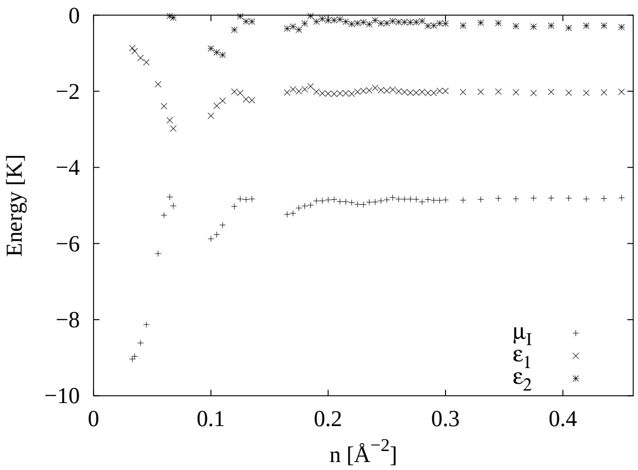

FIGURE 3. The chemical potential μ_I and excited state energie ε_i for ^{3}He in ^{4}He films of coverage n. The gaps indicate coverages with unstable layering, *i.e.* where a ^{4}He film on graphite is microscopically unstable, and hence does not exist.

shows μ_I of ^{3}He, as well as its excited states in Hartree approximation, as a function of n. ^{3}He binding energies have been discussed extensively in Ref. [**CKS97**].

Fig.4 shows μ_I of H, focusing on thick films (the emulation of films beyond $n = 0.45$ Å^{-2} is explained below), where we have also checked the sensitivity of μ_I on retardation effects, modeled by a correction factor $(1+\frac{z}{\lambda})^{-1}$ for the substrate potential, with $\lambda = 200$Å [**CC92**]. Not surprisingly, the attractive Van der Waals tail of the substrate potential pulls the H atom stronger to the ^{4}He film and increases the binding energy with decreasing film thickness. The full curve is a fit of the function

$$\bar{\mu}(d) = \mu(\infty) + U_{\rm sub}(d + D) \tag{236}$$

where we have set $\mu(\infty) = -0.99$K, the chemical potential of H on the 522Å film. This formula assumes that the free surface Andreév state is located at a distance D from the film, and its energy is decreased by the value of the substrate potential at that point. For films $n \leq 0.45$Å^{-2}, which have been calculated separately without employing the thick film approximation of shifting the potential, μ is not very smooth, and the variations about the fit can be regarded as the numerical uncertainty of the ground state optimization.

It is also interesting to know the H-He pair correlation function for H adsorbed on ^{4}-He. This is relevant in calculations of the optical spectrum for adsorbed H, for example. One can also use it to calculate the hyperfine frequency shift. This is interesting in the context of the cryogenic hydrogen maser, not as a necessary input, but as an interesting piece of associated physics.

There are two related ways to look at the pair distribution function which give, while related, different pieces of information. The starting quantity is the general pair distribution

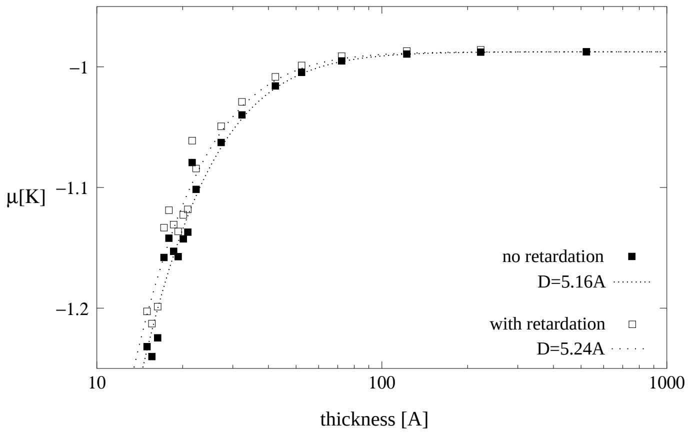

FIGURE 4. The Andreev state energy for H on films of several thicknesses, with (full square) and without retardation (outline square). The dotted lines are simple fits, with the fit parameter D being an effective distance of H from the film surface, see text.

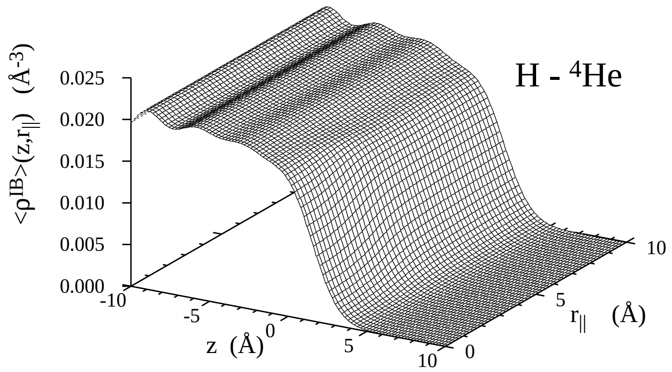

FIGURE 5. The figure shows the correlation hole $\langle \rho^{IB} \rangle (z, r_{||})$ as defined in Eq. (239) around an impurity in it's ground state for a H atom on a ^{4}He films with areal density $n = 0.45\,\text{Å}^{-2}$.

which is, in our geometry, a function of three variables

$$g^I(\mathbf{r}_0, \mathbf{r}) \equiv g^I(z_0, z, \left|\mathbf{r}_0^{||} - \mathbf{r}^{||}\right|) \,. \tag{237}$$

The z-coordinate of the impurity should be taken at the average location of the impurity ground state, in other words we define an average pair distribution function as

$$\langle g^I \rangle (\mathbf{r}) \equiv \int dz_0 \rho_1^I(z_0) g^I(z_0, z, |\mathbf{r}_0^{||} - \mathbf{r}^{||}|) \,. \tag{238}$$

This average pair distribution function describes the local environment of the impurity. Information on the distribution of ^{4}He atoms in the vicinity of the impurity is contained in the averaged two body density, which is the density of ^{4}He atoms subject to the condition that the impurity is located in its ground state at $r_{\|} = 0$, i.e.

$$\left\langle \rho^{IB} \right\rangle (\mathbf{r}) \equiv \rho_1(z) \left\langle g^I \right\rangle (\mathbf{r}) = \rho_1(z) \int dz_0 \rho_1^I(z_0) g^I(z_0, z, |\mathbf{r}_0^{\|} - \mathbf{r}^{\|}|), \tag{239}$$

The latter quantity is perhaps a little more illustrative, we therefore show $\left\langle \rho^I \right\rangle (\mathbf{r})$ for hydrogen in Fig. 5.

3.2. Scattering: general discussion

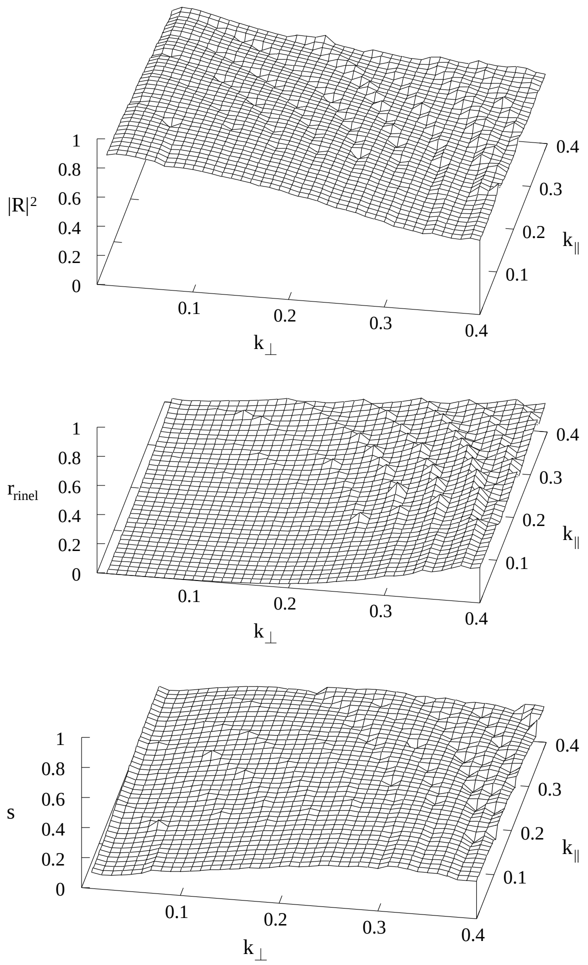

FIGURE 6. The figure shows the elastic reflection probability $|R(k_{\|}, k_{\perp})|^2$, the inelastic reflection probability $r_{\mathrm{inel}(k_{\|},k_{\perp})}$, and the sticking probability $s(k_{\|}, k_{\perp})$ of an H atom impinging on a ^{4}He film of thickness $n = 0.450$ Å^{-2} in dependence of the wave vector $\mathbf{k} = (k_{\|}, 0, k_{\perp})$.

We now turn to the main purpose of this chapter, the results for scattering processes, where in the analysis of our results, we focus on inelastic processes.

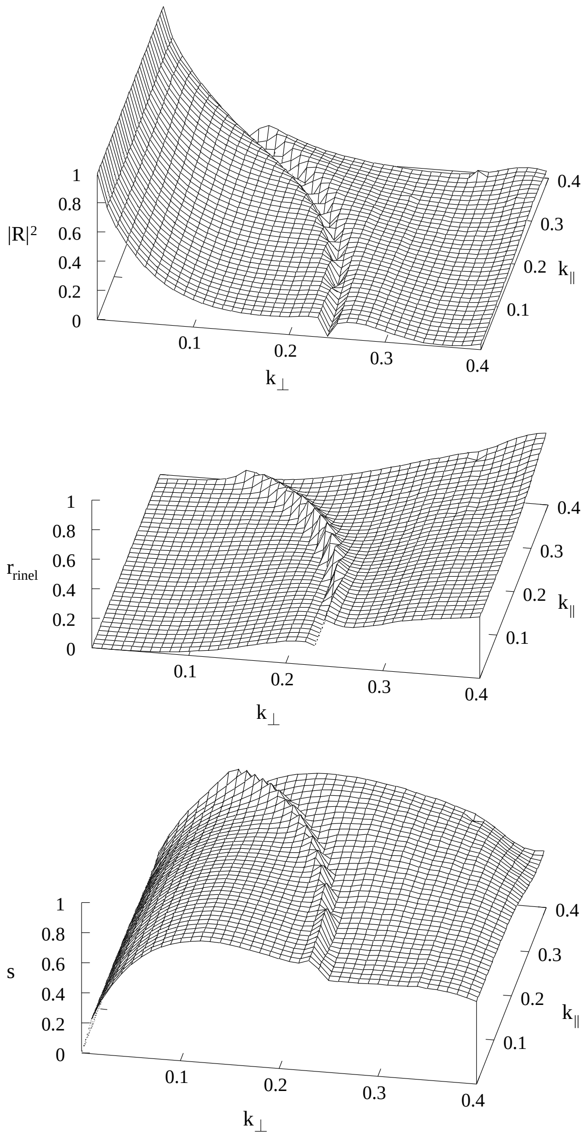

FIGURE 7. Same as Fig. 6 for ^{3}He.

In figures 6 and 7, we show the probabilities for the three types of scattering events off the film of coverage $n = 0.45$ Å^{-2}, for a H and a ^{3}He atom of wave vector $\mathbf{k}$, respectively:

1. the elastic scattering probability $|R(\mathbf{k})|^2$ is the probability to couple only to *virtual* excitations (real part of self energy) such as ripplons and phonons which have a large effect on $|R|^2$ as well as the other two probabilities;
2. the inelastic scattering probability $r_{\rm inel}(\mathbf{k})$, as defined in section 2.1, that the atom excites third sound waves (and, for high enough incident energy and with lower probability, other modes of the film), but still retains enough energy to leave the film;

3. the sticking coefficient $s(\mathbf{k})$, which is the probability that the atom transfers all kinetic energy and the binding energy of the Andreev state (or bound excited state in case of ^{3}He scattering) to the film.

The manifest difference between H and ^{3}He is the smoothness of $|R(\mathbf{k})|^2$, $r_{\rm inel}(\mathbf{k})$, and $s(\mathbf{k})$ as a function of energy and scattering angle for H scattering, as compared to ^{3}He scattering. The noticable ridge in $|R|^2$ for ^{3}He is a substrate-film interface resonance, which is the precursor of a second Andreev state between the film and weaker substrate than graphite, which we found for the metastable cesium adsorbed films [**KZ98**]. For H, the ^{4}He film is not so much a potential well, but a wall (see Fig. 2), therefore the substrate-film resonance as well as other resonances related to the thickness of the film, which can be seen in scattering of ^{3}He are missing for scattering of H atoms.

In Fig.8, $|R(\mathbf{k})|^2$, $r_{\rm inel}(\mathbf{k})$, and $s(\mathbf{k})$ are shown for perpendicular incidence with higher energy resolution. For higher energies up to 10K, impinging H atoms apparently decay into the 3 channels with approximately equal probability. However, the phase space for multi-excitations increases with increasing energy, and the form of the self–energy (163) as well as the current (183) implies that decay into more than two elementary excitations is excluded. Therefore, corrections from multi-excitation processes are to be expected at high scattering energies.

3.3. Low energy sticking of ^{3}He

From experiments [**YDSea93**] as well as calculations [**CC92, KZ98**], it is obvious that, for sufficiently thin films, the effect of universal quantum reflection, $1-|R|^2 \propto k_\perp$, for small incident momenta $\hbar k$, can be suppressed by low lying resonances of the long-ranged tail of the substrate potential, $-C_3/z^3$.

Fig.9 shows the leading coefficient of the expansion of s in $k_\perp$, $s_1 := \lim_{k_\perp\to 0}\frac{s(k_\perp)}{k_\perp}$, for H and ^{3}He scattered at graphite adsorbed ^{4}He films, for the whole series of coverages n for which for which we have carried out the HNC optimization procedure of the film and the H and ^{3}He impurity, respectively. $s_1(^3\mathrm{He})$ exhibits peaks for $n < 0.20\,\text{Å}^{-2}$, whose sharpness decreases with increasing n. The full line is a fit to a Lorentzian. These peaks indicate the accommodation of bound states of ^{3}He in the film as its thickness increases. The peaks of $s(n)$ are less pronounced for larger n and beyond $n = 0.2\text{Å}^{-2}$ we could not distinguish maxima of s from numerical fluctuations. These bound states become more and more dense with increasing n until they form the dense set of bulk modes of ^{3}He solved in ^{4}He. To obtain the binding energy of these states, the full equation of motion (161) would have to be solved for the elastic channel wave function φ_ω, for $\hbar\omega < -\mu_I$; they do not show up in the Hartree equation, which demonstrates the important role of the self energy to lower the excitation energies with respect to the Hartree energies. Therefore, a similarly cautionary comment as for $r_{\rm inel}$ in section 2.6 is applicable to s: in an exact theory, these new bound states are actual decay channels for sticking and are obtained selfconsistently from the equation of motion (161), while here the decay channels are obtained from the Hartree equation (60); hence,

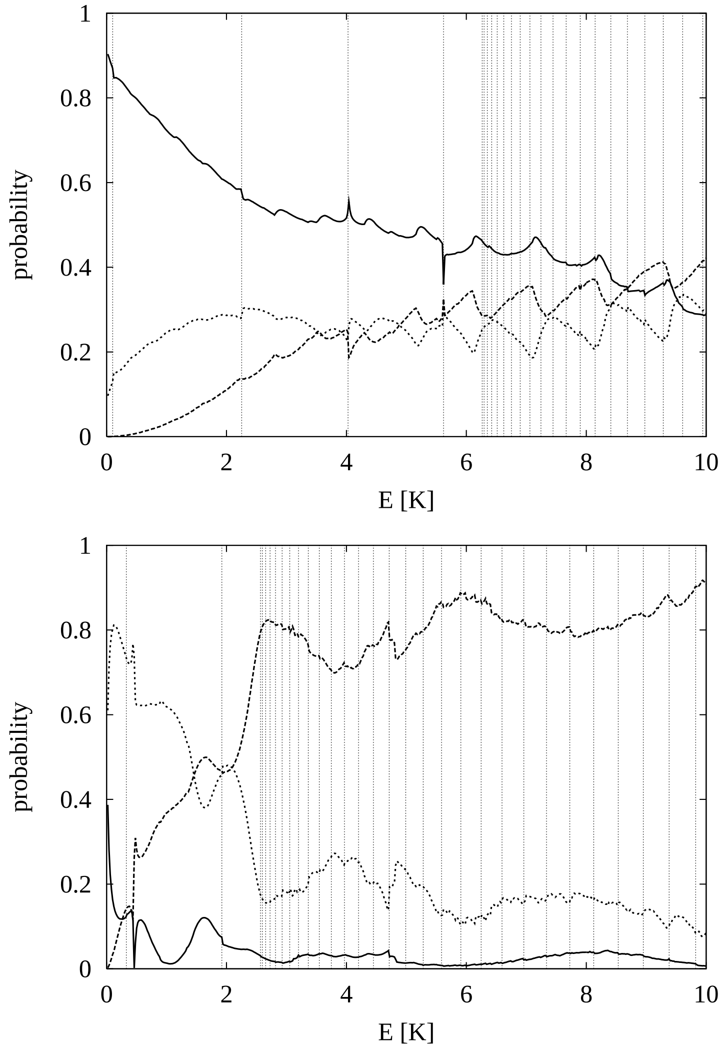

FIGURE 8. The figures shows the elastic (full) and inelastic (dashed) reflection probabilities $|R(E)|^2$ and $r_{\rm inel}$ and the sticking probabilities $s = 1 - |R(E)|^2 - r_{\rm inel}$ for the perpendicular incidence of H (upper figure) and ^{3}He (lower figure) on a graphite adsorbed ^{4}He film of coverage $n = 0.450\,\text{Å}^{-2}$. The threshold energies for channels associated with sticking are indicated with lines, which become a continuum at $E = \mu_I - \mu_B$. For ^{3}He, the sharp drop of $|R(E)|^2$ to zero at $E = 0.45$ K is caused by the resonance at the substrate-film interface.

the occurrence of new bound states does not show up as new decay channels, but only as resonance peak in s as well as a π jump in the phase shift δ of the elastic scattering amplitude $R = |R|e^{2i\delta}$, in accordance with Levinson's theorem [**Tay72**], see below.

For ^{3}He several sticking channels are open. Table 1 splits s_1 into the contribution of the respective channels. Clearly, excitation of a long wave-length third sound wave is the

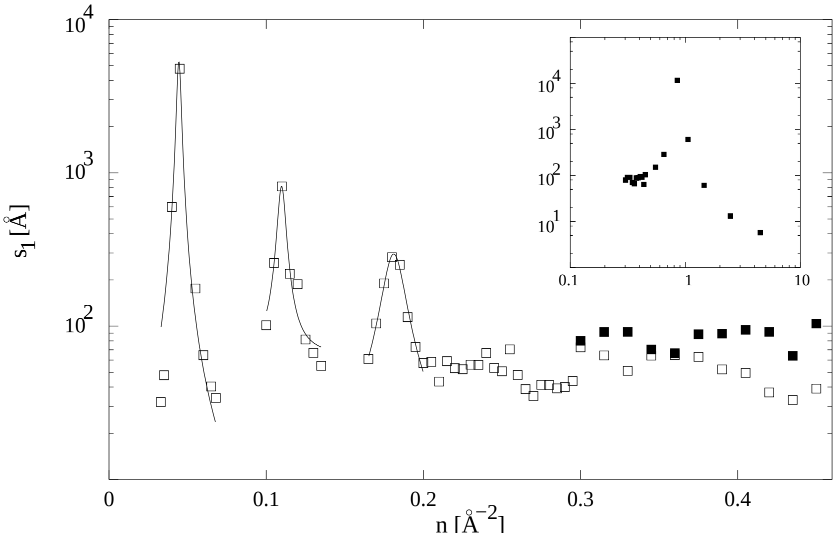

FIGURE 9. The low energy sticking coefficient of ^{3}He (open squares) and H (filled squares), divided by the incident perpendicular momentum $k_\perp$, $s_1 = \lim_{k_\perp \to 0} \frac{s}{k_\perp}$, is plotted as a function of the coverage n of a ^{4}He adsorbed on graphite. s_1 for H scattering at thicker films is shown in the inset.

n[Å^{-2}]	0.200	0.250	0.300	0.375	0.450
total [Å]	57.0	50.8	72.6	63.0	39.1
1—1 [Å]	2.2	1.3	7.3	10.5	<1
1—2 [Å]	19.9	36.3	8.5	7.3	18.2
1—3 [Å]	30.2	8.7	46.4	42.0	15.1
2—1 [Å]	4.7	4.4	<1	<1	<1
2—2 [Å]	–	–	2.8	<1	<1
3—1 [Å]	–	–	7.1	2.0	3.2

TABLE 1. Sticking coefficient $\lim_{k_\perp \to 0} \frac{s(k_\perp)}{k_\perp}$, of ^{3}He on a ^{4}He film of thickness n, adsorbed on graphite. The first row contains the total sticking coefficient, while in the rows below it is split up into the contributions of [film mode m]—[^{3}He state α], where $m = 1$ denotes the ripplon and $\alpha = 1$ denotes the Andreev state. A dash denotes a closed channel.

predominant decay channel, irrespective of the final impurity state. In fact, table 1 shows that trapping into the Andreev state is unlikely compared to trapping into excited impurity states, because due to energy conservation falling into the Andreev state releases more energy than decay into an excited bound state, which excites a third sound mode of longer wave length. The tentative conclusion for ^{3}He scattering at the *free* ^{4}He surface is, that ^{3}He at low energies preferably penetrates into the bulk, after exciting a long wave length ripplon instead of being trapped on the surface which would excite an energetic surface wave with wave length $\lambda \approx 15$Å. Since for sticking the predominance of coupling to third sound above other, more phonon-like modes is accompanied by ^{3}He travelling back and forth through the whole film, emulation of thick films cannot be considered reliable for ^{3}He sticking in the form expained below for hydrogen sticking.

3.4. Low energy sticking of H

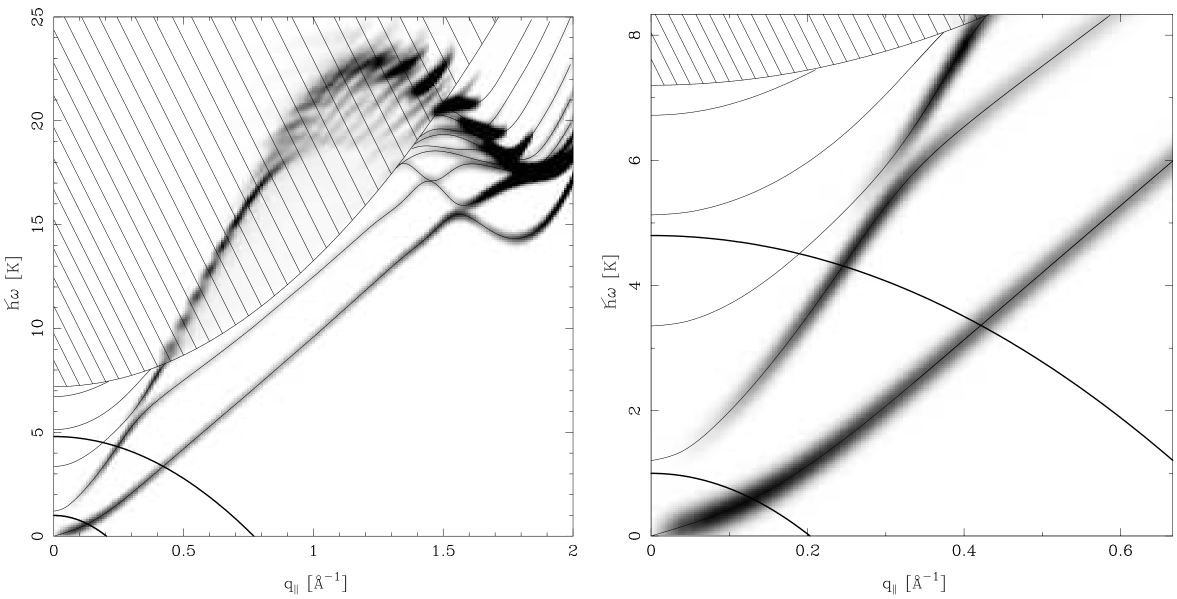

FIGURE 10. The Feynman spectrum (continuum is hatched; $n = 0.45\,\text{Å}^{-2}$) and, also in Feynman approximation, $S(k_{\|}, \omega)$ (broadened with a gaussian of width 0.25K to display its strength in grey scale) are shown. The two thick lines are $|\mu| - \frac{\hbar^2 k_{\|}^2}{2m^I}$ for ^{3}He and H. Hence for vanishing incident energy, their cutting point with the Feynman dispersion yields the Feynman modes excited by decay into the Andreev impurity ground state.

The situation of H scattering is very different from ^{3}He scattering. Since hydrogen has a positive chemical potential (the HNC-Euler-Lagrange theory yields 31.6 K for H in bulk ^{4}He, see the introduction), the number of bound states is not increasing with the film thickness eventually forming a continuum, but for H, the ^{4}He interface is essentially a hard wall beyond a depth of a few Å, see fig.2. Furthermore, the third sound modes created in a sticking process have a wave number of 0.13Å^{-1} which follows from energy conservation and the dispersion relation; in Fig.10, the Feynman spectrum as is appears in the energy denominator of the self energy is shown together with the dynamic structure function for parallel momentum transfer $S(k_{\|}, \omega)$ and $|\mu| - \frac{\hbar k_{\|}^2}{2m^I}$ for both ^{3}He and H. Surface modes of this (and higher) wave number have already attained the free surface limit for the thickest film we have calulated,

$n = 0.45\text{Å}^{-2}$. Therefore – only for H scattering – it is admissible to emulate scattering at thicker film by shifting the substrate potential away from the adsorbed film and filling the gap with homogeneous inert ^{4}He at equilibrium bulk density, $\rho_\infty = 0.0218\text{Å}^{-3}$. What we find is that, due to the much stronger attraction of H to the graphite substrate, the H atom has a weakly bound state in addition to the Andreev ground state, provided that H can come close to the substrate, *i.e.* for thin ^{4}He films. With increasing n, H is pushed away from the energetically favorable well produced by the Van der Waals tail $-C_3/z^3$ and the weakly bound state becomes a low energy resonance — in contrast to ^{3}He, where the situation is reversed: resonances become bound bulk-like modes with increasing n. But in both cases, these resonances lead to an enhancement of the sticking coefficient s_1 of several orders of magnitudes, see inset in Fig.9.

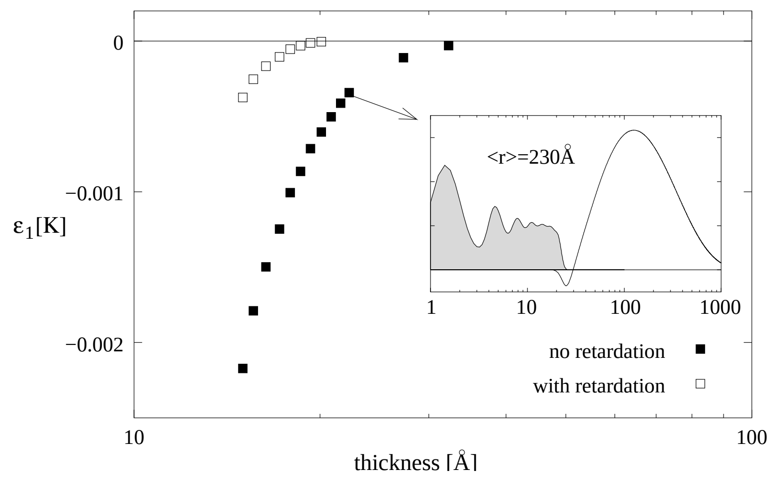

FIGURE 11. Excitation energies of H bound to ^{4}He films of increasing thickness, with (full square) and without retardation (outline square). The inset shows the wave function in Hartree approximation for $n = 0.45\text{Å}^{-2}$.

Fig.12 shows the sticking coefficient of H at the $0.45\,\text{Å}^{-2}$ film, which is 22.2Å thick, and for several thicker, emulated films up to 522Å. The phase shift $\delta(E)$, given by the argument of the elastic reflection coefficient $R = e^{2i\delta}$, is show below $s(n)$. Decreasing the film thickness from 52.2Å to 42.2Å, $\delta(E \to 0)$ increases by π. According to the Levinson theorem [**Tay72**], this jump of $\delta(E \to 0)$ is caused by the increase of the number of states by one; *i.e.* the effect of the graphite substrate on H is strong enough to accomodate a second bound state, in addition to the Andreev state. In Fig.11, we plot the exceptionally low energy of this excited state as a function of film thickness, with and without retardation. The calculation was carried out in Hartree approximation, because, unlike for excited states of ^{3}He in the film, the excited H atom is almost completely *outside* the film, held merely by the Van der Waals tail of the substrate and having no overlap with the self energy.

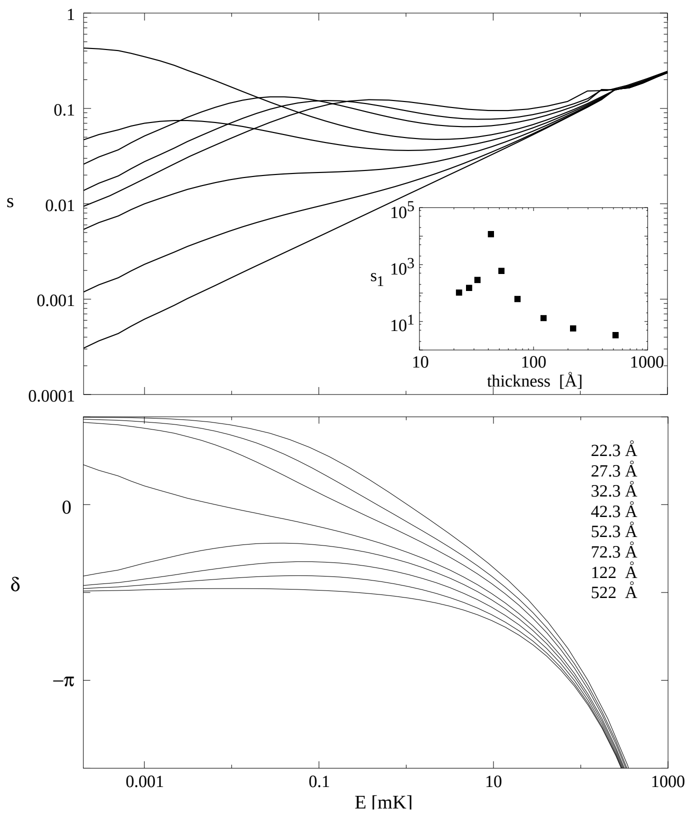

FIGURE 12. The sticking coefficient $s(E)$ of H impinging perpendicularly on a ^{4}He film of coverage $n = 0.450\,\text{Å}^{-2}$ (22.2Åthick), and on thicker films, see text. Below the phase shift $\delta(E)$ is shown, modulo π. For both $\delta(E)$ and $s(E)$ (at $E = 10$mK), higher values correspond to thinner films. Shifting the weakly bound state of H to become a resonance causes $s_1 = \lim_{k_\perp \to 0} \frac{s}{k_\perp}$ to sweep over many orders of magnitude, see inset.

On both sides of the threshold thickness, where the binding energy of the second bound state crosses zero, the sticking coefficient is enhanced in comparison to sticking to the free ^{4}He surface. At the threshold, $s(E)$ is of order unity down to μK. Generally, the closer d is to the threshold thickness, the lower is the energy where the proportionality of s to $k_\perp$ is fulfilled. Specifically, if $s(E, n)$ is plotted as a function of n with E kept fixed, s becomes non-monotonous in n only for energies $E \ll 0.1$mK. In order to examine quantitatively whether a peak in $s(T, d)$ can be observed when the film thickness d is varied, we assume a gas of atomic H characterized by a Maxwell-Boltzman velocity distribution $p(k_z) \propto k_z e^{-\hbar^2 k_z^2/2mk_BT}$ at temperature T [**BW93, GNS95**]. We show in Fig. 13 $s(T, n)$ determined by taking the average $\int dk_z\ s(k_z, d)p(k_z)$, for two temperatures, $T = 0.3mK$ and $T = 0.01mK$. For comparison, we also plot the experimental data points of Ref. [**YDSea93**] at $T = 0.3mK$. It is clear, that $s(0.3\text{mK}, d)$ is still monotonous in d. One has to lower the temperature at least one order of magnitude to discerne a peak in $s(T, d)$.

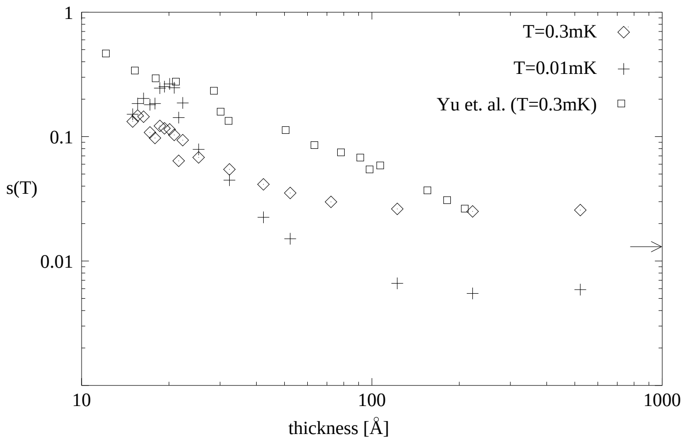

FIGURE 13. For a Maxwell-Boltzman distributed atomic H gas in contact with ^{4}He films of thickness d, $s(T,d)$ is shown for $T = 0.3$mK and $T = 0.01$mK (both with retardation). Also plotted is $s(0.3\text{mK}, d)$ determined experimentally[**YDSea93**] and the arrow indicates the bulk limit, $s(0.3\text{mK}, \infty) \approx 0.013$, which is half our result.

3.5. Low energy inelastic scattering

In section 2.5, a low energy expansion yielded $r_{\text{inel}} = r^0_{\text{inel}} E^2$, where the coefficient r^0_{inel} is given by eq. (217). Fig.14 shows r^0_{inel} as a function of the film coverage, for ^{3}He and H scattering. This quantity is very sensitive to the details of the ground state calculation. Below r^0_{inel}, the third sound velocity c_3 is plotted, which reveals that, for very low coverage, r^0_{inel} even behaves oppositely to what is expected, which would be an approximate proportionality to the inverse forth power of c_3. This apparent strong dependence of the denominator of eq. (217) is probably the reason for the large numerical fluctuations.

The emulation of thick films in the way we used for the calculation of the sticking coefficient for H is not possible for the calculation of the low energy limit of r_{inel}, because the impinging atom couples to ripplons of very long wave-length λ. These modes are basically displacements of the surface of the ^{4}He film of thickness d, which extend the order of $\min(\lambda, d)$ deep into the film. The best we can do in the case of the free ^{4}He surface is to calculate the matrix element (227) for the $0.45\,\text{Å}^{-2}$ film, with the substrate potential set to zero, which yields $2m_I/\hbar^2\,|M_r^{(0)}|^2 = 11.6$, as compared to the value 4 in DWBA. If we use for the surface energy the experimental value $\sigma = 0.28\text{KÅ}^{-2}$, we find $r^0_{\text{inel}} = 0.24\text{K}^{-2}$.

The current numerical uncertainty of the r^0_{inel} results does not warrant a final conclusion, and further work is necessary.

3.6. Angular dependence

In section 2.7, we have already pointed out that the quasi-elastic reflection (direct inelastic scattering peaked in the specular direction) is a consequence of the strong influence

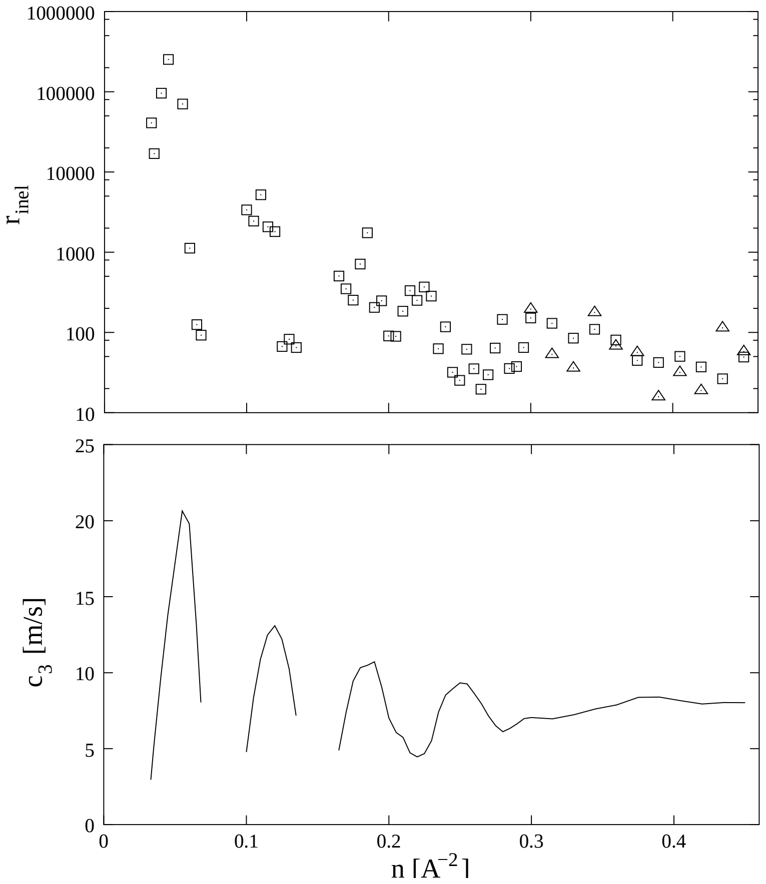

FIGURE 14. The low energy inelastic scattering probability divided by E^2, $\lim_{E\to 0}\frac{r_{\rm inel}}{E^2}$, is shown for ^{3}He (squares) and H (triangles), impinging perpendicularly on ^{4}He films of thickness n adsorbed on graphite. Below the speed of third sound $c_3(n)$ is plotted.

of the third sound surface modes of the ^{4}He film, just as the E^2 proportionality of the total inelastic scattering probability. In Fig.15, the differential, *i.e.* angle dependent inelastic scattering probability devided by k^3, $\frac{1}{k^3}\frac{d\sigma(\theta,k)}{d\theta}$, is shown for ^{3}He and H, respectively, impinging perpendicular on the film with wave number k. Clearly, $\frac{d\sigma(\theta\to 0,k)}{d\theta}$ becomes proportional to k^3. The width of the scattering cone about the specular direction is proportional to k, as it is dictated by $r_{\rm inel}\propto k^4$ for $k\to 0$. Also for finite incident energies, inelastic scattering in specular direction is enhanced by the long range of the interaction between an impurity and third sound modes, which is seen in Fig.16: $\frac{d\sigma(\theta=0,k)}{d\theta}$ is finite.

Turning first to hydrogen scattering, Fig.16 reveals another effect: for H atoms leaving the film almost parallel to its surface, $\theta\to\pi/2$, the scattering probability peaks before it vanishes at $\theta=\pi/2$. This is the same effect as the inhibition of quantum reflection caused by the long range of the Van der Waals attraction of the substrate. For the elastic channel, this leads to a lowering of $|R|^2$ from unity and hence an increase of s at *small* incident energies.

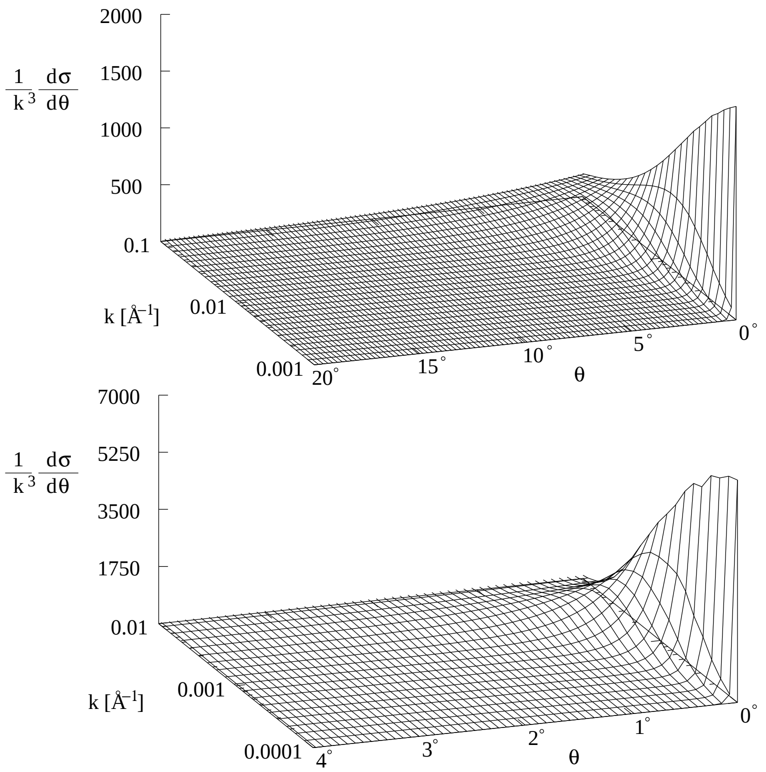

FIGURE 15. For perpendicular incidence of ^{3}He (top) and H (bottom) of incident wave number k on a ^{4}He film of thickness $n = 0.450\,\text{Å}^{-2}$, the differential inelastic scattering probability devided by k^3, $\frac{1}{k^3}\frac{d\sigma(\theta)}{d\theta}$, is shown as a function of k. The range $k = 0.001$ Å^{-1} ... 0.1 Å^{-1} corresponds to an energy range $E = 8.1 \times 10^{-6}$ K ... 0.081 K for ^{3}He, and $E = 2.4 \times 10^{-7}$ K ... 2.4×10^{-3} K for H.

For direct inelastic scattering it leads to an increase of scattering into grazing angles at *any* incident energies, because at these angles the inelastic channel wave functions asymptotically is $e^{ik_{\perp,\text{out}}z}e^{i\mathbf{k}_{\|,\text{out}}\mathbf{r}_\|}$, thus having a small perpenticular momentum just as a low energy elastic channel wave function φ. The low energy resonance at low wave number $k_\perp$, discussed in detail in the previous section for its relevance for s, causes a high probability density for the inelastic channels wave function, thus of course increasing the probability for a decay process into this channel. This explanation for the peak of $\frac{d\sigma(\theta,k)}{d\theta}$ near $\theta = \pi/2$, is readily checked by comparing various film thicknesses: in Fig.17, $\frac{d\sigma(\theta,k)}{d\theta}$ is shown for increasing film thickness. Reaching about 42Å, the probability for inelastic scattering to $\pi/2$ increases dramatically, just as s did. For even thicker films, $\frac{d\sigma(\theta,k)}{d\theta}$ vanishes monotonously with $\theta \to \pi/2$.

At scattering energies above 1K, $\frac{d\sigma(\theta,k)}{d\theta}$ becomes less uniform for ^{3}He as can be seen in Fig.16. The nature of these oscillations can be better understood from studying $d\sigma/dk_{\perp,\text{out}}$, defined by eq. (193), which is the probability to scatter inelastically from an incoming state of wave number $k_{\perp,\text{in}}$ into a state of wave number $k_{\perp,\text{out}}$. In Fig.18 $d\sigma/dk_{\perp,\text{out}}$ is plotted as a

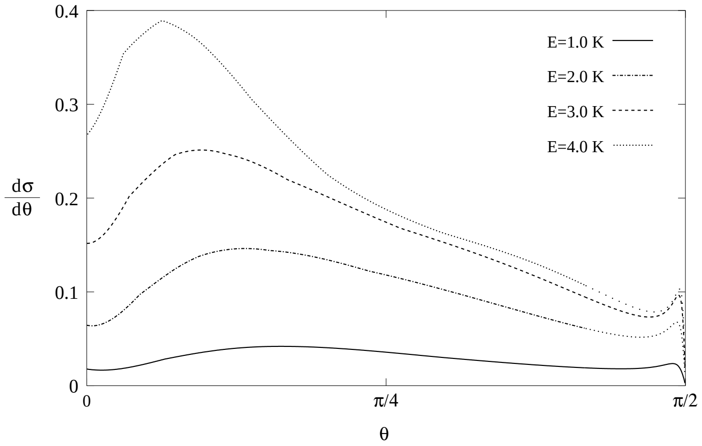

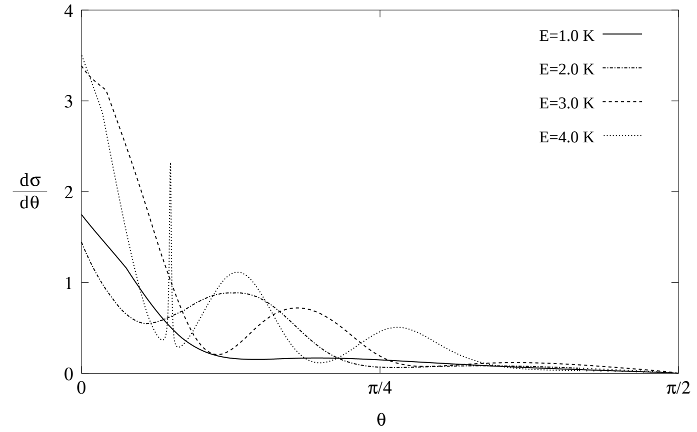

FIGURE 16. For H and ^{3}He impinging perpendicularly on ^{4}He films with energies $E = 1.0; 2.0; 3.0; 4.0$K, the angular dependence of the direct inelastic scattering probability $\frac{d\sigma(\theta)}{d\theta}$ is shown.

function of $k_{\perp,\text{in}}$ and $k_{\perp,\text{out}}$, for perpendicular incidence. Basically, three types of structures can be distinguished:

1. Oscillations independent of $k_{\perp,\text{in}}$, leading to stripes parallel to the $k_{\perp,\text{out}}$-axis in Fig.18. They are cause by a resonance in the elastic channel $\varphi_{k_{\perp,\text{in}}}$.
2. oscillations independent of $k_{\perp,\text{out}}$, caused by a resonance in an inelastic outgoing channel for a final wave number $k_{\perp,\text{out}}$.
3. oscillations oriented diagonally in Fig.18, which we attribute to interference between incoming and outgoing state in the transition matrix element $M_m(\mathbf{k}_m, 0)$. Roughly speaking, these oscillations can be thought of as interference patterns stemming from the Fourier transform of the direct interaction $\nabla X_{m,k_m}(z_0)$ for wave number $k_{\perp,\text{in}} - k_{\perp,\text{out}}$. These oscillations will be distorted, because the channel wave function are not simple plane wave, and $\nabla X_{m,k_m}(z_0)$ changes with k_m which is given by parallel momentum conservation.

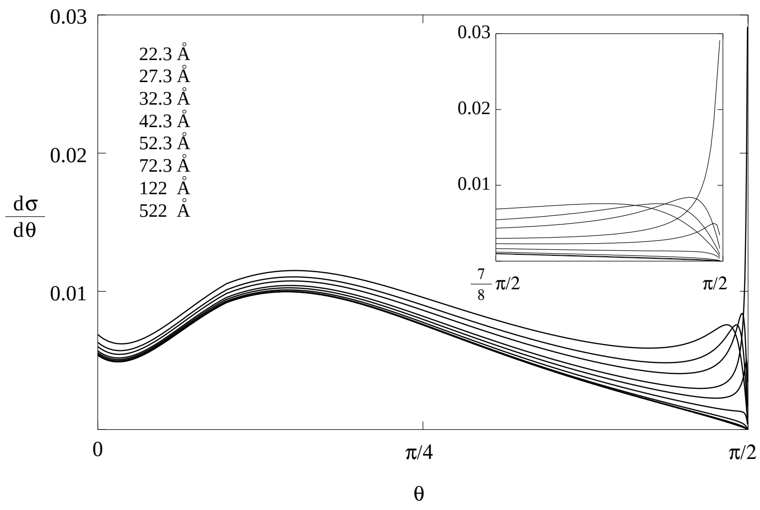

FIGURE 17. For H impinging perpendicularly on ^{4}He films with energy $E = 0.52$K, $\frac{d\sigma(\theta)}{d\theta}$ is shown for various film thicknesses given in the left top corner. Higher values of $\frac{d\sigma(\theta)}{d\theta}$ correspond to thiner film, exept for $\theta \to \pi/2$: there the probability is enhanced by the low energy resonance or weakly bound state of H, analogous to the enhancement of the sticking probability s. The inset shows the $\theta \to \pi/2$ region.

Examples of the first two types of structure are very noticable in Fig.18: sharp resonances occur at $k_{\perp,\mathrm{in}} = 0.24$Å in the elastic channel and in the inelastic channel of final wave number $k_{\perp,\mathrm{out}} = 0.62$Å. The first resonance has been discussed in detail in [**KZ98**]. It is strongly localized between graphite substrate and film, and is the already mentioned precursor of a bound state found for ^{3}He in cesium adsorbed ^{4}He films. The latter is in fact the same substrate-film interface resonance, but because the inelastic channel wave functions are calculated in Hartree approximation, *i.e.* without self energy correction, the resonance energy is much higher: measured from the fully optimized ground state energy, the resonance in the elastic and inelastic channel is at an energy of $0.47\mathrm{K}+|\mu_I| = 5.27$K and $3.1\mathrm{K}+|\mu_I| = 7.9$K, respectively. Hence, the omission of the self energy for the inelastic outgoing channels amounts to a resonance energy which is by about a factor of 1.5 too high – a similar error as for the excitation energy of the roton in Feynman approximation (*i.e.* omitting the self energy correction) for pure ^{4}He. This was to be expected, because also the roton excitation of a finite ^{4}He system is best described as a resonant scattering state, see the previous chapter and Refs. [**CKS98, KZ01**]. For the exact solution of the $(N+1)$-body scattering problem, time reversal symmetry would imply that there is no difference between in- and outgoing channels (in Fig.18, this would mean the horizontal stripe meets the vertical stripe at $k_{\perp,\mathrm{in}} = k_{\perp,\mathrm{out}}$).

Also visible in Fig.18 are interference patterns between elastic and inelastic channels, leading to oscillations oriented approximately diagonally. The interpretation of these oscillations of wave number k implies that the region of interaction between ^{3}He and third sound (the other film modes contribute negligibly to Fig.18) is of the order of $\frac{2\pi}{k} \approx 40$Å, $.i.e$ of the

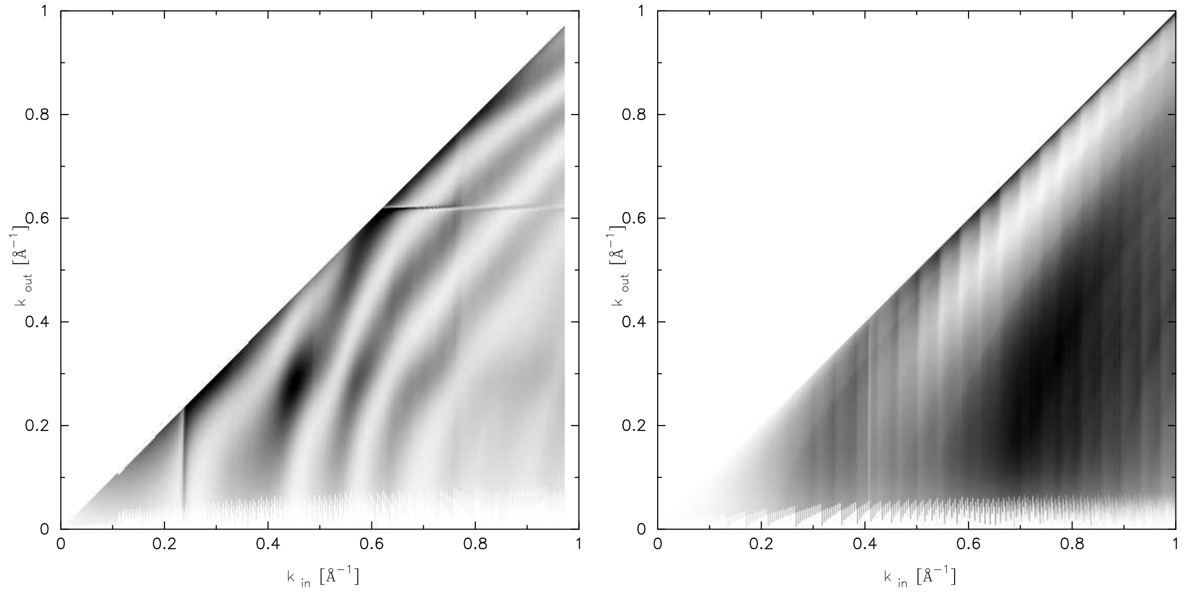

FIGURE 18. For ^{3}He (left) and H (right) impinging perpendicularly on a ^{4}He film ($n = 0.450\,\text{Å}^{-2}$), the inelastic scattering probability is plotted as a function of the initial wave number k_{in} (x-axis) and of the perpendicular component of the final wave number $k_{\perp,\text{out}}$; dark corresponds to high probability.

order of the film thickness. Turning now to the corresponding map for H scattering, we note that, due to the strong repulsion between H and the film, the ripplon interaction region is much smaller, leading to a much broader structure. Only the strong coupling to third sound of very long wave length has large range, as has been explained in section 2.5. This is seen by the sharp peak of $d\sigma/dk_{\perp,\text{out}}$ near $k_{\perp,\text{in}} = k_{\perp,\text{out}}$, especially for H scattering.

3.7. Time-of-flight spectrum

For completeness, we also show time-of-flight spectra, which are obtained from $d\sigma/dk_{\perp,\text{out}}$, eq. (193), by simply transforming from $k_{\perp,\text{out}}$ to time t:

$$\left| \frac{m_I d}{\hbar} \frac{d\sigma_{\perp,\text{inel}}(t)}{dt} \right| = k^2_{\perp,\text{out}} \frac{d\sigma_{\perp,\text{inel}}(k_{\perp,\text{out}})}{dk_{\perp,\text{out}}} \tag{240}$$

where $t = \frac{md}{\hbar k_{\perp,\text{out}}}$. The time-of-flight spectrum thus defined is the inelastically scattered flux per incoming flux through a plane parallel to the film and at a distance d from it. Fig.19 and 20 show $k^2 \frac{d\sigma_{\perp,\text{inel}}(k)}{dk}$ as a function of $1/k$, for H and ^{3}He, respectively, impinging perpendicularly on a ^{4}He film, $n = 0.45\text{Å}^{-2}$. Channels other than third sound open successively with increasing incident energy, which in principle permits measuring the associated excitation energies, but the transition probabilities are negligible compared to excitation of third sound modes. The oscillations of the ^{3}He inelastic scattering probability with exit scattering angle or energy – and hence time of flight – have been discussed in the previous section. The time-of-flight spectrum offers an alternative to the angular dependence to measure the high probability for inelastic scattering into the specular direction, because due to energy conservation atoms emerging from those processes retain almost all their initial energy, which leads to a finite signal of $\frac{d\sigma_{\perp,\mathrm{inel}}(k)}{dk}$ at $k = k_{\mathrm{in}}$.

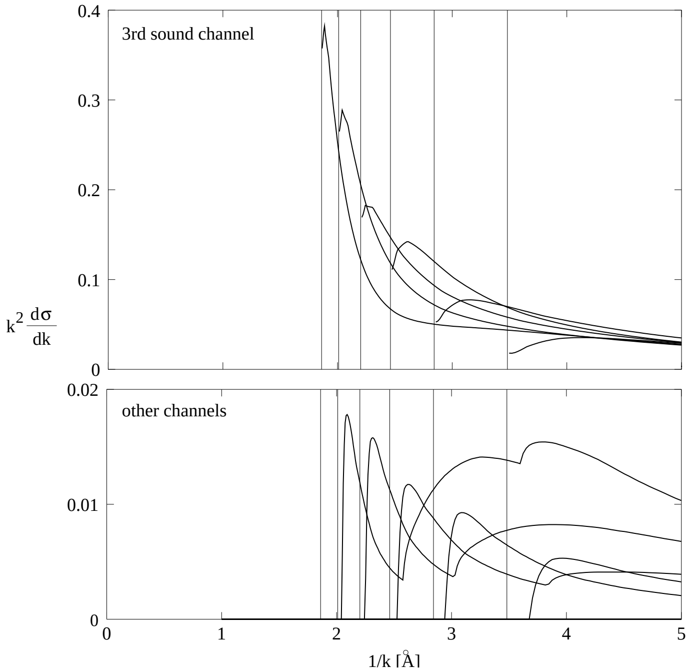

FIGURE 19. The figure shows $k^2 \frac{d\sigma_{\perp,\mathrm{inel}}(k)}{dk}$, with $k = k_{\perp,\mathrm{out}}$ for H scattering, plotted as a function of $1/k$, for pendicular incidence at energies 1K, 2K,..., 6K, on a film of coverage $n = 0.450\,\text{Å}^{-2}$. $k^2 \frac{d\sigma_{\perp,\mathrm{inel}}(k)}{dk}$ is proportional to the time-of-flight spectrum $\frac{d\sigma(t)}{dt}$. The upper figure shows the contribution of the third sound decay channel only, the lower one shows the rest of all other channels. The elastic flux is a δ–peak and is denoted by the vertical lines.

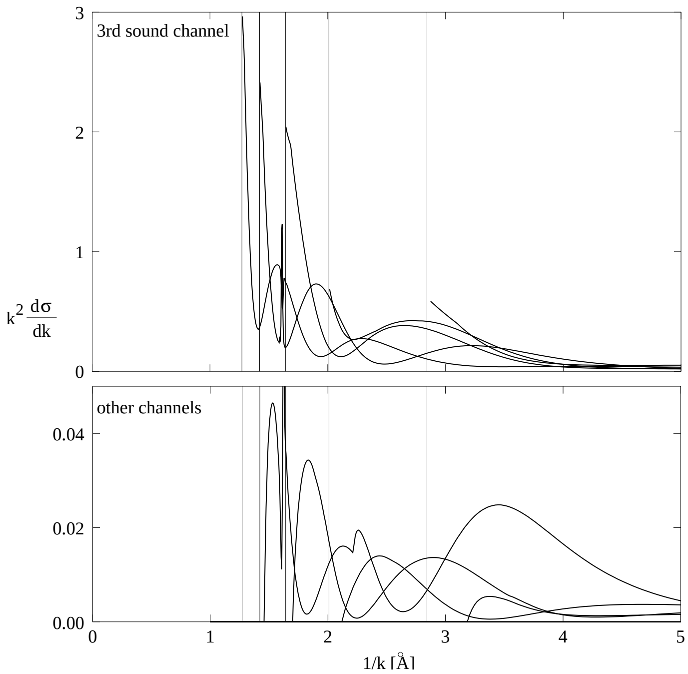

FIGURE 20. Same as Fig.19 for ^{3}He scattering. Incident energies are 1K, 2K,. . . , 5K.

CHAPTER 8

Summary and Conclusions

In this work, we have derived the treatment of the many-body scattering problem in the formulation of the HNC-Euler-Lagrange theory for bosons and for bosons with a single impurity particle. The method was applied to identical particle (^{4}He atoms) scattering and to impurity (^{3}He atoms) scattering at ^{4}He$_N$ droplets of sizes up to $N = 1000$, as well as to impurity scattering off thin ^{4}He films.

For the calculation of the ground state quantities, which is essential as at starting point for dynamical calculations, we relied on earlier work on ^{4}He droplets by Chin and Krotscheck [**CK95b, CK95a**] and on ^{4}He films [**KSE88, EK88, CFK$^+$94, CFKS94, CKS97, Tym95**]. For the calculations of scattering, *i.e.* excited states, we adopted methods for inhomogeneous boson systems which have been applied to ^{4}He films and slabs [**CKT96, CKS98**]. These methods generalize the Feynman approximation by including time-dependent fluctuations of the 2-body correlations which improves the agreement of the energy spectrum with experiment and introduces life-time to excitations. For scattering this means that, in addition to elastic processes such as "quantum scattering" (the conversion between an elementary excitation and a scattered ^{4}He atom), an atom impinging on the droplet can lose energy which gives rise to inelastic cross sections. These inelastic processes were the focus of this work in which we developed the method to calculate their probabilities.

This method consists of expanding the expectation value of the one-body probability current operator to second order in the correlation fluctuations δu_i, which is consistent with solving the equations of motion for δu_i obtained by minimizing the action integral, which is also expanded to second order in δu_i. Cross sections were then obtained by evaluating the current in the asymptotic regime where the interaction energy between scattering atom and droplet vanishes, and where the current fulfills a continuity equation (for impurities it is fulfilled also in the interaction region). In this manner, we obtained a unitary scattering matrix, *i.e.* the probablities for all processes sums up to unity. This does not mean that the formalism accounts for all processes allowed by energy conservation: fluctuating 2-body correlations can account for asymptotically outgoing waves of less than or equal to 2 particles; but, for example, droplet fission cross sections cannot be calculated. For scattering off droplets, *i.e.* finite boson systems, we derived expressions for the cross sections for elastic scattering, inelastic scattering, and – only possible for impurity scattering – adsorption. For impurity scattering off infinitely extended films, the corresponding quantities are the probabilities of specular (elastic) reflection, direct inelastic reflection, and sticking.

Summary of droplet results

Microscopic droplets of ^{4}He are nowadays routinely produced by expanding ^{4}He gas into vacuum, and have found application in spectrocopy of atoms and molecules which are ad/absorbed to/into the droplets serving as a cold matrix which does not perturb the system to be investigated due to the superfluidity of the ^{4}He droplet. Doping the droplets with particles is of course an inelastic scattering process, which is the reason for our interest in this many-body scattering problem. Also, experiments to determine the ripplon excitation energies by ^{3}He scattering off ^{4}He droplets are in preparation. Furthermore, the simplicity of the helium-helium interaction renders scattering off ^{4}He droplets an experimentally accessible model system to test methods of many-body scattering, in contrast for example to scattering of nuclei which is governed by more complicated interactions.

We have chosen helium isotopes as scattering particles, because the comparison of ^{4}He and ^{3}He scattering promised insight into the differences between identical and distinct particle scattering. Appling the methods for ^{3}He to other light atoms will be straightforward. We summarize our most important results:

- The coupling of the impinging atom to a pair of bound droplet excitations leads to resonances of Feshbach type for incident energies below $|\mu_4|$. These resonances can be treated with established methods developed for coupled Hamiltonian formulations of the many-body scattering problem [**Fes58**]. A systematic calculation of the density and life-times of these meta-stable states may be interesting for the investigation of the thermodynamic limit, but has not been carried out for this work.
- The elastic ^{4}He cross section $\sigma_{\rm el}$ describes "quantum scattering", the conversion of the impinging ^{4}He atom to an excitation and back to an atom. If the incident energy E plus the binding energy equals the roton energy, the excitation created during the scattering event is naturally a roton. At and above this energy, $\sigma_{\rm el}$ shows a series of peaks, which confirms our view of the roton-maxon regime of excitations of a finite ^{4}He system as a resonance phenomenon. For small droplets, the roton energy can thus determined from $\sigma_{\rm el}$, although the effect may be to delicate to measure in experiments.
- For higher scattering energies $E = 10 - 15$K, the total cross section $\sigma_{\rm tot}(N)$ as a function of droplet size N extrapolates to approximately twice the classical cross section for $\sigma_{\rm tot}(N=\infty)$, for both, ^{4}He and ^{3}He scattering. This is consistent with a 100% dissipative quantum mechanical scattering process – predominantly inelastic scattering, since the ad-/absorption cross section decreases with increasing energy.
- ^{3}He atoms turned out to constitute an good probe for surface excitations. Despite the inhomogeneity of the droplets, the ripplon dispersion was found as a sharp ridge in $\sigma(E_t, k_t)$, the probability to transfer energy E_t and momentum k_t to the droplet, equivalent to the dynamic structure function $S(k,\omega)$ which is determined by inelastic neutron scattering. The inelastic coupling to rotons was found to be smaller but still significant, and the energy transfer spectrum $\sigma(E_t)$ could be devided into three energy ranges, where ripplon, phonon, and roton excitation dominate, respectively. $\sigma(E_t, k_t)$

for ^{4}He scattering did not yield information about dispersion relations of the droplets; maximal energy transfer occured at about $(E-\mu_4)/2$, the sum of incident and binding energy; it showed little structure in its k-dependence.

- The energies of the first few ripplon modes can be measured by measuring the energy transfer of ^{3}He to the droplet even under experimental conditions, where the sizes of the droplets are unfortunately statistically distributed with a variance of the order of the mean value. If on the other hand, an experiment is devised where also the detector position is varied such that the momentum transfer can be determined, the droplet size distribution is no concern.

Summary of film results

Superfluid ^{4}He films are used in atomic hydrogen experiments as inert cell coating, which is free of magnetic impurities. For these experiments, scattering probabilities, especially for sticking of H to the film, are an important quantity. Therefore, our application of the HNC-Euler-Lagrange theory on scattering off films focused on atomic hydrogen, and, for the purpose of comparison, on ^{3}He. H is strongly repelled from the film while ^{3}He has a positive solvation energy in bulk helium. Hence, H and ^{3}He represent two model cases which should cover a large portion of light particle scattering. We summarize our most important results:

- The sticking probability s, which vanishes linearly with the momentum of the scattering atom, is sensitive to the Van der Waals tail of the substrate potential. We found two essentially different types resonances, near which s becomes large: (i) H has a single bound state of binding energy 1K at the free ^{4}He surface but for thin films the attraction of the substrate can introduce a weakly bound excited state far above the film and of binding energy of the order of millikelvin; at the film thickness, at which this excited state turns into a resonance, s can become very large. To our knowledge, these weakly bound states have not been experimentally observed, while the enhancement of s due to low energy resonances has been measured. (ii) Due to its negative chemical potential of -2.7K in bulk ^{4}He, ^{3}He has, in addition to the Andreev ground state on the film surface, an increasing number of bound states in the film with increasing film thickness. For film thicknesses up to 20Å, the creation of these bulk-like states from scattering resonances can be seen as pronounced peaks in s.
- We found an unexpected low energy behavior to the inelastic scattering probability $r_{\rm inel} \propto E^2$, which is a consequence of the long range and strength of the coupling between atom and long wave-length third sound waves. This allows the excitation of ripplons with the atom still far away from the film, where the probability density of the atom is not suppressed by quantum reflection. The same mechanism leads to the focusing of the inelastically scattered beam in the specular direction (quasi-elastic scattering).
- The low energy resonance induced by the substrate potential, which enhances sticking at low incident energy, also enhances, for arbitrary incident energy, direct inelastic

scattering into directions almost parallel to the film: $d\sigma/d\theta$ for H scattering exhibits a peak near $\theta = \pi/2$, which is most pronounced at the critical film coverage, where the low energy resonance turns into a weakly bound state.

- The probability $d\sigma/dk_{\perp,\mathrm{out}}$ to inelastically scatter from the elastic channel with momentum $\hbar k_{\mathrm{in}}$ into a channel with outgoing perpendicular momentum $\hbar k_{\perp,\mathrm{out}}$ was found to have a oscillatory structure which we could relate to an effective range of interaction between atom and surface excitations, which is small for H due to the repulsion from the film, and of the order of the film thickness for ^{3}He.

APPENDIX A

Definitions

1. Notation

The following conventions are adopted:

- Where appropriate, the argument of a function depending on coordinates $\mathbf{r}_1, \ldots, \mathbf{r}_n$ is replaced by the indices $1, \ldots, n$:

$$\begin{aligned}
&\rho_n(\mathbf{r}_1, \ldots, \mathbf{r}_n; \mathbf{r}'_1, \ldots, \mathbf{r}'_n) \equiv \rho_n(1, \ldots, n; 1', \ldots, n') \ , \\
&\delta u_2^I(\mathbf{r}_0, \mathbf{r}_i) \equiv \delta u_2^I(0, i) \\
&\delta(\mathbf{r}_j - \mathbf{r}_j) \equiv \delta(i, j) \ , \quad \text{etc.}
\end{aligned}$$

  In the same fashion, we will often abbreviate the integration measure:

$$\begin{aligned}
\int d^3r_{n+1} d^3r_N \ |\Phi_0(\mathbf{r}_1, \ldots, \mathbf{r}_N)|^2 \ &\equiv \ \int d(n+1) \ldots dN \ |\Phi_0(1, \ldots, N)|^2 \ , \\
\int d^3r_1 \ \rho_1(\mathbf{r}_1) U_{\text{ext}}(\mathbf{r}_1) \ &\equiv \ \int d1 \ \rho_1(1) U_{ext}(1) \ , \quad \text{etc.}
\end{aligned}$$

- Throughout the text, the coordinates $\mathbf{r}_i$, $i = 1, \ldots, N$ refer to ^{4}He atoms and $\mathbf{r}_0$ to an impurity particle. This convention identifies for example $g_2^I(\mathbf{r}_0, \mathbf{r}_1) = g_2^I(0, 1)$ to be the pair distribution function between an impurity and a ^{4}He atom, while $g_2^B(\mathbf{r}_1, \mathbf{r}_2) = g_2^B(1, 2)$ is the pair distribution function between two "background" ^{4}He atoms. Therefore, if coordinate-dependent functions are written with their arguments, the superscript I or B as well as index denoting the number of particles will often be omitted, e.g.

$$g^I(0,1) \equiv g(0,1) \ , \qquad g_n^B(1, \ldots, n) \equiv g(1, \ldots, n) \ , \qquad \text{etc.}$$

- Quantum numbers characterizing single particle states in three dimensions are triplets of scalar quantum numbers. In expressions valid in any inhomogeneous system we will abbreviate this triplet by a single index, say n, and only when specializing to film or droplet geometry, all three quantum numbers are written. Otherwise the translation is

$$\begin{aligned}
&\text{films:} \qquad && n \equiv (n, \mathbf{q} = (q_x, q_y)) \qquad && \sum_n \equiv \int \frac{d^2q}{(2\pi)^2} (\sum_n + \int dn) \\
&\text{droplets:} \qquad && n \equiv (n, \ell_n, m_n) \qquad && \sum_n \equiv \sum_{\ell_n=0}^{\infty} \sum_{m_n=-\ell_n}^{\ell_n} (\sum_n + \int dn)
\end{aligned}$$

Note that the quantum number associated with the z–direction (films) or the radial direction (droplets) is partly discrete, partly continuous. For brevity, we often simply write $\sum_n$, but mean the full spectrum.

- For inhomogeneous systems, convolution integrals of the type $\int d3\ B(1,3)\rho(3)C(3,2)$ frequently occur. It is useful to define new quantities
$$\tilde{A}(1) = \sqrt{\rho(1)}A(1)\ , \qquad \tilde{B}(1,2) = \sqrt{\rho(1)\rho(2)}B(1,2)\ , \qquad \text{etc.}$$
because then these integrals become operator-operator products, operator-vector products, or scalar products,
$$\begin{aligned} [\tilde{B} * \tilde{C}](1,2) &:= \int d3\ \tilde{B}(1,3)\tilde{C}(3,2) = \sqrt{\rho(1)\rho(2)}\int d3\ B(1,3)\rho(3)C(3,2) \qquad (241)\\ [\tilde{B} * \tilde{A}](1) &:= \int d3\ \tilde{B}(1,3)\tilde{A}(3) = \sqrt{\rho(1)}\int d3\ B(1,3)\rho(3)A(3)\\ [\tilde{A} * \psi] &:= \int d3\ \tilde{A}(3)\psi(3) \end{aligned}$$

2. Number densities and distribution functions

The N–body ground state properties associated with an n–body operator
$$\hat{A} = \sum_{i_1 \neq \cdots \neq i_n} a(i_1, \ldots, i_n)$$
can be written as
$$\langle \hat{A} \rangle = \int d1 \ldots dn\ \left[a(1', \ldots, n')\rho(1, \ldots, n; 1', \ldots, n')\right]_{i=i'}$$
where
$$\rho(1, \ldots, n; 1', \ldots, n') = \frac{N!}{(N-n)!}\frac{\int d(n+1)\ldots dN\ \Phi_0(1,\ldots,n,n+1,\ldots N)^* \Phi_0(1',\ldots,n',n+1,\ldots N)}{\int d1 \ldots dN\ |\Phi_0(1,\ldots,N)|^2}$$
is the n-body density matrix. In practice, $n \ll N$: the kinetic energy operator $-\sum_i \frac{\hbar}{2m_i}\nabla_i^2$ and the current operator $\sum_i \frac{\hbar}{2m_i}\delta(\mathbf{r}_i - \mathbf{r})\nabla_i + c.c.$ are one–body operators, the interaction operator of two particle $\sum_{i<j} V(i,j)$ is a two–body operator, and so on.

The basic ingredient of the HNC-Euler-Lagrange theory are n–body number densities $\rho(1,\ldots,n)$, i.e. the correlation functions without the autocorrelation terms, denoted by $\langle \cdots \rangle_c$,
$$\begin{aligned} \rho(1,\ldots,n) &= \langle \Phi_0 | \hat{\rho}(\mathbf{r}_1)\ldots\hat{\rho}(\mathbf{r}_n)|\Phi_0\rangle_c\\ &= \langle \sum_{i_1 \neq i_2 \neq \cdots \neq i_n} \delta(\mathbf{r}_1 - \mathbf{r}_{i_1})\ldots\delta(\mathbf{r}_n - \mathbf{r}_{i_n})\rangle\\ &= \frac{n!}{\langle\Phi_0|\Phi_0\rangle}\frac{\delta\langle\Phi_0|\Phi_0\rangle}{\delta u_n(1,\ldots,n)} \qquad \text{(Jastrov-Feenberg ansatz)} \end{aligned}$$

which evaluates the probability to find n different particles at coordinates $\mathbf{r}_1,\ldots,\mathbf{r}_n$ simultaneously, and which is just the diagonal part of the n–body density matrix, $\rho(1,\ldots,n;1,\ldots,n)$. For the ground state Φ_0 of N bosons,

$$\rho(1,\ldots,n) = \frac{N!}{(N-n)!}\frac{\int d(n+1)\ldots dN\ |\Phi_0(1,\ldots,n,n+1,\ldots N)|^2}{\int d1\ldots dN\ |\Phi_0(1,\ldots,N)|^2} \tag{242}$$

The n–body density of the ground state of N bosons and an impurity particle $\Phi_0(0,1,\ldots,N)$ is

$$\rho(0,1,\ldots,n-1) = \frac{N!}{(N-n+1)!}\frac{\int dn\ldots dN\ |\Phi_0(0,1,\ldots,n-1,n,\ldots N)|^2}{\int d0d1\ldots dN\ |\Phi_0(0,1,\ldots,N)|^2} \tag{243}$$

and, if the n bodies exclude the impurity particle,

$$\rho(1,\ldots,n) = \frac{N!}{(N-n)!}\frac{\int d0d(n+1)\ldots dN\ |\Phi_0(0,1,\ldots,n,n+1,\ldots N)|^2}{\int d0d1\ldots dN\ |\Phi_0(0,1,\ldots,N)|^2}\,. \tag{244}$$

Important properties of ρ_n, which should also be fulfilled by approximations of ρ_n:

1. Short-range Structure: For strongly repulsive potentials as the helium interaction, ρ_n has to vanish if two particles approach each other
$$\rho(1,\ldots,n)\to 0 \qquad \text{if } |\mathbf{r}_i-\mathbf{r}_j|\to 0 \text{ for any pair } i,\ j. \tag{245}$$
2. Cluster Property: For finite-ranged potentials (or potentials falling off fast enough like the Helium interaction), $\rho(i_1,\ldots,i_n)$ factorizes if m particle coordinates are removed from the rest, but all n coordinates are still inside the system, i.e. where $\rho(i)>0$
$$\begin{aligned}\rho(1,\ldots,n) &\longrightarrow \rho(1,\ldots,m)\rho(m+1,\ldots,n)\\ &\text{for}\quad |\mathbf{r}_k-\mathbf{r}_l|\to\infty,\ k\in\{1,\ldots,m\},\ l\in\{m+1,\ldots,n\}\,,\end{aligned} \tag{246}$$
and accordingly for densities involving the impurity particle.
3. The Sequential Relation is an immediate consequence of the definition of ρ_n:
$$\int dn\ \rho(1,\ldots,n) = (N-n+1)\rho(1,\ldots,n-1)\,. \tag{247}$$

The n–body probability distributions $g(1,\ldots,n)$ and $g(0,\ldots,n-1)$ are defined as

$$g(1,\ldots,n) = \frac{\rho(1,\ldots,n)}{\rho(1)\cdots\rho(n)} \tag{248}$$

$$g(0,\ldots,n-1) = \frac{\rho(0,\ldots,n-1)}{\rho(0)\cdots\rho(n-1)}\,. \tag{249}$$

The cluster property (246) assures that g_n approaches unity if all n particles are far from each other; furthermore, (245) implies the according short range structure in g_n:

$$g(1,\ldots,n)\to 1 \qquad \text{if } |\mathbf{r}_i-\mathbf{r}_j|\to\infty \text{ for all } i,\ j \tag{250}$$

$$g(1,\ldots,n)\to 0 \qquad \text{if } |\mathbf{r}_i-\mathbf{r}_j|\to 0 \text{ for any pair } i,\ j \tag{251}$$

Related to the pair distribution function g_2 is the static structure (integral) operator[1] for pure ^{4}He and single impurities in ^{4}He

$$
\begin{aligned}
S(1,2) &= \delta(1,2) + \sqrt{\rho(1)}[g(1,2) - 1]\sqrt{\rho(2)} && (252)\\
S(0,1) &= \sqrt{\rho(0)}[g(0,1) - 1]\sqrt{\rho(1)}\,. && (253)
\end{aligned}
$$

3. Wigner's 3-j symbols

We summarize those relations between spherical harmonics, 3-j symbols and 6-j symbols which are needed in the derivation of ^{4}He droplet cross sections in chapter 6. The formulas are taken from "Angular Momentum in Quantum Mechanics" by A. R. Edmonds [**Edm60**] and from "Atoms and Molecules", by M. Weissbluth [**Wei78**].

The 3-j symbol is proportional to the Clebsch-Gordon coefficient

$$
\begin{aligned}
\begin{pmatrix} j_1 & j_2 & j_3 \\ m_1 & m_2 & m_3 \end{pmatrix} &= \frac{(-1)^{j_1+j_2-m_3}}{\sqrt{2j_3+1}}(j_1,m_1;j_2,m_2|j_1,j_2,j_3;-m_3)\\
&= 0\,,\ \text{if } \Delta(j_1,j_2,j_3) = 0 \ \text{ or } \ m_1+m_2+m_3 \neq 0
\end{aligned}
$$

for integer angular momenta: $\begin{pmatrix} \ell_1 & \ell_2 & \ell_3 \\ 0 & 0 & 0 \end{pmatrix} = 0\,,$ if $\Delta(\ell_1,\ell_2,\ell_3) = 0$ or $\ell_1+\ell_2+\ell_3$ is not even

Important relations are

$$
\begin{aligned}
&\int d\Omega\; Y_{\ell_1,m_1}(\Omega)Y_{\ell_2,m_2}(\Omega)Y_{\ell_3,m_3}(\Omega) = \\
&= \sqrt{\frac{(2\ell_1+1)(2\ell_2+1)(2\ell_3+1)}{4\pi}} \begin{pmatrix} \ell_1 & \ell_2 & \ell_3 \\ 0 & 0 & 0 \end{pmatrix} \begin{pmatrix} \ell_1 & \ell_2 & \ell_3 \\ m_1 & m_2 & m_3 \end{pmatrix} =: \begin{bmatrix} \ell_1 & \ell_2 & \ell_3 \\ m_1 & m_2 & m_3 \end{bmatrix} \qquad (254)
\end{aligned}
$$

$$
\begin{pmatrix} j_1 & j_2 & j_3 \\ m_1 & m_2 & m_3 \end{pmatrix} = (-1)^{j_1+j_2+j_3} \begin{pmatrix} j_1 & j_2 & j_3 \\ -m_1 & -m_2 & -m_3 \end{pmatrix} \qquad (255)
$$

$$
\sum_{m_1,m_2} \begin{pmatrix} j_1 & j_2 & j_3 \\ m_1 & m_2 & m_3 \end{pmatrix} \begin{pmatrix} j_1 & j_2 & j_3' \\ m_1 & m_2 & m_3' \end{pmatrix} = \frac{1}{2j_3+1}\delta_{j_3,j_3'}\delta_{m_3,m_3'}\Delta(j_1,j_2,j_3) \qquad (256)
$$

$$
\begin{aligned}
&\sum_{m_1',m_2',m_3'} (-1)^{\ell_1+\ell_2+\ell_3+m_1'+m_2'+m_3'} \begin{pmatrix} j_1 & \ell_2 & \ell_3 \\ m_1 & m_2' & -m_3' \end{pmatrix} \begin{pmatrix} \ell_1 & j_2 & \ell_3 \\ -m_1' & m_2 & m_3' \end{pmatrix} \begin{pmatrix} \ell_1 & \ell_2 & j_3 \\ m_1' & -m_2' & m_3 \end{pmatrix} = \\
&\qquad = \begin{pmatrix} j_1 & j_2 & j_3 \\ m_1 & m_2 & m_3 \end{pmatrix} \begin{Bmatrix} j_1 & j_2 & j_3 \\ \ell_1 & \ell_2 & \ell_3 \end{Bmatrix} \qquad (257)
\end{aligned}
$$

where $\Delta(j_1,j_2,j_3)$ is the triangular condition requiring that the three j_i can from a triangle. The 3-j symbol is invariant under cyclic permutation of pairs (j_i,m_i) and changes sign according to $(-1)^{j_1+j_2+j_3}$ for non-cyclic permutations.

[1] also called cumulant correlation function, see appendix of [**Puo97**]

APPENDIX B

Single Particle Green's Functions

The 2-body correlation fluctuation δu_2, appearing in the ^{4}He and ^{3}He self energies (52) and (67) of the elastic channel wave equations (53) and (66) and in the inelastic currents derived in chapter 5, can be expressed in terms of the Green's function of the Feynman equation (43) and of the Hartree equation (60), for ^{4}He and ^{3}He respectively. Here these Green's functions are briefly discussed for spherical and film geometry. For an exhausive discussion of single particle Green's functions see [**Eco79, MF53a**].

The Green's function (operator) G is the resolvent of the linear integro-differential equation $(z-L)f = u$, i.e. the inverse of $z-L$, where L is a linear Hermitean operator and z is a complex number

$$(z-L)G(z) = I \qquad G(z) = (z-L)^{-1}\,. \tag{258}$$

G can be expanded in the eigensystem $\{f_n\}$ of L, $L|f_n\rangle = E_n|f_n\rangle$

$$G(z) = \sum_n \frac{|f_n\rangle\langle f_n|}{z-E_n} \tag{259}$$

which has poles on the real axis if z coincides with a discrete eigenvalue and a branch cut along the real axis corresponding to the continuous spectrum. In the latter case, the prescription for $z \in \mathbb{R}$ is to take the limit $\lim_{\varepsilon\to 0} G(z \pm i\varepsilon) =: G^{\pm}(z)$; in that case $G^{\pm}(z)$ is complex.

Provided the operator L has enough symmetries as to be suitably separable by introducing appropriate coordinates (as it is the case for spherical and film geometry), the expression (259) for G can be simplified. In the coordinate space representation:

$$G(1,2;z) = \sum_i b_i^*(\mathbf{y}_1)G_i(x_1,x_2;z)b_i(\mathbf{y}_2) \tag{260}$$

where $\{b_i\}$ is the basis set of two trivial dimensions with corresponding coordinates $\mathbf{y}_i$ separable from the non-trivial part L_i of L; G_i is the one-dimensional Green's function $(z-L_i)^{-1}$.

	spherical	planar
x	r	z
$\mathbf{y}$	$\Omega = (\theta,\phi)$	$\mathbf{r}^{\parallel} = (x,y)$
i	(ℓ,m)	$\mathbf{q} = (q_x,q_y)$
$b_i(\mathbf{y})$	$Y_{\ell,m}(\Omega)$	$e^{i\mathbf{q}\mathbf{r}^{\parallel}}$

In the following section, G is given for the impurity Hartree equation, and in the next section G is determined at least asymptotically for the Feynman equation. Both Green's functions are given only for the droplet and the film geometry (spherical symmetry and translational invariance in two directions); more on the expansion of the Green's function in generalized coordinate systems can be found in [**MF53b**].

1. Hartree Equation Green's Function

The impurity Hartree equation $H\eta = E\eta$ is a plain one-body Schrödinger equation for a particle under the influence of the potential $V_H(0) = \frac{\hbar^2}{2m_I}\frac{\nabla\sqrt{\rho(0)}}{\sqrt{\rho(0)}}$. In this case the one-dimensional Green's function $G_i(E)$, with E *in the continuum*, can be determined by matching the regular and irregular solutions of $H_i f_i = E f_i$, η and χ

spherical	planar
$\eta_{\ell,k} \to k\ j_\ell(kr + \delta_\ell(k))$	$\eta_k \to \sin(kz + \delta(k))$
$\chi^\pm_{\ell,k} \to ik\ h^\pm_\ell(kr)$	$\chi^\pm_k \to e^{\pm ikz}$

such that they meet the boundary conditions and reproduce the delta peak at $x_1 = x_2$, $(E - H_i)G_i(x_1, x_2; E) = \delta(x_1 - x_2)$. For the full $G(E)$, $E = \frac{\hbar^2 k^2}{2m_I}$, one finds for

spherical geometry:

$$G^\pm(\mathbf{r}, \mathbf{r}'; E > 0) = \sum_{\ell,m} Y_{\ell,m}(\Omega) \sum\!\!\!\!\!\!\!\int_{k'} \frac{\eta_{k',\ell}(r)\eta^*_{k',\ell}(r')}{E \pm i\varepsilon - E_{k',\ell}} Y^*_{\ell,m}(\Omega') \tag{261}$$

$$= \sum_{\ell,m} Y_{\ell,m}(\Omega) \underbrace{\left(-\frac{2m_I}{\hbar^2}\frac{1}{k}\right)\eta_{k,\ell}(r_<)\chi^\pm_{k,\ell}(r_>)e^{\pm i\delta_\ell(k)}}_{=:\, G_\ell(r, r', E)} Y^*_{\ell,m}(\Omega') \tag{262}$$

where $\sum\!\!\!\!\!\!\int$ denotes summation $\sum_n$ over bound states and integration $\int \frac{dk}{\pi/2}$ over continuum states[1], for which $E_{k,\ell} = \frac{\hbar^2 k^2}{2m_I}$. Similarily for

planar geometry:

$$G^\pm(\mathbf{r}, \mathbf{r}'; E > 0) = \int \frac{d^2q}{(2\pi)^2} e^{i\mathbf{q}\mathbf{r}^{\|}} \sum\!\!\!\!\!\!\!\int_{k'} \frac{\eta_{k'}(z)\eta^*_{k'}(z')}{E \pm i\varepsilon - E_{k'}} e^{-i\mathbf{q}\mathbf{r}'^{\|}} \tag{263}$$

$$= \int \frac{d^2q}{(2\pi)^2} e^{i\mathbf{q}\mathbf{r}^{\|}} \underbrace{\left(-\frac{2m_I}{\hbar^2}\right)\frac{1}{k}\eta_k(z_<)\chi^\pm_k(z_>)e^{\pm i\delta(k)}}_{=:\, G(z, z', E)} e^{-i\mathbf{q}\mathbf{r}'^{\|}} \tag{264}$$

For planar geometry, the one-dimensional Green's function $G(z, z', E)$ associated with the perpendicular motion is independent of the parallel quantum number $\mathbf{q}$.

[1] The 2 in $2/\pi$ comes from the normalization of the regular solutions η, and the π from the density of states in the infinite *half* space $[0, \infty[$.

2. Feynman Equation Green's Function

The Feynman equation $H\psi = \hbar\omega[S * \psi]$ differs from the Hartree equation in that it is nonlocal (S is an integral operator), and that it appears to be non-Hermitean. Hermiticity is readily achieved by the transformation $f := [S^{1/2} * \psi]$

$$\int d2\ [S^{-1/2} * H * S^{-1/2}](1,2)f(2) = \hbar\omega f(1) \qquad \text{with} \quad f(1) = \int d2\ S^{1/2}(1,2)\psi(2)\,.$$

Like the local Hartree equation, the Feynman equation is separable to a one-dimensional equation for each subspace i (see table above)

$$\int dx_2\ [S_i^{-1/2} * H_i * S_i^{-1/2}](x_1,x_2)f_i(x_2) = \hbar\omega_i f_i(x_2) \tag{265}$$

Unfortunately, the Green's function of this nonlocal integro-differential equation cannot be be constructed by matching the regular and irregular solutions at $x_1 = x_1$, as is easily seen: assuming $G_i(x_1,x_2) = \alpha f(x_<)\chi(x_>)$, the effect of an integral operator $K(x_1,x_2)$ is

$$\int_0^\infty dx\ K(x_1,x)G_i(x,x_2) = \chi_i(x_2)\int_0^{x_2} dx\ K(x_1,x)f_i(x) + f_i(x_2)\int_{x_2}^\infty dx\ K(x_1,x)\chi_i(x)$$

which can attain the form of a symmetrized product $f\chi$ only if $K(x_1,x) = 0$ for $x < x_1$ and $x > x_1$ simultaneously, i.e. if K is a local operator. In the limit $x_2 \to \infty$ however, $G_i = \alpha f(x_<)\chi(x_>)$ satisfies $\int dx_2\ [S_i^{-1/2} * H_i * S_i^{-1/2} - \hbar\omega](x_1,x_2)G_i(x_1,x_3) = \delta(x_1 - x_3)$, because the integral operator $S_i^{-1/2}$ has only a finite nonlocal range. Hence we find for

spherical geometry:

$$\begin{aligned} G^\pm(\mathbf{r},\mathbf{r}';E>0) &= \sum_{\ell,m} Y_{\ell,m}(\Omega)G_\ell(r,r';E)Y^*_{\ell,m}(\Omega') \\ &\longrightarrow \sum_{\ell,m} Y_{\ell,m}(\Omega)\left(-\frac{2m_B}{\hbar^2}\right)\frac{1}{k}[S_\ell^{1/2} * \psi_{k,\ell}](r_<)\chi^\pm_{k,\ell}(r_>)e^{\pm i\delta_\ell}Y^*_{\ell,m}(\Omega') \\ &\qquad \text{for} \quad r\to\infty \text{ and/or } r'\to\infty \end{aligned} \tag{266}$$

and for

planar geometry:

$$\begin{aligned} G^\pm(\mathbf{r},\mathbf{r}';E>0) &= \int \frac{d^2q}{(2\pi)^2}e^{i\mathbf{q}\mathbf{r}^\parallel}G_q(z,z';E)e^{-i\mathbf{q}\mathbf{r}'^\parallel} \\ &\longrightarrow \int \frac{d^2q}{(2\pi)^2}e^{i\mathbf{q}\mathbf{r}^\parallel}\left(-\frac{2m_I}{\hbar^2}\right)\frac{1}{k}[S_q^{1/2} * \psi_{k,q}](z_<)\chi^\pm_{k,q}(z_>)e^{\pm i\delta_q(k)}e^{-i\mathbf{q}\mathbf{r}'^\parallel} \\ &\qquad \text{for} \quad z\to\infty \text{ and/or } z'\to\infty \end{aligned} \tag{267}$$

If the functions f_n in (259) are the Feynman states ψ_n or their adjoint states ϕ_n or a combination, we use subscripts to indicate which Green's function is meant, e.g.

$${}_{\phi\psi}G(z) = \sum_n \frac{|\phi_n\rangle\langle\psi_n|}{z-E_n} = \sum_n \frac{S^{1/2}|f_n\rangle\langle f_n|S^{-1/2}}{z-E_n} = S^{1/2}\,G(z)\,S^{-1/2}\,. \tag{268}$$

APPENDIX C

Nonlinear Equations of Motion

Conversely, steady superfluid flow involves a velocity field, which is divergence-free (div $\mathbf{v}_s$)*; the simplest example of such a flow is the vortex structure studied in Chapter 8. Such "hydrodynamic" flow is beyond the range of perturbation theory. The condensate has a really different structure, which must be accounted for from the very beginning of the calculation. In such cases, one must abandon the response function method, and rely on a direct description of superfluid flow.*
"The Theory of Quantum Fluids", D. Pines and P. Nozieres [**PN66b**]

In the discussion of the excitations, which are obtained by linear response to an infinitesimal perturbation of the system in its ground state, we observed in section 5 of chapter 3 that certain modes of the system (e.g. vortices, see the introductory quote) cannot be described by linearizing the equations of motion. In section 5 of chapter 5, it was shown that the second order current necessary for calculating mass transport, is not conserved in pure ^{4}He (while it is conserved in the asymptotic regime, which is all we need for the unitarity of the scattering matrix); and we remarked how this violation is remedied by refraining from linearizition. We show now how this comes about, in the simplest possible approximation: allowing only for fluctuations of the 1-body correlations, i.e. the nonlinear generalization of the Feynman approximation.

For a wave function

$$\Phi(1,\ldots,N;t) \;=\; \frac{1}{\mathcal{N}}\, e^{\sum_i \delta u(i;t)/2}\, \Phi_0(1,\ldots,N)$$

the Lagrange functional $L = \int dt\, \mathcal{L}$ derived in section 2 of chapter 3 for an arbitrary diagonal correlation operator $\delta U(t)$ becomes

$$L \;=\; \int_{t_1}^{t_2} dt \left\{ \frac{\hbar^2}{8m} \int d1\; \rho[\delta u_R](1;t)\; |\nabla_1 \delta u(1;t)|^2 + \frac{\hbar}{2} \int d1\; \rho[\delta u_R](1;t)\; \delta \dot{u}_I(1;t) \right\}$$

The stationarity condition $\delta L = 0$ yields 2 coupled equations for the 2 unknown functions $\delta u_R = \Re e\, \delta u$ and $\delta u_I = \Im m\, \delta u$

$$\frac{\delta L}{\delta u_R(1;t)} = 0 \quad \Leftrightarrow \tag{269}$$

$$-\frac{\hbar^2}{2m}\nabla_1\rho[\delta u_R](1;t)\nabla_1\delta u_R(1;t)+\frac{\hbar^2}{4m}\int d2\ \tilde{S}(1,2;t)\ \left\{[\nabla_2\delta u_R(2;t)]^2+[\nabla_2\delta u_I(2;t)]^2\right\}+$$
$$+\hbar\int d2\ \tilde{S}[\delta u_R](1,2;t)\ \delta\dot{u}_I(2;t)=0$$

and

$$\frac{\delta L}{\delta u_I(1;t)}=0 \quad \Leftrightarrow \tag{270}$$

$$-\frac{\hbar^2}{2m}\nabla_1\rho[\delta u_R](1;t)\nabla_1\delta u_I(1;t)\ -\ \hbar\dot{\rho}[\delta u_R](1;t)=0 \tag{271}$$

where $\rho[\delta u_R](1;t)$ denotes the 1-body density $\langle\Phi(t)|\hat{\rho}(1)|\Phi(t)\rangle$, and $S[\delta u_R](1,2;t)$ the static structure function with respect to the time-dependent wave function $\Phi(t)$; both are functionals of δu_R. After linearization these two equations would be equivalent, and could be cast into a single equations for δu, namely the Feynman equation (43); solving them is straightforward. However, solving the above nonlinear, coupled, time-dependent partial integro-differential equations (269) and (271) implies a tremendous effort in inhomogeneous systems — and we have not even taken into account fluctuations of the 2-body correlations.

1. Mass current conservation

As a first step to cast (269) and (271) into a familiar form, we show that the latter is the conservation equation of the 1-body current, which is given by

$$\begin{aligned}\mathbf{j}[\delta u_R,\delta u_I](1;t) &= \\ &= \frac{1}{\langle\Psi|\Psi\rangle}\int d1\ldots dN\ \Psi^*(1\ldots N;t)\frac{\hbar}{2mi}\sum_k[\delta(\mathbf{r}-\mathbf{r}_k)\nabla_k-\nabla_k\delta(\mathbf{r}-\mathbf{r}_k)]\Psi(1\ldots N;t)\\ &= \frac{\hbar}{2m}\rho[\delta u_R](1;t)\nabla\delta u_I(1;t)\end{aligned}$$

Hence the minimization of L with repect to δu_I directly yields the continuity equation

$$\nabla\cdot\mathbf{j}[\delta u_R,\delta u_I](1;t)+\dot{\rho}[\delta u_R](1;t)=0$$

The current is conserved to all orders in δu.

2. Momentum flow

The nonlinear equations of motion for δu_R and δu_I can be brought into a familiar set of equations, namely the hydrodynamic Euler equations for an ideal fluid, *i.e.* the "two fluid" model of ^{4}He at $T=0$.[1] Eq. (271) has already the right form and expresses mass conservation. Eq. (269) is the momentum conservation equation, which is seen be applying

[1] Using the extension of the HNC-Euler-Lagrange theory to finite temperatures [**CKSC93**], a microscopic derivation of the two fluid model for T well below the λ-transition might be possible.

the inverse of the static structure operator, $S^{-1}(1,2;t) = I - \tilde{X}(1,2;t)$, and then the gradient operator. This yields (arguments except t are omitted now)

$$\frac{1}{m}\nabla\frac{1}{\sqrt{\rho(t)}}(I-\tilde{X}(t)) * H_1(t) * \frac{\delta\tilde{u}_R(t)}{2} + (\mathbf{v}_s(t)\cdot\nabla)\mathbf{v}_s(t) + \dot{\mathbf{v}}_s(t) = 0$$

where we defined the superflow velocity

$$\mathbf{v}_s(t) = \frac{\hbar}{2m}\nabla\delta u_I(t)$$

and used $\nabla(\mathbf{a}\cdot\mathbf{b}) = \mathbf{a}\times(\nabla\times\mathbf{b}) + \mathbf{b}\times(\nabla\times\mathbf{a}) + \mathbf{b}\cdot\nabla\ \mathbf{a} + \mathbf{a}\cdot\nabla\ \mathbf{b}$. The operator $H_1(t) = H_1[\delta u_R](1;t)$ is formally defined as in eq. (18), but with with the *fluctuating* density $\rho[\delta u_R](1;t)$ instead of the ground state density.

The complicated pressure term simplifies considerably if we assume small δu_R: $\tilde{X}(1,2;t)$ and $H_1(1;t)$ may be replaced by their repsective ground state value; to first order, the real part of the 1-body fluctuation is $\delta\tilde{u}_R/2 = (I-\tilde{X}) * (\delta\rho/\sqrt{\rho})$. Using the 2-body E.-L. equation for the ground state (24),

$$\frac{1}{m}\nabla\frac{1}{\sqrt{\rho}}(H_1 + 2\tilde{V}_{ph}) * (\frac{1}{\sqrt{\rho}}\,\delta\rho(t)) + (\mathbf{v}_s(t)\cdot\nabla)\mathbf{v}_s(t) + \dot{\mathbf{v}}_s(t) = 0$$

which is the equation of motion of the superflow (*i.e.* the Navier-Stokes equation of an ideal fluid), with a pressure term which is valid down to microscopic length scales, unlike expressions used in phenomenlogical treatments.

$\delta^2 E := \frac{1}{4}(\frac{\delta\rho}{\sqrt{\rho}}|H_1 + 2\tilde{V}_{ph}|\frac{\delta\rho}{\sqrt{\rho}}$ is the energy increase caused by a static density fluctuation see Ref. [**Zil97**] for a discussion. Specifically, for plane wave fluctuations in bulk, $\delta\rho = \delta\rho_k e^{i\mathbf{kr}}$,

$$\frac{1}{m\rho}\nabla(\frac{\hbar^2 k^2}{2m} + 2\tilde{V}_{ph}(k))\delta\rho_k(t) + (\mathbf{v}_s(t)\cdot\nabla)\mathbf{v}_s(t) + \dot{\mathbf{v}}_s(t) = 0\,.$$

To check the validity of this flow equation derived in the framework of a microscopic theory, we take the limit of fluctuations on a macroscopic range. For $k \to 0$, the Fourier tranform of the particle-hole potential becomes $V_{ph}(0+) = mc^2 = \partial P/\partial\rho$ (apart from corrections due to the fact that the elementary diagrams cannot be summed up exactly). Thus, for slowly varying fluctuations of low amplitude, we get the hydrodynamic flow equation

$$-\nabla\frac{P(t)}{\rho} = m(\mathbf{v}_s(t)\cdot\nabla)\mathbf{v}_s(t) + m\dot{\mathbf{v}}_s(t) = m\frac{d}{dt}\mathbf{v}_s(t)\,.$$

Bibliography

[AHS99] V. Apaja, J. Halinen, and M. Saarela. Soft excitation modes of quantum bose fluids; a precursor of solidification. In *Condensed Matter Theories*, volume 14. Nova, 1999.

[AMW87] R. A. Aziz, F. R. W. McCourt, and C. C. K. Wong. A new determination of the ground state interatomic potential for he_2. *Molec. Phys*, 61:1487, 1987.

[And66] A. F. Andreev. Surface tension of weak helium isotope solutions. *JETP*, 23(5):939, 1966.

[Apa00] V. Apaja. *Collective Excitations and Stability of Quantum Fluids*. PhD thesis, Department of Physical Sciences, Theoretical Phycics, University of Oulu, Finland, 2000.

[AS98] V. Apaja and M. Saarela. Current patterns in the phonon-maxon-roton excitations in ^{4}He. *Phys. Rev. B*, 57(9):5358, 1998.

[BBS82] J. Böheim, W. Brenig, and J. Stutzki. On the low energy limit of reflection and sticking coefficients in atom surface scattering. II. long range forces. *Z. Phys. B*, 48:43–49, 1982.

[BC49] J. Boronat and J. Casulleras. Monte carlo analysis of an interatomic potential for he. *Phys. Rev. B*, 49(13):8920, 49.

[BGG94] G. P. Brivio, T. B. Grimley, and G. Guerra. Quantum theory of sticking: various approaches and simple model. *Surf. Sci*, 320:344–354, 1994.

[Bis98] R. F. Bishop. The coupled cluster method. In Jesús Navarro and Artur Polls, editors, *Microscopic Quantum Many-Body Theories and Their Applications*, volume 510 of *Lecture Notes in Physics*, pages 1–70. Springer, 1998.

[BL95] E. R. Bittner and J. C. Light. Many-body effects and resonances in universal quantum sticking of cold atoms to surfaces. *J. Chem. Phys.*, 102(6):2614, 1995.

[Bor98] G. Boronat. Diffusion monte carlo for excited states: Application to liquid helium. In Jesús Navarro and Artur Polls, editors, *Microscopic Quantum Many-Body Theories and Their Applications*, volume 510 of *Lecture Notes in Physics*, pages 359–379. Springer, 1998.

[BW93] J. J. Berkhout and J. T. M. Walraven. Scattering of hydrogen atoms from liquid-helium surfaces. *Phys. Rev. B*, 47(14):8886, 1993.

[Cam78] C. E. Campbell. The structure of quantum fluids. In C. A. Croxton, editor, *Progress in Liquid Physics*, chapter 6, pages 213–308. John Wiley & Sons, Ltd., 1978.

[CC75] C. C. Chang and M. Cohen. Microscopic theory of surface excitations in superfluid ^{4}he. *Phys. Rev. B*, 11(3):1059, 1975.

[CC77] C. C. Chang and C. E. Campbell. Energy and structure of the ground state of liquid ^{4}he. *Phys. Rev. B*, 15:4238–4255, 1977.

[CC92] C. Carraro and M. W. Cole. Role of long-range forces in H sticking to liquid ^{4}He. *Phys. Rev. B*, 45(22):12930, 1992.

[CC98] C. Carraro and M. W. Cole. Sticking coefficient at ultralow energy: quantum reflection. *Prog. Surf. Sci.*, 57(1):61–93, 1998.

[CCKS97] C. E. Campbell, B. E. Clements, E. Krotscheck, and M. Saarela. Thermodynamics of boson quantum films. *PRB*, 55(6):3769–3791, 1997.

[CEKS93] B. E. Clements, J. Epstein, E. Krotscheck, and M. Saarela. Structure of boson quantum films. *Phys. Rev. B*, 48(10):7450, 1993.

[Cep95] D. M. Ceperley. Path integrals in the theory of condensed helium. *Rev. Mod. Phys.*, 67(2):279–355, 1995.

[CF59] J. W. Clark and E. Feenberg. *Phys. Rev.*, 113:388, 1959.

[CFK+94] B. E. Clements, H. Forbert, E. Krotscheck, H. J. Lauter, M. Saarela, and C. J. Tymczak. Dynamics of boson quantum fluids. *Phys. Rev. B*, 50(10):6958, 1994.

[CFKS94] B. E. Clements, H. Forbert, E. Krotscheck, and M. Saarela. ^{4}He on weakly attractive substrates: structure stability, and wetting behavior. *J. of Low Temp. Phys.*, 95(5/6):849, 1994.

[CGK+96] B. E. Clements, H. Godfrin, E. Krotscheck, H. Lauter, P. Leiderer, V. Passiouk, and C. J. Tymczak. Excitations in a thin liquid ^{4}He film from inelastic neutron scattering. *Phys. Rev. B*, 53(18):12242, 1996.

[CK92] D. P. Clougherty and W. Kohn. Quantum theory of sticking. *Phys. Rev. B*, 46:4921, 1992.

[CK95a] S. A. Chin and E. Krotscheck. Systematics of pure and doped ^{4}He clusters. *Phys. Rev. B*, 52(14):10405, 1995.

[CK95b] S. A. Chin and E. Krotscheck. Systematics of pure and doped ^{4}He clusters. *Phys. Rev. Lett.*, 74:1143, 1995.

[CKS94] B. E. Clements, E. Krotscheck, and M. Saarela. Analytic structure of long-wavelength excitations in ^{4}He surfaces. *Z. Physik B*, 94:115–122, 1994.

[CKS97] B. E. Clements, E. Krotscheck, and M. Saarela. Impurity dynamics in boson quantum films. *Phys. Rev. B*, 55(9):5959, 1997.

[CKS98] C. E. Campbell, E. Krotscheck, and M. Saarela. Quantum sticking, scattering and transmission of ^{4}He atoms from superfluid ^{4}He surfaces. *Phys. Rev. Lett.*, 80:2169, 1998.

[CKSC93] B. E. Clements, E. Krotscheck, J. A. Smith, and C. E. Campbell. Statistical mechanics of strongly correlated bose quantum fluids. *Phys. Rev. B*, 47(9):5239, 1993.

[CKT96] B. E. Clements, E. Krotscheck, and C. J. Tymczak. Multiphonon excitations in boson quantum films. *Phys. Rev. B*, 53(18):12253, 1996.

[CW71] R. A. Cowley and A. D. B. Woods. Inelastic scattering of thermal neutrons from liquid helium. *Can. J. Phys.*, 49:177–200, 1971.

[DDH81] R. J. Donnelly, J. A. Donnelly, and R. N. Hills. Specific heat and dispersion curve for helium–II. *J. Low Temp. Phys*, 44:471, 1981.

[DWW78] G. Das, A. F. Wagner, and A. C. Wahl. *J. Chem. Phys.*, 68:4917, 1978.

[Eco79] E. N. Economou. *Green's Functions in Quantum Physics*, volume 7 of *Solid-State Sciences*. Springer, 1979.

[Edm60] A. R. Edmonds. *Angular Momentum in Quantum Mechanics*. Princeton University Press, 2nd edition, 1960.

[EF78] D. O. Edwards and P. P. Fatouros. Theory of atomic scattering at the free surface of ^{4}He. *Phys. Rev. B*, 17(5):2147, 1978.

[EK88] J. Epstein and E. Krotscheck. Structure and excitations of liquid-helium films. *Phys. Rev. B*, 37:1666, 1988.

[EP76a] P. M. Echenique and J. B. Pendry. Reflectivity of liquid ^{4}He surfaces to ^{4}He atoms. *Phys. Rev. Lett.*, 37(9):561, 1976.

[EP76b] P. M. Echenique and J. B. Pendry. Scattering of ^{4}He atoms form the surface of liquid ^{4}He at 30mk. *J. Phys. C*, 9:3183, 1976.

[Eps92] J. Epstein. *Structure, Excitations and Impurity Dynamics of Liquid Helium.* PhD thesis, Texas A&M University, 1992.

[EST88] D. Eichenauer, A. Scheidemann, and J. P. Toennies. Liquid drop and optical model calculations of elastic, vibrationally inelastic and absorptive scattering of ^{4}He from ^{4}He$_n$–clusters. *Z. Phys. D*, 8:295–304, 1988.

[Far75] J. E. G. Farina. *Quantum theory of scattering processes: General principles and advanced topics*, volume 5 of *The international encyclopedia of physical chemistry and chemical physics, topic 2.* Pergamon Press, 1st edition, 1975.

[FC56] R. P. Feynman and M. Cohen. Energy spectrum of the exitations in liquid helium. *Phys. Rev.*, 102(5):1189, 1956.

[Fee69] E. Feenberg. *Theory of Quantum Fluids.* Academic Press, 1969.

[Fes58] H. Feshbach. Unified theory of nuclear reactions. *Ann. Phys.*, 5:357, 1958.

[Fes62] H. Feshbach. Unified theory of nuclear reactions. ii. *Ann. Phys.*, 19:287–313, 1962.

[Fey54] R. P. Feynman. Atomic theory of the two fluid model of liquid helium. *Phys. Rev.*, 94(2):262, 1954.

[For75] D. Forster. *Hydrodynamics, Fluctuations, Broken Symmetry, and Correlation Functions*, volume 47 of *Frontiers in Physics.* W. A. Benjamin, 1975.

[GNS95] W. Greiner, L. Neise, and H. Stöcker. *Thermodynamics and Statistical Mechanics.* Springer, New York, 1995.

[Gol86] V. V. Goldman. Kapitza conductance between gaseous atomic hydrogen and liquid helium. *Phys. Rev. Lett.*, 56(6):612, 1986.

[Goo71] Frank O. Goodman. Role of the attractive potential in gas-surface interaction theory. *J. Chem. Phys.*, 55(12):5742, 1971.

[Gsp95] J. Gspann. Atomic impact experiments with free ^{3}He and ^{4}He clusters. *Z. Phys.*, 98:405–411, 1995.

[GTV98] S. Grebenev, J. P. Toennies, and A. F. Vilesov. Superfluidity within a small helium-4 cluster: The microscopic andronikashvili experiment. *Science*, 279:2083, 1998.

[Gua98] R. Guardiola. Monte carlo methods in quantum many-body theories. In Jesús Navarro and Artur Polls, editors, *Microscopic Quantum Many-Body Theories and Their Applications*, volume 510 of *Lecture Notes in Physics*, pages 269–336. Springer, 1998.

[GW67] Marvin L. Goldberger and Kenneth M. Watson. *Collision Theory.* Wiley, 3rd edition, 1967.

[Hal95] Robert B. Hallock. The properties of multilayer ^{3}He - ^{4}He mixture films. volume XIV, chapter 5, pages 321–443. North-Holland, Amsterdam, 1995.

[Hal98] R. B. Hallock. The magic of helium-3 in two, or nearly two, dimensions. *Physics Today*, 1998.

[HCGG93] J. W. Halley, C. E. Campbell, Clayton F. Giese, and K. Goetz. New approach to the observation of the condensate fraction in superfluid helium-4. *Phys. Rev. Lett.*, 71(15):2429, 1993.

[HM86] J. P. Hansen and I. R. McDonald. *Theory of Simple Liquids.* Academic Press, 1986.

[HS89] T. W. Hijmans and G. V. Shlyapnikov. Small angle inelastic scattering of hydrogen atoms from a liquid He surface. *Phys. Lett. A*, 142(1):45, 1989.

[HWS92] T. W. Hijmans, J. T. M. Walraven, and G. V. Shlyapnikov. Influence of the substrate on the low-temperature limit of the sticking probability of hydrogen atoms on he films. *Phys. Rev. B*, 45(5):2561, 1992.

[Jac74] H. W. Jackson. Mutual properties of exact and certain approximate forms of the dynamic structure function $S(k,\omega)$. *Phys. Rev. A*, 9:964, 1974.

[JBH84] R. Jochemsen, A. J. Berlinsky, and W. N. Hardy. The diffusion cross section for atomic hydrogen in helium gas at low temperature and the H-He potential. *Can. J. Phys.*, 62(8):751759, 1984.

[KDL00] J. Klier, I. Doicescu, and P. Leiderer. First *dc*-measurements of electrons on liquid helium: the helium-FET. *Proceedings of QFS 2000*, 2000.

[KHP$^+$00] Y. Kwon, P. Huang, M. V. Patel, D. Blume, and K. B. Whaley. Quantum solvation and molecular rotations in superfluid helium clusters. *J. Chem. Phys.*, 113(16):6469–6501, 2000.

[KK76] A. K. Kerman and S. E. Koonin. Hamiltonian formulation of time-dependent variational principles for the many-body system. *Ann. Phys.*, 100:332, 1976.

[KKZ99] S. Kilić, E. Krotscheck, and R. Zillich. Binding of two helium atoms in confined geometries. *J. of Low Temp. Phys.*, 116(3/4):245, 1999.

[KPM$^+$98] E. Krotscheck, J. Paaso, M.Saarela, K. Schörkhuber, and R. Zillich. Single particle and fermi liquid properties of ^{3}He-^{4}He mixtures. *Phys. Rev. B*, 58:12282, 1998.

[Kro85a] E. Krotscheck. Liquid helium on a surface: ground state, excitations, condensate fraction, and impurity potential. *Phys. Rev. B*, 32(9):5713, 1985.

[Kro85b] E. Krotscheck. Theory of inhomogeneous quantum system: II. linear response and collective excitations in bose systems. *Phys. Rev. B*, 31:4258–4266, 1985.

[Kro86] E. Krotscheck. Optimal three-body correlations and elementary diagrams in liquid ^{4}He. *Phys. Rev. B*, 33(5):3158, 1986.

[Kro98a] E. Krotscheck. Inhomogeneous quantum liquids: Statics, dynamics, and thermodynamics. In J. Navarro and A. Polls, editors, *Microscopic Quantum Many-Body Theories and Their Applications*, Lecture Notes in Physics, page 187. Springer, 1998.

[Kro98b] E. Krotscheck. Inhomogeneous quantum liquids: Statics, dynamics, and thermodynamics. In Jesús Navarro and Artur Polls, editors, *Microscopic Quantum Many-Body Theories and Their Applications*, volume 510 of *Lecture Notes in Physics*, pages 187–250. Springer, 1998.

[KS93a] E. Krotscheck and M. Saarela. Hydrogen isotope and ^{3}He impurities in liquid ^{4}He. *J. of Low Temp. Phys.*, 90(5/6):415, 1993.

[KS93b] E. Krotscheck and M. Saarela. Theory of ^{3}He–^{4}He mixtures: Energetics, structure, and stability. *Phys. Rep.*, 232(1):1–86, 1993.

[KSE88] E. Krotscheck, M. Saarela, and J. Epstein. Impurity states in liquid-helium films. *Phys. Rev. B*, 38:111, 1988.

[KT92] E. Krotscheck and C. J. Tymczak. Dynamic structure factor of quantum liquid films. *Phys. Rev. B*, 45(1):217, 1992.

[KZ98] E. Krotscheck and R. Zillich. Scattering of ^{3}He atoms from ^{4}He surfaces. *Phys. Rev. B*, 58:5707, 1998.

[KZ99] E. Krotscheck and R. Zillich. Atom scattering from helium droplets. In G. S. Agnastostatos, editor, *Condensed Matter Physics*, volume 3 of *23rd Workshop on Condensed Matter Theories*. Nova Science Publishers, 1999.

[KZ01] E. Krotscheck and R. Zillich. The dynamics of ^{4}He droplets. *J. Chem. Phys.*, 2001. submitted.

[LDPS95] A. Lastri, F. Dalfovo, L. Pitaevskii, and S. Stringari. Dispersion of ripplons in superfluid ^{4}He. *J. of Low Temp. Phys.*, 98(3/4):227, 1995.

[Lek70] J. Lekner. Theory of surface states of ^{3}He atoms in liquid ^{4}He. *Philos. Mag.*, 22:669, 1970.

[LGB59] J. M. J. Van Leeuwen, J. Groeneveld, and J. De Boer. New method for the calculation of the pair correlation function. I. *Physica*, 25:792, 1959.

[LJSD36a] J. E. Lennard-Jones, F. R. Strachan, and A. F. Devonshire. The interaction of atoms and molecules with solid surfaces. III - the condensation and evaporation of atoms and molecules. *Proc. R. Soc. London*, 156:6–28, 1936.

[LJSD36b] J. E. Lennard-Jones, F. R. Strachan, and A. F. Devonshire. The interaction of atoms and molecules with solid surfaces. IV - the condensation and evaporation of atoms and molecules. *Proc. R. Soc. London*, 156:29–36, 1936.

[LST93] M. Lewerenz, B. Schilling, and J. P. Toennies. A new scattering deflection method for determining and selecting the sizes of large liquid clusters of ^{4}He. *Chem. Phys. Let.*, 206(1,2,3,4):381, 1993.

[McC95] P. V. E. McClintock. Ions and the landau critical velocity in He-II. *Z. Phys.*, 98:429–434, 1995.

[Mes85] Albert Messiah. *Quantenmechanik*, volume 2. de Gruyter, 2nd edition, 1985.

[MF53a] P. M. Morse and H. Feshbach. *Methods of Theoretical Physics*, volume 2. McGraw-Hill, 1953.

[MF53b] P. M. Morse and H. Feshbach. *Methods of Theoretical Physics*, volume 1. McGraw-Hill, 1953.

[MO78] I. R. McDonald and O'Gorman. *Phys. Chem. Liq.*, 78:57, 1978.

[MVSS93] A. C. Maan, B. J. Verhaar, H. T. C. Stoof, and I. F. Silvera. Surface-state hydrogen maser. *Phys. Rev. A*, 48(5):3921, 1993.

[New66] R. G. Newton. *Scattering Theory of Waves and Particles*. McGraw-Hill, 1966.

[NO88] John W. Negele and Henri Orland. *Quantum Many-Particle Systems*. Frontiers in Physics. Addison-Wesley, 1988.

[Owe81] J. C. Owen. Effective mass of one ^{3}He atom in liquid ^{4}He. *Phys. Rev. B*, 23:5815–5823, 1981.

[PD99] P. M. Platzman and M. I. Dykman. Quantum computing with electrons floating on liquid helium. *Science*, 284(16):1967, June 1999.

[PN66a] David Pines and Philippe Nozieres. *The Theory of Quantum Fluids*, volume 1. W. A. Benjamin Inc., 1966.

[PN66b] David Pines and Philippe Nozieres. *The Theory of Quantum Fluids*, volume 2. W. A. Benjamin Inc., 1966.

[PO56] O. Penrose and L. Onsager. Bose-einstein condensation and liquid helium. *Phys. Rev.*, 104(3):576, 1956.

[Puo97] M. Puoskari. *Integral Equation Theories of Simple Classical and Bose Liquids*. PhD thesis, University of Oulu, Finland, 1997.

[Puo99] M. Puoskari. Optimization of multiparticle correlations in bose fluids. *Physica Scripta*, 60:387–400, 1999.

[Rea97] L. Reatto. Progress in the theory of inhomogeneous ^{4}He. In C. Caccamo, J.-P. Hansen, and G. Stell, editors, *New Approaches to Problems in Liquid State Theory*, volume 529 of *NATO Science Series C: Mathematical and Physical Sciences*, page 459. Kluwer Academic Publishers, 1997.

[RG97] L. Reatto and D. E. Galli. What is a roton? In D. Neilson and R. F. Bishop, editors, *Recent Progress in Many-Body Theories*, volume 9, page 271. World Scientific, 1997.

[Rim00] A. Rimnac. Calculation of atom scattering processes on clean and adsorbate covered surfaces. Univ. Linz, 2000.

[Rip79] G. Ripka. A practical guide to the hypernetted chain method applied to fermi and bose systems. *Phys. Rep.*, 56:2, 1979.

[RR78] M. Rasetti and T. Regge. Helium droplets as analogs of heavy nuclei. In J .Tuvalds and T. Regge, editors, *Quantum Liquids*, pages 227–236. North-Holland, 1978.

[RS79] M. Reed and B. Simon. *Methods in Modern Mathematical Physics: Scattering Theory*, volume 3. Academic Press, 1979.

[Saa71] W. F. Saam. Origin of bound states of ^{3}He atoms on free superfluid ^{4}He surfaces. *Phys. Rev. A*, 4(3):1278, 1971.

[Saa86] M. Saarela. Elementary excitations in quantum fluids: application to liquid ^{4}He. *Phys. Rev. B*, 33(7):4596, 1986.

[Saa95] M. Saarela. Excitation spectrum of a ^{3}He impurity in ^{4}He. In E. Schachinger, H. Mitter, and H. Sormann, editors, *Recent Progress in Many-Body Theories*, volume 4, pages 93–100, New York, 1995. Plenum Press.

[Sch88] F. Schwabl. *Quantenmechanik*. Springer, 1988.

[SE88] D. R. Swanson and D. O. Edwards. Path-integral theory of the scattering of ^{4}He atoms at the surface of liquid ^{4}He. *Phys. Rev. B*, 37(4):1539, 1988.

[SHC97] A. K. Setty, J. W. Halley, and C. E. Campbell. Variational monte carlo studies of the rate of transmission of an atomic helium bem through a slab of superfluid helium by a condensate mediated process. *Phys. Rev. Lett.*, 79(20):3930, 1997.

[SHES95] F. Stienkemeier, J. Higgins, W. E. Ernst, and G. Scoles. Spectroscopy of alkali atoms and molecules attached to liquid ^{4}He clusters. *Z. Phys.*, 98:413–416, 1995.

[SK95] M. Saarela and F. V. Kusmartsev. Many-body structure of quantum vortices in thin ^{4}He films. *Phys. Lett. A*, 202:317, 1995.

[SMH$^+$99] F. Stienkemeier, F. Meier, A. Hägele, H. O. Lutz, E. Schreiber, C. P. Schuls, and I. V. Hertel. Coherence and relaxation in potassium-doped helium droplets studied by femtosecond pump-probe spectroscopy. *Phys. Rev. Lett.*, 83(12):2320, 1999.

[SVY$^+$98] A. I. Safonov, S. A. Vasilyev, I. S. Yasnikov, I. I. Lukashevich, and S. Jaakola. Observation of quasicondensate in two-dimensional atomic hydrogen. *Phys. Rev. Lett.*, 81:4545, 1998.

[Tay72] J. R. Taylor. *Scattering Theory*. John Wiley & Sons, 1972.

[TSV90] E. Tiesinga, H. T. C. Stoof, and B. J. Verhaar. Reflection of hydrogen atoms from the surface of superfluid helium. *Phys. Rev. B*, 41(13):8886, 1990.

[TV98] J. P. Toennies and A. F. Vilesov. Spectroscopy of atoms and molecules in liquid helium. *Annu. Rev. Phys. Chem.*, 49:1, 1998.

[TVW01] J. Peter Toennies, Andrej F. Vilesov, and K. Birgitta Whaley. Superfluid helium droplets: an ultracold nanolaboratory. *Physics Today*, 54(2):31, 2001.

[TWW76] J. Peter Toennies, W. Welz, and G. Wolf. *Chem. Phys. Lett.*, 44:5, 1976.

[Tym95] C. J. Tymczak. *Excitations in Liquid Helium-4 Films*. PhD thesis, Texas A&M University, May 1995.

[Wei78] M. Weissbluth. *Atoms and Molecules*. Academic Press, 1978.

[Wya98] A. F. G. Wyatt. Evidence of a bose-einstein condensate in liquid ^{4}He from quantum evaporation. *Nature*, 391:56, 1998.

[YDSea93] Ite A. Yu, J. M. Doyle, J. C. Sandberg, and et al. Evidence for universal quantum reflection of hydrogen from liquid ^{4}He. *Phys. Rev. Lett.*, 71(10):1589, 1993.

[Zil97] R. E. Zillich. Streuung von ^{3}He Atomen an dünnen ^{4}He Filmen. Univ. Linz, 1997.